Studies Of Dynamic Properties Of Mass Transport Processes

Thesis Submitted For The Degree Of

DOCTOR OF PHILOSOPHY (SCIENCE)

in

Physics (Theoretical)

by

Animesh Hazra

Department of Physics

University of Calcutta

2025

Acknowledgements

I would like to express my deepest gratitude to Prof. Punyabrata Pradhan for his invaluable guidance, encouragement, and unwavering support throughout the course of my Ph.D. His insightful ideas and mentorship have played a crucial role in shaping both my research and this thesis. I am also sincerely grateful to my thesis committee members, Prof. Jaydeb Chakrabarti and Prof. Manoranjan Kumar, for their thoughtful assessment, constructive suggestions, and engaging discussions during the annual evaluation sessions. In addition, I wish to thank Prof. Subhrangsu Sekhar Manna for his helpful discussions and critical comments on several projects and presentations during my tenure.

I gratefully acknowledge the S.N. Bose National Centre for Basic Sciences (SNBNCBS) under the Department of Science and Technology, Government of India, for providing funding support and an excellent research environment. I am also thankful to the Centre for access to the Cray supercomputing facility, which was essential in carrying out several parts of this research.

At SNBNCBS, I have been fortunate to interact with and learn from many wonderful people. I am thankful to my research group seniors Dhiraj Da, Anirban Da, and Tanmoy Da for their constant guidance and engaging discussions, both academic and otherwise. My juniors from this group, Aniket, Koushik (Das), and Anol, I always enjoyed discussing with them, and I wish them all the best in their future endeavours. I also valued interacting with Monali and Rajit during their project work. I would also like to mention Ritwick, Chandradip, Pallabi, Debojit, and Sabuj, with whom I have had several interactions in academia and shared a memorable trip near Bengaluru.

I am thankful to the gardeners for their hard work in keeping the campus beautiful, and to the other staff members for maintaining our hostel. I am indebted to the administrative staff — Nibedita Ma'am, Chandrakana Di, Rupam Da, and Joydeep Da — for their kind and timely help in various official matters. I am also grateful to faculty members Amitabha Lahiri, Suman Chakraborty, M. Sanjay Kumar, Sunandan Gangopadhyay, and others for the valuable lessons during my master's coursework, as well as to the many inspiring talks delivered in departmental seminars and the Bose Colloquium, which enriched my academic journey. I would also like to acknowledge the student mess facility and all the staff members for their support; being part of the mess committee (2020–21) was a memorable experience, as was serving as the sports coordinator (2022-23) for Muktangan with Shinjini, where we successfully organised sports activities. Beyond academics, I truly enjoyed spending time on the cricket field and interacting with many seniors, and I

am especially thankful to Biswajit (Panda) Da, Shashank Da (for our Fin15 finance club discussions), Subham Da, Premashish Da, Atul Da, Anirban (Paul) Da, and many others for their guidance and companionship.

I would also like to mention that the foundation of my PhD journey was laid during my undergraduate years at Ramakrishna Mission Vivekananda Centenary College, Rahara. I am grateful to have had inspiring teachers such as RK, ADC, AP, and CKD Sir, whose constant motivation and guidance encouraged me to pursue this path. I am also thankful to my college batchmates Saikat, Anirban, Prasanna, Ishitwa, and many others for discussions on various topics in physics. I remain deeply indebted to my teachers — Dipankar, Debrata, Bikas, and many others during higher secondary, as well as Kajol, Sankar Ghorai, Sudarson, and many others from secondary school — all of whom played a significant role in shaping my interest in academia. Also, I would like to thank my school friends — Sagar, Subhasis, Sankar, Kartik, Ayan, Subhadip, Saheb and many others — for their enduring friendship over the years. I have cherished the times spent with them during school life.

I deeply cherish the memories with my MSc batchmates (IPhD 2018): Anirban, Ankita, Avik, Arnab, Gaurav, Ishita, Rajdeep, Shubham, Soumen, Soham, Varsha, and Viswajit. Together, we shared countless moments — from birthday celebrations and night cricket matches to cooking sessions. After my master's, I am thankful to my friends from our PhD circle who made this journey even more special. I fondly recall Anirban's trip planning and restaurant suggestions, Avik's engaging discussions on politics and sports, Soumen's dedication as our "masterchef," Ishita's ever-ready for tea, Rajdeep's energy and creativity in drama scripts, Soham's humour in making memes and singing, Koushik's eagerness to explore local places and food, Shinjini's beautiful singing, and Sudipta's spontaneous plans. I am also thankful to other batchmates, Shashank (Shekhar Pandey), Rajib, and Manoj, for their companionship. Apart from the institute, I feel truly fortunate to have Subhra by my side.

I am deeply indebted to my family. Maa and Baba have always been my greatest source of strength and encouragement, even while remaining curious about what a PhD truly means. My elder brother (Dada), who serves in the Indian Army, has been a constant inspiration, and I feel proud to be his brother. His unwavering support during difficult times has been invaluable in helping me pursue higher studies. I am thankful to my Boudimoni (sister-in-law) for her encouragement and to Puchki (my niece), whose presence has been a source of happiness in our family.

Dedicated to My Parents

Publications

PAPERS TO BE INCLUDED IN THE PH.D. THESIS

1. **Dynamic fluctuations of current and mass in nonequilibrium mass transport processes**, Animesh Hazra, Anirban Mukherjee and Punyabrata Pradhan, J. Stat. Mech.: Theory Exp. 2024(8), 083205.

2. **Hyperuniformity in mass transport processes with center-of-mass conservation: some exact results**, Animesh Hazra, Anirban Mukherjee and Punyabrata Pradhan, J. Stat. Mech.: Theory Exp. 2025(2), 023201.

3. **Generic power laws in higher-dimensional lattice models with multi-directional hopping**, Animesh Hazra, Tanmoy Chakraborty, Anirban Mukherjee and Punyabrata Pradhan (accepted in Phys. Rev. E; arXiv.2503.18365).

OTHER PUBLICATION

1. **Anomalous relaxation and hyperuniform fluctuations in center-of-mass conserving systems with broken time-reversal symmetry**, Anirban Mukherjee, Dhiraj Tapader, Animesh Hazra and Punyabrata Pradhan, Phys. Rev. E **110**(2), 024119 (2024), doi:10.1103/PhysRevE.110.024119.

Notation

The following notation is used throughout the chapters:

L System size (number of lattice sites).

M Total mass in the system.

d Dimensionality of the system.

$\bar{\rho} = M/L^d$ Global density.

ζ Chipping (stickiness) parameter.

$m_i(t)$ Mass at site i in one dimension lattice.

$m(\mathbf{r}, t)$ Mass at site $\mathbf{r}$ at time t in d-dimensions.

ξ_i Random fraction of chipped mass at site i.

$\tilde{S}_{\mathcal{J}}(f)$ Power spectrum of instantaneous bond current.

$\tilde{S}_{M_l}(f)$ Power spectrum of subsystem mass.

$\mathcal{W}(y)$ Scaled bond current fluctuations

D Bulk-diffusion coefficient

χ Mobility

$\Gamma^{\alpha\beta}(\mathbf{r})$ Fluctuating current strength at position $\mathbf{r}$.

$B(\mathbf{r})$: Bond current correlation function.

$\delta(\mathbf{r})$ Discrete Dirac delta function.

$\hat{e}_\alpha$ Unit vector along direction α.

$S(\mathbf{q})$ Static structure factor.

$S(\mathbf{q}, t)$ Dynamic structure factor.

$\mathcal{Q}_\alpha(\mathbf{r}, T)$ Time-integrated bond current at bond $(\mathbf{r}, \mathbf{r} + \hat{e}_\alpha)$ up to time T.

$\mathcal{J}_i(\mathbf{r}, t)$ Instantaneous bond current at space $\mathbf{r}$ and time t.

$C^{AB}(\mathbf{r}, t)$ Dynamic current correlations of two observable $A(\mathbf{0}, t)$ and $B(\mathbf{r}, t)$.

Abstract

This thesis investigates steady-state static and dynamic fluctuations in nonequilibrium mass transport processes on periodic lattices, with a focus on systems possessing either a single conservation law (mass) or two conservation laws (mass and center of mass, CoM). Using a microscopic analytical framework, we study a broad class of mass-chipping models−describing fragmentation, diffusion, and aggregation−as well as threshold-activated conserved sandpile models (e.g., Oslo and Manna) in one and two dimensions.

For a single (mass) conservation law and in one dimension, we identify distinct temporal regimes in current fluctuations, governed by a universal scaling function that bridges subdiffusive and diffusive behavior. A frequency-domain analysis reveals dimension-dependent scaling laws for current power spectra, $S_J(f) \sim S_J(0) + f^{d/2}$, characteristic of mass-conserving systems. In contrast, CoM conservation modifies the scaling to $S_J(f) \sim f^{1+d/2}$, demonstrating fluctuation suppression due to the additional constraint.

On the static side, structure factors in systems with CoM conservation scale as $S(q) \sim q^2$ in the small–wave number limit, consistent with class-I spatial hyperuniformity. Remarkably, in models with multidirectional hopping—where multiple chunks of mass or particles can simultaneously leave a lattice site in different directions—the structure factor exhibits a non-analytic q^2 dependence. This mechanism breaks detailed balance while preserving isotropy and homogeneity, leading to robust power-law $\sim 1/r^{d+2}$ correlations even far from criticality.

Overall, the thesis establishes a unified framework between microscopic models and hydrodynamic theory, providing fundamental insights into transport phenomena, fluctuation suppression, and hyperuniformity in complex driven systems, with broader implications for nonequilibrium statistical mechanics and materials science.

থিসিস সারসংক্ষেপ (বাংলা)

এই থিসিসটি পর্যায়ক্রমিক ল্যাটিসের ওপর ভারসাম্যহীন ভর পরিবহন প্রক্রিয়ার স্থির-অবস্থা স্ট্যাটিক এবং গতিশীল ফ্লাকচুয়েশন (ওঠানামা) নিয়ে গবেষণা করে, যেখানে একটি (ভর) বা দুটি (ভর এবং ভরের কেন্দ্র,) সংরক্ষণ সূত্র রয়েছে। একটি মাইক্রোস্কোপিক বিশ্লেষণাত্মক কাঠামো ব্যবহার করে, আমরা এক এবং দুই মাত্রায় বিস্তৃত ভর-বিভাজন মডেল—যা খণ্ডন, প্রসারণ এবং একীকরণ বর্ণনা করে—এবং থ্রেশহোল্ড-অ্যাক্টিভেটেড সংরক্ষিত স্যান্ডপাইল মডেল (যেমন, অসলো এবং মান্না) অধ্যয়ন করি।

একমাত্রিক ভর সংরক্ষণ সূত্রের ক্ষেত্রে, আমরা বর্তমানের ওঠানামায় স্বতন্ত্র সময়গত ব্যবস্থা শনাক্ত করি, যা একটি সার্বজনীন স্কেলিং ফাংশন দ্বারা নিয়ন্ত্রিত হয় এবং সাবডিফিউসিভ ও ডিফিউসিভ আচরণের মধ্যে সংযোগ স্থাপন করে। ফ্রিকোয়েন্সি-ডোমেন বিশ্লেষণ বর্তমান পাওয়ার স্পেকট্রার জন্য মাত্রা-নির্ভর স্কেলিং নিয়ম প্রকাশ করে, , যা ভর-সংরক্ষণ ব্যবস্থার বৈশিষ্ট্য। এর বিপরীতে, ভরের কেন্দ্র সংরক্ষণ স্কেলিং পরিবর্তন করে করে $S_J(f) \sim f^{d/2}$, যা অতিরিক্ত সীমাবদ্ধতার কারণে ফ্লাকচুয়েশন হ্রাস করে।

স্থির অবস্থার দিকে, ভর কেন্দ্র সংরক্ষণ সহ সিস্টেমের কাঠামো ফ্যাক্টরগুলি ক্ষুদ্র-তরঙ্গ সংখ্যা সীমাতে $S(q) \sim q^2$ হিসাবে স্কেল করে, যা ক্লাস-I স্থানিক হাইপারইউনিফর্মিটির সাথে সামঞ্জস্যপূর্ণ। লক্ষণীয়ভাবে, বহু-দিকনির্দেশক হপিং সহ মডেলগুলিতে—যেখানে একাধিক ভরের খণ্ড বা কণা একই সাথে বিভিন্ন দিকে একটি ল্যাটিস সাইট ছেড়ে যেতে পারে—কাঠামো ফ্যাক্টরটি একটি অ-বিশ্লেষণাত্মক q^2 নির্ভরতা প্রদর্শন করে। এই প্রক্রিয়াটি ডিটেইলড ব্যালেন্সকে ভেঙে দেয় এবং আইসোট্রপি ও সমজাতীয়তাকে অক্ষুণ্ণ রাখে, যা সংকটাপন্ন বিন্দু থেকে অনেক দূরেও ঘনত্ব সহসম্বন্ধ $\sim 1/r^{d+2}$ অনুসারে হ্রাস পায়।

সামগ্রিকভাবে, এই থিসিসটি মাইক্রোস্কোপিক মডেল এবং হাইড্রোডাইনামিক তত্ত্বের মধ্যে একটি সমন্বিত কাঠামো স্থাপন করে, যা পরিবহন প্রক্রিয়া, ওঠানামা দমন, এবং জটিল চালিত সিস্টেমের হাইপারইউনিফর্মিটি সম্পর্কে মৌলিক অন্তর্দৃষ্টি প্রদান করে, যার ভারসাম্যহীন স্ট্যাটিসটিক্যাল মেকানিক্স এবং পদার্থ বিজ্ঞানের জন্য ব্যাপক প্রভাব রয়েছে।

Contents

List of Figures

List of Tables

1

Introduction

Dynamical systems are ubiquitous in natural and engineered systems, spanning over a wide range of spatial and temporal scales − from the motion of subatomic particles to the motions of bodies in the cosmos, and from microseconds to billions of years. Indeed, these systems have a common underlying feature: they are made up of numerous degrees of freedom that change with time, usually in complicated and unforeseen ways. The core problem of physics and allied sciences is to understand their large-scale static and dynamical properties from the underlying microscopic dynamical laws. Such predictive power would have profound consequences in various fields, such as in predicting market trends for strategic choices, weather forecasting to calculating the exact future position of a celestial body. This objective, though, is unattainable for most systems because of the complex many-body interactions between their vast components, the precise dynamical evolution of which is usually unknown or experimentally inaccessible.

Therefore, for statistical physicist and mathematicians, a suitable path has been to take a probabilistic (stochastic) description, where the coarse-grained microscopic dynamics involving particles, mass, or energy, rather than being purely deterministic as in Newtonian or Hamiltonian dynamics, are assumed to happen quite randomly (though perhaps with correlations). Indeed, characterizing fluctuations—of static or of dynamic observables—is a fundamental issue in statistical mechanics and is taken naturally through the investigation of stochastic processes observed in nature. Notably, fluctuations in most instances follow the celebrated central limit theorem (CLT). For instance, in a homogeneous system, the variance of particle number (or mass / energy) within a region of radius R, usually increases linearly with the volume $\sigma(R)^2 \sim R^d$. However, there are some prominent exceptions, where the scaling does not quite hold. Consider, for example, the giant number fluctuations (GNF), one such exception where the variance increases more rapidly than the CLT would suggest. The GNFs have been seen in many active matter systems, such as

flocks of birds, bacterial colonies, self-propelled particles and driven granular media [1], among others. A second deviation from the CLT can arise when large-scale density variations are inhibited instead of enhanced—a state known as "superhomogeneous" [2] or "hyperuniform" [3], with a vanishing structure factor for long wavelengths, $S(q \to 0) \to 0$ [3, 4]. Hyperuniformity was originally identified in ordered materials like perfect crystals and quasi-crystals, but later work has demonstrated its existence in disordered structures, for example, the venation pattern in leaf [5], the pattern of cone cells in avian retinas [6], and even in some jammed particulate packings [7]. Of course, it is highly desirable to understand the dynamical mechanism, which would lead to such a hyperuniform state of matter. In this thesis, we aim to theoretically characterize hyperuniformity using minimal model systems, which exhibit anomalously suppressed density and current fluctuations.

Analytically tractable models exhibiting such fluctuation phenomena are rare, and finding them itself constitutes the important first step in understanding the macroscopic behavior of interacting-particle systems. Indeed, minimal models (typically, on a lattice) provide an important testing ground for their theoretical studies. The simplest example is perhaps the systems of (simple) random walkers, in which non-interacting particles diffuse freely on a lattice. By introducing hard-core exclusion yields the simple symmetric exclusion process (SSEP), a paradigmatic interacting particle system with an excluded-volume constraint, for which both static and dynamic fluctuations can be computed exactly [8, 9]. A second type of interacting system is the zero-range process (ZRP) [10], in which local hop rates depend solely on the local occupation number, and for which condensation transitions and other interesting behaviour are possible.

More intricate cases arise in threshold-activated systems, where mass transfer takes place only when the mass at a given site exceeds a critical threshold m_c, thus introducing strongly nonlinear mass-dependent hopping rates. Examples include the Bak–Tang–Wiesenfeld (BTW) model and the Manna model [11, 12], among several other variants, with or without more-than-one conservation laws, symmetries and dimensions. These models, though central to studies of self-organised criticality [11], are notoriously difficult to handle analytically, even in their active phase far from from the absorbing phase transition point. A simpler alternative arises by considering continuous masses instead of discrete particles and removing the threshold condition. This gives rise to a class of models, called mass chipping models (MCMs) [13, 14]—the primary focus of this thesis. Notably, despite being far from equilibrium, MCMs remain analytically tractable even in the presence of non-trivial spatial correlations. Several well-known processes fall within this class, including the Kipnis–Marchioro–Presutti (KMP) model [15] and the random average process (RAP) [16].

In this thesis, we study a broad classes of MCMs and threshold-activated systems like conserved sandpiles, extending them to higher dimensions and with more than one conservation laws and symmetries. We demonstrate that, despite the simplicity of the dynamical rules, they display rich static and dynamical behavior, which however can be characterized theoretically (in fact, in many cases, exactly). To this end, we calculate both static fluctuations (via the structure factor) and dynamic fluctuations (such as the bond current and its power spectrum in the frequency domain),

thereby revealing how fluctuation behaviour depends on system dimensionality. We then consider an additional centre-of-mass conservation law and investigate its impact on fluctuation properties. Our analysis shows that this extra conservation strongly suppresses fluctuations, leading to hyperuniform states. For MCMs, these results are derived exactly from the microscopic dynamics, providing one of the few (exact) analytically solvable examples of hyperuniformity in a many-body system [4].

1.1 Minimalistic description of interacting systems

The study of many-particle systems offers a fascinating window into how complex behaviors can emerge from simple, local rules. While Newtonian mechanics provides an exact—though often intractable—framework for a few interacting bodies, the complexity increases dramatically as the number of particles grows. At macroscopic scales, tracking individual particle trajectories becomes not only computationally prohibitive, but also physically perhaps not entirely required; instead, the focus shifts to emergent collective behaviour arising from the interactions within the whole system. This is the realm where statistical and probabilistic methods become indispensable. In modern statistical physics, many-body interactions are explored through a variety of simplified and minimalistic, yet insightful models. For example, the symmetric simple exclusion process (SSEP) represents fermionic-like hardcore interactions in equilibrium systems of discrete particles [9]. Similarly, zero-range processes model bosonic systems, providing a minimal model system to study phenomena such as condensation transitions, etc. [17]. Also, beyond equilibrium, threshold-activated systems—such as the Manna [12] and the Oslo sandpiles [18] capture scale-invariant behavior, observed in nature. Indeed, these model systems are well studied for the power-law correlations and "$1/f$" noise[11], they generate in steady states. For the purpose of analytical tractability, one usually considers an important class of models is *mass chipping models* (MCMs) [13–15, 19–22], which have been intensively studied in the past several decades. These models typically describe transport and redistribution (i.e., fragmentation, diffusion and aggregation) of a continuous conserved mass, albeit without a threshold activation condition (see panel (f) of Fig. 1.1). Despite their apparent simplicity, such models mimic various nonequilibrium phenomena [15, 23–27] and exhibit rich emergent behavior, including nontrivial spatial correlations and dynamic fluctuations, such as enhancement or suppression of fluctuations, etc. Although these models offer valuable insights in capturing a range of characteristics observed in driven systems, formulating a unified statistical mechanics framework, beginning with the microscopic dynamical rules, remains a major challenge so far. In this thesis, we have taken up the task of characterizing various static and dynamic characteristics, including the hydrodynamic ones, through microscopic approaches based on the Markov processes described below.

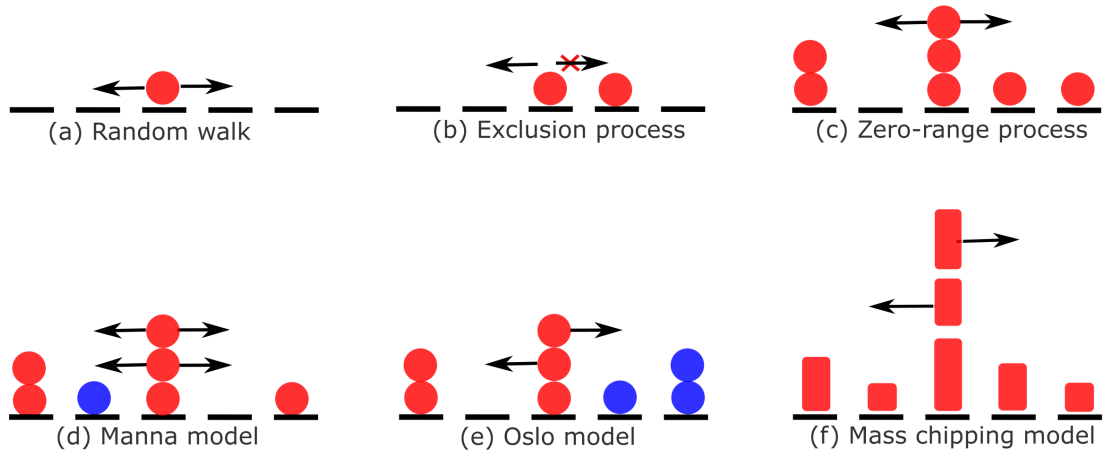

Figure 1.1: *Schematic diagram of various one-dimensional lattice models:* (a) Random walker model with no interaction, representing a single particle diffusing freely on a lattice; (b) Exclusion process with hard-core (fermionic-type) interaction, where each site can be occupied by at most one particle; (c) Zero-Range Process (ZRP) with bosonic-type interaction, where the hopping rate depends solely on the number of particles (mass) at the departure site; (d) Manna model, a sandpile-type system with stochastic toppling and threshold dynamics; (e) Oslo model, another threshold-driven system with bosonic interactions and center-of-mass conserving dynamics; (f) Mass Chipping Model (MCM), which involves many-body continuous mass redistribution without any threshold condition, unlike sandpile models.

1.2 Markov Processes

In the study of stochastic dynamics, theory of Markov processes provides a simple, but useful, framework for modeling systems, where constituents molecules or atoms (or, "agents" in active matter systems) can be interacting with each other. In a Markov process, one considers a space of configurations or "states", where the state of a system at the future (infinitesimal) time-step depends only on the present state of the system, independent of the past trajectory [28, 29]. Many important models in statistical mechanics and mass transport—including exclusion processes, threshold-activated (sandpile) models, and mass chipping models—can be naturally formulated as continuous-time Markov processes. The time evolution of dynamical quantities in such systems can be studied within either discrete-time or continuous-time Markov process formulations. In both approaches, and their relevance to nonequilibrium transport models, we consider a continuous-time Markov process. For a continuous-time Markov process, the probability that the system jumps from configuration n to configuration n' during an infinitesimal time interval dt is given by $W_{n'n}, dt$. The evolution of the probability $P_n(t)$ of finding the system in state n at time t is governed by the Master equation:

$$\frac{dP_n(t)}{dt} = \sum_{n' \neq n} W_{nn'} P_{n'}(t) - \sum_{n' \neq n} W_{n'n} P_n(t). \tag{1.1}$$

Here, $W_{nn'}$ denotes the transition rate from state n' to state n. The first term signifies the sum of all 'gain' processes (probability flux entering n from other states

n'), while the second term represents all 'loss' processes (probability leaving n to other states). The above Eq. 1.1 can be rewritten in a more compact, matrix-centric form:

$$\frac{dP_n(t)}{dt} = \sum_k \mathbb{W}_{nk} P_k(t) \tag{1.2}$$

where the transition rate matrix $\mathbb{W}_{nk}$ is defined as:

$$\mathbb{W}_{nk} = W_{nk} - \delta_{nk} \sum_{n'} W_{n'k}.$$

The normalisation condition $\mathbb{W}_{nn} = -\sum_{n' \neq n} \mathbb{W}_{n'n}$, ensures that each column of the transition rate matrix $\mathbb{W}$ sums to zero. The solution of the master equation mentioned in (1.2) is

$$P_n(t) = e^{\mathbb{W}t} P(0), \tag{1.3}$$

where $P(0)$ is the probability vector of the initial state.

Detailed balance condition

In the stationary state, the left-hand side of the master equation (Eq. (1.2)) vanishes, which yields the condition

$$\sum_k \mathbb{W}_{nk} P_k^{\mathrm{st}} = 0, \tag{1.4}$$

where $\mathbb{W}_{nk} = W_{nk} - \delta_{nk} \sum_\ell W_{\ell n}$ is the generator of the Markov process. This condition ensures probability conservation and defines the stationary distribution P_k^{st}. For systems that satisfy the *detailed balance* condition, the dynamics are time-reversible at the microscopic level. The condition implies that for any sequence of three states a, b, and c, the product of forward transition rates around a loop equals the product of the reverse transitions:

$$W_{ab} W_{bc} W_{ca} = W_{ac} W_{cb} W_{ba}. \tag{1.5}$$

A more commonly used and direct form of the detailed balance condition relates the transition rates and the stationary distribution:

$$W_{nk} P_k^{\mathrm{st}} = W_{kn} P_n^{\mathrm{st}}. \tag{1.6}$$

This implies that the probability current between any pair of configurations vanishes in both directions, and there are no net loops in configuration space. In equilibrium systems, the detailed balance condition is typically satisfied, and the stationary distribution takes the form of the Boltzmann distribution:

$$P_n^{\mathrm{st}} = \frac{1}{Z} e^{-\beta E_n}, \tag{1.7}$$

where E_n is the energy of configuration n, $\beta = 1/(k_B T)$ is the inverse temperature, and Z is the partition function. The transition rates W_{nk} in such systems are often chosen to satisfy detailed balance with respect to this equilibrium distribution:

$$\frac{W_{nk}}{W_{kn}} = e^{-\beta(E_n - E_k)}. \tag{1.8}$$

In contrast, for nonequilibrium systems, detailed balance is violated, and the stationary state typically exhibits non-zero probability currents. These systems cannot generally be described by a Boltzmann distribution, and their steady states must be determined from the full master equation without relying on energy-based principles.

1.3 Equilibrium mass-transport processes

In order to build an initial understanding of large-scale collective behavior in many-body systems, it is natural to begin with equilibrium models. In such systems, the dynamics eventually relax to a steady state that is well described by the principles of equilibrium statistical mechanics. The defining feature of equilibrium models is that the probability of finding the system in a microscopic configuration n is determined solely by the energy $E(n)$ of that configuration and the temperature of the thermal reservoir with which the system is in contact. Formally, the steady-state probability distribution is given by the Boltzmann–Gibbs measure,

$$P^{(\mathrm{Eq})}(n) = \frac{e^{-\beta E(n)}}{Z(\beta)}, \tag{1.9}$$

where $\beta = 1/k_B T$ is the inverse temperature, k_B is the Boltzmann constant, and $Z(\beta)$ is the partition function ensuring normalization. The partition function is defined as $Z(\beta) = \sum_n e^{-\beta E(n)}$, and it encodes all equilibrium thermodynamic information about the system. This formulation applies to systems in contact with a single thermal bath at fixed temperature T. However, equilibrium models can also be defined for isolated systems where the total number of particles is conserved, without introducing temperature explicitly. In such cases, stochasticity arises not from coupling to a thermal reservoir but from the dynamical rules of the model itself. Classic examples include random walks, the symmetric simple exclusion process (SSEP), and the zero-range process, where the global particle density plays the role of the controlling parameter. In these models, particles hop from site to site according to prescribed stochastic rules, and the stationary measure can be characterized without reference to a Hamiltonian or temperature.

Simple random walk

Let us begin with the classic random walk, the flagship model of stochastic motion (see Fig. 1.1(a)). Consider a particle that, at every discrete time step, hops either to the left or right with equal probability. If we denote the position of the walker at time t by $X(t) \in [0, L-1]$, and each step is independent, the dynamics are governed by the recurrence relation:

$$P(X, t+dt) = \frac{1}{2}P(X-1, t) + \frac{1}{2}P(X+1, t) \tag{1.10}$$

where $P(X, t)$ is the probability that the walker finds itself at position X at time t, in a system size of L. This deceptively simple recurrence gives rise to diffusive behavior and captures how randomness at the smallest scale can drive predictable

macroscopic patterns. In the continuum limit, $X/L \to x$ and $t/L^2 \to \tau$, the above relation converges to the diffusion equation:

$$\frac{\partial P(x,\tau)}{\partial \tau} = D\frac{\partial^2 P(x,\tau)}{\partial x^2}, \tag{1.11}$$

with $D = 1/2$ is the bulk-diffusion coefficient for the symmetric random walk. The general solution to the above diffusion equation for an initial distribution $P(x, 0)$, on an infinite domain, is:

$$P(x,\tau) = \frac{1}{\sqrt{4\pi D\tau}} \int_{-\infty}^{\infty} P(x',0) \exp\left(-\frac{(x-x')^2}{4D\tau}\right) dx' \tag{1.12}$$

For an initial delta function at $x = x_0$:

$$P(x,0) = \delta(x - x_0)$$

the solution simplifies to:

$$P(x,\tau) = \frac{1}{\sqrt{4\pi D\tau}} \exp\left(-\frac{(x-x_0)^2}{4D\tau}\right). \tag{1.13}$$

This solution represents the propagator of the diffusion process: the probability distribution remains centered at the initial location x_0, but spreads out over time with a characteristic width (standard deviation) of $\sigma(\tau) = \sqrt{2D\tau}$. This scale sets the speed at which perturbations spread in the system, highlighting how random microscopic motion can lead to universal macroscopic laws.

Symmetric Simple Exclusion Process

The Symmetric Simple Exclusion Process (SSEP) is one of the most fundamental and widely studied models of stochastic transport in interacting particle systems. It serves as a minimal model for diffusive dynamics with hard-core exclusion, where particles hop randomly, but two particles cannot occupy the same site. Despite its simplicity, the SSEP captures key features of interacting systems such as current fluctuations, boundary-driven steady states, and hydrodynamic scaling.

Model: The SSEP is defined on a one-dimensional periodic lattice of L sites, where each site i can be either empty or occupied by a single particle (see schematic diagram Fig. 1.1(b)). The configuration of the system is specified by a set of occupation numbers $\{m_0, m_1, \ldots, m_{L-1}\}$ with $m_i = 0$ or 1. The dynamics proceed as follows:

- Each particle attempts to hop to its left or right neighboring site with an equal rate (typically set to 1).
- The hop is only successful if the target site is empty, enforcing the exclusion principle.
- The total number of particles $M = \sum_i m_i$ or global density $\bar{\rho} = M/L$ is conserved.

It is worth noting that the SSEP model satisfies the detailed balance (DB) condition, $P^{st}(C)W_{C'C} = P^{st}(C')W_{CC'}$, where the steady-state distribution of a configuration $P^{\rm st}(C)$ is given by the Boltzmann weight. However, a nonequilibrium version of the model can be realized by imposing an external density gradient at the system boundaries, which induces a finite current in configuration space and thereby leads to a violation of detailed balance in the bulk.

Diffusive relaxation: In the SSEP, the coarse-grained density field $\rho(x = X/L, \tau = t/L^2) = \langle m_X(t)\rangle$ evolves according to a diffusion equation,

$$\frac{\partial \rho(x,\tau)}{\partial \tau} = D\frac{\partial^2 \rho(x,\tau)}{\partial x^2}, \tag{1.14}$$

where the diffusion constant takes the value $D = 1/2$ for symmetric hopping rates. This relation highlights that the SSEP exhibits purely diffusive behavior at large scales. The associated particle current is given by Fick's law, taking the linear form

$$j^{(d)}(x,\tau) = -D\nabla\rho(x,\tau), \tag{1.15}$$

which shows that the diffusive flux is proportional to the negative gradient of the local density field.

Density correlations: Although the SSEP model involves nearest-neighbor hard-core interactions (particles cannot overlap), its equal-time density correlations can be computed exactly due to the simplicity of the steady state. The connected density correlation function is defined as $\langle m_i m_j\rangle_c = \langle m_i m_j\rangle - \bar{\rho}^2$ where $\bar{\rho} = M/L$ is the average density. A straightforward combinatorial calculation gives

$$\langle m_i m_j\rangle_c = \begin{cases} \bar{\rho}(1-\bar{\rho}), & \text{for } i = j, \\ -\dfrac{\bar{\rho}(1-\bar{\rho})}{L-1}, & \text{for } i \neq j. \end{cases} \tag{1.16}$$

Thus, correlations vanish between distinct sites in the thermodynamic limit ($L \to \infty$), and only on-site fluctuations remain,

$$\langle m_i m_j\rangle_c = \bar{\rho}(1-\bar{\rho})\delta_{ij}. \tag{1.17}$$

Structure factor: The static structure factor is defined as the Fourier transform of the connected correlations,

$$S(q) = \frac{1}{L}\sum_{i,j}^{L} e^{iq(j-i)}\langle m_i m_j\rangle_c. \tag{1.18}$$

Substituting the correlation result, one finds that in the thermodynamic limit, the structure factor is independent of q:

$$S(q) = \bar{\rho}(1-\bar{\rho}). \tag{1.19}$$

This constant structure factor indicates that the SSEP is *not hyperuniform*: density fluctuations remain random and uncorrelated at large scales, as expected for a system with a flat, product-measure steady state.

Zero-Range Process (ZRP)

The Zero-Range Process (ZRP) is a paradigmatic stochastic model of mass or particle transport where hopping rates depend only on the departure site's occupation. Unlike exclusion processes (e.g., SSEP), it allows multiple particles per site, leading to bosonic-type statistics and phenomena such as clustering and condensation. Due to its simplicity, ZRP has been widely applied to model traffic jams, granular clustering, wealth condensation, and nonequilibrium phase transitions in transport and network systems [17, 30, 31].

Model: Consider a one-dimensional lattice of L sites, where each site i holds a non-negative integer number of particles $m_i \in \{0, 1, 2, \dots\}$. The total number of particles $M = \sum_{i=1}^{L} m_i$ is conserved. The dynamics are defined by the following rule:

- A particle at site i attempts to hop to a neighboring site (e.g., to $i+1$ or $i-1$) at a rate $u(m_i)$, which depends only on the number of particles m_i at the departure site.
- The hop is successful regardless of the occupation at the target site—hence "zero-range" interaction.

The function $u(m)$ is called the *rate function*, and its choice determines the qualitative behavior of the model.

Factorized Steady State: Let us consider $P(\{m_i\}, t)$ be the probability of the system being in configuration $\{m_i\} = m_1, m_2, \cdots, m_{L-1}$ at time t. The time evolution follows the master equation, typical of Markov processes. A remarkable feature of the ZRP is that its stationary state often takes a *factorized form*:

$$P^{st}(\{m_i\}) = \frac{1}{Z_{L,M}} \prod_{i=1}^{L} f(m_i), \tag{1.20}$$

where the weight function $f(m)$ is related to the hopping rate as:

$$f(m) = \prod_{k=1}^{m} \frac{1}{u(k)}, \quad f(0) = 1, \tag{1.21}$$

and $Z_{L,M}$ is the normalization (partition function) that ensures conservation of the total mass M. This factorized steady state is a distinctive feature of ZRP and makes it analytically tractable compared to many-body interacting systems with spatial correlations.

Condensation Transition: For certain choices of rate functions, particularly when $u(m)$ decays slowly for large m (e.g., $u(m) = 1 + b/m$), the system exhibits a *condensation transition*. In this phase, a finite fraction of the total mass accumulates at a single site, while the rest of the system remains in a fluid phase with a homogeneous background density. Moreover, it is a well-established result that for the choice of hopping rate $u(m) = 1 + b/m$, the system exhibits condensation

when the density exceeds the critical value $\rho > \rho_c = \frac{1}{b-2}$, provided $b > 2$. In this context, it is important to note that the mass fluctuations $\langle m^2 \rangle$, which quantify physical fluctuations in the system, diverge for $2 < b < 3$, leading to anomalous fluctuations. Therefore, in order to obtain the standard form of condensation with finite fluctuations, one must consider densities above the critical point and restrict to $b > 3$.

Density relaxation: The time evolution equation of the coarse-grained density field $\rho(x, \tau)$ evolves according to the follwing equation,

$$\frac{\partial \rho(x,\tau)}{\partial \tau} = \frac{\partial^2 u(x,\tau)}{\partial x^2}, \tag{1.22}$$

where the effective diffusion coefficient is density-dependent and given by $D(\rho) = (1/2)(du/d\rho)$, with $u(\bar{\rho}) = \langle u(m_i) \rangle = \langle u_i \rangle$ denoting the average hopping rate at mean density $\bar{\rho}$ [32]. Importantly, relaxation remains diffusive in the fluid phase; however, the bulk diffusion constant differs from that of the SSEP model (where $D = 1/2$). The corresponding diffusive current can be written as

$$\langle j_i^{(d)}(t) \rangle = -\frac{1}{2} \langle u_{i+1}(t) - u_i(t) \rangle, \tag{1.23}$$

which highlights the density-dependent transport properties.

Density correlation: The ZRP exhibits density correlations that follow a structure analogous to those in the SSEP. Specifically, the connected two–point correlation function takes the form

$$\langle m_i m_j \rangle_c = \frac{u(\bar{\rho})}{2D(\bar{\rho})} \delta_{i,j}, \tag{1.24}$$

where $u(\bar{\rho})$ is the average hopping rate at mean density $\bar{\rho}$, and $D(\bar{\rho})$ is the density-dependent diffusion coefficient. This result indicates that correlations are purely local, i.e., they vanish for $i \neq j$. Consequently, the structure factor turns out to be flat,

$$S(q) = \frac{u(\bar{\rho})}{2D(\bar{\rho})}, \tag{1.25}$$

demonstrating that the system exhibits random, non-hyperuniform fluctuations in its stationary state, similar to the SSEP model (see Eq. (1.19)).

1.4 Nonequilibrium Mass-Transport Processes

Nonequilibrium systems often involve local interactions and stochastic dynamics that do not obey detailed balance, leading to rich and diverse steady states. The violation of detailed balance can occur in several situations. For example, in a driven system coupled to two heat baths at different temperatures T_1 and T_2, instead of a single bath, a nonzero heat current flows through the system. Similarly, a density gradient induces a particle current, while the application of an external field also drives the system out of equilibrium. Apart from such external drives, there are examples of

internally driven systems, such as the asymmetric exclusion process [33]. Another class of examples is threshold-activated models, where the system can transition from an absorbing state to an active state, but the reverse transition is not allowed—thus clearly violating detailed balance [12, 18].

Continuous mass transport models, such as mass chipping models, provide further examples where the number of possible configurations is unbounded, and detailed balance is violated as well. In this work, we consider minimal nonequilibrium lattice models to explore fundamental aspects of nonequilibrium steady states, fluctuations, and phase transitions. Specifically, we focus on two broad classes: (i) continuous mass transport models, such as mass chipping models[20, 34], and (ii) threshold-activated models, such as the Manna and Oslo models.

Kipnis–Marchioro–Presutti (KMP) model

The Kipnis–Marchioro–Presutti (KMP) model was introduced in [15] as a minimalistic framework to study heat transport. In this model, each site i contains a non-negative continuous mass (or energy) $m_i(t) \geq 0$. At each update step, a bond $(i, i+1)$ is randomly chosen, and the total energy on the bond is redistributed: a random fraction $\xi \in U(0,1)$ of the combined energy $(m_i + m_{i+1})$ is assigned to site i, and the remainder $(1-\xi)(m_i + m_{i+1})$ is assigned to site $i+1$. We consider a periodic system, such that the global density (or average energy per site) $\bar{\rho} = \sum_i m_i/L$ is conserved. Now, the transport coefficients of the model are known exactly: the bulk diffusion constant D and the mobility (or conductivity) χ are

$$D = \frac{1}{2}; \quad \chi(\bar{\rho}) = \frac{\bar{\rho}^2}{2}. \tag{1.26}$$

Another simple feature of this model is that the steady-state density–density (or energy–energy) correlation is short-ranged and takes the form

$$\langle m_i m_j \rangle_c = \bar{\rho}^2 \delta_{ij}. \tag{1.27}$$

Thus, the KMP model displays qualitatively similar equilibrium properties to the SSEP, but differs in its microscopic dynamics: unlike SSEP, the KMP model violates detailed balance. Its simplicity, exact solvability, and nontrivial transport properties have made it a paradigmatic model for the study of nonequilibrium statistical mechanics. A generalized version of this model is also studied in this thesis (see Sec.2.4); importantly, the $\zeta = 0$ limit of MCM III corresponds to the KMP model (also see Table 2.13).

Mass Chipping Models (MCMs)

Mass Chipping Models (MCMs) describe the stochastic redistribution of a continuous scalar quantity—interpreted as "mass"—on a lattice. The mass at each site i, denoted by $m_i \in \mathbb{R}_{\geq 0}$, evolves via local update rules in which a fraction of the mass is "chipped off" and transferred to one or more neighboring sites. A typical rule is as follows: at unit rate, a site i is selected. A fraction ξ_i of its mass is retained, while the remaining portion, $m_i\tilde{\xi}_i$, is chipped off. This chipped mass may be fragmented into random parts and then redistributed to the neighboring sites, often in a symmetric manner.

Several variants of this general model have been investigated in the past, each differing in the details of the chipping and redistribution dynamics [13, 34, 35]. Despite these differences, a unifying feature of MCMs is that the resulting diffusive current has a simple gradient structure:

$$\mathcal{J}i^{(d)}(t) = D\big[\langle mi + 1(t) - m_i(t)\rangle\big], \tag{1.28}$$

where D is the bulk diffusion coefficient. Importantly, D is constant, which is independent of the global density, highlighting a key simplification in the transport behavior of these models.

In addition to the current, other transport coefficients can also be computed exactly. For instance, the density–density correlation functions exhibit nontrivial spatial structure, even though the steady state remains exactly solvable. The mobility factor is found to take the form

$$\chi(\rho) = \text{Const.}\rho^2, \tag{1.29}$$

where the prefactor depends on the specific microscopic details of the model but not on the density itself[34].

This combination of exact solvability and nontrivial correlations makes MCMs a powerful framework for analyzing fluctuations in systems with conserved quantities. In particular, they provide an analytically tractable setting for studying hydrodynamic transport coefficients, fluctuation–dissipation relations, and statistics of dynamic quantities like bond-current in both one and higher dimensions.

Threshold-Activated systems: The Manna and Oslo Models

Another important class of nonequilibrium systems consists of *threshold-activated models*, where a discrete amount of mass or particles is redistributed only when the local occupation exceeds a critical threshold. These models are central to the study of self-organized criticality (SOC) and absorbing-state phase transitions. The canonical example is the sandpile model, which was first introduced by Bak, Tang, and Wiesenfeld (BTW) as a paradigmatic model of SOC and the origin of "$1/f$" noise in nature [11]. In the BTW model, each active site topples deterministically by transferring $z_c = 4$ particles, one to each nearest neighbor in two dimensions.

Later, stochastic generalizations of particle transfer were proposed. The best-known example is the Manna model [12], where particles are redistributed randomly among neighboring sites during a toppling. This stochasticity gives rise to more robust power-law scaling of avalanche distributions. Importantly, in systems with periodic boundaries, the Manna model exhibits a well-defined absorbing-state phase transition: there exists a critical particle density ρ_c below which the system evolves into an absorbing state with no further activity, while for $\rho > \rho_c$ the system remains in an active steady state [36]. Near this transition, it is widely believed that the model develops long-range correlations as the correlation length diverges; however, this picture is not universally valid, particularly in higher dimensions where different scaling behavior may emerge [37–39].

The Manna Model. In the Manna model, each site i holds an integer number of particles $m_i \in \mathbb{Z}_{\geq 0}$. A site becomes *active* if $m_i \geq 2$, and it topples by transferring exactly two particles to neighboring sites chosen at random. Due to this stochastic redistribution, the only conserved quantity in the periodic system is the total density. Interestingly, additional conservation laws can emerge in special deterministic variants of the model. For example, in one dimension, if two particles are deterministically moved—one to the left neighbor and one to the right—then the system acquires an extra conserved quantity, leading to distinct dynamical behavior [40].

Generalizations of the Manna model to higher dimensions, sometimes called conserved Manna-class (CoMC) models, have also been explored, where mass transfer along axial directions provides a natural extension of the threshold-activation mechanism. From a hydrodynamic perspective, these models exhibit a fundamentally different transport structure than Mass Chipping Models. The diffusive current can be expressed in terms of the gradient of the local *activity field*, $\hat{a}(\mathbf{r}, t)$, as

$$\mathcal{J}_i^{(d)}(t) = a_i(t) - a_{i+1}(t). \tag{1.30}$$

Here, the gradient is taken of a non-conserved quantity (the activity), in contrast with MCMs where it is the mass itself. This lack of a purely conservative gradient structure makes the model far more challenging to treat analytically. Nevertheless, with suitable approximations, significant progress has been made in deriving coarse-grained hydrodynamic descriptions for density and current fluctuations [36, 41, 42].

The Oslo Model. The Oslo model, originally proposed to describe granular pile experiments, represents another archetype of threshold-activated dynamics. Unlike the Manna model, particle transfer in the Oslo model is deterministic: when a site topples, it transfers one grain to a nearest neighbor. The stochasticity instead arises from the local threshold, which is redrawn randomly after each toppling event. Concretely, a site i becomes active when its local height m_i exceeds its threshold $m_c \in \{2, 3\}$, after which m_c is reset randomly.

Despite its simplicity, the Oslo model captures several hallmark features of self-organized criticality: scale-invariant avalanche statistics, nontrivial spatiotemporal correlations, and critical fluctuations without fine-tuning of parameters. Most notably, its dynamics are density-conserving, which leads to the emergence of *hyperuniformity*—a remarkable state of matter in which large-scale density fluctuations are strongly suppressed. This is quantified by the static structure factor,

$$S(q) \sim q^{\alpha}, \tag{1.31}$$

where $\alpha > 0$ characterizes the degree of hyperuniformity. In the Oslo model, numerical studies have reported $\alpha \simeq 0.5$ at criticality [43], while away from criticality $\alpha \simeq 2.0$ [44]. Consequently, the Oslo model is hyperuniform across all densities, in agreement with broader theoretical considerations on hyperuniform systems [4, 45].

1.5 Hyperuniformity

The concept of hyperuniformity, also referred to as "superhomogeneity," was originally introduced in the context of static systems, where the suppression of large-scale

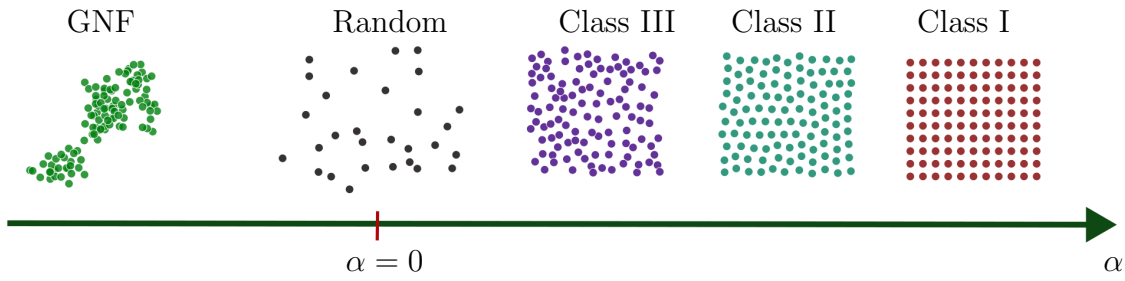

Figure 1.2: Schematic two-dimensional point patterns illustrating different fluctuation regimes: Class I (strong hyperuniformity), Class II (marginal hyperuniformity), Class III (weak hyperuniformity), Random (Poisson), and Anti-hyperuniform or giant number fluctuations(GNF).

density fluctuations gives rise to unusual structural properties intermediate between crystalline order and disordered phases [2, 4, 45]. Hyperuniform systems are characterized by anomalously reduced density fluctuations at long wavelengths. Unlike typical disordered systems (such as gases and liquids), which exhibit random fluctuations at all scales, hyperuniform systems display long-range order without periodic crystalline symmetry. Such exotic states of matter have been observed across diverse natural and biological systems, including vein patterns in leaves [5], the photoreceptor arrangement in the chicken retina [6], and cellular structures in biological tissues [46–48].

In general, fluctuations in static systems can be quantified through the structure factor $S(\mathbf{q})$. In the thermodynamic limit, at small wave numbers $|\mathbf{q}| \to 0$, the structure factor typically follows a power-law form, $S(\mathbf{q}) \sim q^{\alpha}$, where the exponent α characterizes the nature of fluctuations. For instance, $\alpha = 0$ corresponds to random (Poissonian) fluctuations, while $\alpha < 0$ indicates the presence of giant number fluctuations (GNF) [49] (see schematic of two dimensional points pattern in 1.2). Mathematically, hyperuniformity is defined by the condition

$$\lim_{\mathbf{q}\to 0} S(\mathbf{q}) = 0,$$

which signifies the vanishing of density fluctuations at the largest length scales. Equivalently, in real space, the number variance within a spherical observation window of radius R grows more slowly than the window volume, scaling as R^{d-1} (with spatial dimension d), in contrast to the R^d scaling expected for typical disordered systems. Based on the rate at which $S(\mathbf{q})$ vanishes as $|\mathbf{q}| \to 0$, hyperuniform systems are further classified into three types:

- **Class I**: $S(\mathbf{q}) \sim |\mathbf{q}|^{\alpha}$ with $\alpha > 1$. Found in crystals and quasicrystals; number variance grows as R^{d-1}.
- **Class II**: $S(\mathbf{q}) \sim |\mathbf{q}|$, corresponding to marginal suppression; $\mathrm{Var}[N(R)] \sim R^{d-1} \log R$.
- **Class III**: $S(\mathbf{q}) \sim |\mathbf{q}|^{\alpha}$ with $0 < \alpha < 1$; the suppression is weaker but still sub-Poissonian.

Dynamical Hyperuniformity: In the temporal scale, one can also define a *dynamical* version of hyperuniformity, which concerns the fluctuations of dynamical

observables in extended nonequilibrium systems. Dynamical hyperuniformity usually refers to the suppression of fluctuations of time-integrated or temporally coarse-grained quantities. These observables can be chosen depending on the physical system under study, such as the dynamical structure factor, the activity field, or time-integrated particle currents. A particularly illustrative case is that of the *time-integrated bond current*, defined as

$$\mathcal{Q}_i(T) = \int_0^T \mathcal{J}_i(t)\, dt, \tag{1.32}$$

where $\mathcal{J}_i(t)$ is the instantaneous current across a bond $(i, i+1)$ at time t, and T is the observation time. The variance of $\mathcal{Q}_i(T)$ at large time ($T > L^2$) typically grows as a power law in T:

$$\langle \mathcal{Q}(T)^2 \rangle \sim T^{\lambda}, \tag{1.33}$$

with this exponent λ, determine the nature of dynamic fluctuations in the system. In conventional diffusive systems, one expects $\lambda = 1$, corresponding to normal scaling of fluctuations with time (i.e. diffusive fluctuations obeying the central limit theorem). However, when the exponent satisfies

$$0 \leq \lambda < 1, \tag{1.34}$$

the fluctuations grow sublinearly with T, indicating a suppression of temporal fluctuations relative to ordinary diffusive behavior. This regime is referred to as *dynamical hyperuniformity* [50].

From a theoretical perspective, dynamical hyperuniformity can be understood as the temporal analogue of static hyperuniformity: while the latter describes the anomalous suppression of fluctuations in the static structure factor $S(q)$ as $q \to 0$, the former characterizes anomalously small fluctuations of dynamical observables in the long-time limit $T \to \infty$. This analogy provides a unifying language to describe fluctuation suppression both in spatial and temporal domains, and suggests deep links between nonequilibrium dynamics, conservation laws, and universality classes.

1.6 Macroscopic Fluctuation Theory (MFT)

Fluctuating Hydrodynamics: The macroscopic time evolution of fluctuations in interacting many-body systems is often described within the framework of fluctuating hydrodynamics [51, 52]. At large length and time scales, only the slow modes associated with conserved quantities survive, while non-conserved fields decay rapidly. For instance, if the particle number is conserved, the relevant hydrodynamic field is the density, denoted by $\rho(x,t)$. Conservation of total density imposes the continuity equation,

$$\frac{\partial \rho(x,t)}{\partial t} + \frac{\partial \mathcal{J}(x,t)}{\partial x} = 0, \tag{1.35}$$

where $\mathcal{J}(x,t)$ represents the local fluctuating current. In fluctuating hydrodynamics, for a large system of size L, the current is typically decomposed as

$$\mathcal{J}(x,t) = -D(\rho(x,t))\frac{\partial \rho(x,t)}{\partial x} + \xi(x,t), \tag{1.36}$$

where $D(\rho)$ is the density-dependent diffusion coefficient, and $\xi(x,t)$ is a stochastic noise term accounting for microscopic fluctuations. This noise is generally assumed to be Gaussian and delta-correlated (white noise):

$$\langle \xi(x,t) \rangle = 0, \quad \langle \xi(x,t)\, \xi(x',t') \rangle = \frac{2\chi(\rho(x,t))}{L}\, \delta(x-x')\, \delta(t-t'). \tag{1.37}$$

Here, $\chi(\rho)$ is the mobility (or noise strength), which together with $D(\rho)$ satisfies a fluctuation–dissipation relation in equilibrium systems, while in nonequilibrium contexts it plays a central role in governing large-scale fluctuations; here L is the size of the original microscopic system. Taking the ensemble average of Eq. (1.36), the fluctuating contribution vanishes, yielding the deterministic diffusive current

$$\langle \mathcal{J}(x,t) \rangle = -D(\rho(x,t))\, \partial_x \rho(x,t), \tag{1.38}$$

which corresponds to Fick's law of diffusion. This simple structure underlies the hydrodynamic description of a wide range of stochastic lattice gases and nonequilibrium systems. Apart from taking an ensemble average, one can also consider the *space-time averaged current*. This is defined as

$$q_\tau = \int_0^1 dx \int_0^\tau \mathcal{J}(x,\tau')\, d\tau', \tag{1.39}$$

which represents the total integrated current over both spatial and temporal domains. The fluctuations of this space-time averaged current can be directly obtained from the noise correlations in Eq. (1.37), yielding

$$\langle q_\tau^2 \rangle = \frac{2\chi(\rho)}{L}\, \tau. \tag{1.40}$$

This result shows that the variance of the integrated current grows linearly with the averaging time τ, with a prefactor determined by the noise strength $\chi(\rho)$ and system size L. Furthermore, this expression is directly related to the microscopic bond current fluctuations. Specifically, one finds

$$\langle \mathcal{Q}_i(T)^2 \rangle = L^2 \langle q_\tau^2 \rangle = \frac{2\chi(\rho)}{L}\, T, \tag{1.41}$$

which recovers the asymptotic scaling form of bond-current fluctuations discussed earlier with $i = xL$ and $T = \tau L^2$. A microscopic derivation of this result has been obtained explicitly for mass-chipping models in the large-system limit (see Eq. (2.60) in Chapter 2).

Macroscopic Fluctuation Theory (MFT): The central aim of the MFT is to provide a unified framework for describing fluctuations and large deviations in nonequilibrium systems with conserved quantities, such as mass or particle number. It generalizes the ideas of fluctuating hydrodynamics by systematically incorporating both the deterministic evolution of conserved fields and their stochastic deviations.

In particular, under the assumption of local equilibrium, the density field in a small interval $(x, x+\Delta x)$ can be represented by a smooth density profile $\rho(x,\tau)$,

together with an associated current profile $\mathcal{J}(x,\tau)$. The probability of observing such a path can be expressed as

$$\mathcal{P}[\rho(x,\tau)|\rho(x,\tau_0)] \sim \int \mathcal{D}\mathcal{J}\,\mathcal{D}\rho\,\exp\left(-L\int_0^1 dx\int_{\tau_0}^{\tau} d\tau'\frac{\big(\mathcal{J}+D(\rho)\,\partial_x\rho\big)^2}{4\chi(\rho)}\right), \tag{1.42}$$

given an initial profile $\rho(x,\tau_0)$. The above expression can also be written in terms of a large deviation principle as

$$\mathcal{P}[\rho(x,\tau)|\rho(x,\tau_0)] \sim e^{-L\mathcal{F}(\rho(x,\tau))},$$

where $\mathcal{F}$ is the large deviation functional, often interpreted as a nonequilibrium free energy functional that quantifies deviations from typical hydrodynamic behavior. Analogously, for time-integrated bond current, $\mathcal{Q}_i(T)/T = q/L$, the distribution follows

$$\mathcal{P}\left(\frac{\mathcal{Q}_i(T)}{T}=\frac{q}{L}\right) \sim e^{-\tau L I(q)}, \tag{1.43}$$

where $I(q)$ is the rate function, characterizing the large deviations of current fluctuations. The symmetry of the rate function is constrained by the *fluctuation theorem*,

$$I(q)-I(-q) = \lim_{\tau\to\infty}\frac{1}{\tau}\int_0^1 dx\int_0^{\tau} d\tau'\,\frac{\mathcal{J}\,\rho' D(\rho)}{\chi(\rho)}. \tag{1.44}$$

Thus, on a hydrodynamic scale, the MFT not only predicts the average hydrodynamic behavior but also determines the full distribution of dynamical fluctuation variables such as density and current through their large deviation functions. This framework has been successfully applied to a wide variety of many-body systems under different boundary conditions [52–55].

However, the short-time behavior cannot be predicted through the MFT formalism. Moreover, the direct application of MFT has not yet been rigorously established for hyperuniform systems. In this thesis, we have provided a microscopic dynamical approach, which not only derives the hydrodynamic behavior, but also captures the fluctuations, thus providing a suitable formulation a fluctuating hydrodynamic (the MFT-like) framework for such systems. In particular, for center-of-mass–conserving systems, the mobility $\chi(\rho)$ "vanishes" [44, 56], leading to the breakdown of the standard MFT formalism. This remains an open problem. In this thesis, while we are able to compute the second moment of current fluctuations for both hyperuniform and non-hyperuniform systems, obtaining the full current distribution remains a significant and unsolved challenge.

1.7 Outline of the thesis

Provided below is a brief chapter-wise outline of the remainder of the thesis.

Chapter 2: We study steady-state dynamical fluctuations of currents and mass in several variants of random average processes on a periodic lattice of L sites.

These processes generically violate detailed balance in the bulk and exhibit nontrivial spatial structure: their steady states are not governed by a Boltzmann–Gibbs measure and can display finite-range correlations. Using a fully microscopic approach, we exactly compute the second cumulants (variances) of time-integrated currents, $\langle \mathcal{Q}_i^2(T)\rangle_c$ across a single bond i and $\langle \mathcal{Q}_{sub}^2(l,T)\rangle_c$ across a subsystem of size l, as well as the two-point dynamic correlation function for subsystem mass. In particular, for large $L \gg 1$, we show that the variance $\langle \mathcal{Q}_i^2(T)\rangle_c$ of cumulative bond current grows linearly, $\sim T$, at short times $T \sim \mathcal{O}(1)$, subdiffusively as $\sim T^{1/2}$ in the intermediate window $1 \ll T \ll L^2$, and crosses back to linear diffusive growth $\sim T$ for long times $T \gg L^2$. The scaled subsystem current cumulant $\lim l \to \infty, T \to \infty \langle \mathcal{Q}_{sub}^2(l,T)\rangle_c/2lT$ converges to the density-dependent mobility $\chi(\rho)$ when the subsystem-size limit is taken before the large-time limit, but vanishes if the limits are reversed. Strikingly, the bond-current variance admits a universal scaling form: the rescaled quantity $D\langle \mathcal{Q}_i^2(T)\rangle_c/2\chi L \equiv \mathcal{W}(y)$ depends only on the scaled time $y = DT/L^2$, with D the bulk diffusion constant. This single scaling function $\mathcal{W}(y)$ seamlessly connects the subdiffusive and diffusive growth regimes. Power spectra of current and mass fluctuations are likewise determined exactly and expressed in terms of associated scaling functions. Finally, we derive microscopic analogues of equilibrium Green–Kubo and Einstein relations, establishing exact connections between steady-state current fluctuations, the operational mobility (defined via response to an external field), and subsystem mass fluctuations.

Chapter 3: We investigate steady-state static and dynamic properties of a broad class of mass transport processes defined on a periodic hypercubic lattice of volume L^d, where both the total mass and the *center of mass* (CoM) are conserved, while detailed balance is violated in the bulk. Our focus is on models in one and two spatial dimensions ($d = 1, 2$). Using an exact microscopic approach, we determine the decay (or growth) exponents of several key dynamic and static correlation functions. Although the additional constraint imposed by CoM conservation (CoMC) restricts the dynamics, we demonstrate that density relaxation remains diffusive. However, the fluctuation properties show striking deviations from systems with only a single (mass) conservation law: both static and dynamic fluctuations are significantly suppressed, leading in some cases to extreme ("class-I") hyperuniformity. In the thermodynamic limit, the long-time growth of the variance $\langle \mathcal{Q}^2(T)\rangle_c$ of the time-integrated bond current $\mathcal{Q}(T)$ across a bond is found to follow $\langle \mathcal{Q}^2(T)\rangle_c \simeq A_1 T + A_2 + A_3 T^{-d/2}$. We exactly determine the exponents that govern the small-frequency behavior of the current power spectrum, $S_J(f) \simeq A_1 + \text{Const.} f^{\psi_J}$, with $\psi_J = 3/2$ in $d = 1$ and $\psi_J = 2$ in $d = 2$. Correspondingly, the unequal-time bond current correlations decay as $t^{-5/2}$ in $d = 1$ and t^{-3} in $d = 2$. Interestingly, for certain parameter regimes and dimensions, the prefactor A_1 vanishes, resulting in the eventual *saturation* of current variance − an indication of class-I *dynamic hyperuniformity*. Finally, we compute the static structure factor $S(q)$, which exhibits a quadratic dependence on the wave number, $S(q) \sim q^2$ in the small-q limit. This confirms the emergence of class-I *spatial hyperuniformity* in CoM-conserving transport processes.

Chapter 4: We demonstrate that lattice models in $d > 1$ dimensions with mass conservation and multidirectional hopping dynamics display robust power-law correlations for generic parameter choices, persisting even far from any phase transition (if present). The central mechanism behind this algebraic decay is the *multidirectional*

hopping process, where multiple chunks of mass or particles can simultaneously leave a site in different directions, thereby breaking detailed balance. The models studied are continuous-time Markov processes that remain diffusive, spatially homogeneous, and *lattice-rotation symmetric*, with no net mass current. By combining hydrodynamic arguments with exact microscopic analysis, we show that in $d > 1$ the steady-state density–density and "activity"–density correlations universally decay as $\sim 1/r^{d+2}$ at large separations $r = |\mathbf{r}|$. Moreover, we compute the precise amplitude of this decay for several models, expressed in terms of the density-dependent diffusion coefficient and mobility tensor. Our framework, in particular, elucidates how centre-of-mass–conserving dynamics − relevant for disordered *hyperuniform* states of matter − naturally give rise to such long-ranged correlations.

Chapter 5: In this chapter, we conclude the thesis with a summary of the models studied, their fluctuation properties, and the implications in the broader context of nonequilibrium statistical mechanics of driven systems in general.

2

Dynamical properties of mass chipping models

2.1 Introduction

Characterizing static and dynamic properties of mass (or energy) transport processes is a fundamental problem in nonequilibrium statistical physics; it helps develop a simple theoretical understanding of a variety of natural phenomena involving rather complex many-body interactions among constituents that facilitate transport of mass in a far-from-equilibrium setting. Such processes are abundant in nature and manifest themselves in cloud formation [23], heat conduction [15], propagation of forces in granular media [24, 57], river network formation [25], self-assembly of lipid droplets on cell surfaces [26], traffic flow [27], and wealth distribution in a population [21, 58, 59], among others. Minimal lattice models, which were widely studied in the literature to understand transport in interacting-particle systems, are those of simple exclusion processes (SEPs) and zero-range processes (ZRPs). Another class of models, which has drawn significant attention in the past, is that of the conserved-mass transport processes, also called *mass chipping models* (MCMs), where mass is probabilistically transferred from one site to another (usually either of the nearest neighbor ones) [13–15, 20, 24, 34, 57, 60, 61]; indeed some of these models are related to *random average processes* (RAPs) [16], which have also generated a lot of interest. Interestingly, the steady-state measures of MCMs on a closed geometry, unlike that for SEPs and ZRPs, violate detailed balance, are not usually described by the equilibrium Boltzmann-Gibbs distribution, and, in most cases, are *a-priori* not known. Indeed, these processes are inherently driven out of equilibrium

This chapter is based on the paper, **Dynamic fluctuations of current and mass in nonequilibrium mass transport processes**, Animesh Hazra, Anirban Mukherjee and Punyabrata Pradhan, J. Stat. Mech.: Theory Exp. 2024(8), 083205.

and generate nontrivial spatial structures, where there can be nonzero (finite) spatial correlations present in the systems, thus making exact dynamic characterization of the steady state a challenging problem.

Recently, a theoretical framework for driven diffusive systems, known as macroscopic fluctuation theory (MFT) [52, 54], has been developed for studying fluctuations of coarse-grained (hydrodynamic) variables such as density $\rho(x,\tau)$ and current $j(x,\tau)$, where x and τ are suitably rescaled position and time, respectively. The MFT is a generalization of the Onsager-Machlup theory of *near-equilibrium systems* to the theory of far-from-equilibrium ones [62, 63]. Its main ingredients are the density-dependent transport coefficients, namely the bulk-diffusion coefficient $D(\rho)$ and the mobility $\chi(\rho)$ (equivalently, the conductivity), which govern density relaxation and current fluctuation on macroscopic scales [55, 64–66]. Despite a simple prescription of the MFT, calculating the transport coefficients as a function of density and other parameters is difficult, especially for many-body systems, where spatial correlations are nonzero. The difficulty stems primarily from the fact that the averages of various observables, which are necessary to calculate the transport coefficients, must be computed in the nonequilibrium steady state, which is not described by the Boltzmann-Gibbs distribution and, moreover, is not explicitly known in most cases. Perhaps not surprisingly, apart from SEPs [33, 67–72] and ZRPs [10, 73], which have a product-measure steady state [74], there are very few examples of exact microscopic characterization of dynamic fluctuations in interacting-particle systems.

Of course, MCMs, which constitute a paradigm for out-of-equilibrium many-body systems, are an exception. Indeed, because they could be analytically tractable, MCMs provide a level playing field for exact microscopic calculations of various time-dependent quantities, such as static density correlations and dynamic tagged-particle correlations, which have been extensively explored in the past [14, 34, 75]. However, except for the Kipnis-Marchioro-Presutti (KMP)-like models [76, 77] and the SEP [78], which satisfy detailed balance, rigorous microscopic characterization of the precise quantitative connection between fluctuation and transport have not been done for nonequilibrium mass-transport processes having nontrivial spatial structures in the bulk. Indeed, it would be quite interesting to relate the microscopic dynamic properties of mass and current to the macroscopic transport coefficients and thus to derive the MFT [54] for such models from "first-principles" calculations.

In this chapter, by using a microscopic approach, we exactly calculate steady-state dynamic correlations for subsystem current and mass in a broad class of one-dimensional mass-chipping models (MCMs) on a ring of L sites. In these models, a site i is associated with a continuous variable, called mass, $m_i \geq 0$, where the total mass in the systems remains conserved. With some specified rates, a certain fraction of mass at a site gets fragmented or chipped off from the parent mass, diffuses *symmetrically*, and coalesces with mass at one of the nearest neighbor sites. The MCMs have been intensively studied in various contexts in the past decades [13, 14, 20, 34, 75, 79], and some of their variants can be mapped to a class of transport processes, called the *random averaging processes* (RAPs) [16], which can be related to the so called Hammersley process [19]. Note that, for symmetric transfer (i.e., diffusion) of masses, although there is no net mass flow in the steady state on a ring

geometry, the probability currents in the configuration space can still be nonzero and the Kolmogorov criteria for equilibrium can be shown to get violated [80]. As mentioned before, despite the steady-state measures for generic parameter values are not known [13, 14, 20, 75], the MCMs are amenable to exact theoretical studies. For example, the spatial correlation function of mass has been exactly calculated before in some of the variants of MCMs [14, 20, 60, 81, 82]. Furthermore, the mean-squared fluctuation of the position of a single tagged particle as well as the dynamic correlations of two tagged particles in related models - the RAPs - have been calculated exactly using microscopic and hydrodynamic calculations [82–84].

The primary focus of our study is the cumulative time-integrated currents - $\mathcal{Q}_i(T)$ and $\mathcal{Q}_{sub}(l,T)$ in a time interval $[0,T]$ across a bond $(i,i+1)$ and a subsystem of size l, respectively, in the steady state. We exactly calculate the second cumulant, or the variance, of bond current $\langle \mathcal{Q}_i^2(T)\rangle_c = \langle \mathcal{Q}_i^2(T)\rangle - \langle \mathcal{Q}_i(T)\rangle^2$ as a function of time T and show that the second cumulant exhibits three distinct temporal behaviors (note that, on a periodic domain, $\langle \mathcal{Q}_i(T)\rangle = 0$ in the steady state and therefore $\langle \mathcal{Q}_i^2(T)\rangle_c = \langle \mathcal{Q}_i^2(T)\rangle$). Initially, for small times $T \ll 1/D$, the temporal growth of the current cumulant is linear in time T, where D is the bulk-diffusion coefficient (a constant). For moderately large times, i.e., for $1/D \ll T \ll L^2/D$ with L being the system size, the temporal fluctuation grows subdiffusively, having a $T^{1/2}$ growth. Finally, at very large times $T \gg L^2/D$, the growth again becomes linear in time. We find that, even in the presence of nonzero spatial correlations, the qualitative behavior of the current fluctuations, except for the prefactors, have characteristics, which are similar to that in the SEP. Remarkably, independent of the details of the mass-transfer rules of the models, the suitably scaled bond-current fluctuation $\langle \mathcal{Q}_i^2(T)\rangle D/2\chi L$, with $\chi(\rho)$ being the density-dependent (collective) particle mobility, as a function of the scaled time $y = DT/L^2$, which is finite while $T, L \gg 1$, can be expressed in terms of a universal scaling function $\mathcal{W}(y)$. The scaling function is exactly calculated and is shown to have the following asymptotic behavior,

$$\mathcal{W}(y) = \begin{cases} (y/\pi)^{1/2} & \text{for } y \ll 1, \\ y & \text{for } y \gg 1. \end{cases} \tag{2.1}$$

This demonstrates that the intermediate-time $T^{1/2}$ and long-time T growths of bond-current fluctuation, quite interestingly, are connected through a *single* scaling function $\mathcal{W}(y)$. Furthermore, we show that the two-point correlation for the instantaneous current as a function of time t has a delta-correlated part at $t = 0$ and a long-ranged (power-law) negative part, which decays via a $t^{-3/2}$ power law. The corresponding power spectrum of current $S_{\mathcal{J}}(f)$ is calculated analytically and it exhibits a low-frequency power-law behavior $f^{1/2}$ in the frequency regime $D/L^2 \ll f \ll 1$. Similarly, the power spectrum $S_{M_l}(f)$ for subsystem mass is calculated exactly and is shown to have a low-frequency power-law divergence $f^{-3/2}$. We have also calculated the scaling functions when the rescaled power spectra for current and mass are expressed in terms of the scaled frequency fL^2/D.

Next, by using "first-principles" microscopic dynamical calculations, we rigorously establish a nonequilibrium fluctuation relation between scaled subsystem mass and space-time integrated current fluctuations in the steady state. We calculate the scaled fluctuation of the cumulative current $\mathcal{Q}_{sub}(l,T)$, summed over a subsystem

of size l and integrated up to time T. We show that, in the steady state, the scaled second cumulant or the variance $\langle \mathcal{Q}^2_{sub}(l,T)\rangle_c = \langle \mathcal{Q}^2_{sub}(l,T)\rangle - \langle \mathcal{Q}_{sub}(l,T)\rangle^2$ of subsystem current converges to the density-dependent particle mobility $\chi(\rho)$, i.e.,

$$\sigma^2_{\mathcal{Q}} \equiv \lim_{l\to\infty, T\to\infty} \frac{\langle \mathcal{Q}^2_{sub}(l,T)\rangle}{lT} = 2\chi(\rho), \tag{2.2}$$

where we have used $\langle \mathcal{Q}_{sub}(l,T)\rangle = 0$ in the steady state and taken the infinite subsystem-size limit $l \to \infty$ first, followed by the infinite time limit $T \to \infty$; notably, in the opposite order of limits, the left-hand side of the above equation simply vanishes. By explicitly calculating the scaled subsystem mass fluctuation $\sigma^2_M = \lim_{l\to\infty}\langle \Delta M^2_l\rangle/l$, where $\langle \Delta M^2_l\rangle = \langle M^2_l\rangle - \langle M_l\rangle^2$ is the fluctuation of mass in a subsystem of size l, we then derive a nonequilibrium fluctuation relation between mass and current fluctuations,

$$\sigma^2_M = \frac{\sigma^2_{\mathcal{Q}}}{2D}, \tag{2.3}$$

which is a modified version of the celebrated Einstein relation for equilibrium systems. Furthermore, provided there is a small biasing force $\tilde{F}$ (suitably scaled), which generates a drift current $J_{drift} = \chi_{op}(\rho)\tilde{F}$ along the direction of the force, we derive a nonequilibrium version of the Green-Kubo-like fluctuation-response relation,

$$\chi_{op}(\rho) \equiv \left[\frac{\partial J_{drift}}{\partial \tilde{F}}\right]_{\tilde{F}=0} = \frac{\sigma^2_{\mathcal{Q}}}{2}; \tag{2.4}$$

the above relation directly connects the "operational mobility" or, equivalently, the response to an applied force, to the current fluctuations in the nonequilibrium steady state.

2.2 Models

In this section, we consider a class of conserved-mass transport processes, where (continuous) masses get chipped off and diffuse to neighboring sites with constant rates. These models are an example of interacting many-body systems, which have nontrivial spatial structure in the bulk and belong to the generalized versions of the well-known random average processes (RAPs), which have been intensively studied throughout the past decades. The original version of these model systems was first introduced by Ferrari and Fontes in Ref. [16] and its variants were then studied in Ref. [14] by Rajesh and Majumdar and in Ref. [20] by Krug. Later on, in Refs. [13, 85], these models have been further generalized to several other variants. In this chapter, we collectively call these transport processes as mass chipping models (MCMs).

An important defining characteristic of MCMs is that the mass-chipping rate depends on neither the destination nor the departure sites. As we discuss later, this has some simplifying consequences for the hierarchy of correlation functions (two-point and higher-order ones), which closes because the local diffusive current is linear in local mass variables [see the "linearity property" in eq. (2.11)]. Moreover, MCMs have an interesting feature that the variance of subsystem mass is proportional

to the square of the mass density, leading to a remarkable (static) property that the subsystem mass distributions, irrespective of dynamical details, have a form of gamma distribution [13, 14, 20, 85, 86]. However, dynamic fluctuation properties of mass and current in MCMs remain largely unexplored and are investigated here.

To this end, we consider three widely-studied variants of mass chipping models - MCM I, MCM II, and MCM III, which differ in the details of their microscopic dynamics, but the total mass in the system for all three variants remains conserved. We define the models on a one-dimensional periodic lattice with sites labeled by $i = 0, 1, \cdots, L-1$. A continuous mass variable $m_i \geq 0$ is associated with a site i, with the total mass $M = \sum_{i=0}^{L} m_i$ being conserved. In Fig. 2.1, we present schematic diagrams that represent the underlying microscopic dynamics of these three models. The continuous-time dynamical update rules are provided below.

MCM I: A site i is updated with unit rate, where the following events of fragmentation and chipping take place at the site. During the fragmentation process, a (constant) ζ fraction of mass m_i is retained at the site, while $\tilde{\zeta} = 1 - \zeta$ a fraction of mass m_i is chipped off. Subsequently, a random fraction ξ_i of the chipped-off mass, $\tilde{\zeta} m_i \xi_i$, is then transferred to the right nearest neighbor, while the remaining fraction of the chipped-off mass, $\tilde{\zeta} m_i (1 - \xi_i)$, is transferred to the left nearest neighbor. Here $\xi_i \in [0, 1]$ is independent and identically distributed (i.i.d.) random variables, having a uniform distribution. For convenience, we also define $\tilde{\xi}_i = 1 - \xi_i$, which is used throughout. This class of models have been considered, e.g., in Refs. [13, 34, 86].

MCM II: A site i is updated with unit rate, where ζ fraction of mass at the site is retained, while $\tilde{\zeta} = 1 - \zeta$ fraction of mass is chipped off. Then a random fraction ξ_i of the chipped-off mass, $\tilde{\zeta} m_i \xi_i$, is transferred either to the left or to the right neighbor, with an equal probability $1/2$. The remaining fraction of the chipped-off mass, $\tilde{\zeta} m_i (1 - \xi_i)$, is subsequently deposited back to site i. This class of models has been considered, e.g., in Refs. [14, 20, 85].

MCM III: A bond $(i, i+1)$ is updated with unit rate, where remixing of masses at the bond takes place as follows. A fraction $\tilde{\zeta} = 1 - \zeta$ of mass is chipped off from each of the sites at the chosen bond, i.e., $\tilde{\zeta} m_i$ and $\tilde{\zeta} m_{i+1}$ from the sites i and $i+1$, respectively, are chipped off. Subsequently, a random fraction, ξ_i, of the combined chipped-off masses is transferred to site $i+1$, while the $\tilde{\xi}_i = 1 - \xi_i$ fraction is transferred to site i. This class of model has been considered, e.g., in Refs. [15, 21, 58, 59]. Note that MCM III with $\zeta = 0$ is the celebrated Kipnis-Marchioro-Presutti (KMP) model [15].

These models, except some specific parameter values, do not satisfy detailed balance [80], and the steady-state microscopic weights are not known. Indeed, it is possible to generalize the above models to several other variants, such as finite-range mass-chipping models, where mass can be transferred to a certain, say $2K$, number of neighboring sites. However, as long as the mass-chipping rate is constant, all these variants will have similar large-scale dynamical properties, and, for simplicity, we confine ourselves to the MCMs with $K = 1$.

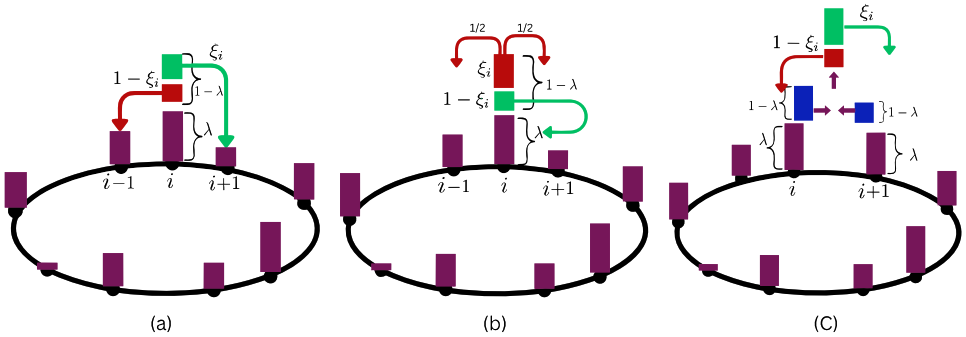

Figure 2.1: *Schematic representation of the mass-chipping models MCM I, MCM II, and MCM III:* (a) In MCM I, a site i on a periodic lattice (shaped as a dark oval) having mass m_i (dark violet), retains a fraction ζ of its mass (dark violet), while a random fraction ξ_i of the chipped-off mass (green) migrates to the right neighbor, and the remaining fraction of the chipped mass(red) moves to the left side. (b) In MCM II, a random fraction ξ_i of chipped-off mass(red) moves either left or right nearest neighbor with equal probability, while the rest of the chipped mass(green) is deposited back to the same site i. (c) In MCM III, a fraction equivalent to $1-\zeta$ of the mass (blue) is chipped off from sites i and $i+1$. This extracted mass is then recombined and subsequently redistributed in a way such that site i receives a random fraction of $1-\xi_i$ (red), while site $i+1$ acquires a fraction of ξ_i (green).

2.3 Theory: MCM I

In this section, we study in detail the first variant of mass chipping models (MCM I) on a periodic one-dimensional lattice of size L; for the other models (MCMs II and III), we briefly discuss the results, which can be derived following the techniques developed in this section. We define local mass density as $\rho_i(t) = \langle m_i(t) \rangle$ at site i and time t, while the global density is defined as $\bar{\rho} = M/L$. Notably, unlike in MCMs II and III, a site in MCM I is stochastically updated in a way that simultaneously impacts its two immediate neighbors; this particular update rule results in nonzero spatial correlations in the system. We now explicitly write down the stochastic update rules for mass $m_i(t)$ at site i and time t during an infinitesimal time interval $(t, t+dt)$,

$$m_i(t+dt) = \begin{cases} \textbf{event} & \textbf{prob.} \\ m_i(t) - \tilde{\zeta} m_i(t) & dt \\ m_i(t) + \tilde{\zeta}\xi_{i-1} m_{i-1}(t) & dt \\ m_i(t) + \tilde{\zeta}\tilde{\xi}_{i+1} m_{i+1}(t) & dt \\ m_i(t) & (1-3dt), \end{cases} \tag{2.5}$$

where $\xi_j \in (0,1)$ is a random variable, which, for simplicity, is taken to be uniformly distributed; generalization of the results to other distributions is straightforward. Using the above dynamical update rules, the time-evolution of local mass can be written as

$$\frac{d}{dt} \langle m_i(t) \rangle = D(\zeta) \left(\langle m_{i-1}(t) \rangle - 2 \langle m_i(t) \rangle + \langle m_{i+1}(t) \rangle \right), \tag{2.6}$$

where $D(\zeta) = \tilde{\zeta}/2$ is the bulk-diffusion coefficient for MCM I. Note that the bulk-diffusion coefficient D is independent of density, leading to some important simplifications in the hierarchy for mass and current correlation functions, which, as we show later, actually close.

2.3.1 Definitions and notations

At this point, we introduce time-integrated bond current $\mathcal{Q}_i(t)$, which is the cumulative current across the bond $(i, i+1)$ in a time interval $(0, t)$. The current across the i^{th} bond during an infinitesimal time interval $[t, t+dt]$ is $\mathcal{J}_i(t)dt$, where instantaneous bond current is defined as

$$\mathcal{J}_i(t) \equiv \frac{d\mathcal{Q}_i(t)}{dt}, \tag{2.7}$$

and therefore we simply have

$$\mathcal{Q}_i(t) = \int_0^t dt' \mathcal{J}_i(t'). \tag{2.8}$$

We must mention here that, throughout the chapter, we consider statistics of current (and mass) in the steady state only. That is, we start at an initial time $t = -\infty$, wait for the system to settle into its steady state, and then we start measuring current and mass, say, at time $t = 0$.

We can express eq.(2.6), the time-evolution equation for local density $\rho_i(t) = \langle m_i(t) \rangle$, in terms of a (discrete) continuity equation,

$$\frac{d}{dt}\rho_i(t) = \langle \mathcal{J}_i(t) - \mathcal{J}_{i+1}(t) \rangle. \tag{2.9}$$

It is useful to decompose the instantaneous bond current as the sum of a diffusive component $\mathcal{J}_i^{(d)}(t)$ and a fluctuating component $\mathcal{J}_i^{(fl)}$,

$$\mathcal{J}_i(t) = \mathcal{J}_i^{(d)}(t) + \mathcal{J}_i^{(fl)}(t), \tag{2.10}$$

where we identify the diffusive current to be

$$\mathcal{J}_i^{(d)}(t) \equiv D(\zeta)\big[m_i(t) - m_{i+1}(t)\big]. \tag{2.11}$$

Here, it is important to note that the bulk-diffusion coefficient $D(\zeta)$ depends only on the chipping parameter ζ, *not* on density ρ. Not only does the model possess the so-called "gradient-property" [54], but also the local diffusive current, which is proportional to the (discrete) gradient of mass, is actually a *linear* function of local *mass* variables. This "linearity property" applies even to other variants of MCMs, such as the finite-range versions discussed in the model section. Indeed, as shown later in the calculation scheme, the aforementioned linearity property is crucial for ensuring a linear structure for mass and current correlations, whose hierarchy would then close, making the problem of computing current fluctuation in MCMs exactly solvable. Furthermore, we note that the average fluctuating current $\langle \mathcal{J}_i^{(fl)} \rangle = 0$ is

zero, implying $\langle \mathcal{J}_i(t) \rangle = \langle \mathcal{J}_i^{(d)}(t) \rangle$. Indeed, one could interpret $\mathcal{J}_i^{(fl)}(t)$ as a fast-varying "noise" current around the slow-varying diffusive ("hydrodynamic") current $\mathcal{J}_i^{(d)}(t)$. As we show later, the statistics of fluctuating current $\mathcal{J}_i^{(fl)}(t)$ is, in fact, delta-correlated in time and short-ranged in space, whereas the diffusive current $\mathcal{J}_i^{(d)}(t)$ is long-ranged in time (a power law) and short-ranged in space.

For convenience, we introduce the following notation for correlation function $C_r^{AB}(t,t')$ involving any two local observable $A_i(t)$ and $B_j(t')$, with $t \geq t'$,

$$\begin{aligned} C_{r=|j-i|}^{AB}(t,t') &= \langle A_i(t) B_j(t') \rangle - \langle A_i(t) \rangle \langle B_j(t') \rangle \\ &\equiv \langle A_i(t) B_j(t') \rangle_c, \end{aligned} \tag{2.12}$$

where $r = |j-i|$ is the relative distance. We denote the spatial Fourier transform of the correlation function $C_r^{AB}(t,t')$ as given below

$$\tilde{C}_q^{AB}(t,t') = \sum_{r=0}^{L-1} C_r^{AB}(t,t') e^{iqr}, \tag{2.13}$$

where $q = 2\pi s/L$ and $s = 0, 1, \ldots, L-1$; the inverse Fourier transform is given by

$$C_r^{AB}(t,t') = \frac{1}{L} \sum_q \tilde{C}_q^{AB}(t,t') e^{-iqr}. \tag{2.14}$$

2.3.2 Calculation scheme

In this section, we describe our calculation scheme for MCM I in detail. The stochastic dynamical rules for time-integrated current $\mathcal{Q}_i(t)$ in an infinitesimal time interval $(t, t+dt)$ can be written as

$$\mathcal{Q}_i(t+dt) = \begin{cases} \textbf{event} & \textbf{prob.} \\ \mathcal{Q}_i(t) + \tilde{\zeta}\xi_i m_i(t) & dt, \\ \mathcal{Q}_i(t) - \tilde{\zeta}\xi_{i+1} m_{i+1}(t) & dt, \\ \mathcal{Q}_i(t) & (1-2dt). \end{cases} \tag{2.15}$$

The above update rules allow us to derive the time-evolution equation for the first moment of the time-integrated bond-current $\mathcal{Q}_i(t)$ as follows:

$$\frac{d\langle \mathcal{Q}_i(t) \rangle}{dt} = D\langle m_i(t) - m_{i+1}(t) \rangle = \langle \mathcal{J}_i^{(d)}(t) \rangle. \tag{2.16}$$

Using the update rule as in eq. (2.15), the infinitesimal time-evolution equation for the following product of the time-integrated currents at two different times t and t' $(t > t')$ can be written as

$$\mathcal{Q}_i(t+dt)\mathcal{Q}_{i+r}(t') = \begin{cases} \textbf{event} & \textbf{prob.} \\ [\mathcal{Q}_i(t) + \tilde{\zeta}\xi_i m_i(t)]\mathcal{Q}_{i+r}(t') & dt, \\ [\mathcal{Q}_i(t) - \tilde{\zeta}\xi_{i+1} m_{i+1}(t)]\mathcal{Q}_{i+r}(t') & dt, \\ \mathcal{Q}_i(t)\mathcal{Q}_{i+r}(t') & (1-2dt). \end{cases} \tag{2.17}$$

Now, by utilizing Eq.(2.16), we immediately arrive at the time-evolution equation for the unequal-time current-current correlation function,

$$\frac{d}{dt}C_r^{\mathcal{Q}\mathcal{Q}}(t,t') = C_r^{\mathcal{J}^{(d)}\mathcal{Q}}(t,t'). \tag{2.18}$$

Interestingly, while calculating the time derivative of current (or related observables), Eq. (2.18) can be simply obtained by using a convenient thumb rule, where one takes the time derivative inside angular brackets as

$$\frac{d}{dt}\left\langle \mathcal{Q}_i(t)\mathcal{Q}_{i+r}(t')\right\rangle_c = \left\langle \frac{d\mathcal{Q}_i(t)}{dt}\mathcal{Q}_{i+r}(t')\right\rangle - \left\langle \frac{d\mathcal{Q}_i(t)}{dt}\right\rangle \left\langle \mathcal{Q}_{i+r}(t')\right\rangle. \tag{2.19}$$

Then, by replacing the instantaneous current by $d\mathcal{Q}_i(t)/dt \equiv D(m_i - m_{i+1}) + \mathcal{J}_i^{(fl)}$ and subsequently dropping the noise correlation as $\langle \mathcal{J}_i^{(fl)}(t)\mathcal{Q}_{i+r}(t')\rangle = 0$ for $t > t'$, we get Eq. (2.18).

By using Eq. (2.11) into rhs of Eq. (2.18), we express the time evolution of unequal-space-time current-current correlation function in terms of the unequal-space-time mass-current correlation function,

$$\frac{d}{dt}C_r^{\mathcal{Q}\mathcal{Q}}(t,t') = D\big(C_r^{m\mathcal{Q}}(t,t') - C_{r-1}^{m\mathcal{Q}}(t,t')\big). \tag{2.20}$$

From the equation presented above, it is evident that the calculation of the unequal-time mass-current correlation, denoted as $C_r^{m\mathcal{Q}}(t,t')$, is now necessary to calculate the unequal-time current-current correlation $C_r^{\mathcal{Q}\mathcal{Q}}(t,t')$. The time evolution of the correlation function $C_r^{m\mathcal{Q}}(t,t')$ can be obtained by using infinitesimal-time update rules for the following mass-current product at a later time $t + dt$ as

$$m_i(t+dt)Q_{i+r}(t') = \begin{cases} \textbf{event} & \textbf{prob.} \\ [m_i(t) - \tilde{\zeta}m_i(t)]Q_{i+r}(t') & dt \\ [m_i(t) + \tilde{\zeta}\xi_{i-1}m_{i-1}(t)]Q_{i+r}(t') & dt \\ [m_i(t) + \tilde{\zeta}\tilde{\xi}_{i+1}m_{i+1}(t)]Q_{i+r}(t') & dt \\ m_i(t)Q_{i+r}(t') & (1-3dt). \end{cases} \tag{2.21}$$

Using the above update rule, the time evaluation of unequal-time mass-current can be expressed in the following form,

$$\frac{d}{dt}C_r^{m\mathcal{Q}}(t,t') = D\langle (m_{i+1}(t) - 2m_i(t) + m_{i-1}(t))\mathcal{Q}_{i+r}(t')\rangle_c = D\sum_k \Delta_{r,k}C_k^{m\mathcal{Q}}(t,t'), \tag{2.22}$$

where $\Delta_{r,k} = \delta_{r-1,k} - 2\delta_{r,k} + \delta_{r+1,k}$ is the discrete Laplacian. Equations (2.20) and (2.22) can be expressed in terms of the Fourier modes as defined in Eq. (2.13),

$$\frac{d}{dt}\tilde{C}_q^{\mathcal{Q}\mathcal{Q}}(t,t') = D\tilde{C}_q^{m\mathcal{Q}}(t,t')\left(1 - e^{iq}\right), \tag{2.23}$$

and

$$\frac{d}{dt}\tilde{C}_q^{m\mathcal{Q}}(t,t') = -D\omega_q\tilde{C}_q^{m\mathcal{Q}}(t,t'), \tag{2.24}$$

where the eigenvalue of the discrete Laplacian is written as

$$\omega_q = 2\left(1 - \cos q\right). \tag{2.25}$$

Note that $\tilde{C}_q^{\mathcal{QQ}}(t,t')$ and $\tilde{C}_q^{m\mathcal{Q}}(t,t')$ are the Fourier transforms of the quantities $C_r^{\mathcal{QQ}}(t,t')$ and $C_r^{m\mathcal{Q}}(t,t')$, respectively. Now, Eq.(2.23) and Eq.(2.24) can be integrated to have

$$\tilde{C}_q^{\mathcal{QQ}}(t,t') = D\int_{t'}^{t} dt''\tilde{C}_q^{m\mathcal{Q}}(t'',t')\left(1-e^{iq}\right) + \tilde{C}_q^{\mathcal{QQ}}(t',t'), \tag{2.26}$$

and

$$\tilde{C}_q^{m\mathcal{Q}}(t,t') = e^{-D\omega_q(t-t')}\tilde{C}_q^{m\mathcal{Q}}(t',t'), \tag{2.27}$$

respectively. The Eqs. (2.26) and (2.27) suggest that the equal-time correlation of current-current $C_r^{\mathcal{QQ}}(t',t')$ and mass-current $C_r^{m\mathcal{Q}}(t',t')$ are required to obtain the respective unequal-time correlation function.

The time-evolution equation for the equal-time current-current spatial correlation $C_r^{\mathcal{QQ}}(t,t)$ can be written from the infinitesimal update rules for the product of the following random variables,

$$\mathcal{Q}_i(t+dt)\mathcal{Q}_{i+r}(t+dt) = \begin{cases} \textbf{event} & \textbf{prob.} \\ \mathcal{Q}_i\mathcal{Q}_{i+r} + \tilde{\zeta}\left(\xi_i m_i - \tilde{\xi}_{i+1}m_{i+1}\right)\mathcal{Q}_{i+r} & \\ +\tilde{\zeta}\left(\xi_{i+r}m_{i+r} - \tilde{\xi}_{i+r+1}m_{i+r+1}\right)\mathcal{Q}_i & dt, \\ \mathcal{Q}_i\mathcal{Q}_{i+r} + \tilde{\zeta}^2(\xi_i^2 m_i^2 + \tilde{\xi}_{i+1}^2 m_{i+1}^2) & \delta_{r,0}dt, \\ \mathcal{Q}_i\mathcal{Q}_{i+r} - \tilde{\zeta}^2\xi_i\tilde{\xi}_i m_i^2 & \delta_{r,-1}dt, \\ \mathcal{Q}_i\mathcal{Q}_{i+r} - \tilde{\zeta}^2\xi_{i+1}\tilde{\xi}_{i+1}m_{i+1}^2 & \delta_{r,1}dt, \\ \mathcal{Q}_i\mathcal{Q}_{i+r} & 1-\sum dt, \end{cases} \tag{2.28}$$

where $\sum = 1 + \delta_{r,0} + \delta_{r,1} + \delta_{r,-1}$ represents the total exit rate. From the above update rules, we can deduce the following time-evolution equation,

$$\frac{d}{dt}\left\langle \mathcal{Q}_i(t)\mathcal{Q}_{i+r}(t)\right\rangle_c = D\left\langle (m_i - m_{i+1})\mathcal{Q}_{i+r}\right\rangle_c + D\left\langle \mathcal{Q}_i(m_{i+r} - m_{i+r+1})\right\rangle_c + \Gamma_r, \tag{2.29}$$

where Γ_r can be written in terms of the steady-state single-site mass fluctuation (which is a function of $\bar{\rho}$) as follows:

$$\Gamma_r(\bar{\rho}) = \frac{\tilde{\zeta}^2}{6}\langle m_i^2\rangle(4\delta_{r,0} - \delta_{r,1} - \delta_{r,-1}). \tag{2.30}$$

For convenience, we now introduce the following quantity,

$$\chi(\bar{\rho}) \equiv \frac{\tilde{\zeta}^2}{6}\langle m_i^2\rangle \tag{2.31}$$

which, as we show later, is nothing but the density-dependent transport coefficient, called the mobility $\chi(\bar{\rho}) = \lim_{T\to\infty, L\to\infty} L\left\langle \mathcal{Q}_i^2(T)\right\rangle_c / 2T$ - the scaled second cumulant

of the bond-current fluctuation, where the infinite-time limit $T \to \infty$ has to be taken first; note that, in the steady state, as the average $\langle \mathcal{Q}_i(T) \rangle = 0$, the second cumumant (or, the variance) and the second moment are equal, i.e., $\langle \mathcal{Q}_i^2(T) \rangle_c = \langle \mathcal{Q}_i^2(T) \rangle$, and we use them interchangeably. As we shall demonstrate later, the mobility $\chi(\bar{\rho})$ can be exactly equated to another transport coefficient, which we call an "operational" mobility $\chi_{op}(\bar{\rho})$ and is a ratio of the current (response) to a small externally applied biasing force (perturbation) [80]. As shown later in eq. (2.50), the analytic expression for the second moment $\langle m_i^2 \rangle$ of single-site mass in the steady state can be written in terms of the chipping parameter $\tilde{\zeta}$ and density $\bar{\rho}$ as

$$\langle m_i^2 \rangle = \frac{3}{(3 - 2\tilde{\zeta})} \bar{\rho}^2, \tag{2.32}$$

which is proportional to the square of density. The above density dependence of the second moment (and the variance) of local mass is rather generic for a broad class of MCMs, not just MCM I (though the pre-factor can differ depending on dynamical rules). Indeed, it is a direct consequence of the linear dependence of the (local) diffusive current on (local) mass, as encoded in the linearity property in eq. (2.11).

We now substitute Eq.(2.31) into Eq.(2.30) to express $\Gamma_r(\bar{\rho})$ in terms of the system's density-dependent mobility $\chi(\bar{\rho})$ as

$$\Gamma_r(\bar{\rho}) = 4\chi(\bar{\rho})\delta_{r,0} - \chi(\delta_{r,1} + \delta_{r,-1}). \tag{2.33}$$

It is interesting to note that Γ_r has a direct connection to the steady-state mass-mass correlation C_r^{mm}, through the relation

$$\Gamma_r = 2DC_r^{mm}. \tag{2.34}$$

Later, we demonstrate that the quantity Γ_r is related to the spatial correlation function for the fluctuating ("noise") current. This reveals a direct relationship between (noise) current fluctuation and density fluctuation, as well as the crucial role of steady-state spatial structure in determining large-scale dynamic properties. This is precisely how density and current fluctuations, as well as relaxation properties (via bulk-diffusivity), are inextricably linked to one another, culminating in an equilibrium-like Einstein relation, as shown later.

Now, by using the following formula

$$D \langle (m_i - m_{i+1}) \mathcal{Q}_r \rangle_c = \frac{D}{L} \sum_q (1 - e^{iq}) \tilde{C}_q^{m\mathcal{Q}}(t,t) e^{-iqr} \tag{2.35}$$

in Eq.(2.29) and performing some algebraic manipulations, we obtain

$$\frac{d}{dt} C_r^{\mathcal{Q}\mathcal{Q}}(t,t) = \frac{D}{L} \sum_q (1 - e^{iq}) \tilde{C}_q^{m\mathcal{Q}}(t,t)(2 - \omega_{qr}) + \Gamma_r, \tag{2.36}$$

where $\omega_{qr} = 2\,(1 - \cos(qr))$ [see Eq.(2.25)]. After integrating both sides of the above equation, we obtain the equal-time current-current correlation function,

$$C_r^{\mathcal{Q}\mathcal{Q}}(t,t) = \int_0^t dt' \Gamma_r(t') + \frac{D}{L} \int_0^t dt' \sum_q \tilde{C}_q^{m\mathcal{Q}}(t',t')(1 - e^{iq})(2 - \omega_{qr}). \tag{2.37}$$

To explicitly obtain the above equal-time correlation for current, we need to calculate the equal-time correlation function $C_r^{m\mathcal{Q}}(t,t)$ by using the following infinitesimal-time update rule,

$$m_i(t+dt)\mathcal{Q}_{i+r}(t+dt) = \begin{cases} \textbf{event} & \textbf{prob.} \\ m_i\mathcal{Q}_{i+r} + \tilde{\zeta} m_i(\xi_{i+r}m_{i+r} - \tilde{\xi}_{i+r+1}m_{i+r+1}) & \\ +\tilde{\zeta}\left(\tilde{\xi}_{i+1}m_{i+1} - m_i + \xi_{i-1}m_{i-1}\right)\mathcal{Q}_{i+r} & dt, \\ m_i\mathcal{Q}_{i+r} - \tilde{\zeta}^2(\xi_i m_i^2 + \tilde{\xi}_{i+1}^2 m_{i+1}^2) & \delta_{r,0}dt \\ m_i\mathcal{Q}_{i+r} + \tilde{\zeta}^2(\tilde{\xi}_i m_i^2 + \xi_{i-1}^2 m_{i-1}^2) & \delta_{r,-1}dt, \\ m_i\mathcal{Q}_{i+r} + \tilde{\zeta}^2\tilde{\xi}_{i+1}\xi_{i+1}m_{i+1}^2 & \delta_{r,1}dt, \\ m_i\mathcal{Q}_{i+r} - \tilde{\zeta}^2\xi_{i-1}\tilde{\xi}_{i-1}m_{i-1}^2 & \delta_{r,-2}dt, \\ m_i\mathcal{Q}_{i+r} & 1-\sum dt, \end{cases} \tag{2.38}$$

where $\sum = 1 + \delta_{r,0} + \delta_{r,1} + \delta_{r,-1} + \delta_{r,-2}$ is the total exit rate. Using the above dynamical update rules, we obtain the following time-evolution equation,

$$\frac{d}{dt}C_r^{m\mathcal{Q}}(t,t) = D\left(C_{r-1}^{m\mathcal{Q}} - 2C_r^{m\mathcal{Q}} + C_{r+1}^{m\mathcal{Q}}\right) + A_r, \tag{2.39}$$

where the quantity A_r - a source term in an inhomogeneous (discrete) Laplace equation - is given by

$$A_r = \frac{\tilde{\zeta}}{2}\langle m_i m_{i+r} - m_i m_{i+r+1}\rangle_c - \frac{5\tilde{\zeta}^2}{6}\langle m_i^2\rangle\delta_{r,0} + \frac{\tilde{\zeta}^2}{6}\langle m_i^2\rangle\delta_{r,1} - \frac{\tilde{\zeta}^2}{6}\langle m_i^2\rangle\delta_{r,-2}, \tag{2.40}$$

which we now proceed to calculate in the steady state.

It is evident here that the quantity A_r is related to equal-time spatial correlation for mass, which can be calculated by using the following infinitesimal-time update rules,

$$m_i(t+dt)m_{i+r}(t+dt) = \begin{cases} \textbf{event} & \textbf{prob.} \\ \tilde{\zeta}\left(\tilde{\xi}_{i+1}m_{i+1} + \xi_{i-1}m_{i-1}\right)m_{i+r} & \\ +\tilde{\zeta}m_i(\tilde{\xi}_{i+r+1}m_{i+r+1} + \xi_{i+r-1}m_{i+r-1}) & \\ (1-2\tilde{\zeta})m_i m_{i+r} & dt, \\ m_i m_{i+r} + \tilde{\zeta}^2(m_i^2 + \tilde{\xi}_{i+1}^2 m_{i+1}^2 + m_{i-1}^2\xi_{i-1}^2) & \delta_{r,0}dt, \\ m_i m_{i+r} - \tilde{\zeta}^2(\tilde{\xi}_{i+1}m_{i+1}^2 + \xi_i m_i^2) & \delta_{r,1}dt, \\ m_i m_{i+r} + \tilde{\zeta}^2(\tilde{\xi}_i m_i^2 + \xi_{i-1}m_{i-1}^2) & \delta_{r,-1}dt, \\ m_i m_{i+r} - \tilde{\zeta}^2\xi_{i+1}\tilde{\xi}_{i+1}m_{i+1}^2 & \delta_{r,2}dt, \\ m_i m_{i+r} - \tilde{\zeta}^2\xi_{i-1}\tilde{\xi}_{i-1}m_{i-1}^2 & \delta_{r,-2}dt, \\ m_i m_{i+r} & 1-\sum dt, \end{cases} \tag{2.41}$$

where $\sum = 1 + \delta_{r,0} + \delta_{r,1} + \delta_{r,-1} + \delta_{r,-2} + \delta_{r,2}$ is the total exit rate. Using the above dynamical update rules, we obtain the time evolution equation for spatial

mass-mass correlation,

$$\frac{d}{dt}C_r^{mm}(t,t) = 2D\sum_k \langle m_0 \Delta_{r,k} m_k \rangle_c + B_r, \tag{2.42}$$

where the source term B_r in the steady state can be expressed in terms of the second moment of single-site mass, i.e.,

$$B_r = \frac{\tilde{\zeta}^2 \langle m_i^2 \rangle}{6}[10\delta_{r,0} - 6(\delta_{r,1} + \delta_{r,-1}) + (\delta_{r,2} + \delta_{r,-2})]. \tag{2.43}$$

Then, by using the steady-state condition $dC_r^{mm}(t,t)/dt = 0$, we obtain the equation for the steady-state spatial correlation for mass,

$$2D\left[C_{r+1}^{mm} - 2C_r^{mm} + C_{r-1}^{mm}\right] + B_r = 0. \tag{2.44}$$

The structure of the above equation [similar to the Poisson equation, albeit a discrete one] for the two-point (equal-time) mass-mass correlation in the steady state is quite generic for models satisfying a linearity property (i.e., the bulk-diffusion coefficient being constant) analogous to eq. (2.11). As illustrated below, an explicit analytical solution to the dynamical correlations for current and mass actually hinges on the solvability of the above equation.

Indeed, in the case of MCM I (as well as MCM II and III), eq. (2.44) can be readily solved by employing a generating function

$$G(z) = \sum_{r=0}^{\infty} C_r^{mm} z^r. \tag{2.45}$$

The following generating function method differs from the one used in [34] and is presented here for completeness of the various calculations, and the derivations of the fluctuation relations, discussed in the subsequent sections. By multiplying both sides of Eq.(2.44) by z^r and then summing over r, we solve for the generating function,

$$G(z) = \frac{C_0^{mm}[6 - (10 - 6z + z^2)\tilde{\zeta}] - 6zC_1^{mm} - (10 - 6z + z^2)\bar{\rho}^2}{6(1-z)^2}, \tag{2.46}$$

where we use the following identities, $\sum_{r=0}^{\infty} C_{r+1}^{mm} z^r = [G(z) - C_0^{mm}]/z$, $\sum_{r=0}^{\infty} C_{r-1}^{mm} z^r = C_1^{mm} + zG(z)$, and $\langle m_i^2 \rangle = C_0^{mm} + \bar{\rho}^2$. Note that $G(z)$ has a second-order pole at $z = 1$. However, by considering the fact that $G(z = 1)$ represents the sum of density correlations and thus it should be finite, we find that $\lim_{z\to 1} G(z)$ must also be finite. Therefore, the numerator and its derivative must vanish as $z \to 1$. From these root-cancellation conditions, we get the following two equations,

$$C_0^{mm}(6 - 5\tilde{\zeta}) - 6C_1^{mm} - 5\bar{\rho}^2 = 0, \tag{2.47}$$

and

$$2\tilde{\zeta}C_0^{mm} + 3C_1^{mm} - 2\bar{\rho}^2 = 0. \tag{2.48}$$

By solving the above equations, we finally obtain the generating function,

$$G(z) = \frac{2\tilde{\zeta}\bar{\rho}^2}{3-2\tilde{\zeta}} - \frac{\tilde{\zeta}\bar{\rho}^2}{2(3-2\tilde{\zeta})}z, \tag{2.49}$$

which immediately leads to the explicit analytical expression for the steady-state spatial correlation function C_r^{mm} for mass,

$$C_r^{mm} = \langle m_i m_{i+r}\rangle - \bar{\rho}^2 = \begin{cases} \frac{2\tilde{\zeta}}{3-2\tilde{\zeta}}\bar{\rho}^2 & \text{for } r=0 \\ -\frac{\tilde{\zeta}}{2(3-2\tilde{\zeta})}\bar{\rho}^2 & \text{for } |r|=1 \\ 0 & \text{otherwise.} \end{cases} \tag{2.50}$$

Now, the steady-state spatial correlation function for mass can be readily expressed in terms of the particle mobility $\chi(\bar{\rho})$,

$$C_r^{mm} = \frac{\chi(\bar{\rho})}{\tilde{\zeta}}(4\delta_{r,0} - \delta_{r,1} - \delta_{r,-1}). \tag{2.51}$$

Furthermore, by summing both sides of Eq. (2.51) over r, we obtain a fluctuation relation between mass fluctuation and the mobility (equivalently, the current fluctuation),

$$\sum_{r=-\infty}^{\infty} C_r^{mm} = \frac{2\chi(\bar{\rho})}{\tilde{\zeta}}. \tag{2.52}$$

In the steady state, we can write $A_r(\bar{\rho})$ by simply using Eq.(2.51) in Eq.(2.40),

$$A_r(\bar{\rho}) = -\frac{5}{2}\chi(\bar{\rho})(\delta_{r,0} - \delta_{r,-1}) + \frac{1}{2}\chi(\delta_{r,1} - \delta_{r,-2}). \tag{2.53}$$

We now express Eq. (2.39) in the Fourier space as

$$\frac{d}{dt}\tilde{C}_q^{m\mathcal{Q}}(t,t) = -D\omega_q \tilde{C}_q^{m\mathcal{Q}}(t,t) + \tilde{f}_q(t), \tag{2.54}$$

where the Fourier transform of the source term A_r is given by

$$\tilde{f}_q = -\chi(1-e^{-iq})\left(1 + \frac{1}{2}\omega_q\right). \tag{2.55}$$

Equation (2.54) can be integrated to obtain

$$\tilde{C}_q^{m\mathcal{Q}}(t',t') = \int_0^{t'} dt'' e^{-D\omega_q(t'-t'')}\tilde{f}_q(t''), \tag{2.56}$$

which appears in Eqs. (2.37) and (2.27) and can be now used to calculate the equal-time current-current and unequal-time mass-current correlation functions.

2.3.3 Time-integrated current fluctuation

In this section, we use the theoretical framework outlined in the preceding section to compute the time-integrated bond-current fluctuation for MCM I exactly. To this end, we insert Eq. (2.56) into Eq. (2.37), yielding an explicit expression for the time-integrated bond-current fluctuation,

$$C_r^{\mathcal{Q}\mathcal{Q}}(t,t) = \int_0^t dt' \Gamma_r(t') + \frac{D}{L}\sum_q \int_0^t dt' \int_0^{t'} dt'' e^{-D\omega_q(t'-t'')} \tilde{f}_q(t'')(1-e^{iq})[2-\omega_{qr}]. \tag{2.57}$$

Now, by using Eqs. (2.57), (2.56), (2.27), and (2.26), we finally obtain the desired expression for the unequal-time current-current correlation function,

$$\begin{aligned} C_r^{\mathcal{Q}\mathcal{Q}}(t,t') =& t'\Gamma_r - \frac{\chi D}{L}\sum_q \int_0^{t'} \mathrm{d}t'' \int_0^{t''} \mathrm{d}t''' \, e^{-D\omega_q(t''-t''')}\omega_q(1+\frac{1}{2}\omega_q)(2-\omega_{qr}) \\ & - \frac{\chi D}{L}\sum_q \int_{t'}^{t} \mathrm{d}t'' \int_0^{t'} \mathrm{d}t''' \, e^{-D\omega_q(t''-t''')}\omega_q(1+\frac{1}{2}\omega_q)e^{-iqr}. \end{aligned} \tag{2.58}$$

We obtain, in the steady state, the second cumulant or the variance of time-integrated bond-current $\langle \mathcal{Q}_i^2(T)\rangle_c = \langle \mathcal{Q}_i^2(T)\rangle - \langle \mathcal{Q}_i(T)\rangle^2 = C_0^{\mathcal{Q}\mathcal{Q}}(T,T)$ from Eq.(2.58), by putting $t' = t = T$ and $r = 0$,

$$\langle \mathcal{Q}_i^2(T)\rangle_c = \langle \mathcal{Q}_i^2(T)\rangle = \frac{2\chi T}{L} + \frac{2\chi}{L}\sum_{n=1}^{L-1}\left(1+\frac{\omega_n}{2}\right)\frac{(1-e^{-D\omega_n T})}{D\omega_n}, \tag{2.59}$$

where $\omega_n = 2(1-\cos(2\pi n/L))$, with $n = 1, \cdots, L-1$ and we have used steady-state average $\langle \mathcal{Q}_i(T)\rangle = 0$. If we first take the limit $T \to \infty$ (i.e., corresponding to the time domain $T \gg L^2$), we immediately obtain in the leading order,

$$\langle \mathcal{Q}_i^2(T)\rangle \simeq \frac{2\chi T}{L} + \frac{\chi}{D}\left(\frac{L}{6} - \frac{1}{L}\right) = \frac{2\chi T}{L}\left[1 + \mathcal{O}\left(\frac{L^2}{DT}\right)\right]. \tag{2.60}$$

By performing the asymptotic analysis of Eq. (2.59), we can identify two distinct time regimes, that correspond to two of the following cases.

Case 1: Small-time regime $DT \ll 1$

In the limit $DT \ll 1$, the system does not have sufficient time for building up spatial correlations at neighboring sites, resulting in the bond-current fluctuation having no information of the spatial structure in the system. In equation (2.59), we expand the exponential up to linear order for $DT \ll 1$ and obtain

$$\langle \mathcal{Q}_i^2(T)\rangle = \frac{2\chi T}{L} + \frac{2\chi}{L}\sum_{n=1}^{L-1}\left(1+\frac{\omega_n}{2}\right)T. \tag{2.61}$$

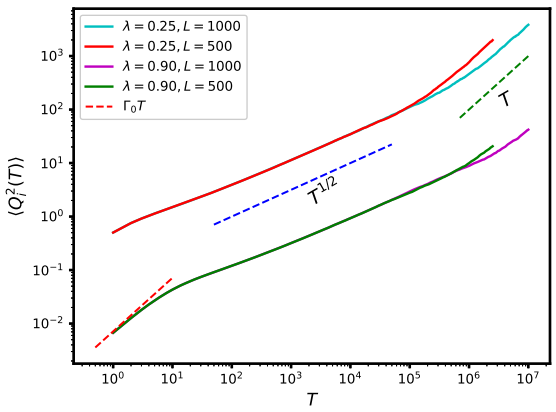

Figure 2.2: The second cumulant, or the variance, $\langle \mathcal{Q}_i^2(T)\rangle_c = \langle \mathcal{Q}_i^2(T)\rangle$ of time-integrated bond-current in the steady state plotted as a function of time T for various chipping parameter and system sizes. The cyan ($\zeta = 0.25$, $L = 1000$), magenta ($\zeta = 0.90$, $L = 1000$), red ($\zeta = 0.25$, $L = 500$), and green ($\zeta = 0.90$, $L = 500$) lines represent simulation data for global density $\bar{\rho} = 1$. The red dashed line represents the behavior $\Gamma_0 T$ for $\zeta = 0.90$ as mentioned in Eq.(2.62), while the blue and green dashed lines represent sub-diffusive $\sim T^{1/2}$ and diffusive $\sim T$ growth, respectively, as mentioned in Eq.(2.70).

To further simplify it, we use the identity $\sum_{n=1}^{L-1} \omega_n = 2L$, resulting in

$$\langle \mathcal{Q}_i^2(T)\rangle = \Gamma_0 T = 4\chi T, \tag{2.62}$$

where Γ_0 is the strength of fluctuating current as mentioned in Eq.(2.33) and later calculated exactly.

In Figure 2.2, we present simulation data for the second cumulant, or the variance, $\langle \mathcal{Q}_i^2(T)\rangle_c = \langle \mathcal{Q}_i^2(T)\rangle$ of time-integrated bond-current in the steady state plotted as a function of time T. The plot shows three distinct behaviors of temporal growth of the current fluctuations: Short-time linear ($\sim T$), intermediate-time subdiffusive ($\sim T^{1/2}$), and long-time linear ($\sim T$) growths. We have examined the effects of chipping by varying the values of $\zeta = 0.25$ and 0.90 for two different system sizes $L = 500$ and $L = 1000$. Also, we provide two plots concerning current fluctuations that overlap in the region $DT \ll 1$ for two system sizes with ζ kept fixed.

Case 2: Long-time regime $DT \gg 1$

In the limit $DT \gg 1$, spatial correlations gradually build up in the system. Interestingly, Eq. (2.60) suggests that, in the large-time limit ($T \gg L^2$), $\langle \mathcal{Q}_i^2(T)\rangle$ asymptotically approaches $2\chi T/L$, indicating that there are only three macroscopic parameters - the bulk-diffusion coefficient D, the mobility χ, and system size L - which are relevant and thus can be used to characterize the large-scale temporal growth in the system. Indeed, one would expect that $\langle \mathcal{Q}_i^2(T)\rangle$ and T should be related through a precise scaling combination involving the above mentioned macroscopic quantities. To precisely quantify this scaling regime, we define a scaled

second moment of steady-state time-integrated bond-current, in the limit of large $T, L \gg 1$, i.e.,

$$\lim_{T,L\to\infty} \frac{D\langle \mathcal{Q}_i^2(T)\rangle}{2\chi L} = \mathcal{W}\left(y = \frac{DT}{L^2}\right), \tag{2.63}$$

where $\mathcal{W}(y)$ is a scaling function, with the scaling variable $y = DT/L^2$ being finite, and can be exactly written as

$$\mathcal{W}(y) = \lim_{L\to\infty}\left[y + \frac{1}{L^2}\sum_q \left(1+\frac{\omega_q}{2}\right)\frac{1-e^{-\omega_q L^2 y}}{\omega_q}\right], \tag{2.64}$$

where $\omega_q = 2(1-\cos q)$, with $q = 2\pi n/L$ and $n = 1, 2, \cdots, L-1$. In the right hand side of Eq. (2.64), the scaling function $\mathcal{W}(y)$ can be approximately written in terms of the following integral representation,

$$\mathcal{W}(y) \simeq y + \lim_{L\to\infty}\frac{1}{\pi L}\int_{2\pi/L}^{\pi} dq \frac{\left(1-e^{-L^2 y\omega(q)}\right)}{\omega(q)} + \lim_{L\to\infty}\frac{1}{2\pi L}\int_{2\pi/L}^{\pi} dq\left(1-e^{-L^2 y\omega(q)}\right). \tag{2.65}$$

By using variable transformation $z = \omega(q)L^2$ in Eq. (2.65) and taking the infinite system-size limit $L\to\infty$, we obtain the following expression,

$$\mathcal{W}(y) \simeq y + \frac{1}{2\pi}\int_{4\pi^2}^{\infty} dz \frac{(1-e^{-zy})}{z^{3/2}}, \tag{2.66}$$

where we have used the fact that the third term on the right-hand side of eq. (2.65) gives a subleading $o(1/L)$ contribution, which vanishes in the scaling limit. After performing the integration explicitly, we finally write

$$\mathcal{W}(y) \simeq y + \sqrt{\frac{y}{\pi}}\mathrm{erfc}(2\pi\sqrt{y}) + \frac{1-e^{-4\pi^2 y}}{4\pi^2}, \tag{2.67}$$

where $\mathrm{erfc}(z) = 1-\mathrm{erf}(z)$ and the error function is given by

$$\mathrm{erf}(z) = \frac{2}{\sqrt{\pi}}\int_0^z e^{-t^2} dt. \tag{2.68}$$

From Eq. (2.67), we straightforwardly determine the asymptotic form of $\mathcal{W}(y)$ in the following two regimes of large and small y,

$$\mathcal{W}(y) \simeq \begin{cases} \sqrt{y/\pi} & \text{for } y \ll 1 \\ y & \text{for } y \gg 1. \end{cases} \tag{2.69}$$

In Fig. 2.3, we plot the scaled time-integrated bond-current fluctuation $\langle \mathcal{Q}_i^2(T)\rangle D/(2\chi L)$ as a function of scaled time DT/L^2 for different chipping parameters and system sizes for global density $\bar{\rho} = 1$. The colored lines are obtained from simulations, and the black solid line corresponds to theory as in Eq.(2.64). Two guiding (dashed) lines, which represent subdiffusive $\sim y^{1/2}$ behavior (blue) at early (but still large)

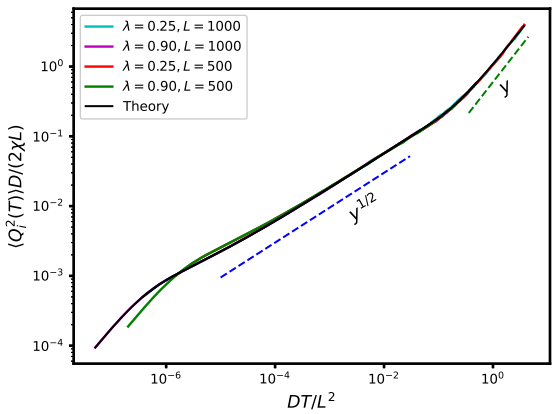

Figure 2.3: Scaled time-integrated bond-current fluctuation, $\langle \mathcal{Q}_i^2(T)\rangle D/(2\chi L)$, in the steady state is plotted against scaled time DT/L^2 for different chipping parameters and system sizes at a global density of $\bar{\rho} = 1$. The cyan ($\zeta = 0.25$, $L = 1000$), magenta ($\zeta = 0.90$, $L = 1000$), red ($\zeta = 0.25$, $L = 500$), and green ($\zeta = 0.90$, $L = 500$) lines represent simulation data. The two guiding dashed lines depict subdiffusive $\sim y^{1/2}$ growth (blue) at early times, followed by a diffusive $\sim y$ growth (green) at long times. These trends are based on the scaling function $\mathcal{W}(y)$ [as in Eq.(2.69)]. The black solid line corresponds to theoretical results [as in Eq.(2.64)] and demonstrates an excellent agreement with simulations.

times, followed by diffusive growth as $\sim y$ (green) at long times, as given in Eq. (2.69).

Thus, by combining all three temporal regimes discussed above, we summarize the asymptotic behaviors of the time-integrated bond-current $\langle \mathcal{Q}_i^2(T)\rangle$ as

$$\langle \mathcal{Q}_i^2(T)\rangle = \begin{cases} 4\chi T & \text{for } DT \ll 1, \\ \frac{2\chi}{\sqrt{D\pi}} T^{1/2} & \text{for } 1 \ll DT \ll L^2, \\ \frac{2\chi}{L} T & \text{for } DT \gg L^2, \end{cases} \tag{2.70}$$

where it is interesting to note that the second and third regimes are indeed related through a *single* scaling function $\mathcal{W}(y)$.

Space-time integrated current fluctuations

In this section, we focus on the second cumualnt, or the variance, $\langle \mathcal{Q}_{sub}^2(l,T)\rangle_c = \langle \mathcal{Q}_{sub}^2(l,T)\rangle - \langle \mathcal{Q}_{sub}(l,T)\rangle^2 = \langle \mathcal{Q}_{sub}^2(l,T)\rangle$ (as steady-state $\langle \mathcal{Q}_{sub}(l,T)\rangle = 0$) of the cumulative (space-time integrated) particle current $\mathcal{Q}_{sub}(l,T) = \sum_{i=0}^{l-1} \mathcal{Q}_i(T)$ across a subsystem of size l and up to time T in the steady state. The subsystem-current fluctuation can be written as

$$\langle \mathcal{Q}_{sub}^2(l,T)\rangle = \left\langle \sum_{i=1}^{l-1} \mathcal{Q}_i(T) \sum_{j=1}^{l-1} \mathcal{Q}_j(T) \right\rangle, \tag{2.71}$$

where the sum on the right-hand side can be expressed in terms of the (equal-time) current-current dynamic correlations,

$$\langle \mathcal{Q}^2_{sub}(l,T)\rangle = lC_0^{\mathcal{Q}\mathcal{Q}}(T,T) + \sum_{r=1}^{l-1} 2(l-r)C_r^{\mathcal{Q}\mathcal{Q}}(T,T). \tag{2.72}$$

By using Eq.(2.57) in the above equation and then employing the following identity,

$$\sum_{r=1}^{l-1} 2(l-r)(2-\omega_{rq}) = 2\left(\frac{\omega_{lq} - l\omega_q}{\omega_q}\right), \tag{2.73}$$

we obtain, after some algebraic manipulations, the following expression,

$$\begin{aligned}\langle \mathcal{Q}^2_{sub}(l,T)\rangle &= 2\chi lT + 2\chi T(1-\delta_{l,L}) - \frac{2\chi D}{L} \\ &\times \sum_q \frac{(D\omega_q T - 1 + e^{-\omega_q DT})}{(\omega_q D)^2}\left(1+\frac{\omega_q}{2}\right)\omega_{ql},\end{aligned} \tag{2.74}$$

where $\omega_q = 2(1-\cos q)$ with $q = 2\pi n/L$ and $n = 1, 2, \cdots, L-1$. The subsystem size l comes into play through the Fourier mode ω_{ql} alone. We now derive the asymptotic dependence of Eq.(2.74) on the subsystem size l and time T, first by considering the limit $T \gg 1$ followed by $l \gg 1$, and then by reversing the order of the limits, i.e., $l \gg 1$ followed by $T \gg 1$.

Case 1: $T \gg 1$ and $l \gg 1$

We first consider the limit $T \gg 1$ followed by the limit $l \gg 1$; in that case, Eq. (2.74) simplifies to

$$\langle \mathcal{Q}^2_{sub}(l,T)\rangle \simeq \frac{2\chi l^2 T}{L} + \frac{2\chi D}{L}\sum_q \frac{(1-e^{-D\omega_q T})}{D^2\omega_q^2}\left(1+\frac{\omega_q}{2}\right)\omega_{ql}. \tag{2.75}$$

In the limit of $L \to \infty$, the sum in the above equation can be approximated as an integral,

$$\langle \mathcal{Q}^2_{sub}(l,T)\rangle \simeq \frac{2\chi D}{\pi}\int_0^\pi dq \frac{(1-e^{-D\omega(q)T})}{D^2\omega(q)^2}\left[1+\frac{\omega(q)}{2}\right]\omega(ql). \tag{2.76}$$

Then, by using the approximation $\omega(lq) \simeq l^2q^2$ for a finite subsystem size l, and a variable transformation $z = DTq^2$, we obtain the following expression,

$$\langle \mathcal{Q}^2_{sub}(l,T)\rangle \simeq \frac{\chi l^2\sqrt{T}}{\pi\sqrt{D}}\int_0^\infty dz(1-e^{-z})z^{-3/2}, \tag{2.77}$$

which, by using the identity $\int_0^\infty dz(1-e^{-z})z^{-3/2} = 2\sqrt{\pi}$, leads to the asymptotic form,

$$\frac{\langle \mathcal{Q}^2_{sub}(l,T)\rangle}{lT} \simeq \frac{2\chi}{\sqrt{\pi D}}\frac{l}{\sqrt{T}}. \tag{2.78}$$

Case 2: $l \gg 1$ and $T \gg 1$

In this specific order of limits, where $l \gg 1$ limit is taken first and then $T \gg 1$ limit, equation (2.74) can be expressed in an integral form,

$$\frac{\langle \mathcal{Q}^2_{sub}(l,T)\rangle}{lT} \simeq 2\chi + \frac{2\chi}{l} + \frac{4\chi D}{lT\pi}\int_0^\pi dq \frac{[D\omega(q)T - 1 + e^{-\omega(q)DT}]}{D^2\omega(q)^2}, \tag{2.79}$$

where we use an approximation $\omega(ql) \simeq 2$. Again, by using the variable transformation $z = DTq^2$, we obtain

$$\frac{\langle \mathcal{Q}^2_{sub}(l,T)\rangle}{lT} \simeq 2\chi + \frac{2\chi}{l} - \frac{2\chi\sqrt{DT}}{\pi l}\int_0^\infty dz(z - 1 + e^{-z})z^{-\frac{5}{2}}. \tag{2.80}$$

By using the identity $\int_0^\infty dz(z - 1 + e^{-z})z^{-5/2} = 4\sqrt{\pi}/3$ in the above equation, we find the following asymptotic behavior,

$$\frac{\langle \mathcal{Q}^2_{sub}(l,T)\rangle}{lT} \simeq 2\chi - \frac{8\chi}{3}\frac{\sqrt{D}}{\pi}\frac{\sqrt{T}}{l} \tag{2.81}$$

Hence, the asymptotic expression for the variance of the cumulative subsystem current, as given in eq. (2.74), in fact depends on the order of limits for $T \gg 1$ and $l \gg 1$, i.e.,

$$\frac{\langle \mathcal{Q}^2_{sub}(l,T)\rangle}{lT} \simeq \begin{cases} \frac{2\chi}{\sqrt{\pi D}}\frac{l}{\sqrt{T}} & \text{for } T \gg 1, l \gg 1, \\ 2\chi - \frac{8\chi}{3}\frac{\sqrt{D}}{\pi}\frac{\sqrt{T}}{l} & \text{for } l \gg 1, T \gg 1. \end{cases} \tag{2.82}$$

The first expression in the above equation results from taking the limits in the following sequence: first $T \gg 1$ and then $l \gg 1$. In this specific order of limits, the scaled function $\langle \mathcal{Q}^2_{sub}(l,T)\rangle/lT$ decreases as $1/\sqrt{T}$ and eventually diminishes as T approaches infinity. On the other hand, if we reverse the order of limits, i.e., first $l \gg 1$ limit and $T \gg 1$ limit, we derive the second asymptotic expression as in Eq.(2.82). Notably, when infinite subsystem-size limit $l \to \infty$ is taken first, the scaled variance of the subsystem current converges to a finite number - twice the mobility 2χ - as T increases,

$$\sigma^2_{\mathcal{Q}} \equiv \lim_{T\to\infty}\left[\lim_{l\to\infty}\frac{\langle \mathcal{Q}^2_{sub}(l,T)\rangle_c}{lT}\right] = \lim_{T\to\infty}\left[\lim_{l\to\infty}\frac{\langle \mathcal{Q}^2_{sub}(l,T)\rangle}{lT}\right] = \sum_r \Gamma_r, \tag{2.83}$$

where we have used $\langle \mathcal{Q}_{sub}(l,T)\rangle = 0$ in the steady state. Indeed the fluctuation relation as in Eq. (2.83) could be viewed as a nonequilibrium version of the Green-Kubo relation, which is well known for equilibrium systems. If we consider $l = L \gg 1$ (corresponding to the case when the bond current is summed over the entire system), we can recast the above fluctuation relation as

$$\lim_{L\to\infty}\frac{\langle \mathcal{Q}^2_{sub}(L,T)\rangle}{LT} = 2\chi = \sum_r \Gamma_r. \tag{2.84}$$

Interestingly, the above expression is valid for any finite time T. This is due to the fact that, by definition, the diffusive part of the total current vanishes over the full

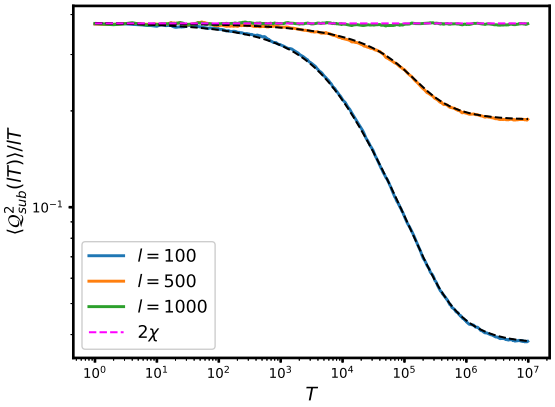

Figure 2.4: The scaled cumulant, or the variance, $\langle \mathcal{Q}^2_{sub}(l,T)\rangle_c = \langle \mathcal{Q}^2_{sub}(l,T)\rangle$ of space-time-integrated subsystem current in the steady state is plotted as a function of time T for various subsystem sizes $l = 100$ (lower blue solid line), 500 (middle orange solid line), and 1000 (top solid green line). The chipping parameter for the model is chosen to be $\zeta = 0.25$, with a system size of $L = 1000$ and a global density of $\bar{\rho} = 1$. The black dashed line in the plot corresponds to the theoretical prediction derived from Eq.(2.74), and it precisely aligns with the respectable simulation data. Moreover, when the subsystem size equals the full system size, i.e., $l = L$, $\langle \mathcal{Q}^2_{sub}(L,T)\rangle/LT$ follows the behavior of 2χ (magenta dashed lines), as indicated by Eq.(2.84).

system size, i.e., $\sum_{i=1}^{L} \mathcal{J}_i^{(d)} = 0$. As a result, we are left with the space-time current having only the contribution from the fluctuating part, thus leading to the sum rule $\sum_r \Gamma_r = 2\chi$ as given in eq. (2.84).

In Figure 2.4, we plot the scaled cumulant, or the variance, $\langle \mathcal{Q}^2_{sub}(l,T)\rangle_c = \langle \mathcal{Q}^2_{sub}(l,T)\rangle$ of space-time-integrated subsystem-current fluctuation against time T for various subsystem sizes: $l = 100$ (blue line), $l = 500$ (orange line), and $l = L = 1000$ (green line). The black dashed lines represent theoretical predictions that closely match the simulation data. A magenta dotted line at 2χ overlays the data when $l = L$, indicating a limit where $l \to \infty$ is taken first. Notably, for smaller subsystem sizes, i.e., when $T \to \infty$ limit is taken first, $\langle \mathcal{Q}^2_{sub}(l,T)\rangle/lT$ tends to zero.

2.3.4 Instantaneous bond-current fluctuations

In this section, we calculate the spatio-temporal correlation function $C_r^{\mathcal{J}\mathcal{J}}(t) = \langle \mathcal{J}_i(t)\mathcal{J}_{i+r}(0)\rangle_c$ of the instantaneous bond current $\mathcal{J}_i(t)$ from the already calculated correlation function involving time-integrated bond current and show that the instantaneous bond current is negatively correlated in time. This is accomplished by taking a double derivative of the time-integrated bond current correlation as follows,

$$C_r^{\mathcal{J}\mathcal{J}}(t,t') = \left[\frac{d}{dt}\frac{d}{dt'} C_r^{\mathcal{Q}\mathcal{Q}}(t,t')\right]. \tag{2.85}$$

Here, with the understanding that $t \geq t'$, we proceed to differentiate Eq.(2.58) twice with respect to time, resulting in the expression

$$C_r^{\mathcal{J}\mathcal{J}}(t,t') = \Gamma_r \delta(t-t') - \frac{\chi D}{L} \sum_q e^{-D\omega_q(t-t')} \omega_q \left(1 + \frac{\omega_q}{2}\right) e^{-iqr}. \tag{2.86}$$

To investigate the temporal behavior of instantaneous bond current, we set $r = 0$ and $t > t' = 0$ in Eq.(2.86) and simplify the expression, to obtain the integral form of the bond current correlation as

$$C_0^{\mathcal{J}\mathcal{J}}(t,0) \simeq \frac{\chi D}{\pi} \int_0^\pi dq e^{-D\omega(q)t} \omega(q) \left[1 + \frac{\omega(q)}{2}\right], \tag{2.87}$$

where we take the thermodynamic limit $L \to \infty$ and $\omega(q) = 2(1 - \cos q)$. Now, by approximating $\omega(q) \simeq q^2$ and making a variable transformation $z = Dq^2 t$, we rewrite the above equation as

$$C_0^{\mathcal{J}\mathcal{J}}(t,0) \simeq -\frac{\chi t^{-\frac{3}{2}}}{2\pi\sqrt{D}} \int_0^\infty z^{\frac{1}{2}} e^{-z} dz, \tag{2.88}$$

where we have ignored the subleading term $O(t^{-5/2})$. We note that the sign of the dynamic correlation function for bond current is negative as given in Eq.(2.88). Finally, by using the integral $\int_0^\infty z^{1/2} e^{-z} dz = \sqrt{\pi}/2$, the asymptotic form of the dynamic current correlation function can be expressed as

$$C_0^{\mathcal{J}\mathcal{J}}(t,0) \simeq \Gamma_0 \delta(t) - \frac{\chi}{4\sqrt{\pi D}} t^{-3/2}. \tag{2.89}$$

Notably, the negative (second) part in the right hand side of the above equation exhibits long-range power-law behavior, solely due to the contribution from the dynamic correlation involving the diffusive current, i.e., $C_0^{\mathcal{J}^{(d)}\mathcal{J}^{(d)}}(t,0) \sim t^{-3/2}$. On the other hand, the fluctuating current is short-ranged $C_r^{\mathcal{J}^{(fl)}\mathcal{J}^{(fl)}}(t,0) = \delta(t)\Gamma_r$, which is delta-correlated in time and where Γ_r represents the space-dependent strength of the fluctuating current. This particular behavior should be contrasted with that for the symmetric simple exclusion processes [78], where, due to the lack of spatial correlations, the strength does not depend on space variable r (the temporal part is, however, delta-correlated as in the mass chipping models).

Now, to obtain the spatial correlation of instantaneous current, we calculated the two-point correlation function calculated at the same time, $t = t'$, but at different space points separated by a distance r. In that case, Eq.(2.86) can be expressed as:

$$C_r^{\mathcal{J}\mathcal{J}}(t,t) = \Gamma_r \delta(0) - \frac{\chi D}{L} \sum_q \omega_q \left(1 + \frac{\omega_q}{2}\right) e^{-iqr}. \tag{2.90}$$

After some algebraic manipulations, the above equation can be expressed in terms of the steady-state ($t \to \infty$) density correlation C_r^{mm},

$$C_r^{\mathcal{J}\mathcal{J}} = \Gamma_r \delta(0) - D^2[3C_r^{mm} - (C_{r-1}^{mm} + C_{r+1}^{mm})]. \tag{2.91}$$

In the above equation, we can see that the spatial length scale associated with the instantaneous current is intimately connected to the space-dependent strength Γ_r of the instantaneous current. There is an interesting observation: As Γ_r directly influences the density correlation C_r^{mm}, we find that, in the steady state, the spatial extent over which the instantaneous bond currents are correlated is inherently short-ranged and, moreover, is characterized by the same length scale, which governs the spatial density correlations. In contrast to the dynamic correlation of the fluctuating current, which constitutes two distinct components - (i) the fluctuating current, which is short-ranged both in terms of spatial and temporal dependencies, and (ii) the diffusive current, which is characterized by its short-ranged spatial behavior, but the long-ranged (power law) temporal behavior ($\sim t^{-3/2}$).

We also study the power spectrum for the instantaneous bond current $\mathcal{J}_i$, which, by using the *Wiener-Khinchin theorem* [87], can be expressed as

$$S_{\mathcal{J}}(f) = \int_{-\infty}^{\infty} dt C_0^{\mathcal{J}\mathcal{J}}(t,0) e^{2\pi i f t}. \tag{2.92}$$

By putting $r = 0$ and $t' = 0$ in Eq. (2.86), we integrate the right hand side of the above equation to obtain

$$S_{\mathcal{J}}(f) = \frac{2\chi(\bar{\rho})}{L} + \frac{2\chi(\bar{\rho})}{L} \sum_q \left(1 + \frac{\omega_q}{2}\right) \frac{4\pi^2 f^2}{D^2\omega_q^2 + 4\pi^2 f^2}, \tag{2.93}$$

where $\omega_q = 2(1-\cos q)$ with $q = 2\pi n/L$ and $n = 1, 2, \cdots, L-1$. By subtracting the zero-th mode ($f = 0$), we rewrite the above expression through a suitably defined power spectrum $\tilde{S}_{\mathcal{J}}(f) = S_{\mathcal{J}}(f) - S_{\mathcal{J}}(0)$,

$$\tilde{S}_{\mathcal{J}}(f) = \frac{2\chi(\bar{\rho})}{L} \sum_q \left(1 + \frac{\omega_q}{2}\right) \frac{4\pi^2 f^2}{D^2\omega_q^2 + 4\pi^2 f^2}. \tag{2.94}$$

Now we rescale frequency as $\tilde{y} = fL^2/D$ and introduce a scaling function $\mathcal{H}$, that relates, for large $f^{-1}, L \gg 1$, to $\tilde{S}_{\mathcal{J}}(f)$ as

$$\lim_{f^{-1},L\to\infty} \mathcal{H}\left(\frac{L^2 f}{D}\right) = \frac{L\tilde{S}_{\mathcal{J}}(f)}{2\chi(\bar{\rho})} = \lim_{f^{-1},L\to\infty} \sum_q \left(1 + \frac{\omega_q}{2}\right) \frac{4\pi^2 \left(\frac{L^2 f}{D}\right)^2}{L^4\omega_q^2 + 4\pi^2 \left(\frac{L^2 f}{D}\right)^2}. \tag{2.95}$$

The above expression can be represented in an integral form and, for small frequencies and in the thermodynamic limit $L \to \infty$, we obtain a scaling regime as discussed below. Furthermore, Eq. (2.95) shows that, as $\tilde{y} \to \infty$, the scaled power spectrum of instantaneous currents diverges with the system size as $2L-1$ [see Fig. 2.5]. The above-mentioned scaling function for the power spectrum of instantaneous bond current as a function of scaled frequency $\tilde{y}$ has an integral representation in the lower frequency regime $D/L^2 \ll f \ll 1$. The integral representation, to a good approximation, is given by

$$\mathcal{H}(\tilde{y}) \simeq \lim_{L\to\infty} \frac{L}{\pi} \int_{2\pi/L}^{\pi} dq \left[1 + \frac{\omega(q)}{2}\right] \frac{1}{1 + \frac{L^4\omega(q)^2}{4\pi^2\tilde{y}^2}}, \tag{2.96}$$

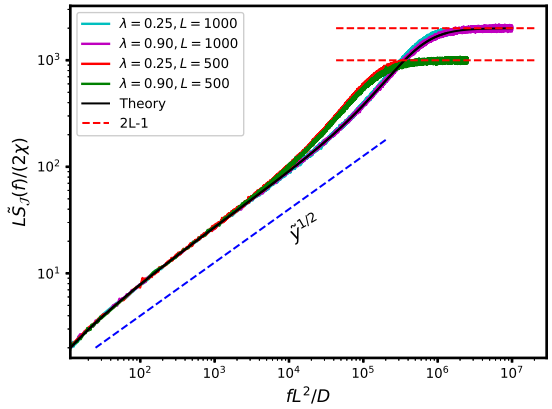

Figure 2.5: The scaled power spectrum of instantaneous current, $L\tilde{S}_{\mathcal{J}}(f)/(2\chi)$, in the steady state is plotted as a function of scaled frequency $L^2 f/D$ for various chipping parameters and system sizes. The cyan solid line corresponds to $\zeta = 0.25$ and $L = 1000$, the magenta solid line corresponds to $\zeta = 0.90$ and $L = 1000$, the red solid line corresponds to $\zeta = 0.25$ and $L = 500$, and the green solid line corresponds to $\zeta = 0.90$ and $L = 500$, all at a global density of $\bar{\rho} = 1$. The blue dashed line shows $\tilde{y}^{1/2}$ scaling behavior in the low-frequency regime as in Eq.(2.97) and red dashed lines represent $L\tilde{S}_{\mathcal{J}}(f)/(2\chi)$ diverges as system size $2L-1$ at the high-frequency limit. The solid color lines represent the simulation results, while the black solid line represents the theoretical prediction from Eq.(2.95).

where $\omega(q) = 2(1-\cos q)$. Now after variable transformation $z = \omega(q)L^2$ and then by taking $L \to \infty$, we obtain the following expression of the scaling function,

$$\mathcal{H}(\tilde{y}) \simeq \frac{1}{2\pi}\int_0^\infty \frac{dz}{z^{1/2}[1+\frac{z^2}{4\pi^2\tilde{y}^2}]} \simeq \sqrt{\frac{\tilde{y}\pi}{4}}. \tag{2.97}$$

In Fig. 2.5, one can see that the scaled power spectrum of the instantaneous bond current, denoted as $L\tilde{S}_{\mathcal{J}}(f)/(2\chi)$, plotted against the scaled frequency $L^2 f/D$ for various chipping parameters and system sizes, where global density $\bar{\rho} = 1$. The simulation results are depicted by using solid colored lines, while the black solid line represents theoretical predictions from Eq.(2.95), which agree very well with the simulation data. Additionally, in the lower scaled-frequency range, we have included a guiding line representing $\tilde{y}^{1/2}$ behavior, as specified in Eq.(2.97). According to Eq.(2.97), the power spectrum of instantaneous current displays a power-law behavior $f^{1/2}$ in the low-frequency regime. Indeed, it can be immediately inferred that, in the temporal domain, the correlation of instantaneous current has a scaling behavior of $\langle \mathcal{J}_0(t)\mathcal{J}_0(0)\rangle \sim t^{-3/2}$ power-law decay, which is consistent with Eq. (2.89).

2.3.5 Subsystem mass fluctuations

In the previous sections, we have performed a detailed study of dynamic current-current correlation and the associated power spectrum for instantaneous current. In this section, we study the power spectrum for subsystem mass fluctuation. To

this end, we first calculate the two-point dynamic correlation function $C_r^{mm}(t,0) = \langle m_i(t)m_{i+r}(0)\rangle - \langle m_i(t)\rangle \langle m_{i+r}(0)\rangle$ for local mass. By employing the microscopic update rules, we derive the time-evolution equation for $C_r^{mm}(t,0) \equiv C_r^{mm}(t)$,

$$\begin{aligned}\frac{d}{dt}C_r^{mm}(t) &= D\sum_k \Delta_{0,k}\left\langle m_k(t)m_r(0)\right\rangle_c \\ &= D\sum_k \Delta_{0,k}C_k^{mm}(t).\end{aligned} \tag{2.98}$$

The solution of the above equation can be written in terms of Fourier modes,

$$\tilde{C}_q^{mm}(t) = e^{-D\omega_q t}\tilde{C}_q^{mm}(0), \tag{2.99}$$

where $\tilde{C}_q^{mm}$ is the Fourier transform of C_r^{mm}. The equal-time two-point mass correlation function $C_r^{mm}(0)$ corresponds to the steady-state mass-mass correlation C_r^{mm} mentioned in Eq.(2.51). At this point, one can check that the equal-time mass correlation C_r^{mm} has a direct connection with the scaled subsystem-mass fluctuation,

$$\sigma_M^2 \equiv \lim_{l\to\infty}\frac{\langle M_l^2\rangle - \langle M_l\rangle^2}{l} = \sum_{r=-\infty}^{r=\infty} C_r^{mm} = \frac{\chi}{D}, \tag{2.100}$$

where boundary contribution of C_r^{mm} has been neglected in the limit of large subsystem size $l \to \infty$.

Note that, in Eq. (2.100), the density-dependent transport coefficient - the collective particle mobility $\chi(\bar{\rho})$ - is defined purely from current fluctuations in the systems, where the particle-hopping rates are strictly symmetric in either direction. Indeed, the essence of the recently developed macroscopic fluctuation theory for diffusive systems [54] is that for "gradient-type models", the current fluctuations can be alternatively calculated using a slightly different approach, where the particle-hopping rates are biased in a certain direction. Essentially, this amounts to applying a small biasing force in that direction so that the hopping rates become slightly asymmetric and a small current is generated in the system. Interestingly, this particular scheme leads to the definition of another transport coefficient, which we call an "operational" mobility and characterizes the response (i.e., the small current generated) of the system to a small biasing force field F; for simplicity, the biasing field is assumed to be constant throughout. Indeed, in Ref. [80], one of us previously introduced such a biasing force, which modifies the original unbiased (symmetric) hopping rates of the MCMs. Of course, in the absence of the force F, we recover the original time-evolution equation (2.6)). In that case, a time-evolution equation for local density field, as opposed to the unbiased scenario as in Eq.(2.6)), is given by [80]

$$\frac{d\rho_i}{dt} = \frac{\tilde{\zeta}}{2}(\rho_{i+1} - 2\rho_i + \rho_{i-1}) + \frac{\tilde{\zeta}^2}{12}F\left(\left\langle m_{i-1}^2\right\rangle - \left\langle m_{i+1}^2\right\rangle\right), \tag{2.101}$$

where we denote local density $\rho_i(t) = \langle m_i(t)\rangle$ at site i. By scaling space and time as $x = i/L$ and $\tau = t/L^2$ and the biasing force as $F = \tilde{F}/L$, the time-evolution equation for density field $\rho(x,\tau)$ as a function of the rescaled space and time variables can be

expressed in terms of a continuity equation,

$$\begin{aligned}\partial_\tau \rho(x,\tau) &= -\partial_x \left[-D\partial_x \rho(x,\tau) + \chi_{op}\tilde{F}\rho(x,\tau) \right] \\ &= -\partial_x J(x,\tau),\end{aligned} \tag{2.102}$$

where the total local current $J = J_{diff} + J_{drift}$ is written as the sum of the diffusive current $J_{diff} = -D\partial_x \rho(x,\tau)$ and drift current $J_{drift} = \chi_{op}\tilde{F}$; here the two transport coefficients - the bulk-diffusion coefficient and the "operational" mobility are given by $D = \tilde{\zeta}/2$ and $\chi_{op} = \langle m_i^2 \rangle /6$, respectively. The latter identity immediately implies, directly through Eq.(2.31), a fluctuation-response relation between the operational mobility and the current fluctuation,

$$\chi_{op}(\bar{\rho}) \equiv \left[\frac{\partial J_{drift}}{\partial \tilde{F}} \right]_{\tilde{F}=0} = \sigma_Q^2 \equiv \chi(\bar{\rho}). \tag{2.103}$$

In other words, here we have derived a *nonequilibrium* version of the celebrated Green-Kubo relation for (near) equilibrium systems. We can immediately derive a nonequilibrium version of another celebrated relation for systems in equilibrium, called the Einstein relation, which connects the scaled mass fluctuation, the bulk-diffusion coefficient and the "operational" mobility, i.e.,

$$\chi_{op} \equiv \left[\frac{\partial J_{drift}}{\partial \tilde{F}} \right]_{\tilde{F}=0} = D\sigma_M^2, \tag{2.104}$$

where we have used the already derived fluctuation relation as given in Eq.(2.100). Notably, the above equation is exact for the MCMs studied in this chapter and the above analysis constitutes a rigorous microscopic derivation of the Green-Kubo-like fluctuation-response relation in a system having a nonequilibrium steady state. Furthermore, by using Eq.(2.83) and Eq. (2.100), we can immediately derive another nonequilibrium fluctuation relation, between the fluctuation of mass and that of current, as expressed in the following equation,

$$\sigma_M^2 = \frac{\sigma_Q^2}{2D}. \tag{2.105}$$

It is not difficult to see that the above relation is nothing but a slightly modified version of the equilibrium-like Einstein relation as given in Eq. (2.104). While the above set of fluctuation relations are quite well established in the context of equilibrium systems, their existence in systems having a nonequilibrium steady state is, however, nontrivial, and there is no rigorous proof for it in nonequilibrium many-particle systems in general. Indeed, some theoretical understanding has been gradually emerging for a somewhat restricted class of nonequilibrium systems having diffusive bulk dynamics, which violate detailed balance in the bulk to which these MCMs belong.

Now, in order to solve Eq. (2.99), we must determine the steady-state mass-mass correlation, whose Fourier modes are given by

$$C_q^{mm} = \frac{\chi}{D}\left(1 + \frac{\omega_q}{2}\right). \tag{2.106}$$

We substitute the above into Eq. (2.99) to obtain

$$\tilde{C}_q^{mm}(t) = \frac{\chi}{D} e^{-D\omega_q t} \left(1 + \frac{\omega_q}{2}\right). \tag{2.107}$$

Finally, by using inverse Fourier transform of the above equation, we get the correlation function as a function of time,

$$C_r^{mm}(t) = \frac{\chi}{D} \frac{1}{L} \sum_q e^{-iqr} e^{-D\omega_q t} \left(1 + \frac{\omega_q}{2}\right). \tag{2.108}$$

To calculate the large-time asymptotics, we express the above expression by setting $r = 0$ and write it in an integral form as

$$C_0^{mm}(t) \simeq \frac{\chi}{\pi D} \int_0^\pi dq e^{-D\omega(q)t} \left[1 + \frac{\omega(q)}{2}\right]. \tag{2.109}$$

We approximate $\omega(q) \approx q^2$, perform a variable transformation $z = Dtq^2$ and simplify the above equation as

$$C_0^{mm}(t) \simeq \frac{\chi}{\pi D\sqrt{4Dt}} \int_0^\pi z^{-\frac{1}{2}} e^{-z} dz, \tag{2.110}$$

where the subleading term $O(t^{-3/2})$ is neglected. By using the integral $\int_0^\infty z^{-\frac{1}{2}} e^{-z} dz = \sqrt{\pi}$ in the above equation, we obtain the desired asymptotic expression,

$$C_0^{mm}(t) \simeq \frac{\chi}{D\sqrt{4\pi D}} t^{-1/2}. \tag{2.111}$$

We now consider a subsystem of size $l < L$ with a total mass $M_l(t) = \sum_{i=0}^{l-1} m_i(t)$ and calculate the unequal-time correlation function $C^{M_l M_l}(t, 0) \equiv C^{M_l M_l}(t)$ for subsystem mass,

$$C^{M_l M_l}(t) = \left\langle \sum_{i=0}^{l-1} m_i(t) \sum_{j=0}^{l-1} m_j(0) \right\rangle_c. \tag{2.112}$$

Upon simplifying the above equation, we obtain the following identity

$$C^{M_l M_l}(t) = l C_0^{mm}(t) + \sum_{r=1}^{l-1} (l - r) \left[C_r^{mm}(t) + C_{-r}^{mm}(t)\right]. \tag{2.113}$$

After substituting Eq.(2.108) into the above equation and by performing some algebraic manipulations, we arrive at the expression,

$$C^{M_l M_l}(t) = \frac{\chi}{D} \frac{1}{L} \sum_q e^{-D\omega_q t} \left(1 + \frac{\omega_q}{2}\right) \frac{\omega_{lq}}{\omega_q}. \tag{2.114}$$

Now, we derive the asymptotic behavior of the dynamic correlation function $C^{M_l M_l}(t)$ for subsystem mass, which appeared in Eq.(2.114). At time $t = 0$, it takes a maximum value and, subsequently, it decays as a function of time t. To extract the time

dependence, we isolate $C^{M_l M_l}(t)$ by subtracting it from its maximum value and then express the equation in an approximate integral form as

$$C^{M_l M_l}(0) - C^{M_l M_l}(t) \simeq \frac{2\chi}{\pi D} \int_0^\pi dq \left[1 - e^{-D\omega(q)t}\right] \left[1 + \frac{\omega(q)}{2}\right] \frac{1}{\omega(q)}. \tag{2.115}$$

Again, by approximating $\omega(q) \approx q^2$ and performing a variable transformation $z = Dtq^2$, we simplify the above equation in the leading order as

$$C^{M_l M_l}(0) - C^{M_l M_l}(t) \simeq \frac{\chi\sqrt{t}}{\pi\sqrt{D}} \int_0^\infty z^{-3/2}(1 - e^{-z})dz. \tag{2.116}$$

By using $\int_0^\infty z^{-3/2}(1 - e^{-z})dz = 2\sqrt{\pi}$, we obtain the asymptotic expression of the dynamic correlation function for the subsystem mass,

$$C^{M_l M_l}(t) - C^{M_l M_l}(0) \simeq -\frac{2\chi}{\sqrt{\pi D}} t^{1/2}. \tag{2.117}$$

We can also calculate the power spectrum of subsystem mass fluctuation $S_{M_l}(f)$ by calculating the Fourier transform of Eq. (2.114),

$$S_{M_l}(f) = \lim_{T\to\infty} \int_{-T}^{T} dt\ C^{M_l M_l}(t, 0) e^{2\pi i f t}. \tag{2.118}$$

Upon performing the aforementioned integration, we derive the desired expression for the power spectrum,

$$S_{M_l}(f) = \frac{2\chi}{L} \sum_q \left(1 + \frac{\omega_q}{2}\right) \frac{\omega_{lq}}{\omega_q^2 D^2 + 4\pi^2 f^2}, \tag{2.119}$$

where $\omega_q = 2(1 - \cos q)$, with $q = 2\pi n/L$ and $n = 1, 2, \cdots, L-1$. We then obtain another scaling function, denoted as $\mathcal{F}$, that connects, for large $f^{-1}, L \gg 1$, the power spectrum $S_{M_l}(f)$ to a scaled frequency as

$$\lim_{f^{-1},L\to\infty} \mathcal{F}\left(\frac{L^2 f}{D}\right) = \frac{D^2}{2\chi L^3} S_{M_l}(f) = \lim_{f^{-1},L\to\infty} \sum_q \left(1 + \frac{\omega_q}{2}\right) \frac{\omega_{lq}}{L^4\omega_q^2 + 4\pi^2 (L^2 f/D)^2}, \tag{2.120}$$

where the scaling function can be well approximated through the following integral representation,

$$\mathcal{F}(\tilde{y}) \simeq \lim_{L\to\infty} \frac{L}{\pi} \int_{2\pi/L}^{\pi} dq \left[1 + \frac{\omega(q)}{2}\right] \frac{\omega(lq)}{4\pi^2\tilde{y}^2 + L^4\omega(q)^2}. \tag{2.121}$$

For large subsystem size $1 \ll l < L$, the function $\omega(lq)$ exhibits high-frequency oscillations with values in the range of $[0, 4]$, leading to an approximation of $\omega(lq) \approx 2$. Additionally, we use the transformation $z = \omega(q)L^2$ and then by taking $L \to \infty$, we obtain the following expression of the scaling function,

$$\mathcal{F}(\tilde{y}) \simeq \frac{1}{4\pi^3\tilde{y}^2} \int_0^\infty \frac{dz}{z^{1/2}\left(1 + \frac{z^2}{4\pi^2\tilde{y}^2}\right)}, \tag{2.122}$$

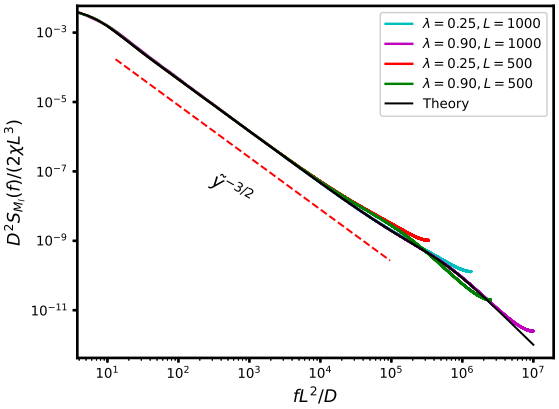

Figure 2.6: The scaled subsystem mass power spectrum, $D^2\tilde{S}_{M_l}(f)/(2\chi L^3)$, in the steady state is plotted as a function of the scaled frequency $L^2 f/D$ for various chipping parametre and system sizes. The lines, colored cyan ($\zeta = 0.25$, $L = 1000$), magenta ($\zeta = 0.90$, $L = 1000$), red ($\zeta = 0.25$, $L = 500$), and green ($\zeta = 0.90$, $L = 500$), represent simulation data, all obtained at a global density of $\bar{\rho} = 1$. In the low-frequency range, the red dashed line demonstrates a scaling behavior of $\mathcal{F}(\tilde{y})$ as $\tilde{y}^{-3/2}$ [as in Eq.(2.123)]. The black solid line corresponds to theoretical predictions [as mentioned in Eq.(2.120)].

which, after evaluating the integral, leads to the asymptotic form of the scaled power spectrum of the subsystem mass fluctuation,

$$\mathcal{F}(\tilde{y}) \simeq \frac{(\tilde{y}\pi)^{-3/2}}{4}. \tag{2.123}$$

The above equation implies that, in a low-frequency regime, the power spectrum of the subsystem mass displays a power-law behavior $f^{-\psi_M}$ with an exponent of $\psi_M = 3/2$. It is also evident that, in the temporal domain, the correlation of the subsystem mass $\langle M_l(t)M_l(0)\rangle_c$ scales as $t^{\psi_M - 1}$, which is, interestingly, a $t^{1/2}$ power-law growth.

In Fig. 2.6, we plot the scaled power spectrum $D^2\tilde{S}_{M_l}(f)/(2\chi L^3)$ for subsystem mass as a function of the scaled frequency $L^2 f/D$ for various chipping parameters and system sizes, along with theoretical predictions provided there as black solid line for comparison purpose. The power spectrum exhibits a power-law scaling in the low-frequency range, with the red dashed line indicating a $\tilde{y}^{-3/2}$ behavior. The simulation results (solid colored lines) are in excellent agreement with the theoretical predictions (black solid line).

2.4 Model: MCM II

In this section, we apply the theoretical framework developed in the previous sections for calculating various dynamic quantities for MCM II and present the significant findings for the system.

2.4.1 Time-integrated current fluctuation

The time-integrated bond-current fluctuation for MCM II is described by the expression as given in eq. (2.124). In this case, the strength of the fluctuating current is characterized by $\Gamma_r = 2\chi\delta_{0,r}$, where the bulk diffusion coefficient is given by $D = \tilde{\zeta}/4$ and the density-dependent mobility $\chi(\bar{\rho}) = \tilde{\zeta}^2\bar{\rho}^2/2(3-2\tilde{\zeta})$ remains identical to that for MCM I [see Eqs. (2.31) and (2.32)]. It is worth mentioning that, for MCM II, both the steady-state density correlation C_r^{mm} and the strength of the fluctuating current Γ_r are delta-correlated, indicating the absence of nearest-neighbor correlations (see Table I for comparison between models); also Γ_r and C_r^{mm} are related by a scaling factor (the bulk diffusivity D) as given in Eq.(2.34), and this particular relationship holds true for this model as well.

For MCM II, we proceed to calculate the second cumulant or the variance $\langle \mathcal{Q}_i^2(T)\rangle_c = \langle \mathcal{Q}_i^2(T)\rangle = C_0^{QQ}(t,t)$ of time-integrated bond-current fluctuation in the steady-state for equal time $t' = t = T$ and in the same space, i.e., $r = 0$. The resulting expression is as follows:

$$\langle \mathcal{Q}_i^2(T)\rangle = \frac{2\chi T}{L} + \frac{2\chi}{L}\sum_{n=1}^{L-1}\frac{(1-e^{-D\omega_n T})}{D\omega_n}, \tag{2.124}$$

where $\omega_n = 2(1-\cos(2\pi n/L))$, with $n = 1, \cdots, L-1$. If we take the $T \to \infty$ limit first in the above equation, we get the following expression,

$$\langle \mathcal{Q}_i^2(T)\rangle \simeq \frac{2\chi T}{L} + \frac{\chi L}{6D} = \frac{2\chi T}{L}\left[1 + \mathcal{O}\left(\frac{L^2}{DT}\right)\right]. \tag{2.125}$$

It is worth noting that the term $\chi L/6D$ in the above equation can be neglected since the leading contribution will arise from the term $2\chi T/L$ as $T \gg L^2$. In the smaller time regime where $DT \ll 1$, Eq.(2.124) can be simplified as

$$\langle \mathcal{Q}_i^2(T)\rangle = \Gamma_0 T = 2\chi T, \tag{2.126}$$

where the strength of the fluctuating current Γ_0 is equal to 2χ, which differs from the value in the case of MCM I (as demonstrated in Eq.(2.33)). Furthermore, in the regime where $DT \gg 1$, we find that the scaling function $\mathcal{W}(y)$, with the scaling variable $y = DT/L^2$, has the exactly same form as presented in Eq.(2.67), as found in MCM I. In left panel of Figure 2.7, We plot the second cumulant or the variance of time-integrated bond-current, $\langle \mathcal{Q}_i^2(T)\rangle_c = \langle \mathcal{Q}_i^2(T)\rangle$, as a function of time T. We highlight the early-time behavior of $\langle \mathcal{Q}^2(T)\rangle$, which scales as $\Gamma_0 T$ and is described in Eq.(2.126). Additionally, in the right panel of the figure, we plot the scaled fluctuation $\langle \mathcal{Q}_i^2(T)\rangle D/(2\chi L)$ of the time-integrated bond current as a function of the scaled time DT/L^2. We include guiding lines that illustrate the asymptotic behavior of the scaling function $\mathcal{W}(y)$. Thus the overall behavior for the temporal growth of the time-integrated bond-current fluctuation exhibits three distinct (asymptotic) regimes:

$$\langle \mathcal{Q}_i^2(T)\rangle = \begin{cases} 2\chi T & \text{for } DT \ll 1 \\ \frac{2\chi}{\sqrt{D\pi}}T^{1/2} & \text{for } 1 \ll DT \ll L^2 \\ \frac{2\chi}{L}T & \text{for } DT \gg L^2. \end{cases} \tag{2.127}$$

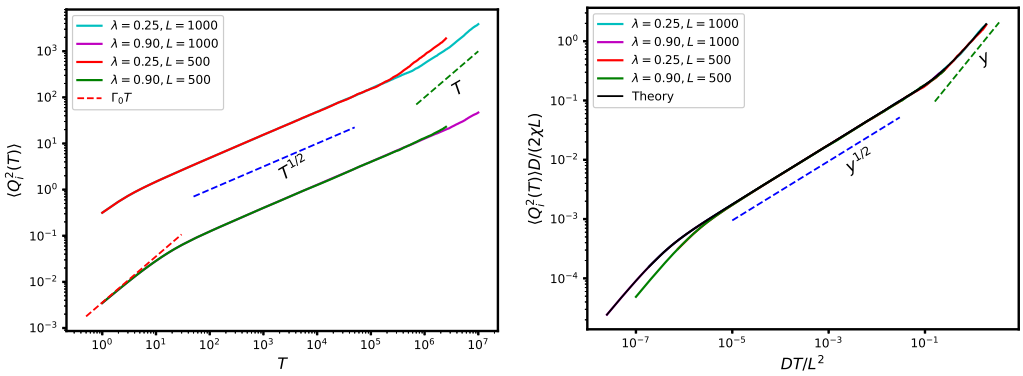

Figure 2.7: *Left panel:* We plot the second cumulant, or the variance, $\langle \mathcal{Q}_i^2(T) \rangle_c = \langle \mathcal{Q}_i^2(T) \rangle$ of time-integrated bond-current in the steady state as a function of time T for various chipping parameters and system sizes. For both this panel, the cyan ($\zeta = 0.25$, $L = 1000$), magenta ($\zeta = 0.90$, $L = 1000$), red ($\zeta = 0.25$, $L = 500$), and green ($\zeta = 0.90$, $L = 500$) lines represent simulation data at a global density of $\bar{\rho} = 1$. The red dashed line corresponds to the behavior $\Gamma_0 T$ for $\zeta = 0.90$ (refer to Eq.(2.126)), while the blue and green dashed lines represent sub-diffusive growth, approximately scaling as $\sim T^{1/2}$, and diffusive growth, approximately scaling as $\sim T$, respectively, as discussed in Eq.(2.127) *Right panel:* We plot the scaled time-integrated bond-current fluctuation, $\langle \mathcal{Q}_i^2(T) \rangle D/(2\chi L)$, in the steady state as a function of scaled time DT/L^2 for various chipping parameters and system sizes. The two dashed lines serve as a guide, indicating that $\mathcal{W}(y)$ exhibits sub-diffusive growth $\sim y^{1/2}$ (in blue) at early (hydrodynamic) times, followed by diffusive growth as $\sim y$ (in green) at long times [as in Eq.(2.69)]. The solid color lines illustrate the simulation results, while the black solid line represents the theoretical results obtained from Eq.(2.124) upon suitable scaling.

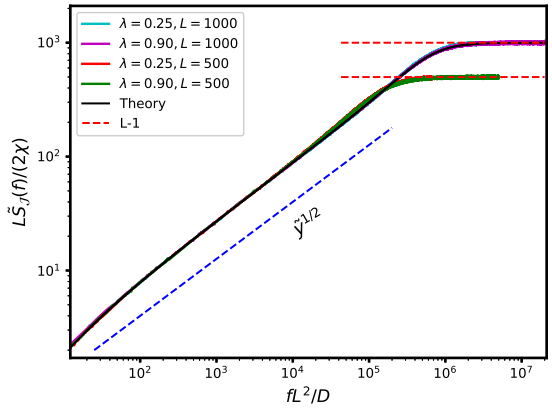

Figure 2.8: The scaled power spectrum of instantaneous current, $L\tilde{S}_{\mathcal{J}}(f)/(2\chi)$, in the steady state is plotted as a function of scaled frequency $L^2 f/D$ for various chipping parameters and system sizes. The cyan solid line corresponds to $\zeta = 0.25$ and $L = 1000$, the magenta solid line corresponds to $\zeta = 0.90$ and $L = 1000$, the red solid line corresponds to $\zeta = 0.25$ and $L = 500$, and the green solid line corresponds to $\zeta = 0.90$ and $L = 500$, all at a global density of $\bar{\rho} = 1$. The blue dashed line shows $\tilde{y}^{1/2}$ scaling behavior in the low-frequency regime as in Eq.(2.97) and red dashed lines represent $L\tilde{S}_{\mathcal{J}}(f)/(2\chi)$ diverges as system size $L-1$ at the high-frequency limit. The solid color lines represent the simulation results, while the black solid line represents the theoretical predictions of Eq.(2.128) upon suitable scaling.

2.4.2 Instantaneous bond-current fluctuations

Using the theory presented in Section 2.3, we also compute the power spectrum of the instantaneous bond current $\mathcal{J}_i(t)$ in MCM II. The expression for the power spectrum can be written as

$$\tilde{S}_{\mathcal{J}}(f) = \frac{2\chi(\bar{\rho})}{L} \sum_{q} \frac{4\pi^2 f^2}{D^2\omega_q^2 + 4\pi^2 f^2}, \tag{2.128}$$

where $\omega_q = 2(1 - \cos q)$ with $q = 2\pi n/L$ and $n = 1, 2, \cdots, L-1$. The above expression exhibits an asymptotic behavior $\mathcal{H}(\tilde{y}) \sim \tilde{y}^{1/2}$ in the low-frequency regime, quite similar to that for MCM I as mentioned in Eq.(2.97). Furthermore, $\mathcal{H}(\tilde{y})$ diverges as $L-1$ in the limit $\tilde{y} \to \infty$ (i.e., for $T \gg L^2$).

In Figure 2.8, the scaled power spectrum $L\tilde{S}_{\mathcal{J}}(f)/(2\chi)$ of the instantaneous bond current is plotted against the scaled frequency $L^2 f/D$. Simulation and theoretical results are found to be in excellent agreement with each other. Additionally, in the low-frequency range, we have included a guiding line $\sim \tilde{y}^{1/2}$, which is obtained from the integral representation of Eq.(2.128). This behavior is consistent with what was mentioned earlier in the context of MCM I.

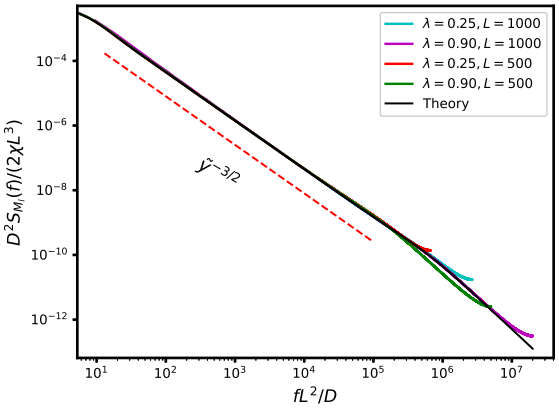

Figure 2.9: The scaled subsystem mass power spectrum, $D^2\tilde{S}_{M_l}(f)/(2\chi L^3)$, in the steady state is plotted as a function of scaled frequency $L^2 f/D$ for various chipping parametre and system sizes. The cyan solid line corresponds to $\zeta = 0.25$ and $L = 1000$, the magenta solid line corresponds to $\zeta = 0.90$ and $L = 1000$, the red solid line corresponds to $\zeta = 0.25$ and $L = 500$, and the green solid line corresponds to $\zeta = 0.90$ and $L = 500$, all at a global density of $\bar{\rho} = 1$. The red dashed line shows a $\tilde{y}^{-3/2}$ scaling behavior in the low-frequency regime. The solid color lines represent the simulation results, while the black solid line represents the theoretical predictions of Eq.(2.129) upon suitable scaling, which matches the simulation data.

2.4.3 Subsystem mass fluctuations

For MCM II, we compute another time-dependent quantity - the power spectrum $S_{M_l}(f)$ for subsystem mass,

$$S_{M_l}(f) = \frac{2\chi}{L} \sum_q \frac{\omega_{vq}}{\omega_q^2 D^2 + 4\pi^2 f^2}. \tag{2.129}$$

We can now calculate the scaling function $\mathcal{F}(\tilde{y})$ associated with the above-mentioned power spectrum of subsystem mass. Notably, it exhibits a $\tilde{y}^{-3/2}$ power-law behavior in the low-frequency regime, similar to that observed in the case of MCM I mentioned in Eq.(2.123). In Figure 2.9, the scaled subsystem-mass power spectrum $D^2\tilde{S}_{M_l}(f)/(2\chi L^3)$ is plotted against the scaled frequency $L^2 f/D$ for various chipping parameters and system sizes. The red dashed line exhibits a $\tilde{y}^{-3/2}$ power-law behavior in the low-frequency regime. The solid color lines represent the simulation results and the black solid line corresponds to the theoretical predictions from Eq.(2.129), which matches quite well with the simulation data when suitably scaled.

2.5 MCM III

In this section, we compute the dynamic correlations for current and mass in the case of MCM III, which has been extensively investigated in the past, to explain wealth distribution in a population [21, 58, 59]. It is worth noting that, upon appropriate scaling, the dynamic correlations for MCM III turn out to be similar to those for

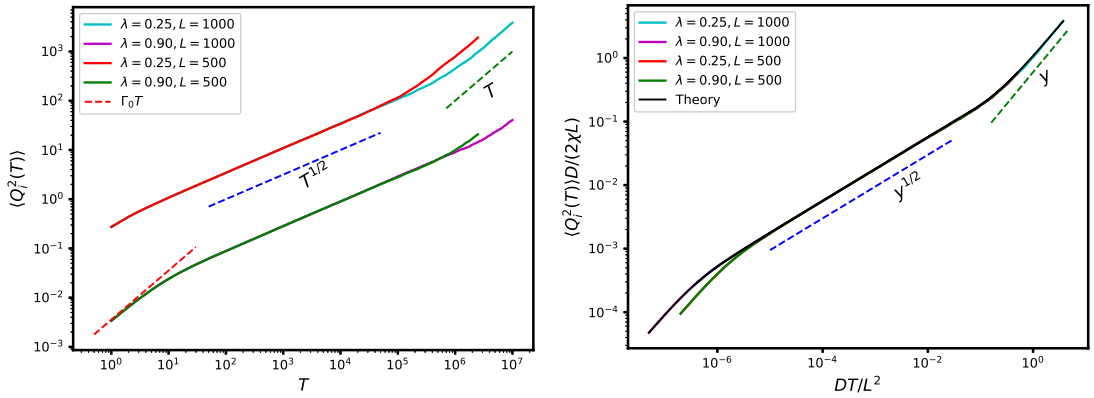

Figure 2.10: *Left panel:* The second cumulant, or the variance, $\langle \mathcal{Q}_i^2(T)\rangle_c = \langle \mathcal{Q}_i^2(T)\rangle$ of time-integrated bond-current in the steady state is plotted as a function of time T for various chipping parameter and system sizes. For both this panel, the cyan ($\zeta = 0.25$, $L = 1000$), magenta ($\zeta = 0.90$, $L = 1000$), red ($\zeta = 0.25$, $L = 500$), and green ($\zeta = 0.90$, $L = 500$) lines represent simulation data for global density $\bar{\rho} = 1$. The red dashed line represents the behavior $\Gamma_0 T$ for $\zeta = 0.90$ [see Eq(2.126)], while the blue and green dashed lines represent sub-diffusive $T^{1/2}$ and diffusive T growth, respectively, as mentioned in Eq.(2.127). *Right panel:* The plot shows the scaled time-integrated bond-current fluctuation, $\langle \mathcal{Q}_i^2(T)\rangle D/(2\chi L)$, in the steady state as a function of scaled time DT/L^2 for different chipping parameter and system sizes. The two dashed lines serve as guides, indicating that $\mathcal{W}(y)$ exhibits sub-diffusive $y^{1/2}$ growth (blue) at early times, followed by diffusive y growth (green) at later times [as in Eq.(2.69)]. Solid-color lines represent simulations, while the black solid line represents the theoretical prediction obtained from Eq.(2.124), which perfectly matches the simulation data when suitably scaled.

MCM II, due to the fact that both these models exhibit similar density correlations (with vanishing neighboring correlations).

2.5.1 Time-integrated current fluctuation

The time-integrated bond current fluctuation in MCM III takes an identical form to that of MCM II, as shown in Eq.(2.124). Indeed the strength Γ_0 of the fluctuating current and the particle χ are the same as in MCM II. Also the bulk diffusivity $D = \tilde{\zeta}/2$ for MCM III is again independent of density.

In left panel of Figure 2.10, we plot the second cumulant or the variance of time-integrated bond-current, $\langle \mathcal{Q}_i^2(T)\rangle_c = \langle \mathcal{Q}_i^2(T)\rangle$, as a function of time T in the steady state. The early-time behavior of $\langle \mathcal{Q}_i^2(T)\rangle$, which scales as $\Gamma_0 T$ according to Eq.(2.126), is highlighted. In the right panel, we plot the scaled fluctuation of the time-integrated current, $\langle \mathcal{Q}_i^2(T)\rangle D/(2\chi L)$, as a function of scaled time DT/L^2. Solid color lines represent simulation results, while the black solid line represents the theoretical prediction obtained from Eq.(2.124), which agrees well with the simulation data when appropriately scaled. Guiding lines illustrate the asymptotic behavior of the scaling function $\mathcal{W}(y)$.

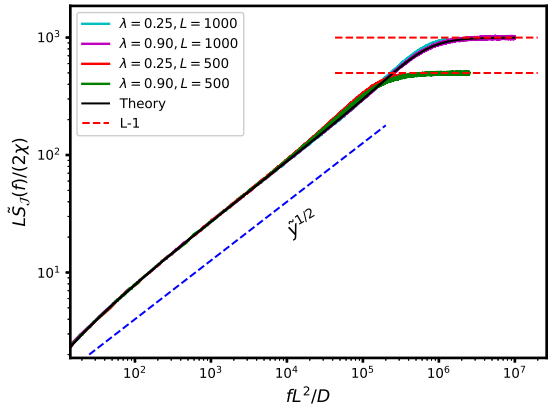

Figure 2.11: The scaled power spectrum of instantaneous current, $L\tilde{S}_{\mathcal{J}}(f)/(2\chi)$, in the steady state is plotted as a function of scaled frequency $L^2 f/D$ for various chipping parameters and system sizes. The cyan solid line corresponds to $\zeta = 0.25$ and $L = 1000$, the magenta solid line corresponds to $\zeta = 0.90$ and $L = 1000$, the red solid line corresponds to $\zeta = 0.25$ and $L = 500$, and the green solid line corresponds to $\zeta = 0.90$ and $L = 500$, all at a global density of $\bar{\rho} = 1$. The blue dashed line shows $\tilde{y}^{1/2}$ scaling behavior in the low-frequency regime and the red dashed lines represent the power spectrum diverges as $L - 1$ at the high-frequency limit. The solid color lines represent the simulation results, while the black solid line represents the theoretical predictions of Eq.(2.128) upon suitable scaling, which fully matches the simulation data.

2.5.2 Instantaneous bond-current fluctuations

For MCM III, the power spectrum of instantaneous bond current exhibits the same form as mentioned in Eq.(2.128), with $D = \tilde{\zeta}/2$ and the particle mobility $\chi(\bar{\rho}) = \tilde{\zeta}^2\bar{\rho}^2/2(3-2\tilde{\zeta})$ being the same as above mentioned MCMs (MCM I and MCM II). In Fig. 2.11, the scaled power spectrum $L\tilde{S}_{\mathcal{J}}(f)/(2\chi)$ of the instantaneous bond current is plotted against the scaled frequency $L^2 f/D$. Both simulation and theoretical results are shown to have an excellent agreement with each other. Additionally, in the low-frequency range, we have included a guiding line $\sim \tilde{y}^{1/2}$; this particular behavior is consistent with what was mentioned earlier in the context of MCM I [see Eq.(2.97)].

2.5.3 Subsystem Mass fluctuations

In this section, we discuss the subsystem-mass power spectrum, which has the same form as in Eq.(2.129). In Figure 2.12, we plot the scaled subsystem mass power spectrum, denoted as $D^2\tilde{S}_{M_l}(f)/(2\chi L^3)$, against the scaled frequency $L^2 f/D$ for various chipping parameters and system sizes. Solid color lines represent simulation results, and the black solid line corresponds to theoretical predictions from Eq.(2.129), in agreement with the simulation data when suitably scaled. The red dashed line shows a $\tilde{y}^{-3/2}$ scaling behavior at low frequencies, as in MCM I [see Eq.(2.123)].

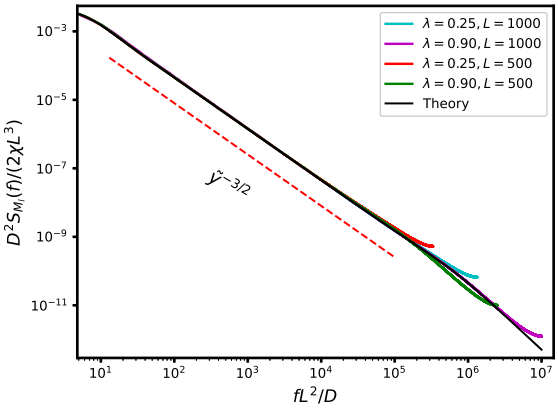

Figure 2.12: The scaled subsystem mass power spectrum, $D^2\tilde{S}_{M_l}(f)/(2\chi L^3)$, in the steady state is plotted as a function of scaled frequency $L^2 f/D$ for various chipping parameter and system sizes. The cyan solid line corresponds to $\zeta = 0.25$ and $L = 1000$, the magenta solid line corresponds to $\zeta = 0.90$ and $L = 1000$, the red solid line corresponds to $\zeta = 0.25$ and $L = 500$, and the green solid line corresponds to $\zeta = 0.90$ and $L = 500$, all at a global density of $\bar{\rho} = 1$. The red dashed line shows a $\tilde{y}^{-3/2}$ scaling behavior in the low-frequency regime. The solid color lines represent the simulation results, while the black solid line represents the theoretical prediction from Eq.(2.129) upon suitable scaling.

2.6 Comparison of models

In this section, we perform a comparative study of various dynamical quantities for the three models studied in this chapter: MCM I, MCM II, and MCM III. In particular, we do a comparative investigation of the scaled variance of time-integrated bond-current described by the scaling function $\mathcal{W}(y)$ with y being the scaled time $y = DT/L^2$, the scaled power spectrum of instantaneous currents $\mathcal{H}(\tilde{y})$, and the scaled subsystem mass power spectrum $\mathcal{F}(\tilde{y})$ with $\tilde{y}$ being the scaled frequency $\tilde{y} = fL^2/D$. In Fig. (2.13), we plot the above-mentioned dynamical quantities as a function of the scaled time and frequencies. Remarkably, despite the different microscopic dynamical rules, there exists a universal scaling regime where all three models, in fact, exhibit the same behavior, where the subdiffusive and diffusive growth of bond-current variance are connected through the same scaling function. However, outside the scaling regime, the temporal growth of the variance of the bond current is linear in time, though the prefactors are different in different models. These differences are accurately captured in both the simulations and the corresponding theoretical predictions, providing insights into the quantitatively different dynamical properties of current fluctuations at small scales.

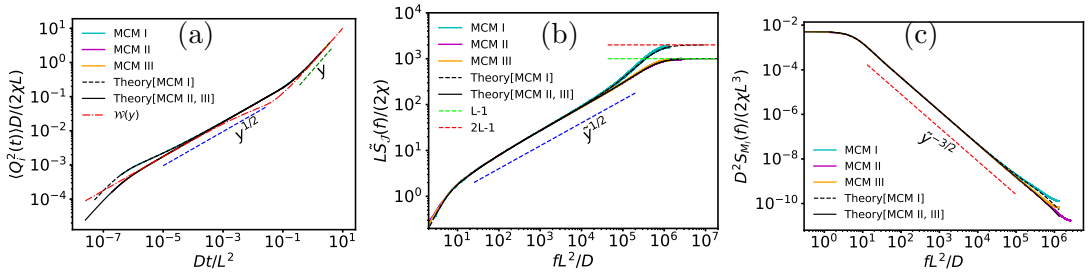

Figure 2.13: Panel (a): Scaled time-integrated bond-current fluctuation, $\langle \mathcal{Q}_i^2(T)\rangle D/(2\chi L)$, as a function of scaled time DT/L^2 for MCM I (blue solid line), MCM II (magenta solid line), and MCM III (orange solid line) in the steady state. The two dashed lines serve as guides, indicating that $\mathcal{W}(y)$ (red dashed; see Eq. (2.67)) exhibits sub-diffusive behavior as $\sim y^{1/2}$ (in blue) at early times, followed by diffusive growth as $\sim y$ (in green) at later times. Panel (b): Scaled power spectrum of instantaneous currents, $L\tilde{S}_{\mathcal{J}}(f)/(2\chi)$, in the steady state is plotted as a function of scaled frequency $L^2 f/D$ for various chipping parameter and system sizes. The blue dashed line represents the $\tilde{y}^{1/2}$ scaling behavior of $\mathcal{H}(\tilde{y})$ in the low-frequency regime. In contrast, the power spectrum exhibits divergence, reaching $2L-1$ (red dashed line) for MCM I and $L-1$ (lime dashed line) for MCM II and MCM III in the high-frequency limit. Panel (c): Scaled subsystem mass power spectrum, $D^2\tilde{S}_{M_l}(f)/(2\chi L^3)$, in the steady state, is plotted as a function of scaled frequency $L^2 f/D$ for various chipping parameters and system sizes. The red dashed line shows a $\tilde{y}^{-3/2}$ scaling behavior of $\mathcal{F}(\tilde{y})$ in the low-frequency regime. In all of these panels, we have used a fixed chipping parameter $\zeta = 0.5$, global density $\bar{\rho} = 1.0$, and a system size of $L = 1000$. Simulation data for MCM I, MCM II, and MCM III are represented by blue, magenta, and orange solid lines, respectively. Black dashed lines correspond to theory for MCM I, while black solid lines represent theory for MCM II and MCM III, respectively.

We provide in Table 2.1 a concise description concerning the similarities and differences among the three models, in terms of their time-dependent properties. To begin with, we highlight the transport coefficients - the bulk-diffusion coefficient D and the particle mobility $\chi(\bar{\rho})$ for each model. Notably, D is constant (independent of density) for all three models; however, the mobility χ is density dependent (proportional to the square of the density). The table displays the density correlation function C_r^{mm} for these models. MCM I possesses finite (nonzero) nearest-neighbor spatial correlations, whereas MCM II and MCM III lack such correlations. The table also presents the strength Γ_r of fluctuating ("noise") current for the models, with each of the models having a distinct value. However, it is important to note that the relationship $\Gamma_r = C_r^{mm}/2D$ holds true for all models; presumably this relation is valid for diffusive systems in general. Lastly, the table compares the source term A_r appearing in the time-evolution equation for the mass-current correlation function, where the Fourier mode $\tilde{f}_q$ of the quantity A_r is useful in explicitly calculating various dynamic quantities).

Quantity	**MCM I**	**MCM II**	**MCM III**
Bulk-diffusion coefficient $\mathbf{D}$	$\frac{\tilde{\zeta}}{2}$	$\frac{\tilde{\zeta}}{4}$	$\frac{\tilde{\zeta}}{2}$
Mobility χ	$\frac{\tilde{\zeta}^2}{2(3-2\tilde{\zeta})}\bar{\rho}^2$	$\frac{\tilde{\zeta}^2}{2(3-2\tilde{\zeta})}\bar{\rho}^2$	$\frac{\tilde{\zeta}^2}{2(3-2\tilde{\zeta})}\bar{\rho}^2$
Density correlation function $\mathbf{C^{mm}_r}$	$\frac{\tilde{\zeta}}{2(3-2\tilde{\zeta})}\bar{\rho}^2[4\delta_{0,r}-\delta_{r,1}-\delta_{r,-1}]$	$\frac{2\tilde{\zeta}}{(3-2\tilde{\zeta})}\bar{\rho}^2\delta_{0,r}$	$\frac{\tilde{\zeta}}{(3-2\tilde{\zeta})}\bar{\rho}^2\delta_{0,r}$
$\mathbf{\Gamma_r}$	$\frac{\tilde{\zeta}^2}{2(3-2\tilde{\zeta})}\bar{\rho}^2[4\delta_{0,r}-\delta_{r,1}-\delta_{r,-1}]$	$\frac{\tilde{\zeta}^2}{(3-2\tilde{\zeta})}\bar{\rho}^2\delta_{r,0}$	$\frac{\tilde{\zeta}^2}{(3-2\tilde{\zeta})}\bar{\rho}^2\delta_{r,0}$
$\mathbf{A_r}$	$\frac{\tilde{\zeta}^2}{4(3-2\tilde{\zeta})}\bar{\rho}^2[-5(\delta_{r,0}-\delta_{r,-1})+(\delta_{r,1}-\delta_{r,-2})]$	$-\frac{1}{2}\frac{\tilde{\zeta}^2}{(3-2\tilde{\zeta})}\bar{\rho}^2(\delta_{r,0}-\delta_{r,-1})$	$-\frac{1}{2}\frac{\tilde{\zeta}^2}{(3-2\tilde{\zeta})}\bar{\rho}^2(\delta_{r,0}-\delta_{r,-1})$
$\tilde{\mathbf{f}}_\mathbf{q}$	$-\frac{\tilde{\zeta}^2}{2(3-2\tilde{\zeta})}\bar{\rho}^2(1-e^{-iq})\left(1+\frac{w_q}{2}\right)$	$-\frac{\tilde{\zeta}^2}{2(3-2\tilde{\zeta})}\bar{\rho}^2(1-e^{-iq})$	$-\frac{\tilde{\zeta}^2}{2(3-2\tilde{\zeta})}\bar{\rho}^2(1-e^{-iq})$

Table 2.1: We highlight various key quantities, which are explicitly required to calculate the steady-state dynamical correlations in MCM I, MCM II, and MCM III. These quantities are the transport coefficients, such as the bulk-diffusion coefficient D and the mobility χ, and, additionally, density correlation function C_r^{mm}, strength Γ_r of fluctuating current, the source term A_r in time-evolution equation for (equal-time) mass-current correlation function, and its Fourier mode $\tilde{f}_q$.

2.7 Summary and Conclusion

In this chapter, we exactly calculate the steady-state dynamic correlation functions for mass and current in a broad class of conserved-mass transport processes, called mass chipping models (MCMs), on a one-dimensional ring. All of these systems, for which our analytical scheme should work, share the following simplifying feature: The mass-chipping rates in the system are constant and do *not* depend on the departure and destination sites, where the mass is chipped off from or is transferred to, respectively. The crucial consequence of the above feature is that the local diffusive current, being a (discrete) gradient of local mass variable, is *a linear function of local mass*; in other words, the bulk-diffusion coefficient is *independent* of density.

Notably, despite having the aforementioned linearity property, these systems, which are nothing but the variants of the intensively studied many-body systems called the random average processes (RAPs) [16], violate detailed balance in the bulk and, unlike simple exclusion processes (SEPs) and zero range processes (ZRPs), have nontrivial spatial structures even on a periodic lattice. Indeed, in most cases (a notable exception being the Kipnis-Marchioro-Presutti (KMP) model [15]), their steady-state measures (on a ring) are not described by the equilibrium Boltzmann-Gibbs distribution and a priori *not* known. For all variants of MCMs considered here, we find three qualitatively different temporal growth regimes for the fluctuation of the time-integrated bond current in the steady state. For initial times, the time-integrated current fluctuation grows linearly with time T, with a proportionality factor being Γ_0, which, however, is a model-dependent quantity and determined here exactly for each of the models. In the intermediate but large time regime $1/D \ll T \ll L^2/D$, with D being the bulk-diffusion coefficient, we find subdiffusive - $T^{1/2}$ - growth of the bond-current fluctuation, where the density-dependent prefactor of $T^{1/2}$ growth are calculated exactly. This subdiffusive growth is again followed by a linear, or diffusive, growth of current fluctuation in the long-time regime ($T \gg L^2$). Furthermore, by using a microscopic approach, we exactly calculate a *model-independent* scaling function $\mathcal{W}(y) \equiv D\langle \mathcal{Q}_i^2(T)\rangle/2\chi L$ as a function of a scaling variable $y = DT/L^2$, where D, χ and L are the bulk-diffusion coefficient, mobility, and system size L, respectively. It is quite interesting that a single scaling function connects both the intermediate-time subdiffusive and long-time diffusive growths of the time-integrated bond-current fluctuations.

We also analytically calculate the dynamic correlation function for instantaneous bond current. We show that similar to the SEP [78], the correlation function for bond current decays as $t^{-3/2}$ even if the MCMs, unlike the SEP on a periodic domain, have nontrivial spatial structures in bulk. Notably, the correlation function has a delta-correlated part at $t = 0$ and its magnitude for $t > 0$ is in fact negative Despite the fact that there is no restriction on single-site occupancy of mass, i.e., mass at a site is unbounded (unlike the SEP), the negative part of the current correlation function is directly responsible for the subdiffusive growth of the bond current fluctuation in the thermodynamic limit. The power-law behavior of dynamic current correlations is consistent with the exact calculation of the current power spectrum $\tilde{S}_{\mathcal{J}}(f)$, which has a low-frequency asymptotic behavior $\tilde{S}_{\mathcal{J}}(f) \sim f^{\psi_{\mathcal{J}}}$ with $\psi_{\mathcal{J}} = 1/2$. Furthermore, we exactly obtain the scaling function $\mathcal{H}(\tilde{y})$, which represents the rescaled power

spectrum of the current $L\tilde{S}_{\mathcal{J}}(f)/2\chi$ as a function of the scaled variable $\tilde{y} = fL^2/D$.

Furthermore, we compute the scaled subsystem mass fluctuation, which is shown to be identically equal to the suitably scaled dynamic fluctuation of the space-time integrated current $\mathcal{Q}_{sub}(l,T)$, divided by a factor of $2D$, with D being the bulk-diffusion coefficient [see Eq.(2.105)]. This particular fluctuation relation in the context of MCMs is nothing but a nonequilibrium version of the celebrated equilibrium Einstein relation. It should be noted that the fluctuation relation requires the scaled fluctuation of space-time integrated current to be calculated in the thermodynamic limit, i.e., by first taking the infinite subsystem size limit $l \to \infty$, followed by the infinite time limit $T \to \infty$. In this specific order of limits, we also show that $\lim_{l\to\infty}\lim_{T\to\infty}\langle\mathcal{Q}^2_{sub}(l,T)\rangle/lT$ is identically equal to the spatial sum of the strength Γ_r of the fluctuating bond current. As a simple consequence of the Einstein relation, the correlation functions of mass and fluctuating current are related via $C^{mm}_r = \Gamma_r/2D$. We also calculate the unequal-time correlation function of the total mass of a subsystem and its power spectrum S_{M_l}, which decays as $S_{M_l} \sim f^{-\psi_M}$, with $\psi_M = 3/2$, consistent with the scaling relation $\psi_{\mathcal{J}} = 2 - \psi_M$ [42]. The scaled power spectrum of subsystem mass, $D^2S_{M_l}(f)/2\chi L^3$, can also be expressed in terms of a scaling function $\mathcal{F}(\tilde{y})$ with scaling variable $\tilde{y} = fL^2/D$.

Notably, the qualitative behavior of time-integrated bond-current fluctuations for all three models are similar, though the prefactors of the temporal growth laws depend on the details of the dynamical rules. In the small-frequency (large-time) domain, the prefactors of the intermediate-time subdiffusive and long-time diffusive growth of the bond current fluctuations can be expressed in terms of the bulk-diffusion coefficient and the particle mobility. However, the large-frequency behavior is not universal in the sense that it depends on the local microscopic properties. More specifically, the differences in the spatial structures of these models manifest themselves in the small-time growth of the time-integrated bond-current fluctuation $\langle\mathcal{Q}^2_i(T)\rangle \simeq \Gamma_0 T$, where Γ_0 is proportional to the single-site mass fluctuation $\langle m^2_i\rangle$, which is different in these three models.

A few remarks are in order. Characterizing dynamic properties of interacting particle systems through microscopic calculations is an important, though difficult, problem in statistical physics. The variants of mass chipping models discussed here have nontrivial steady states, but they are shown to be still analytically tractable and exact results concerning dynamic correlations could be obtained. As discussed in this chapter, depending on their dynamical rules, these models differ from each other in the details of their spatial structures. Model MCM I possesses nonzero spatial correlations, whereas MCM II and III have vanishing neighboring correlations in the thermodynamic limit. However, as mentioned before, all of these models share one noteworthy aspect in common: The bulk-diffusion coefficient, like in the SEP [78], is *independent* of density (this is, however, not the case for the ZRP [32]). In fact, this is precisely why the hierarchy of current and mass correlations closes, and thus, the current fluctuations in these models are exactly solvable. Of course, one may consider numerous additional versions of MCMs, such as those in which mass is transferred to a given number of neighboring sites, say $2K$ (rather than the case with $K = 1$ considered here). In that situation, the system's correlation length may be extended; however, our overall calculation scheme remains suitable due to an

analogous linearity property as encoded in eq. (2.11). Although the mass chipping models have a nontrivial steady state (unknown, in most cases), these models, due to their simple dynamical rules, do not exhibit a phase transition; in other words, there are no singularities present in the transport coefficients. However, through simple variations in the dynamical rules, it is possible to have nontrivial (singular) macroscopic behavior in some of their variants. We must mention here that, though the large-deviation function for the time-integrated bond current can have singular behavior in case of dynamical phase transition [88], the variance of the same involves only small fluctuation and does not have any singularity as such. Indeed, it would be quite interesting to characterize the dynamic properties of current and mass through microscopic calculations in higher dimensions, for systems with more than one conserved quantity [77], for arbitrary initial conditions [89, 90] (for which the scaling function would presumably be different), and when the transport properties are anomalous, such as in the case of zero-range processes at criticality [32].

3

Mass transport processes with center-of-mass conservation

3.1 Introduction

Recently, there has been a surge of interest in characterizing a remarkable state of matter that is amorphous or disordered, yet correlated and known as "hyperuniform" matter [4]. While they lack true long-range order, these many-body systems exhibit long-wavelength density fluctuations that are anomalously suppressed. First, consider an equilibrium disordered fluid with density ρ in d-dimensional space. In that case, the variance of particle number, or mass, M_l in a large subsystem of volume l^d is equal to $\sigma^2(\rho)l^a$, with $a = d$ following the central limit theorem, where $\sigma^2(\rho)$ is the scaled variance of subsystem mass and is proportional to the compressibility. By tuning parameters like temperature and pressure, one can have a state with the exponent a being larger than the dimension ($a > d$); an example of this scenario is an equilibrium critical point (say, that of water and vapor), where fluctuation, or, equivalently, the compressibility, diverges in the thermodynamic limit. Indeed, the opposite also can happen where, in the presence of interactions, particles in a system can dynamically organize themselves in such a fashion that the subsystem-mass fluctuations are greatly reduced as the subsystem size increases, leading to the vanishing compressibility; these systems are "hyperuniform" as $(d-1) \leq a < d$ [3]. In fact, a perfectly *ordered* crystalline state (achieved only at zero temperature) is hyperuniform where $a = d - 1$; other examples include one-component Coulomb gas [91, 92] and jammed granular matter [3, 7], which are incompressible and hyperuniform. Notably, no *disordered* systems, with short-ranged interactions

This chapter is based on the paper, **Hyperuniformity in mass transport processes with center-of-mass conservation: some exact results**, Animesh Hazra, Anirban Mukherjee and Punyabrata Pradhan, J. Stat. Mech.: Theory Exp. 2025(2), 023201.

and at finite temperature, are however, known to exhibit hyperuniformity in equilibrium; rather, for such systems, hyperuniformity has so far been observed only in nonequilibrium settings [93–101]. As discussed above, spatial correlations within a system are quantified by space-integrated (extensive) observables such as subsystem particle number. Similarly, time-integrated observables, such as cumulative particle flux $\mathcal{Q}(T)$ across a surface in the time interval T, can be used to characterize dynamic correlations. Typically, in one-dimensional diffusive systems with a *single* (say, mass) conservation law, the variance $\mathcal{Q}^2(T)$ of time-integrated current in the thermodynamic limit grows sublinearly with time T, i.e., the temporal growth of $\mathcal{Q}^2(T) \sim T^b$ is subdiffusive with $b = 1/2$ [42, 68, 102, 103]; near criticality though, the exponent b can take other values, less [42, 44] or greater (but, still $b < 1$) [32] than one-half. Similar anomalous growth of time-integrated fluctuations can also happen for various other quantities, such as cumulative displacement of a tagged particle in single-file diffusion where $b = 1/2$ [104] or cumulative activity (or, the avalanche size) in one-dimensional sandpiles where, quite interestingly, $b = 0$ [50]; the latter case ($b = 0$) in fact provides an example of an extreme form of hyperuniformity in time domain, analogous to hyperuniformity exponent $a = d - 1$ in space domain. Indeed, the subdiffusive ($b < 1$) temporal growth of the variance of a time-integrated quantity is a manifestation of long-ranged temporal correlations in the system and is called "dynamic hyperuniformity", the notion recently introduced in the context of threshold-activated systems like sandpiles [42, 50]. Exact characterization of such correlations in interacting-particle systems is of relevance also from a general theoretical point of view and has been done in this paper for current fluctuations in nonequilibrium mass transport processes with center-of-mass (CoM) conservation.

Two celebrated models for disordered nonequilibrium systems are the conserved ("fixed-energy") Manna sandpiles [12, 105] and the biased random organization (BRO) [93, 106]. Both the models have been studied in a variety of contexts in the past, including absorbing-phase transition (APT) [36, 105], reversible-irreversible transition in sheared colloids [96, 107], random close packing (RCP) in disordered solids and jamming phenomenon [7, 93, 108–112], etc. Although hyperuniform structures have been envisaged since a long time [3], it was only recently observed that these two models exhibit hyperuniform fluctuations in their (quasi-)nonequilibrium steady states [40, 43, 45, 113, 114]. In the BRO model, provided that they overlap, a pair of particles of, say, unit diameter are given a random kick (displacement) of *identical* magnitude, but in the diametrically *opposite* directions, ensuring that their center of mass remains the same. Consequently, there are two conserved quantities in the system: Total mass and center-of-mass (CoM). Moreover, the microscopic dynamics in the bulk break time-reversal symmetry and the BRO model exhibits hyperuniformity in the so-called "active" phase, which is analogous to the "irreversible" phase of the colloidal system investigated in the experiment [106, 107]. Perhaps not surprisingly, the BRO model is extremely challenging to solve analytically, even in one dimension, due to the nontrivial overlapping condition, which allows for particles hopping only when the particles overlap with each other. Indeed, lately there is a growing interest to develop a rigorous theoretical understanding of how multiple conservation laws determine large-scale properties, concerning density relaxation and current and mass fluctuations, of minimal model systems [51, 115].

In such a scenario, it is highly desirable to examine CoM-conserving models with simpler dynamical rules, allowing the systems to be rigorously dealt with through a microscopic approach.

In one dimension, if the overlapping condition is relaxed and the random displacements depending on the inter-particle gaps are chosen appropriately, the modified model is related to another class of widely studied many-body systems, known as random average processes (RAPs) [9, 14, 16, 20], which consist of interacting particles diffusing on a circle (continuum), but now obeying the (additional) CoM conservation (CoMC). While the particles remain correlated, resulting in a nontrivial spatial structure in the systems, these one-dimensional models allow explicit analytical calculations. For simplicity, in the rest of the paper, we focus on the unbounded versions of these mass transport processes, known as *mass chipping models* (MCMs) [13, 21, 22, 34, 57, 58, 116–118], which are the generalized variants of the Kipnis-Marchioro-Presutti (KMP) models [15, 19] and, in one dimension, can be obtained through an exact mapping [17, 20] of a RAP of L particles on a circle to a system on a ring of L discrete lattice sites having continuous mass. That is, a particle in the RAP can be thought of as a lattice site, and the inter-particle gap is a (continuous) non-negative mass variable assigned to the site; also the dynamical mass transfer rules in the RAP have one-to-one correspondence to the mapped mass transport process. In a related context, an unbounded version of a RAP with an overlapping (threshold) condition, which allows movement of two particles on a line only when the gap between the particles exceed a certain threshold value (the condition differs slightly from that in the BRO model), has received a lot of attention in the last decade. The one-dimensional model is a continuous-mass variant of the discrete-mass Manna sandpile [12, 105], which has been intensively studied to characterize APT with a conserved (density) field [42, 119]. In the MCMs explored here, we do not however impose any threshold condition in microscopic dynamics to make the systems analytically tractable, and consequently the phase transition is lost.

The MCMs break time-reversal symmetry (violating detailed balance) in the bulk for generic parameter values and, consequently, the steady-state probabilities of the microscopic configurations in most cases are not described by the equilibrium Boltzmann-Gibbs distribution and not a-priori known. Throughout the past several decades, they have been extensively studied in the literature in various contexts, such as cloud formation [23], force fluctuation in jammed granular media [57], wealth distribution in a population [21, 116, 120], and traffic flow [27], etc. However, the issue concerning the precise role of an additional conserved quantity, such as CoM, on the relaxation and (static and dynamic) fluctuation properties of these systems has yet to be explored. Indeed, the problem is of general relevance, as there has recently been a surge of interest in characterizing the large-scale properties of systems with multiple conservation laws [115, 121–125], notably in the context of quantum many-body systems like fractonic fluids [126–128].

In this paper, using a microscopic approach, we analytically calculate various static and dynamic correlation functions in a broad class of MCMs having both mass and CoM conservation in $d = 1$ and 2 dimensions (the results can be suitably generalized to arbitrary dimensions). We find that the density relaxation, despite the dynamics being strongly constrained due to the CoM conservation (CoMC), is in

fact diffusive. To substantiate this assertion, we consider, for simplicity, an infinite domain and consider density relaxation by taking a step-like initial density profile $\rho(X, t = 0) = \rho_{in}(X) = \rho_0 + \rho_1$ for $x < 0$ and ρ_0 otherwise. We show the time-dependent relative density profile $\rho(X, t) - \rho_0 = \mathcal{R}(X/\sqrt{t})$ obeys a diffusive scaling, where $\mathcal{R}(z)$ is a scaling function, with the scaled argument $z = X/\sqrt{t}$, and is determined exactly. However, fluctuation properties are strikingly different from that in diffusive systems with a single (mass) conservation law. In the thermodynamic limit, the steady-state second cumulant, or the variance, $\langle \mathcal{Q}^2(T) \rangle_c = \langle \mathcal{Q}^2(T) \rangle - \langle \mathcal{Q}(T) \rangle^2$ of the time-integrated bond current $\mathcal{Q}(T)$ across a bond in the time interval T has the following long-time behavior: $\langle \mathcal{Q}^2(T) \rangle_c = \langle \mathcal{Q}^2(T) \rangle \simeq A_1 T + A_2 + A_3 T^{-d/2}$ (note that $\langle \mathcal{Q}^2(T) \rangle_c = \langle \mathcal{Q}^2(T) \rangle$ as the average bond current $\langle \mathcal{Q}(T) \rangle = 0$ is zero in steady state). The exponents governing the small-frequency behavior of the power spectra $S_J(f) \simeq A_1 + \text{Const.} f^{\psi_J}$ for bond current are exactly determined as $\psi_J = 3/2$ and 2 in $d = 1$ and 2 dimensions, respectively; in d dimensions, we have $\psi_J = (1 + d/2)$. Remarkably, depending on dimensions and microscopic details, the coefficient A_1 can vanish (e.g., for $d = 1$). That is, the variance of time-integrated bond current in the time interval T eventually *saturates* as a function of time T to a density-dependent coefficient $A_2(\rho)$, implying a "dynamic hyperuniformity"; in that case, we have $\langle \mathcal{Q}^2(T) \rangle_c \sim T^b$ with $b = 0$, which signifies an extreme form of hyperuniformity in temporal domain observed previously for avalanche time-series in a one-dimensional sandpile [50]. Furthermore, the long-time (or, equivalently, small-frequency) asymptotics for dynamic (two-point and unequal-time) "cross"-correlation functions for the bond currents in orthogonal directions (e.g., correlations between currents along x and y directions) decay as a power law, where the exponents of the power laws are exactly determined. We also calculate static structure factor $S(q)$, which varies as the square of wave number q in the small-q limit, i.e., $S(q) \sim q^2$ as $q \to 0$. This is a direct consequence of the fact that, in the thermodynamic limit, the spatial integral of the two-point density correlation function for mass is zero in these systems.

We organize the paper as follows. In Sec. 3.2, we introduce a CoM-conserving mass chipping model (MCM), called MCM-CoMC, in one dimension and demonstrate its equivalence to a CoM-conserving random average process (RAP). In Sec. 3.2.1, we derive hydrodynamics of the one-dimensional MCM-CoMC with nearest-neighbor mass transfer; in Sec. 3.2.2, we explore dynamic correlations for the model. In Sec. 3.3, we explore a one-dimensional variant of the MCM-CoMC, which now have microscopic dynamics with finite-range mass transfer. In Secs. 3.4 and 3.5, we introduce a couple of two-dimensional versions of the MCM-CoMCs. We study the asymptotic behavior of the MCM-CoMCs in higher dimensions in Sec. 3.7. Finally, in Sec. 3.8, we summarize the paper with some concluding remarks.

3.2 One-dimensional MCM-CoMC I: Nearest-neighbor mass transfer

In this section, we explore a broad class of conserved-mass transport processes, called mass chipping models (MCMs) [13, 21, 58, 103, 129], where masses fragment, diffuse, and coalesce with the neighboring masses at a constant rate. Because of their analytical tractability, these processes, which are generalized variants of the well-

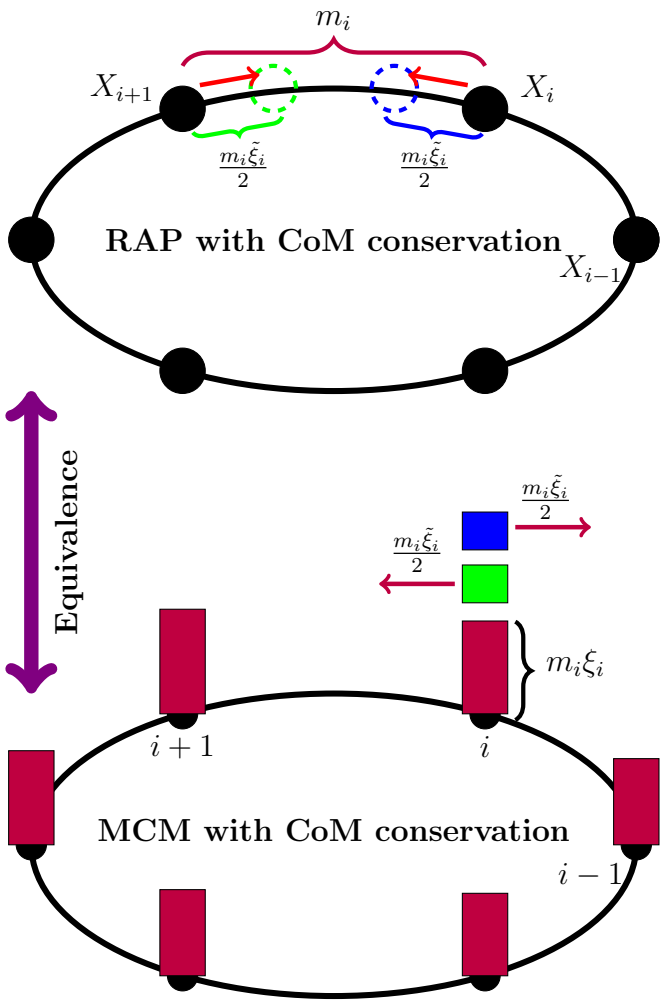

Figure 3.1: *Equivalance between random average process (RAP) and mass chipping model (MCM) with CoM conservation (CoMC) in one dimension through a schematic diagram.* Top panel – *RAP with CoMC*: Two particles (black circles) located at X_i and X_{i+1} are displaced in the opposite directions (inward) by an equal amount, i.e., $m_i\tilde{\xi}_i/2$, where $m_i \equiv X_{i+1} - X_i$ is the inter-particle distance, or gap, between ith and $(i+1)$th particles. Here $\tilde{\xi}_i = (1-\xi_i)$ and ξ_i is a random fraction uniformly distributed in $[0,1]$. Bottom panel – *MCM with CoMC*: A site (represented by a black circle) contains a certain amount of (continuous) mass (dark-violet rectangular bars). During a mass transfer process, a site retains a random fraction ξ_i of its mass m_i, and the remaining fraction of mass, $(1-\xi_i)m_i$, is *equally* divided into two parts, with one being transferred to its left neighbor (green rectangle) and the other to its right neighbor (blue rectangle). In that case, cumulative (time-integrated) current increases by $m_i\tilde{\xi}_i/2$ across bond $(i, i+1)$ and decreases by the same amount across the other bond $(i-1, i)$.

known random average processes (RAPs) [9, 14, 16, 20] or the Kipnis-Marchioro-Presutti (KMP) models [15, 19], have been studied mainly in one dimension in the past. Notably, on a periodic domain, unlike other lattice gases, such as symmetric simple exclusion processes (SSEP) [68, 71] and zero-range processes (ZRPs) [10, 17], MCMs generally violate detailed balance in the bulk due to the broken time-reversal symmetry; consequently, their steady-state measures are in most cases not described by the equilibrium Boltzmann-Gibbs distribution. The detailed definition of a broad class of MCMs, and their connection to other models such as RAPs, can be found in Ref. [103], where relaxation and fluctuation properties have been studied. However, in this work, we impose an *additional* conservation law on the microscopic dynamics, where both mass and center-of-mass (CoM) now remain conserved.

We introduce a model of *MCM with CoM conservation* (MCM-CoMC) and study the role of CoM conservation on the time-dependent (density relaxation and dynamic fluctuation) properties of the system. Let us begin by considering a system on a one-dimensional periodic lattice of size L, where lattice sites are labeled as $i = 0, 1, \ldots, L-1$. A site i is associated with a continuous mass variable $m_i \geq 0$, with the total mass $M = \sum_{i=0}^{L-1} m_i = \rho L$ fixed and ρ being the global density; defining similar CoM-conserving models in higher dimensions d is straightforward and the MCM-CoMCs in $d = 2$ are studied later. We consider a continuous-time process, where mass m_i at site i gets chipped off with unit rate. A random fraction ξ_i of mass m_i is retained and the remaining fraction, $(1 - \xi_i)$, of mass, then gets fragmented in two *equal* halves; one half $(1 - \xi_i)m_i/2$ coalesce with the right-neighbor $(i + 1)$ mass and the other half coalesce with the left-neighbor $(i - 1)$ mass. Evidently, the mass transfer rule locally conserves *mass* as well as *center of mass* (CoM). In Fig. 3.1, we demonstrate the equivalence between two models: the random average process (RAP) with CoM conservation and the mass chipping model (MCM) with CoM conservation. In top panel, we describe a *RAP with CoMC*. In this case, two particles (black circles) located at X_i and X_{i+1} are displaced in the opposite directions (inward) by an equal amount, i.e., $m_i\tilde{\xi}_i/2$, where $m_i \equiv X_{i+1} - X_i$ is the inter-particle distance, or gap, between ith and $(i + 1)$th particles. In bottom panel, we describe a *MCM with CoMC*. In this case, a site (represented by a black circle) contains a certain amount of (continuous) mass (dark-violet rectangular bars). During a mass transfer process, a site retains a random fraction ξ_i of its mass m_i, and the remaining fraction of mass, $(1 - \xi_i)m_i$, is *equally* divided into two parts, with one being transferred to its left neighbor (green rectangle) and the other to its right neighbor (blue rectangle).

For the MCM-CoMC in one dimension, the time evolution of mass at a site i can be expressed in terms of the following infinitesimal-time update rules:

$$m_i(t + dt) = \begin{cases} \textbf{event} & \textbf{prob.} \\ m_i(t) - \tilde{\xi}_i m_i(t) & dt \\ m_i(t) + \frac{\tilde{\xi}_{i+1}}{2} m_{i+1}(t) & dt \\ m_i(t) + \frac{\tilde{\xi}_{i-1}}{2} m_{i-1}(t) & dt \\ m_i(t) & (1 - 3dt), \end{cases} \tag{3.1}$$

where $\tilde{\xi}_i = 1 - \xi_i \in (0, 1)$ is a random variable, drawn from a distribution $\phi(\xi_i)$, with the first and the second moments being denoted as $\langle \xi_i \rangle = \mu_1$ and $\langle \xi_i^2 \rangle = \mu_2$,

respectively. In this paper, we consider, for simplicity, a uniform distribution $\phi(\xi_i) = 1$, with $\mu_1 = 1/2$ and $\mu_2 = 1/3$.

3.2.1 Hydrodynamics

In this section, we investigate the temporal evolution of a density perturbation and its relaxation dynamics. According to the update rule Eq. (3.1), the time evolution of local mass at site X can be written as

$$\frac{d\langle m_X(t)\rangle}{dt} = D\left(\langle m_{X+1}(t) - 2m_X(t) + m_{X-1}(t)\rangle\right). \tag{3.2}$$

Here, $D = \mu_1/2$ is the bulk-diffusion coefficient, which is *independent* of density. Provided we consider density relaxation on a ring of L sites, we can scale position X and time t as $x = X/L$ and $\tau = t/L^2$, and we obtain, from Eq. (3.2),

$$\frac{\partial h(x,\tau)}{\partial \tau} = D\frac{\partial^2 h(x,\tau)}{\partial x^2}, \tag{3.3}$$

which governs the time-evolution equation for scaled density field $h(x = X/L, \tau = t/L^2) = \langle m_X(t)\rangle \equiv \rho_X(t)$. The aforementioned equation is a linear partial differential equation, which can be solved for a given initial condition. For simplicity, to show the diffusive scaling property of a time-dependent density profile, we take an initial density profile being a step-like profile $\rho_X(t = 0) = \rho_{in}(X)$ on an infinite domain as follows:

$$\rho_{in}(X) = \begin{cases} \rho_0 + \rho_1 & \text{for } x < 0 \\ \rho_0 & \text{for } x \geq 0, \end{cases} \tag{3.4}$$

where $\rho_0 = 1$ and $\rho_1 = 3$. We can then directly solve Eq. (3.2) and get the solution of excess density profile $\rho_X(t) - \rho_0 = \mathcal{R}(X/\sqrt{t})$ in terms of a scaling function, $\mathcal{R}(z)$, where the position is scaled by $z = X/\sqrt{t}$. Moreover, by solving the resultant equation

$$-z\frac{d\mathcal{R}}{dz} = D\frac{d^2\mathcal{R}}{dz^2} \tag{3.5}$$

for $\mathcal{R}(z)$ with boundary condition $\mathcal{R}(z \to \infty) = 0$ and $\mathcal{R}(z \to -\infty) = \rho_1$, we immediately obtain the exact scaling solution,

$$\mathcal{R}(z) = \frac{\rho_1}{2}\left[1 - \mathrm{erf}\left(\frac{z}{\sqrt{4D}}\right)\right] \equiv \frac{\rho_1}{2}\mathrm{erfc}\left(\frac{z}{\sqrt{4D}}\right), \tag{3.6}$$

where the scaling variable is defined as $z = x/\sqrt{t}$, and the complementary error function is given by $\mathrm{erfc}(z) = (2/\sqrt{\pi})\int_z^\infty e^{-t^2}dt$.

In Fig. 3.2, the excess density $(\rho_X(t) - \rho_0)$ of a step initial profile is plotted against position x in Panel (a) at various times: $t = 2000$ (orange square), 5000 (green asterisks), 10000(red square), and 20000 (violet triangle). The background density $\rho_0 = 1$, and the initial density profile height $\rho_1 = 3$. In Panel (b), the scaled shifted density profile $\mathcal{R}(z)$ is plotted as a function of the scaling variable $z = x/\sqrt{t}$, with simulation data points matching closely with the analytic solution (purple dashed line), mentioned in Eq. (3.6). One can see that, despite the constrained dynamics due to the additional (CoM) conservation law, the density relaxation in the MCM remains indeed diffusive.

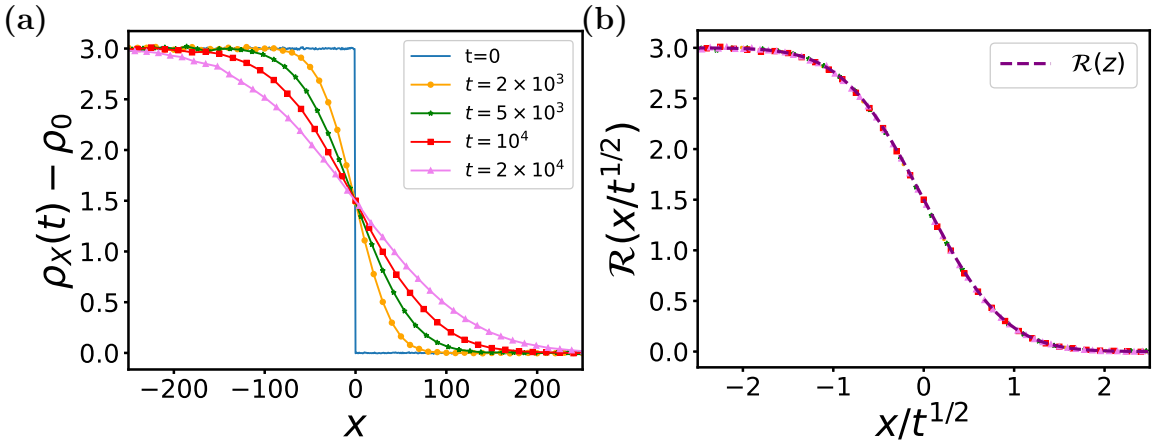

Figure 3.2: *MCM-CoMC I in one dimension.* Panel (a) shows the excess density $(\rho_X(t) - \rho_0)$ of a step initial profile density, plotted against position X at four times: $t = 2000$ (orange square), 5000 (green asterisks), 10000(red square), and 20000 (violet triangle). The background density is $\rho_0 = 1$, and the initial density profile height is $\rho_1 = 3$. Panel (b): The scaled shifted density profile $R(z)$ is plotted as a function of the scaling variable $z = x/\sqrt{t}$. Points represent simulation data, while the purple dashed line is the analytic solution [see Eq. (3.6)].

3.2.2 Dynamic correlations: One dimension

In this section, we calculate various time-dependent quantities in the steady state, including the variance of time-integrated bond current in a finite time interval and dynamic correlations for instantaneous current in one-dimensional MCM-CoMC I. Notably, the global density ρ and the center of mass are conserved in this model, making it particularly interesting to compute these time-dependent quantities exactly. We denote the dynamical correlation function for two observables A and B as $C_r^{AB}(t,t') = \langle A^i(t)B^{i+r}(t')\rangle_c$. The Fourier transform of dynamical correlation function is written as

$$\tilde{C}_q^{AB} = \sum_r C_r^{AB} e^{iqr}, \tag{3.7}$$

and then the inverse Fourier transform is given by

$$C_r^{AB} = \frac{1}{L}\sum_q \tilde{C}_q^{AB} e^{-iqr}. \tag{3.8}$$

More specifically, we are interested in characterizing time-integrated bond current, $\mathcal{Q}_i(T)$, which is defined as the net amount of mass that flows through a bond $(i, i+1)$ in a time interval T in the steady state. That is, if mass δm is transferred from site i (or, $i+1$) to site $i+1$ (i) during an infinitesimal time interval $(t, t+\delta t)$, we measure a positive (negative) instantaneous current $+\delta m/\delta t$ $(-\delta m/\delta t)$ flown through the bond; in other words, the cumulative current increases (decreases) by $+\delta m$ $(-\delta m)$ in that time interval δt. The time-evolution equation for the first moment of the cumulative bond current from the following infinitesimal-time update

rules,

$$\mathcal{Q}_i(t+dt) = \begin{cases} \textbf{event} & \textbf{prob.} \\ \mathcal{Q}_i(t) + \frac{\tilde{\xi}_i m_i(t)}{2} & dt \\ \mathcal{Q}_i(t) - \frac{\tilde{\xi}_{i+1} m_{i+1}(t)}{2} & dt \\ \mathcal{Q}_i(t) & (1-2dt), \end{cases} \tag{3.9}$$

from which we obtain the following equation,

$$\frac{d\langle \mathcal{Q}_i(t)\rangle}{dt} \equiv \langle \mathcal{J}_i(t)\rangle = \frac{\mu_1}{2}\langle m_i(t) - m_{i+1}(t)\rangle\,, \tag{3.10}$$

where we define instantaneous bond current as $\mathcal{J}_i(t) \equiv d\mathcal{Q}_i/dt$. that is, the cumulative (time-integrated) bond current in an infinitesimal time interval δt is given by $\mathcal{Q}_i(\delta t) = \lim_{\delta t\to 0}\int_t^{t+\delta t}\mathcal{J}_i(t)dt$. The instantaneous bond current $\mathcal{J}_i(t) = J^D(t) + \mathcal{J}^{fl}(t)$ can be decomposed into two parts: The diffusive current

$$J^D(t) \equiv \frac{\mu_1}{2}[m_i(t) - m_{i+1}(t)] \tag{3.11}$$

and fluctuating (or, "noise") current $\mathcal{J}^{fl}(t)$; it is evident that $\langle \mathcal{J}^{fl}\rangle = 0$. Note that Eq. (3.10) is linear in local masses; this particular *linearity property* [103] is actually required for obtaining an exact solution to the current statistic in the class of mass transport processes considered in this paper. We can now write the time-evolution equation for the unequal-time ($t > t'$) current correlation function as

$$\frac{d}{dt}C_r^{\mathcal{Q}\mathcal{Q}}(t,t') = \frac{\mu_1}{2}\left[C_r^{m\mathcal{Q}}(t,t') - C_{r-1}^{m\mathcal{Q}}(t,t')\right]. \tag{3.12}$$

The above equation has a quite similar structure as derived in Ref. [103] for MCMs *without* CoM conservation. However, as discussed in the rest of the paper, the explicit solutions to the above equation for MCMs with CoM conservation is qualitatively different from those without the CoM conservation. Now proceeding along the lines of Ref. [103], we take Fourier transform of both sides of the above equation and obtain

$$\frac{d}{dt}\tilde{C}_q^{\mathcal{Q}\mathcal{Q}}(t,t') = \mu_1(1-e^{iq})\frac{\tilde{C}_q^{m\mathcal{Q}}(t,t')}{2}. \tag{3.13}$$

To solve Eq. (3.12), we first need to calculate the unequal-time mass-current correlation function $C_r^{m\mathcal{Q}}(t,t')$, which, in Fourier space, satisfies the following equation,

$$\frac{d}{dt}\tilde{C}_q^{m\mathcal{Q}}(t,t') = -\frac{\mu_1}{2}\lambda_q\tilde{C}_q^{m\mathcal{Q}}(t,t'), \tag{3.14}$$

where

$$\lambda_q = 2(1-\cos q), \tag{3.15}$$

with the wave number $q = 2\pi n/L$ and $n = 1, 2, \cdots, L-1$. We also required to calculate the equal-time current-current spatial correlation function, which in Fourier space can be written as

$$\frac{d}{dt}\tilde{C}_q^{\mathcal{Q}\mathcal{Q}}(t,t) = \mu_1(1-e^{iq})\tilde{C}_q^{m\mathcal{Q}}(t,t) + \tilde{\Gamma}_q, \tag{3.16}$$

where $\tilde{\Gamma}_q = \mu_2\langle m^2\rangle\lambda_q/4$ is related to the strength of fluctuating current as given below:

$$\langle \tilde{\mathcal{J}}_q^{(fl)}(t)\tilde{\mathcal{J}}_{q'}^{(fl)}(t')\rangle = L\tilde{\Gamma}_q\delta_{q,-q'}\delta(t-t'). \tag{3.17}$$

The right-hand side of the above equation indicates that the strength of the fluctuating current is short-ranged (delta correlated) in both spatial and temporal scales [103]. Note that solving Eq. (3.14) requires calculation of equal-time mass-current spatial correlation, which, in the Fourier space, can be written as

$$\frac{d}{dt}\tilde{C}_q^{m\mathcal{Q}}(t,t) = -\frac{\mu_1}{2}\lambda_q\tilde{C}_q^{m\mathcal{Q}}(t,t) + \tilde{f}_q. \tag{3.18}$$

Here the source term $\tilde{f}_q$ can be written in terms of the steady-state density correlation $\tilde{C}_q^{mm}$ as

$$\tilde{f}_q = (1-e^{-iq})\left[D\tilde{C}_q^{mm} - \frac{\mu_2\langle m^2\rangle}{4}\lambda_q\right]. \tag{3.19}$$

Density correlation and structure factor.

It is quite convenient, and instructive, to express the steady-state density correlation function in Fourier mode $\tilde{C}_q^{mm}$. To this end, we write the time evolution of the Fourier mode for equal-time mass-mass correlation function as

$$\frac{d}{dt}\tilde{C}_q^{mm}(t,t) = -2D\lambda_q\tilde{C}_q^{mm}(t,t) + B(q), \tag{3.20}$$

where the quantity $B(q) = \mu_2\langle m^2\rangle\lambda_q^2/4$ depends on the second moment of onsite mass. We readily obtain the solution to the above equation, which is given by

$$\tilde{C}_q^{mm}(t,t) = \left(1-e^{-2D\lambda_q t}\right)\frac{\langle m^2\rangle\mu_2}{8D}\lambda_q, \tag{3.21}$$

which, in the steady state (in the limit $t\to\infty$), leads to the static density correlation function in the Fourier space,

$$\tilde{C}_q^{mm} = \frac{\mu_2\rho^2}{2(2\mu_1-\mu_2)}\lambda_q. \tag{3.22}$$

Now onward, we follow the convention that, if the time argument in the correlation function is not explicitly mentioned, e.g., $\tilde{C}_q^{mm}$ - a function of density and other parameters, it would simply imply that the correlation function is calculated in the steady state and thus does not depend on time. Note that, in this case, the above-mentioned steady-state density-correlation function $\tilde{C}_q^{mm}$ is related to the strength of fluctuating current as

$$\tilde{\Gamma}_q = 2D\tilde{C}_q^{mm}. \tag{3.23}$$

Now by taking inverse Fourier transform, Eq. (3.22) leads to the correlation function in real space as given below:

$$C_r^{mm}(\rho) = \frac{\mu_2\rho^2}{2(2\mu_1-\mu_2)}\left[2\delta_{r,0} - (\delta_{r,1}+\delta_{r,-1})\right], \tag{3.24}$$

which is strictly finite-ranged and valid for any finite L. Moreover, Eq. (3.23) leads to a fluctuation relation between the two-point spatial correlation function for mass and the intensity of fluctuating current,

$$C_r^{mm}(\rho) = \frac{\Gamma_r(\rho)}{2D}. \tag{3.25}$$

Now, to calculate the dynamic structure factor, we define Fourier transform $\delta\tilde{m}_q(t)$ of excess mass $\delta m_i(t) = (m_i(t) - \rho)$ at site i, which satisfies the following time-evolution equation for the Fourier modes $\delta\tilde{m}_q(t)$,

$$\frac{\partial}{\partial t}\delta\tilde{m}_q(t) = -D\lambda_q\delta\tilde{m}_q(t) + (e^{iq} - 1)\tilde{\mathcal{J}}_q^{(fl)}(t). \tag{3.26}$$

In the above equation, the first term on the right-hand side arises from diffusion, and the second term is due to the fluctuating (or the "noise") current. By using Eqs. (3.26) and (3.17) and performing some algebraic manipulations, we obtain the dynamic structure factor,

$$S(q,t) = \frac{\langle|\delta\tilde{m}_q(t)|^2\rangle}{L} = \tilde{C}_q^{mm}(t,t) = \left(1 - e^{-2D\lambda_q t}\right)\tilde{C}_q^{mm}, \tag{3.27}$$

where $\tilde{C}_q^{mm}(t,t)$ and $\tilde{C}_q^{mm} \equiv \lim_{t\to\infty}\tilde{C}_q^{mm}(t,t)$ are the steady-state dynamic and static density-correlation functions, respectively. Exact calculation of dynamic structure factor in a driven many-body system is quite challenging in general and has been done before only in a few cases in the past, e.g., in Refs. [130, 131]. The steady-state static structure factor $S(q) = \lim_{t\to\infty} S(q,t)$ is then given by

$$S(q) = \tilde{C}_q^{mm} = \frac{\mu_2\rho^2}{2(2\mu_1 - \mu_2)}\lambda_q \simeq \frac{\mu_2\rho^2}{2(2\mu_1 - \mu_2)}q^2, \tag{3.28}$$

which vanishes as $q \to 0$; here, in the last step of the above expression, we have used a small-q approximation of $\lambda_q \approx q^2$. Indeed, this particular q-dependence of the structure factor, i.e., $S(q) \sim q^2$ in the limit of small q, implies a "Class-I" hyperuniformity, implying an extreme suppression of density fluctuations in spatial domain, as categorized in Ref. [4].

In panel (a) of Fig. 3.3, we have plotted the steady-state density correlation function C_r^{mm} as a function of spatial distance r. In panel (b) of the same figure, we have plotted the static structure factor $S(q)$ as a function of wave number q. In both panels (a) and (b), the orange dashed lines represent theoretical predictions, which are obtained from Eqs. (3.24) and (3.28), respectively. Simulations are performed for global density $\rho = 1.0$ and system size $L = 1000$, and match quite well with theory.

Calculation of current correlation functions.

To obtain unequal-time current-current correlation function, we first evaluate equal-time current-current and mass-current correlation functions from Eqs. (3.16) and (3.18), respectively. Next, we calculate the unequal time mass-current correlation

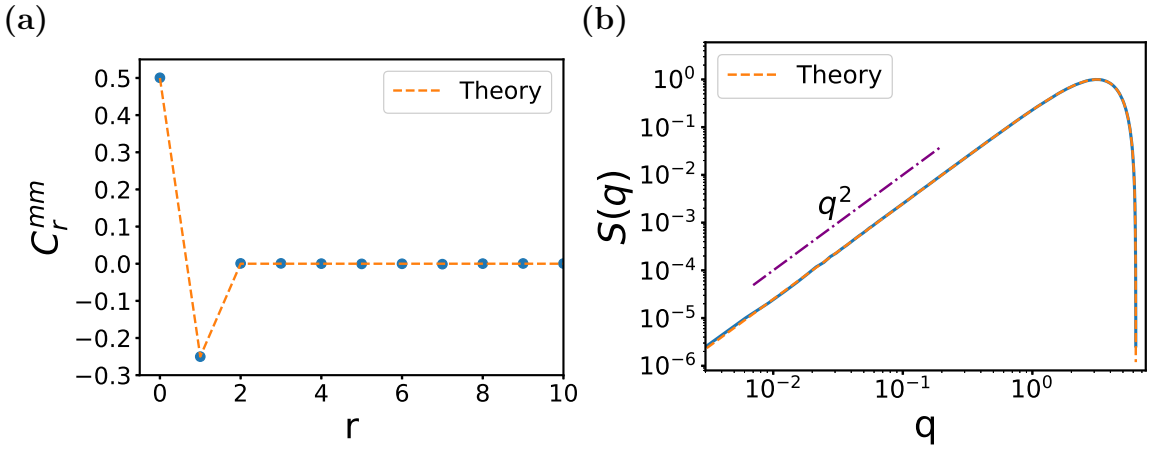

Figure 3.3: *MCM-CoMC I in one dimension.* Panel (a): We plot steady-state density correlation function, C_r^{mm}, as a function of spatial distance r. Panel (b): Steady-state structure factor $S(q)$ is plotted as a function of wave number q. The purple dashed-dotted line represent the asymptotic behavior, which scales as q^2 for small q. In both the panels (a) and (b), the orange dashed lines represent theoretical predictions obtained from Eqs. (3.24) and (3.28), respectively. Simulations are performed for global density $\rho = 1.0$ and system size $L = 1000$.

using Eq. (3.14). Finally, we derive the full solution for the unequal time current-current correlation from Eq. (3.12) in the Fourier representation,

$$\tilde{C}_q^{\mathcal{Q}\mathcal{Q}}(t,t') = \tilde{\Gamma}_q t' - \frac{\mu_2 (D\lambda_q \rho)^2}{(2\mu_1 - \mu_2)} \left[\int_0^{t'} dt'' \int_0^{t''} dt''' e^{-D\lambda_q (t''-t''')} + \frac{1}{2} \int_{t'}^{t} dt'' \int_0^{t''} dt''' e^{-D\lambda_q (t''-t''')} \right]. \tag{3.29}$$

The equal-time bond-current correlation $C_0^{\mathcal{Q}\mathcal{Q}}(T,T) \equiv \langle \mathcal{Q}_i^2(T) \rangle_c$, or the variance (the second cumulant), can now be obtained by first taking the inverse Fourier transform in Eq.(3.29) and then setting $t = t' = T$ and $r = 0$, as follows:

$$\langle \mathcal{Q}_i^2(T) \rangle_c = \langle \mathcal{Q}_i^2(T) \rangle = T \left[\Gamma_0 - D C_0^{mm} \frac{1}{L} \sum_{q \neq 0} \lambda_q \right] + \frac{\mu_2 \rho^2}{(2\mu_1 - \mu_2)} \frac{1}{L} \sum_{q \neq 0} \left(1 - e^{-\frac{\mu_1}{2} \lambda_q T} \right). \tag{3.30}$$

In the long-time regime, by collecting leading-order terms, Eq. (3.30) can be written in the following asymptotic form,

$$\langle \mathcal{Q}_i^2(T) \rangle \simeq A_1 T + A_2 + A_3 T^{-1/2}, \tag{3.31}$$

where A_1, A_2 and A_3 are constant (time-independent) coefficients, which in general depend on density and other model parameters. Quite remarkably, in this case (presumably, generically in one-dimensional models as discussed in the next section), we find that the coefficient corresponding to the first (linear-time-growth) term in the above equation vanishes, i.e.,

$$A_1 = \left[\Gamma_0 - D C_0^{mm} \frac{1}{L} \sum_q \lambda_q \right] = 0, \tag{3.32}$$

obtained by using the identity $\sum_q \lambda_q = 2L$ (note that $\lambda_0 = 0$) and the fluctuation relation $\Gamma_0 = 2DC_0^{mm}$ from Eq. (3.25). Now, in the thermodynamic limit, with $L \to \infty$ and density being fixed, Eq. (3.30) can be written in an integral form as given below:

$$C_0^{\mathcal{Q}\mathcal{Q}}(T,T) \simeq \frac{\mu_2\rho^2}{(2\mu_1-\mu_2)}\frac{1}{\pi}\int_0^\pi dq\left(1-e^{-\frac{\mu_1}{2}\lambda(q)T}\right) \tag{3.33}$$
$$= \frac{\mu_2\rho^2}{(2\mu_1-\mu_2)}\left[1-e^{-\mu_1 T}I_0(\mu_1 T)\right],$$

where $I_0(x) = (1/\pi)\int_0^\pi e^{x\cos q}dq$ is the modified Bessel function of the first kind and we denote $\lambda(q) = 2(1-\cos q)$. By performing an asymptotic analysis, Eq. (3.33) can be written for large time T as follows:

$$\langle \mathcal{Q}_i^2(T)\rangle \simeq \frac{\mu_2\rho^2}{(2\mu_1-\mu_2)} - \frac{\mu_2\rho^2}{(2\mu_1-\mu_2)\sqrt{2\pi\mu_1}}T^{-1/2}, \tag{3.34}$$

where we have used the approximation $\lambda(q) \approx q^2$. That is, in the thermodynamic limit, the variance of time-integrated bond current in a long time interval $T \to \infty$ saturates to a finite value,

$$A_2(\rho) = \frac{\mu_2\rho^2}{(2\mu_1-\mu_2)}, \tag{3.35}$$

through a power-law decay $T^{-1/2}$. The third coefficient A_3 can also be identified from Eq. (3.34) as

$$A_3(\rho) = -\frac{\mu_2\rho^2}{(2\mu_1-\mu_2)\sqrt{2\pi\mu_1}}. \tag{3.36}$$

The fact that the coefficient A_1 vanishes here implies that, in the long-time limit, the variance $\mathcal{Q}_i^2(T)$ of time-integrated bond current in one-dimensional MCM *with* CoM conservation saturates as a function of time T as opposed to growing as $T^{1/2}$ in one-dimensional MCMs *without* CoM conservation [103]. Physically, in the former case, it implies a stronger anti-correlations between currents developing at two different times; it could be understood on the physical ground that, whenever there is a current generated at some point, there is also a reverse current of the same magnitude generated in the opposite direction. This extreme suppression of dynamic current fluctuation is somewhat analogous to extreme suppression of dynamic activity fluctuations previously observed in a model of sandpiles, called the Oslo model, in Ref. [50] (the hyperuniformity exponent $b = 0$ in both cases). Furthermore, the expression in Eq. (3.34) has a quite similar structure to that obtained previously, albeit through an approximate closure scheme, for the one dimensional Oslo model in the far-from-critical regime [44]. However, unlike in the Oslo model, the calculation scheme for MCMs in this paper is exact and the corresponding coefficients A_1, A_2 and A_3 are obtained explicitly as a function of density and the other parameters.

Instantaneous bond-current correlation functions.

We now calculate the temporal correlation of instantaneous current correlations, $C_r^{\mathcal{J}\mathcal{J}}(t,0)$ for $t \geq 0$, which can be expressed as:

$$C_r^{\mathcal{J}\mathcal{J}}(t,0) = \left[\frac{d}{dt}\frac{d}{dt'}C_r^{\mathcal{Q}\mathcal{Q}}(t,t')\right]_{t'=0,t\geq 0} = \Gamma_r\delta(t) - \frac{\mu_1^2\mu_2\rho^2}{8(2\mu_1-\mu_2)}\frac{1}{L}\sum_q e^{-\frac{\mu_1}{2}\lambda_q t}\lambda_q^2 e^{-iqr}. \tag{3.37}$$

In the large system size limit, the above equation with $r = 0$ can be written in the following form:

$$C_0^{\mathcal{J}\mathcal{J}}(t,0) \simeq -\frac{\mu_1^2\mu_2\rho^2}{8(2\mu_1-\mu_2)}e^{-\mu_1 t}\left[2I_0(\mu_1 t) - \frac{I_1(\mu_1 t)}{\mu t}\right], \tag{3.38}$$

where we have taken $t > 0$ and $I_\nu(z)$ denotes the modified Bessel function of the first kind of order ν. Also, in the long-time limit and for large-system-size limit, the Eq. (3.37) with $r = 0$ has the following asymptotic form,

$$C_0^{\mathcal{J}\mathcal{J}}(t,0) \simeq -\frac{3\mu_2\rho^2}{16\sqrt{2\pi\mu_1}(2\mu_1-\mu_2)}t^{-5/2}. \tag{3.39}$$

In Fig. 3.4, panel (a), the variance $C_0^{\mathcal{Q}\mathcal{Q}}(T,T) = \langle \mathcal{Q}_i^2(T)\rangle$ of time-integrated current in a time interval T is plotted as a function of T. The theory line (orange dashed), obtained from Eq. (3.33), matches with the simulation perfectly. The guiding line (purple dash-dot) indicates the saturation value obtained from Eq.(3.35). Panel (b): The relative time-integrated bond-current fluctuation, $A_2(\rho) - C_0^{\mathcal{Q}\mathcal{Q}}(T,T)$, is plotted as a function of time T for both simulation (solid blue line) and theory (orange dashed). The purple dashed-dotted line represents $T^{-1/2}$, as described in Eq.(3.34). Panel (c): Negative of instantaneous bond-current correlation $-C_0^{\mathcal{J}\mathcal{J}}(t,0)$ is plotted as a function of t. The theory line (orange dashed), mentioned in Eq. (3.38), matches the simulation quite well. The asymptotic decay as $t^{-5/2}$ (purple dashed-dotted) is consistent with Eq. (3.39). In all the panels simulation data (blue line) is for system size of $L = 1000$ and a global density $\rho = 1$.

3.3 One-dimensional MCM-CoMC II: Finite-range mass transfer

In this section, we consider a variant of the CoM-conserving mass chipping model on a one-dimensional periodic ring, now with *finite-range* mass-transfer rule, where the chipped-off mass can coalesce with not only the nearest-neighbor masses, but also the next-nearest-neighbor masses. More specifically, mass m_i at site i is chipped off with unit rate and a random fraction ξ_i of mass m_i, i.e., $\xi_i m_i$ is retained, while the remaining fraction of mass $(1-\xi_i)m_i$ is fragmented into two equal halves, each having mass $(1-\xi_i)m_i/2$. These two chunks of fragmented masses then coalesce, with equal probability, either with the two nearest-neighbor masses at $i+1$ and $i-1$ or with the next-nearest-neighbor masses at $i+2$ and $i-2$. It is worth noting that, in a finite-range (say, of range k) mass transfer process, when a random

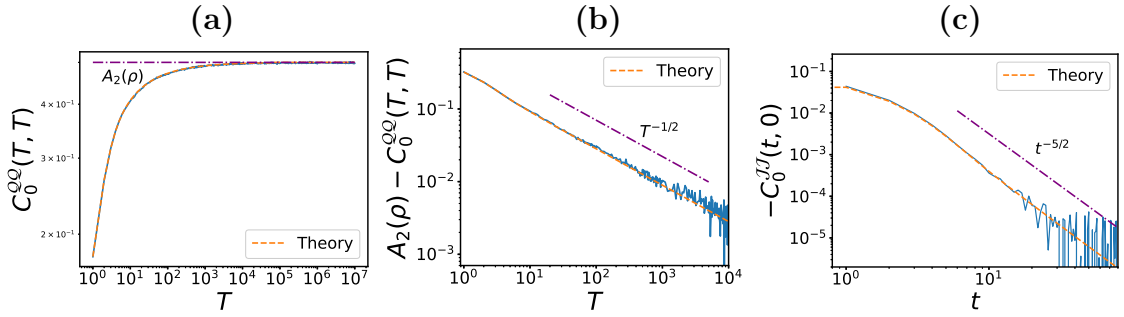

Figure 3.4: *MCM-COM-I in one dimension.* Panel (a): Time-integrated bond-current fluctuation or variance $\langle \mathcal{Q}_i^2(T)\rangle = C_0^{\mathcal{Q}\mathcal{Q}}(T,T)$ is plotted as a function of time T. Theory line (orange dashed), obtained from Eq. (3.33), agrees quite well with simulation perfectly. The guiding line (purple dashed) indicates the saturation value obtained from Eq.(3.35). Panel (b): The relative time-integrated bond-current fluctuation, $A_2(\rho) - C_0^{\mathcal{Q}\mathcal{Q}}(T,T)$, is plotted as a function of time T for both simulation (blue) and theory (orange). The asymptotic $T^{-1/2}$ (purple) is obtained from Eq.(3.34). Panel (c), negative of instantaneous bond-current correlation $-C_0^{\mathcal{J}\mathcal{J}}(t,0)$ is plotted as a function of t. The orange dashed line represents theory as in Eq. (3.38). The purple dashed-dotted line represents the asymptotic power-law decay $t^{-5/2}$, obtained from theory Eq. (3.39). In all panels, simulation data (blue line) is for system size $L = 1000$ and global density $\rho = 1$.

fraction of the chipped-off mass, δm, is transferred from the ith site to $(i+k)$th site (where $k = 2$ in the model considered in this section) during the time interval $(t, t+\delta t)$, the cumulative currents increase by δm across all bonds from $(i, i+1)$ to $(i+k-1, i+k)$. Similarly, if the chipped-off mass, δm, is transferred from the ith site to $(i-k)$th site, the cumulative currents decrease by δm across all bonds from $(i-1, i)$ to $(i-k, i-k+1)$.

We now present simulation results to demonstrate that the qualitative results derived in the previous section are indeed quite robust for one dimensional systems. In Fig. 3.5, panel (a), the excess density profile $(\rho_X(t) - \rho)$ of an initially stepped density profile [see Eq. (3.4)] is plotted against position X at four different times: $t = 2000$ (orange squares), 5000 (green asterisks), 10000 (red squares), and 20000 (violet triangles). Panel (b) depicts the scaled density profile $\mathcal{R}(X/t^{1/2})$ as a function of the scaled position $X/t^{1/2}$. The solution (black dashed line) obtained from Eq. (3.6) with the theoretically obtained bulk-diffusion coefficient $D = 5\mu_1/4$ (different from the model described in the previous section) agrees quite well with the simulation data. In panel (a) of Fig. 3.6, the variance $C_0^{\mathcal{Q}\mathcal{Q}}(T,T)$ of time-integrated bond current is plotted as a function of time T. In panel (b) of the same figure, the relative bond-current fluctuation, $A_2(\rho) - C_0^{\mathcal{Q}\mathcal{Q}}(T,T)$, is plotted as a function of time T. Purple dashed-dotted line is the asymptotic power-law $T^{-1/2}$ as derived in Eq. (3.34). In panel (c), negative of instantaneous bond current correlation, $-C_0^{\mathcal{J}\mathcal{J}}(t,0)$, is plotted as a function of time t. In the all panels, we have taken system size $L = 1000$ and global density $\rho = 1.0$.

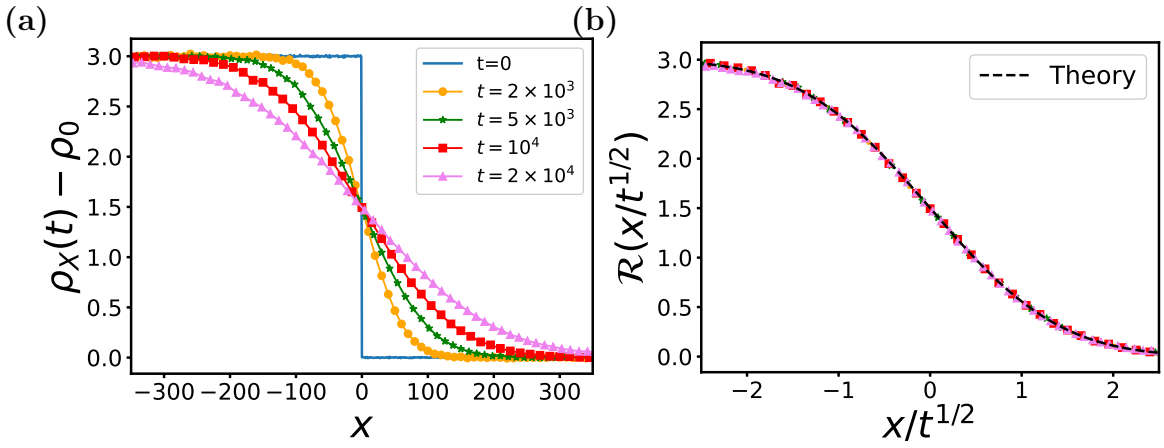

Figure 3.5: *MCM-CoMC II in one dimension.* Panel (a): The excess density $(\rho_X(t) - \rho_0)$ of an initially stepped density profile is plotted against position X at four different times: $t = 2000$ (orange squares), 5000 (green asterisks), 10000 (red squares), and 20000 (violet triangles). The background density is $\rho_0 = 1$, with an initial profile height of $\rho_1 = 3$. Panel (b): The scaled shifted density profile $R(z)$ is plotted against the scaling variable $z = X/t^{1/2}$. Points represent simulation data, while the black dashed line [Eq. (3.6)] indicates the analytic solution with $D = 5\mu_1/4$.

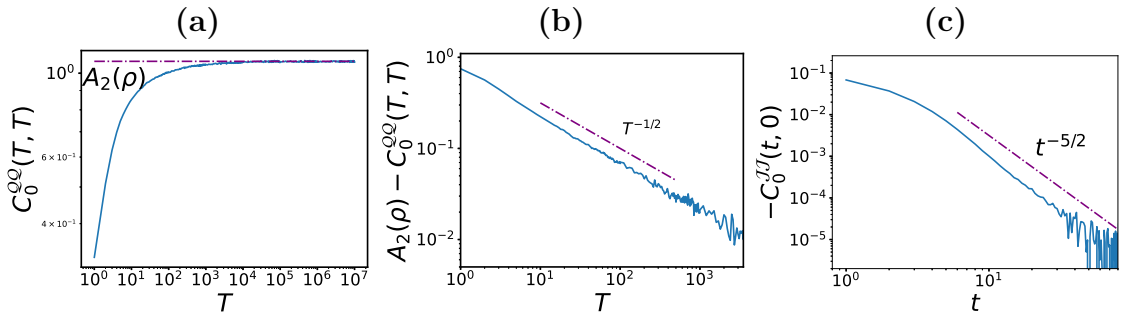

Figure 3.6: *MCM-CoMC II in one dimension.* Panel (a): the time integrated bond-current fluctuation is plotted as a function of time T. The purple dashed-dotted line represent the saturation value $A_2(\rho) = 1.075$(fitted). Panel (b): The relative bond-current fluctuation, $A_2(\rho) - C_0^{\mathcal{Q}\mathcal{Q}}(T,T)$, is plotted as a function of time T. Purple dashed-dotted line is the asymptotic power law decay $T^{-1/2}$, obtained from Eq. (3.34). Panel (c): Negative of instantaneous bond-current correlation $-C_0^{\mathcal{J}\mathcal{J}}(t,0)$ is plotted as a function of time t. The asymptotic line (purple dashed-dotted) is the theoretical estimation obtained from Eq. (3.39). In the all the panels, we have taken system size $L = 1000$ and global density $\rho = 1.0$.

3.4 Two-dimensional MCM-CoMC I

3.4.1 Model and definition of current

In this section, we introduce a model defined on a two-dimensional periodic square lattice with the following dynamical rules; for simplicity, we consider only nearest-neighbor mass transfer. Here, a site (i, j) retains a random fraction of its mass $\xi m_{i,j}$, and the remaining fraction of mass, $(1-\xi)m_{i,j}$, is divided equally into four parts, each having $(1-\xi)m_{i,j}/4$, which is then transferred to each of the four nearest neighbors $(i+1, j)$, $(i-1, j)$, $(i, j+1)$, and $(i, j-1)$.

In a two-dimensional square lattice, the bond current is defined similar to that in the one-dimensional case. The time-integrated bond current along the x direction, denoted as $\mathcal{Q}_x^{i,j}(T)$, represents the net flux of mass between site (i, j) and site $(i+1, j)$ in the time interval T: If an amount of mass δm is transferred from site i to $i+1$ (or, $i+1$ to i) during an time interval, say δt, $\mathcal{Q}_x^{i,j}$ increases (or, decreases) by δm, i.e., $\mathcal{Q}_x^{i,j} \to \mathcal{Q}_x^{i,j} + \delta m$ (or, $\mathcal{Q}_x^{i,j} \to \mathcal{Q}_x^{i,j} - \delta m$). Similarly, the time-integrated bond current along the y direction, denoted as $\mathcal{Q}_y^{i,j}(T)$, represents the net flux of mass through the bond between sites (i, j) and $(i, j+1)$ during the same interval T. The time-integrated bond current $\mathcal{Q}_\alpha^{i,j}(T)$, with $\alpha \in x, y$, can be expressed in terms of the instantaneous bond current $\mathcal{J}_\alpha^{i,j}(t)$ as $\mathcal{Q}_\alpha^{i,j}(T) = \int_t^{t+T} \mathcal{J}_\alpha^{i,j}(t')dt'$, with $\alpha \in x, y$. In the schematic diagram Fig. 3.7, a mass of amount $4\delta m$ is chipped off from site (i, j) and fragmented into 4 equal parts with each of the part δm being transferred to each of its four neighboring sites during the time interval $(t, t+\delta t)$. As a result, along the x axis, a mass δm is transferred from site (i, j) to site $(i+1, j)$, and from site (i, j) to site $(i-1, j)$, thus generating a positive instantaneous current $\mathcal{J}_x^{i,j} = +\delta m/\delta t$ through the bond between sites (i, j) and $(i+1, j)$ and a negative instantaneous current $\mathcal{J}_x^{i-1,j} = -\delta m/\delta t$ through the bond between sites $(i-1, j)$ and (i, j). Similarly, along the y axis, a mass δm is transferred from site (i, j) to site $(i, j+1)$ and from site (i, j) to site $(i, j-1)$), generating a positive instantaneous current $\mathcal{J}_y^{i,j} = +\delta m/\delta t$ through the bond (i, j) and $(i, j+1)$ and a negative instantaneous current $\mathcal{J}_y^{i,j-1} = -\delta m/\delta t$ through the bond $(i, j-1)$ and (i, j).

In two dimensions, the current can flow along x or y axis (or, along both the axes during an infinitesimal time interval as in this particular case MCM-CoMC I considered in this section). Consequently, the current correlations have two distinct components: the correlation function for currents along the same direction, $C_{r,s}^{\mathcal{Q}_x\mathcal{Q}_x}(t, t')$ [or, $C_{r,s}^{\mathcal{Q}_y\mathcal{Q}_y}(t, t')$] and the "cross"-correlation function, $C_{r,s}^{\mathcal{Q}_x\mathcal{Q}_y}(t, t')$ or $C_{r,s}^{\mathcal{Q}_y\mathcal{Q}_x}(t, t')$. For convenience, we use the dynamical correlation for two observables A_x and B_y as $C_{r,s}^{A_xB_y}(t, t') = \langle A_x^{i,j}(t) B_y^{i+r,j+s}(t') \rangle_c$ in the rest of the paper.

3.4.2 Calculation of current correlation functions

The unequal-time ($t > t'$) correlation function for bond currents in the same direction (i.e., the correlation between the current in the x direction at initial time with that at later time), $C_{r,s}^{\mathcal{Q}_x\mathcal{Q}_x}(t, t')$, which in the Fourier domain $\mathbf{q} \equiv (q_x, q_y)$ satisfies

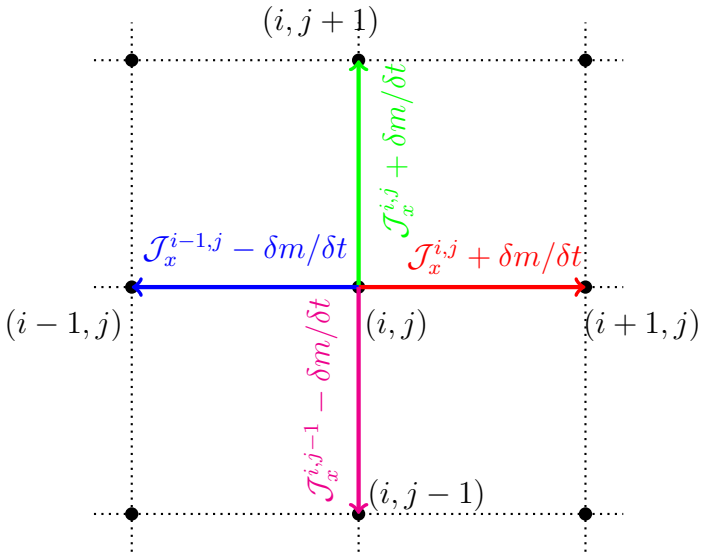

Figure 3.7: The schematic diagram illustrates a mass-update process and the associated instantaneous bond currents across 4 different bonds, resulting from the loss of mass $m_{i,j} - 4\delta m$ at site (i, j) and the gain of mass δm at each of the four neighboring sites in the time interval $(t, t + \delta t)$. During the mass-transfer event, the corresponding instantaneous bond currents are updated as following: $\mathcal{J}_x^{i,j} \to \mathcal{J}_x^{i,j} + \delta m/\delta t$ (rightward, red arrow), $\mathcal{J}_x^{i-1,j} \to \mathcal{J}_x^{i-1,j} - \delta m/\delta t$ (leftward, blue arrow), $\mathcal{J}_y^{i,j} \to \mathcal{J}_y^{i,j} + \delta m/\delta t$ (upward, green arrow), and $\mathcal{J}_y^{i,j-1} \to \mathcal{J}_y^{i,j-1} - \delta m/\delta t$ (downward, magenta arrow).

the following time-evolution equation

$$\frac{d}{dt}\tilde{C}^{\mathcal{Q}_x\mathcal{Q}_x}_{q_x,q_y}(t, t') = D(1 - e^{iq_x})\tilde{C}^{m\mathcal{Q}_x}_{q_x,q_y}(t, t'), \tag{3.40}$$

where $D = \mu_1/4$ is the bulk-diffusion coefficient. Here, we denote the Fourier transform of the two dynamical observables A and B, in two dimensions, as

$$\tilde{C}^{AB}_{q_x,q_y} = \sum_{r,s} C^{AB}_{r,s} e^{iq_x r} e^{iq_y s},$$

and accordingly the inverse Fourier transform is given by

$$C^{AB}_{r,s} = \frac{1}{L^2} \sum_{q_x,q_y} \tilde{C}^{AB}_{q_x,q_y} e^{-iq_x r} e^{-iq_y s}.$$

Now, to solve Eq. (3.40), we need to calculate the unequal-time mass-current correlation function in the Fourier domain, $\tilde{C}^{m\mathcal{Q}_x}_{q_x,q_y}(t, t')$, which satisfies the following equation,

$$\frac{d}{dt}\tilde{C}^{m\mathcal{Q}_x}_{q_x,q_y}(t, t') = -D\omega(q_x, q_y)\tilde{C}^{m\mathcal{Q}_x}_{q_x,q_y}(t, t'), \tag{3.41}$$

with

$$\omega(q_x, q_y) = \lambda(q_x) + \lambda(q_y) \tag{3.42}$$

and $\lambda(q_\alpha) = 2[1 - \cos(q_\alpha)]$ with $\alpha \in [x, y]$. The above-mentioned Eqs. (3.40) and (3.41) are two first-order ordinary differential equations, which can be solved exactly by knowing the following equal-time correlations: $\tilde{C}^{\mathcal{Q}_x\mathcal{Q}_x}_{q_x,q_y}(t,t)$ and $\tilde{C}^{m\mathcal{Q}_x}_{q_x,q_y}(t,t)$ as initial conditions. Further, from the microscopic update rules, we calculate the equal-time current-current correlation in Fourier space-domain, $\tilde{C}^{\mathcal{Q}_x\mathcal{Q}_x}_{q_x,q_y}(t,t)$, which satisfies the following equation,

$$\frac{d}{dt}\tilde{C}^{\mathcal{Q}_x\mathcal{Q}_x}_{q_x,q_y}(t,t) = 2D\tilde{C}^{m\mathcal{Q}_x}_{q_x,q_y}(t,t)(1 - e^{iq_x}) + \tilde{\Gamma}^{xx}_{q_x,q_y}, \tag{3.43}$$

where $\tilde{\Gamma}^{xx}_{q_x,q_y} = \mu_1\mu_2\rho^2\lambda(q_x)/8(2\mu_1 - \mu_2)$ is the corresponding source term. Now, using the microscopic update rule, the time evolution of the equal-time mass-current correlation in the Fourier space, i.e., $\tilde{C}^{m\mathcal{Q}_x}_{q_x,q_y}(t,t)$, satisfies the following equation:

$$\frac{d}{dt}\tilde{C}^{m\mathcal{Q}_x}_{q_x,q_y}(t,t) = -D\omega(q_x,q_y)\tilde{C}^{m\mathcal{Q}_x}_{q_x,q_y}(t,t) + \tilde{f}^{x}_{q_x,q_y}. \tag{3.44}$$

Here the source term $\tilde{f}^{x}_{q_x,q_y} = -\mu_1\mu_2\rho^2(1 - e^{-iq_x})\omega(q_x,q_y)/16(2\mu_1 - \mu_2)$ is evaluated from the knowledge of the steady-state density correlation, which, in Fourier space, can be obtained by solving following equation,

$$\frac{d}{dt}\tilde{C}^{mm}_{q_x,q_y}(t,t) = -2D\omega\tilde{C}^{mm}_{q_x,q_y}(t,t) + \omega^2\frac{\mu_2}{16}\langle m^2\rangle. \tag{3.45}$$

Here we have the bulk-diffusion coefficient $D = \mu_1/4$ and the second moment of mass m_i at a site i as $\langle m^2\rangle \equiv \int m^2 \text{Prob.}[m_i = m]dm$. In the steady-state, we have $d\tilde{C}^{mm}_{q_x,q_y}(t,t)/dt = 0$, and we obtain the desired density correlation function as follows:

$$\tilde{C}^{mm}_{q_x,q_y} = S(q_x,q_y) = \frac{\mu_2\rho^2}{4(2\mu_1 - \mu_2)}\omega(q_x,q_y) \simeq \frac{\mu_2\rho^2}{4(2\mu_1 - \mu_2)}(q_x^2 + q_y^2), \tag{3.46}$$

where the second moment of on-site mass can be explicitly calculated as $\langle m^2\rangle = 2\mu_1\rho^2/(2\mu_1 - \mu_2)$. Notably, the Fourier transform of the density correlation in Eq. (3.46) is related to the structure factor $S(q)$ up to a constant factor. This implies that, in the small-q limit, where $\lambda(q_x) \sim q_x^2$ as $q_x \to 0$, the structure factor $S(q)$ scales as q^2, with $q = \sqrt{q_x^2 + q_y^2}$. Indeed, the vanishing of the static structure factor $S(q)$ at small wave number is a signature of extreme ("class-I") hyperuniformity of spatial density fluctuations [4]. In Fig. 3.8, we provide a heat-map of the steady-state density correlation and structure factor for the two-dimensional mass chipping model. Panel (a) presents a two-dimensional color heat map of the steady-state density correlation function $C^{mm}_{r,s}$ for an MCM on a periodic square lattice with an area of 100×100. In Panel (b), we show the heat map of the structure factor, $S(q_x,q_y)$, in the scaled two-dimensional plane $(Lq_x/2\pi, Lq_y/2\pi)$. Panel (c) depicts the structure factor $S(q)$ as a function of the magnitude $q = \sqrt{q_x^2 + q_y^2}$ of the wave number vector $\mathbf{q} \equiv \{q_x, q_y\}$. For small q values, $S(q)$ exhibits a scaling behavior proportional to q^2, as described by Eq. (3.46). In all panels, the structure factors calculated in the simulations are for an MCM on a periodic lattice with an area of 128×128 and global density $\rho = 1.0$.

We provide below the results for dynamic correlations in the following two cases. In the first case, we calculate the correlation function for currents along the same direction (say, both along x direction). In the second case, we do the same for currents along two perpendicular directions (say, along x and y directions).

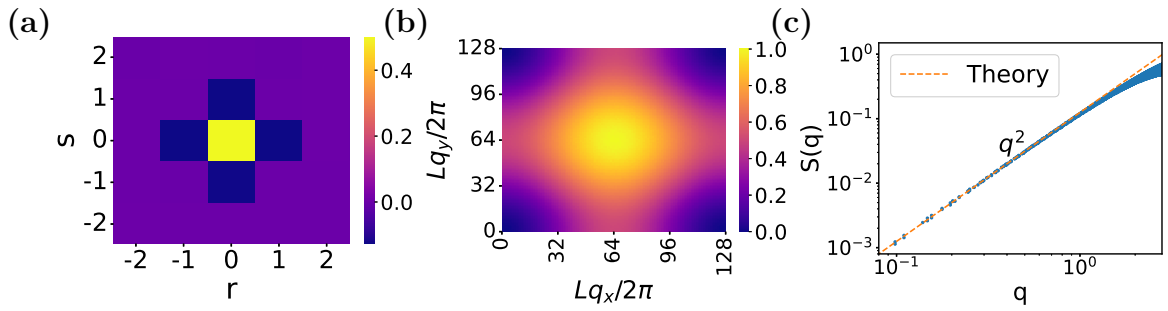

Figure 3.8: *MCM-CoMC I in two dimensions.* Panel (a): Steady-state density correlation $C^{mm}_{r,s}$ is shown in a 2D color heat plot. In this panel we have taken periodic system size of area 100×100. Panel (b): The heat-map of structure factor $S(\mathbf{q})$ is plotted in the two-dimensional (scaled) $\mathbf{q}$-plane. Panel (c): The structure factor $S(q)$ is shown as a function of the magnitude $q = \sqrt{q_x^2 + q_y^2}$. For small-q values, $S(q)$ scales as q^2 [see Eq. (3.46)]. In panel (b) and (c), we take a periodic system of area 128×128. Global density $\rho = 1.0$ for all the panels.

3.4.3 Case I: Correlation between currents along the same direction.

Finally, we obtain a closed set of Eqs. (3.40), (3.41), (3.43), and (3.44) from which, after some algebraic manipulation (e.g., few integrations followed by inverse Fourier transform, which is defined as $C^{AB}_{r,s} = 1/L^2 \sum_{q_x,q_y} \tilde{C}^{AB}_{q_x q_y}$), we are able to calculate the time-integrated bond-current fluctuation of unequal-time $C^{\mathcal{Q}_x\mathcal{Q}_x}_{r,s}(t,t')$. However, by setting $r = s = 0$ and $t = t' = T$, the second cumulant, or the variance, of the time-integrated current $\mathcal{Q}_x(T)$ across a particular bond in x direction and in time interval T can be obtained from $C^{\mathcal{Q}_x\mathcal{Q}_x}_{0,0}(T,T) = \langle[\mathcal{Q}_x(T)]^2\rangle_c$, and it can be expressed explicitly as

$$\langle[\mathcal{Q}_x(T)]^2\rangle_c = C^{\mathcal{Q}_x\mathcal{Q}_x}_{0,0}(T,T) = T\frac{\mu_2\langle m^2\rangle}{8} + \frac{2D}{L^2}\sum_{q_x,q_y}\left[\frac{T}{D\omega} - \frac{(1-e^{-D\omega T})}{(D\omega)^2}\right] \times \lambda_{q_x}\left[D\tilde{C}^{mm}_{q_x,q_y} - \frac{\mu_2}{16}\langle m^2\rangle\omega\right], \tag{3.47}$$

where the summation is over $(q_x, q_y) \neq (0,0)$. The above equation in the long-time regime can be written in the following asymptotic form,

$$\langle[\mathcal{Q}_x(T)]^2\rangle_c = \langle[\mathcal{Q}_x(T)]^2\rangle \simeq A_1 T + A_2 + \frac{A_3}{T} \tag{3.48}$$

After some algebraic manipulation, we obtain from Eq. (3.47) the first coefficient,

$$A_1(\rho) = \frac{\mu_2\langle m^2\rangle}{32}\left[4 - \frac{2}{L^2}\sum_{q_x,q_y}\lambda_{q_x}\right] = 0, \tag{3.49}$$

which, quite interestingly, vanishes as in the case of one-dimensional models discussed in the previous sections; here we have used the identity $\sum_{q_x}\lambda_{q_x} = 2L$. In other words, the coefficient of the leading-order term of Eq. (3.48) having linear ($\sim T$) growth is zero; however, as we show later, this particular behavior may not in

general be observed in two (and higher) dimensions and depends on the microscopic details of the models under consideration. Now, in the thermodynamic limit $L \to \infty$ and keeping density fixed, we can express Eq. (3.47) as the following integral,

$$\langle [\mathcal{Q}_x(T)]^2 \rangle_c = \frac{\mu_2 \rho^2}{2(2\mu_1 - \mu_2)} \frac{1}{(2\pi)^2} \int_0^{2\pi} \int_0^{2\pi} dq_x dq_y \frac{\lambda(q_x)\left(1 - e^{-D\omega T}\right)}{\lambda(q_x) + \lambda(q_y)}, \tag{3.50}$$

For large time T, we have the asymptotic expression of Eq. (3.50) as

$$C_{0,0}^{\mathcal{Q}_x \mathcal{Q}_x}(T,T) \simeq A_2(\rho) \left[1 - \frac{1}{4\pi D} T^{-1}\right], \tag{3.51}$$

where we have used the approximation $\lambda(q_\alpha) \approx q_\alpha^2$ and obtain

$$A_2(\rho) = \lim_{T \to \infty} C_{0,0}^{\mathcal{Q}_x \mathcal{Q}_x}(T,T) = \frac{\mu_2 \rho^2}{4(2\mu_1 - \mu_2)}. \tag{3.52}$$

In other words, at long times, the variance of time-integrated bond current, quite strikingly, saturates to a constant value. Next, we calculate the two-point unequal-time correlation function for bond current (correlation between the currents at unequal times, but both along the same, say x, direction), which can be obtained as

$$C_{0,0}^{\mathcal{J}_x \mathcal{J}_x}(t,0) = \left[\frac{d}{dt}\frac{d}{dt'} C_{0,0}^{\mathcal{Q}_x \mathcal{Q}_x}(t,t')\right]_{t'=0, t \geq 0} = \Gamma_{0,0}^{xx} \delta(t) - \frac{\mu_1^2 \mu_2 \rho^2}{64(2\mu_1 - \mu_2)} \frac{1}{L^2} \sum_{q_x, q_y} e^{-D\omega t} \lambda_{q_x} \omega. \tag{3.53}$$

By taking the infinite-volume limit $L \to \infty$ with $t > 0$ finite, the above expression can be written in an integral form,

$$C_{0,0}^{\mathcal{J}_x \mathcal{J}_x}(t,0) = -\frac{\mu_1^2 \mu_2 \rho^2}{64(2\mu_1 - \mu_2)} \frac{1}{(2\pi)^2} \int_0^{2\pi} \int_0^{2\pi} dq_x dq_y e^{-D\omega t} \lambda(q_x) \omega(q_x, q_y). \tag{3.54}$$

By using the approximation $\lambda(q_\alpha) \approx q_\alpha^2$ in the above equation, we get the asymptotic behavior of instantaneous current correlation function at large times,

$$C_{0,0}^{\mathcal{J}_x \mathcal{J}_x}(t,0) \simeq -\frac{\mu_2 \rho^2}{4\pi \mu_1 (2\mu_1 - \mu_2)} t^{-3}. \tag{3.55}$$

Clearly, as in Eq. (3.55), the decay of the dynamic (two-point) correlation function for bond current in *two* dimensions differs from that of the CoM-conserving models in *one* dimension as shown in Eq. (3.39) for MCMs and in Ref. [44] for the Oslo model.

3.4.4 Case II: Correlation between currents along two perpendicular directions.

The unequal-time ($t > t'$) current correlation between currents along two perpendicular directions x and y can be written as

$$\frac{d}{dt} \tilde{C}_{q_x, q_y}^{\mathcal{Q}_x \mathcal{Q}_y}(t,t') = D(1 - e^{iq_x}) \tilde{C}_{q_x, q_y}^{m \mathcal{Q}_y}(t,t'), \tag{3.56}$$

where unequal-time mass current correlation $\tilde{C}^{m\mathcal{Q}_y}_{q_x,q_y}(t,t')$ satisfy following equation

$$\frac{d}{dt}\tilde{C}^{m\mathcal{Q}_y}_{q_x,q_y}(t,t') = -D\omega(q_x,q_y)\tilde{C}^{m\mathcal{Q}_y}_{q_x,q_y}(t,t'), \tag{3.57}$$

Now to solve Eq. (3.56), we require equal-time correlation function for two cumulative currents $\mathcal{Q}_x$ and $\mathcal{Q}_y$ in the perpendicular directions x and y, respectively,

$$\frac{d}{dt}\tilde{C}^{\mathcal{Q}_x\mathcal{Q}_y}_{q_x,q_y}(t,t) = D(1-e^{iq_x})\tilde{C}^{m\mathcal{Q}_y}_{q_x,q_y}(t,t) + D(1-e^{iq_y})\tilde{C}^{m\mathcal{Q}_x}_{q_x,q_y}(t,t) + \tilde{\Gamma}^{xy}_{q_x,q_y}(\rho), \tag{3.58}$$

where $\tilde{\Gamma}^{xy}_{q_x,q_y}(\rho) = \mu_1\mu_2\rho^2(1-e^{iq_x})(1-e^{-iq_y})/8(2\mu_1-\mu_2)$. Furthermore, following along the lines of the calculations given in section 3.4.2 and explicitly solving the above set of time-evolution equations, we calculate equal-time "cross"-correlation function (i.e., correlation between currents in x and y directions, measured up to time T) for the time-integrated bond current (by setting $r=s=0$),

$$\begin{aligned} C^{\mathcal{Q}_x\mathcal{Q}_y}_{0,0}(T,T) &= \frac{\mu_2\rho^2}{4(2\mu_1-\mu_2)}\frac{1}{L^2}\sum_{(q_x,q_y)\neq(0,0)}\frac{(1-e^{-D\omega T})}{\omega}\Lambda(q_x,q_y) \\ &\simeq B_1T + B_2 + B_3T^{-2}, \end{aligned} \tag{3.59}$$

where we denote

$$\Lambda(q_x,q_y) = [\lambda(q_x)+\lambda(q_y)-\lambda(q_x-q_y)],$$

and B_1, B_2 and B_3 are density-dependent constant coefficients, describing the asymptotic growth law for cross-correlation function. Note that, in this particular case of two-dimensional MCM-CoMC I, the coefficient B_1 of the first term corresponding to the linear-time growth is identically zero and we find

$$B_1 = \frac{\mu_2\langle m^2\rangle}{32}\left[2-\frac{1}{L^2}\sum_{(q_x,q_y)\neq(0,0)}\Lambda(q_x,q_y)\right] = 0; \tag{3.60}$$

this is however not the case for the other two-dimensional case of MCM-CoMC II discussed in the next section and depends on microscopic details. In the thermodynamic limit ($L\to\infty$ and global density ρ being fixed), the summation in the above equation can be written as an integral,

$$C^{\mathcal{Q}_x\mathcal{Q}_y}_{0,0}(T,T) = \frac{\mu_2\rho^2}{4(2\mu_1-\mu_2)}\frac{1}{(2\pi)^2}\int_0^{2\pi}\int_0^{2\pi}dq_xdq_y\frac{(1-e^{-D\omega T})}{\omega}\Lambda(q_x,q_y). \tag{3.61}$$

The form of the second factor $\Lambda(q_x,q_y) = \lambda(q_x)+\lambda(q_y)-\lambda(q_x-q_y)$ in the right hand side (inside the integral) of the above equation is generic in any dimension d, where one considers correlations between currents along any two perpendicular directions (here, x and y); see the sketch of the calculation details given in 3.6. In the above expression, we can write the factor explicitly as $\Lambda(q_x,q_y) = 2(1-\cos(q_x))+2(1-\cos(q_y))-2+2\cos(q_x)\cos(q_y)+2\sin(q_x)\sin(q_y)$. Now the integration over the last term $2\sin(q_x)\sin(q_y)$ in the factor Λ vanishes. Therefore, in the limit of small wave numbers, the remaining terms, in the leading order, can be approximated as

$\lambda(q_x)+\lambda(q_y)-\lambda(q_x-q_y)\approx q_x^2q_y^2/2$, leading to the following asymptotic form of the "cross-correlation" function for cumulative bond currents,

$$C_{0,0}^{\mathcal{Q}_x\mathcal{Q}_y}(T,T)\simeq B_2(\rho)-\frac{2\mu_2\rho^2}{16\mu_1^2(2\mu_1-\mu_2)\pi}T^{-2}, \tag{3.62}$$

which, for large times, saturates to a density-dependent constant,

$$B_2(\rho)=\frac{\mu_2\rho^2}{4(2\mu_1-\mu_2)}\frac{1}{(2\pi)^2}\int_0^{2\pi}\int_0^{2\pi}dq_xdq_y\frac{\Lambda(q_x,q_y)}{\omega}. \tag{3.63}$$

Notably, in the above equation, the dynamic "cross"-correlation function $C_{0,0}^{\mathcal{Q}_x\mathcal{Q}_y}(T,T)$ for time-integrated bond currents along two orthogonal (x and y) directions decays much faster, i.e., as a T^{-2} power law [see panel (e) of Fig. 3.9], as compared to that along the same direction, which decays as T^{-1} [see panel (b) of Fig. 3.9] obtained in Eq. (3.51). Now, we calculate the dynamical cross-correlation function for the instantaneous bond current as

$$C_{0,0}^{\mathcal{J}_x\mathcal{J}_y}(t,0)=\Gamma_{0,0}^{xy}\delta(t)-\frac{\mu_1^2\mu_2\rho^2}{128(2\mu_1-\mu_2)}\frac{1}{L^2}\sum_{q_x,q_y}e^{-D\omega(q_x,q_y)t}\omega(q_x,q_y)\Lambda(q_x,q_y), \tag{3.64}$$

where $\Gamma_{0,0}^{xy}=\mu_2\langle m^2\rangle/16$. Now, in the thermodynamic limit $L\to\infty$, we obtain, for time $t>0$,

$$\begin{aligned}C_{0,0}^{\mathcal{J}_x\mathcal{J}_y}(t,0)&=-\frac{\mu_1^2\mu_2\rho^2}{128(2\mu_1-\mu_2)}\frac{1}{(2\pi)^2}\int_0^{2\pi}\int_0^{2\pi}dq_xdq_ye^{-D\omega(q_x,q_y)t}\omega(q_x,q_y)\Lambda(q_x,q_y)\\&\simeq-\frac{3\mu_2\rho^2}{16\mu_1^2(2\mu_1-\mu_2)\pi}t^{-4}.\end{aligned} \tag{3.65}$$

In panel (a) of Fig. 3.9, we plot the variance $\langle[\mathcal{Q}^x(T)]^2\rangle_c\equiv C_{0,0}^{\mathcal{Q}_x\mathcal{Q}_x}(T,T)$ of time-integrated bond current along x direction in time interval T as a function of time T. In panel (b) of Fig. 3.9, the relative bond-current fluctuation $[A_2(\rho)-C_{0,0}^{\mathcal{Q}_x\mathcal{Q}_x}(T,T)]$, is plotted as a function of time T. The decay follows a T^{-1} power-law behavior as in Eq. (3.51) (purple dot-dashed). In panel (c) of the same figure, the correlation function $C_{0,0}^{\mathcal{J}_x\mathcal{J}_x}(t,0)$ for bond currents in the same (x) direction is plotted as a function of time t. The corresponding cross-correlation function $C_{0,0}^{\mathcal{Q}_x\mathcal{Q}_y}(T,T)$ for time-integrated bond currents along the orthogonal (x and y) directions and the asymptotic behavior of $A_2(\rho)-C_{0,0}^{\mathcal{Q}_x\mathcal{Q}_y}(T,T)$ are plotted as a function of time T in panels (d) and (e), respectively. In panel (f), the cross correlation function $C_{0,0}^{\mathcal{J}_x\mathcal{J}_y}(t,0)$ for bond current is plotted as a function of time t. The dashed-lines (orange) in panels (a), (c), (d), and (f) are obtained from theory as in Eqs. (3.50), (3.54), (3.61) and (3.65), respectively. In all the panels, simulations (blue line) are for periodic system of area 100×100 and global density $\rho=1.0$.

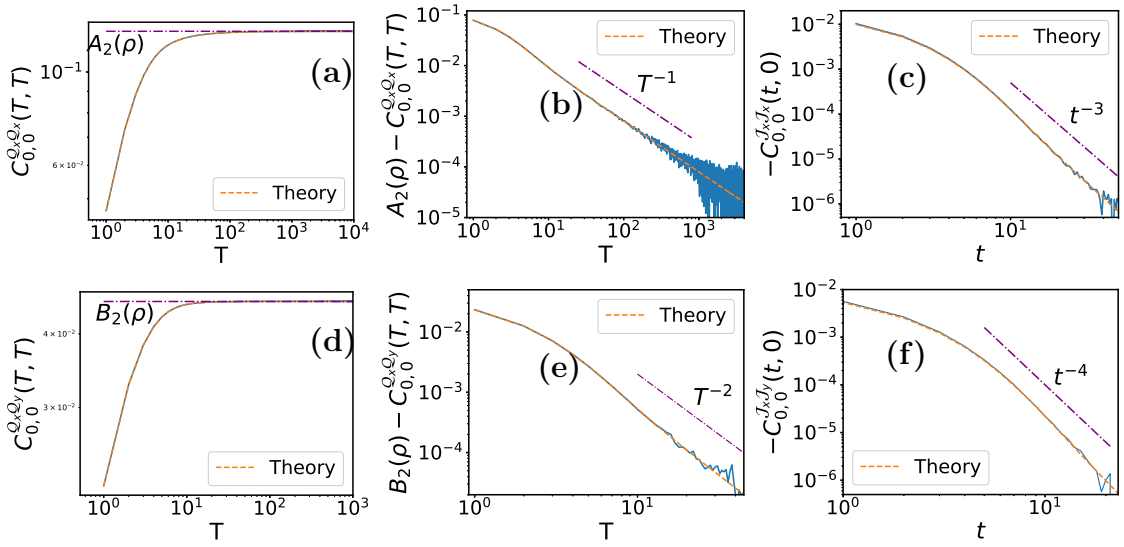

Figure 3.9: *MCM-CoMC I in two dimensions:* Panel (a): Equal-time bond-current fluctuations (in the same direction) $C_{0,0}^{\mathcal{Q}_x\mathcal{Q}_x}(T,T)$ are plotted as a function of time T. Panel (b): The relative bond current fluctuation $A_2(\rho)-C_{0,0}^{\mathcal{Q}_x\mathcal{Q}_x}(T,T)$, is plotted as a function of time T. The decay follows a T^{-1} [see Eq. (3.51)] behavior (purple dot-dashed). Panel (c): The instantaneous current correlation in the same direction, $C_{0,0}^{\mathcal{J}_x\mathcal{J}_x}(t,0)$, is plotted as a function of time t. The cross-correlation of the bond current, $C_{0,0}^{\mathcal{Q}_x\mathcal{Q}_y}(T,T)$ (panel d) , and the asymptotic behavior of $A_2(\rho)-C_{0,0}^{\mathcal{Q}_x\mathcal{Q}_y}(T,T)$ (panel e) are plotted as a function of time T. Panel (f): The cross current correlation, $C_{0,0}^{\mathcal{J}_x\mathcal{J}_y}(t,0)$, is plotted as a function of time t. The dashed-lines (orange) in panels (a), (c), (d), and (f) are obtained from theory as in Eqs. (3.50), (3.54), (3.61) and (3.65), respectively. In all panels, simulations (blue line) have been performed for system of area 100×100 and global density $\rho=1.0$.

3.5 Two-dimensional MCM-CoMC II

In this section, we consider the following model in two dimensional square lattice on a periodic domain. Mass at a site (i, j) is fragmented with unit rate, where the site retains a random fraction $\xi m_{i,j}$ of mass. The remaining mass is chipped off and divided into two equal parts, each of which, having $\tilde{\xi} m_{i,j}/2$ amount of mass, is transferred to each of the two nearest neighbor sites in the horizontal or vertical direction, i.e., either to $(i+1, j)$ and $(i-1, j)$ (horizontal direction) or to $(i, j+1)$ and $(i, j-1)$ (vertical direction), with equal probability. From the time evolution of the density profile, we were able to calculate the bulk-diffusivity $D = \mu_1/4$, which is the same as the value obtained in the previous model discussed in Section 3.4.

3.5.1 Correlation between currents along the same directions.

In this section, we calculate the dynamical correlation of current (correlation in the same direction), i.e., $C_{0,0}^{\mathcal{Q}_x \mathcal{Q}_x}$, in terms of the Fourier modes of the density correlation function $\tilde{C}^{mm}_{q_x,q_y}$ as:

$$C_{0,0}^{\mathcal{Q}_x \mathcal{Q}_x}(T,T) = T\frac{\mu_2\langle m^2\rangle}{4} + \frac{2D}{L^2}\sum_{q_x,q_y}\left[\frac{T}{D\omega} - \frac{(1-e^{-D\omega T})}{(D\omega)^2}\right]\lambda_{q_x}\left[D\tilde{C}^{mm}_{q_x,q_y} - \frac{\mu_2}{8}\langle m^2\rangle\lambda_{q_x}\right], \tag{3.66}$$

where $\tilde{C}^{mm}_{q_x,q_y}$ is Fourier models of the steady-state density correlation function and $C^{mm}_{0,0} + \rho^2 \equiv \langle m^2\rangle > 0$ is the second moment of mass at a single site. In the long-time regime, the above equation can be written in an asymptotic form,

$$C_{0,0}^{\mathcal{Q}_x \mathcal{Q}_x}(T,T) = \langle[\mathcal{Q}_x(T)]^2\rangle_c \simeq A_1 T + A_2 + A_3 T^{-1}, \tag{3.67}$$

where A_1, A_2 and A_3 are constant coefficients. We note that the coefficient of the first term corresponding to the linear-growth is *nonzero* and can be expressed as

$$A_1 = \frac{\mu_2\langle m^2\rangle}{8}\left[2 - \frac{1}{L^2}\sum_{q_x,q_y}\frac{\lambda^2(q_x)}{\omega}\right] \approx \frac{\mu_2\langle m^2\rangle(\pi-2)}{4\pi} \neq 0. \tag{3.68}$$

In Eq. (3.66), we have used the Fourier modes of the steady-state density correlation function $\tilde{C}^{mm}_{q_x,q_y}$, which can in principle be obtained from the following equation,

$$\frac{d}{dt}\tilde{C}^{mm}_{q_x,q_y}(t,t) = -2D\omega\tilde{C}^{mm}_{q_x,q_y}(t,t) + (\lambda^2_{q_x} + \lambda^2_{q_y})\frac{\mu_2}{8}\langle m^2\rangle. \tag{3.69}$$

In the limit $t \to \infty$, the above equation leads to the expression of density correlation function in the Fourier space,

$$\tilde{C}^{mm}_{q_x,q_y} = \frac{\mu_2}{4\mu_1}\langle m^2\rangle\frac{\lambda^2_{q_x} + \lambda^2_{q_y}}{\lambda_{q_x} + \lambda_{q_y}} = \rho S(q_x, q_y). \tag{3.70}$$

In the subsequent analysis, where we obtain various asymptotic behavior for bond current fluctuation and the corresponding exponents, we do not actually require

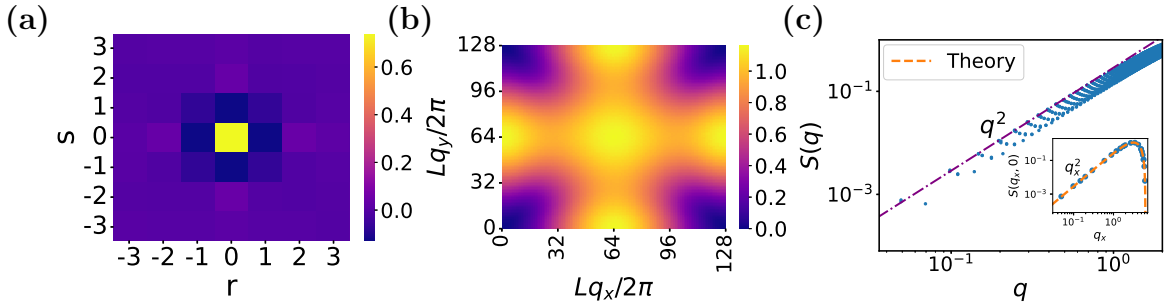

Figure 3.10: Panel (a): The steady-state density correlation $C^{mm}_{r,s}$ is depicted in a 2D color heat plot. In this panel, we have taken a periodic square lattice of area 100×100. Panel (b): The heat-map of steady-state structure factor $S(\mathbf{q})$ is plotted in two-dimensional (scaled) $\mathbf{q}$-plane. Panel (c): The structure factor $S(q)$ is plotted as a function of q. The guiding line (purple dashed-dotted) represents q^2 growth as $q \to 0$. In the inset of panel (c), we have plotted the structure factor $S(q_x, 0)$ as a function of q_x, setting $q_y = 0$ and compared it with theory (orange line) obtained from Eq. (3.70). In panels (b) and (c), we take a periodic square lattice of area $L \times L$ with $L = 128$ and global density $\rho = 1.0$ for the above-mentioned plots.

to explicitly solve for $\langle m^2 \rangle$, which simply appears as a proportionality constant. In panel (a) of Fig. 3.10, we have shown the heat map of steady-state density correlation $C^{mm}_{r,s}$ for system size 100×100. In panel (b), the heat plot of steady-state structure factor $S(\mathbf{q})$ has been plotted in two-dimensional (scaled) $\mathbf{q}$-plane. Panel (c): The structure factor $S(q)$ is plotted as a function of $q = \sqrt{q_x^2 + q_y^2}$. The guiding line (purple dashed-dotted) represents q^2 growth. In the inset of panel (c), we have plotted the structure factor $S(q_x, 0)$ as a function of q_x, setting $q_y = 0$ and theory line (orange) obtained from Eq. (3.70). We have measured structure factor for periodic square lattice of area 128×128. Global density has been taken to be $\rho = 1.0$ for all panels.

Furthermore, after some algebraic manipulations, we can rewrite Eq. (3.66) in the following asymptotic form,

$$
\begin{aligned}
C^{\mathcal{Q}_x\mathcal{Q}_x}_{0,0}(T,T) = \langle (\mathcal{Q}_x)^2 \rangle &= A_1 T + \frac{\mu_2 \langle m^2 \rangle}{(2\pi)^2} \int_0^{2\pi}\int_0^{2\pi} dq_x dq_y (1 - e^{-D\omega T}) \left[\frac{\lambda(q_x)}{\omega}\right]^2 \qquad (3.71) \\
&\simeq \frac{\mu_2 \langle m^2 \rangle (\pi - 2)}{4\pi} T + \frac{\mu_2 \langle m^2 \rangle}{2\pi}(\pi - 1) - \frac{3\mu_2 \langle m^2 \rangle}{8\mu_1 \pi} T^{-1} \\
&\equiv A_1 T + A_2 + A_3 T^{-1},
\end{aligned}
$$

where we use the approximation $\lambda(q_\alpha) \approx q_\alpha^2$. From the above equation, we find that the variance $C^{\mathcal{Q}_x\mathcal{Q}_x}_{0,0}(T,T)$ of time-integrated bond current grows linearly $\sim T$ with time; indeed, this particular growth law is qualitatively different from the other variants of one- and two-dimensional MCM-CoMC studied in the previous sections 3.2.2, 3.3, and 3.4, where A_1 is zero and the variance of time-integrated bond current saturate to a constant value at long times. We next calculate the correlation function, $C^{\mathcal{J}_x\mathcal{J}_x}_{0,0}(t,0) \equiv C^{\mathcal{J}_x\mathcal{J}_x}_{0,0}(t)$, for the bond currents in the same (x)

direction as follows:

$$C_{0,0}^{\mathcal{J}_x\mathcal{J}_x}(t,0) = \Gamma_{0,0}^{xx}\delta(t) - \frac{\langle m^2\rangle\mu_1\mu_2}{64}\frac{1}{L^2}\sum_{q_x,q_y} e^{-D\omega t}\lambda_{q_x}^2, \tag{3.72}$$

with $\Gamma_{0,0}^{xx} = \mu_2\langle m^2\rangle/4$. In the thermodynamic limit and for $t > 0$, the above equation can be written in the following integral form

$$C_{0,0}^{\mathcal{J}_x\mathcal{J}_x}(t,0) = -\frac{\langle m^2\rangle\mu_1\mu_2}{64}\frac{1}{(2\pi)^2}\int_0^{2\pi}\int_0^{2\pi} dq_x dq_y e^{-D\omega t}\lambda^2(q_x) \simeq -\frac{\mu_2\langle m^2\rangle}{32\pi\mu_1}t^{-3}, \tag{3.73}$$

where the above asymptotic expression has been calculated for large time and by using the approximation $\lambda(q) \approx q^2$. Using Eq. (3.72), also the power spectrum for instantaneous bond current can be calculated by taking the Fourier transform of the unequal-time bond current correlation function,

$$S_J(f) = \int_{-\infty}^{\infty} dt C_0^{\mathcal{J}_x\mathcal{J}_x}(t,0)e^{i2\pi ft} = S_J(0) + \frac{\langle m^2\rangle\mu_1\mu_2}{32DL^2}\sum_{q_x,q_y}\frac{\lambda_{q_x}^2}{\omega}\frac{4\pi^2f^2}{4\pi^2f^2 + D^2\omega^2}, \tag{3.74}$$

where the zero-frequency mode of the power spectrum is given by

$$S_J(0) = \frac{\mu_2\langle m^2\rangle}{8}\left[2 - \frac{1}{L^2}\sum_{q_x,q_y}\frac{\lambda^2(q_x)}{\omega}\right] = A_1 \equiv \lim_{T\to\infty}\frac{\langle\mathcal{Q}^2(T)\rangle_c}{T}. \tag{3.75}$$

It should be noted that the coefficient A_1 is actually nonzero for this particular variant in two (and higher) dimensions, signifying that, in temporal domain, time-integrated bond current is not hyperuniform and its variance has a linear growth as a function of time.

3.5.2 Correlation between currents along two perpendicular directions.

Now, we calculate the cross-correlation function for time-integrated bond currents in the two orthogonal directions (x and y) as follows:

$$C_{0,0}^{\mathcal{Q}_x\mathcal{Q}_y}(T,T) = -\frac{\langle m^2\rangle\mu_2}{16}\frac{1}{L^2}\sum_{q_x,q_y}\left[\frac{T}{\omega} - \frac{1-e^{-D\omega T}}{D\omega^2}\right]\Lambda(q_x,q_y)\gamma(q_x,q_y), \tag{3.76}$$

where $\gamma(q_x,q_y) = (2\lambda_{q_x}\lambda_{q_y} + \lambda_{q_x}^2 - \lambda_{q_y}^2)/(\lambda_{q_x} + \lambda_{q_y})$. In the thermodynamic limit, we can write the above equation in an integral form,

$$\begin{aligned} C_{0,0}^{\mathcal{Q}_x\mathcal{Q}_y}(T,T) &= -\frac{\langle m^2\rangle\mu_2}{16(2\pi)^2}\int_0^{2\pi}\int_0^{2\pi} dq_x dq_y\left[\frac{T}{\omega} - \frac{1-e^{-D\omega T}}{D\omega^2}\right]\Lambda(q_x,q_y)\gamma(q_x,q_y) \\ &\simeq -\frac{\langle m^2\rangle\mu_2(10-3\pi)\pi^4}{384}T + \frac{\langle m^2\rangle\mu_2\pi^2(3\pi-8)}{256\mu_1} - \frac{3\langle m^2\rangle\mu_2}{128\mu_1^3\pi}T^{-2}, \\ &\equiv B_1T + B_2 + B_3T^{-2}, \end{aligned} \tag{3.77}$$

where we have used the approximation $\lambda(q_\alpha) \approx q_\alpha^2$. Note that, in the long-time regime, the cross-correlation of the time-integrated current grows linearly with time, where the prefactor of the growth $B_1 < 0$ is *negative*. Physically, this negative sign implies that, if some current is generated along x direction over a time interval T, the current along y-direction flows in the negative direction due to the existence of current loops, or vortices, in two dimensional geometry [132]. However, quite interestingly, the sign of this cross-correlation function $C_{0,0}^{\mathcal{Q}_x\mathcal{Q}_y}$ for orthogonal (along x and y) currents is *positive* for the model (two-dimensional MCM-CoMC I) discussed in the previous section. Similarly, we have calculated the fluctuation of instantaneous current in different direction

$$C_{0,0}^{\mathcal{J}_x\mathcal{J}_y}(t,0) = -\frac{\langle m^2\rangle\mu_2\mu_1}{128}\frac{1}{(2\pi)^2}\int_0^{2\pi}\int_0^{2\pi} dq_x dq_y e^{-D\omega t}\Lambda(q_x,q_y)\gamma(q_x,q_y) \tag{3.78}$$
$$\simeq -\frac{9\langle m^2\rangle\mu_2}{128\mu_1^3\pi}t^{-4},$$

where we use the approximation $\lambda(q_\alpha) \approx q_\alpha^2$. In Fig. 3.11, we have plotted various time-dependent quantities involving current correlations in this model. In panel (a) of Fig. 3.11, the time-integrated bond-current fluctuation $C_{0,0}^{\mathcal{Q}_x\mathcal{Q}_x}(T,T)$ is plotted as a function of time T. In panel (b) of the same figure, the negative of the instantaneous current correlation $C_{0,0}^{\mathcal{J}_x\mathcal{J}_x}(t,0)$ is plotted as a function of time t. In panel (c), the negative of time-integrated "cross"-current correlation $C_{0,0}^{\mathcal{Q}_x\mathcal{Q}_y}$ is plotted as a function of time T. In panel (d), the negative of cross-correlation $C_{0,0}^{\mathcal{J}_x\mathcal{J}_y}(t,0)$ for instantaneous bond current is plotted as a function of time t. The orange dashed lines in all these panels represent the theory lines, where the asymptotic (purple dashed-dotted lines) there are obtained from Eqs. (3.71), (3.73), (3.77), and (3.78), respectively. Here, we have considered a periodic system with area 100×100 and global density $\rho = 1.0$.

3.6 Dynamic correlations in d dimensions: Sketch of the calculations

Let us consider a system on a d-dimensional periodic square lattice, where masses diffuse with both mass and CoM conserved. Now let us denote the time-integrated bond currents as $\mathcal{Q}_\alpha$ and $\mathcal{Q}_\beta$ along two orthogonal directions α and β (like x and y for $d = 2$), respectively. In this case, the unequal-time ($t > t'$) current correlation function in Fourier space can be written as

$$\frac{d}{dt}\tilde{C}_{\mathbf{q}}^{\mathcal{Q}_\alpha\mathcal{Q}_\beta}(t,t') = D(1-e^{iq_\alpha})\tilde{C}_{\mathbf{q}}^{m\mathcal{Q}_\beta}(t,t'), \tag{3.79}$$

where $\mathbf{q}$ is d-dimensional wave-number vector with q_α being the component of $\mathbf{q}$ along direction α. Equation (3.79) has a similar structure to that in one dimension, with D being the bulk-diffusion coefficient. To solve the above equation, we require the unequal-time mass-current correlation, which satisfies the following equation:

$$\frac{d}{dt}\tilde{C}_{\mathbf{q}}^{m\mathcal{Q}_\beta}(t,t') = -D\omega(\mathbf{q})\tilde{C}_{\mathbf{q}}^{m\mathcal{Q}_\beta}(t,t'), \tag{3.80}$$

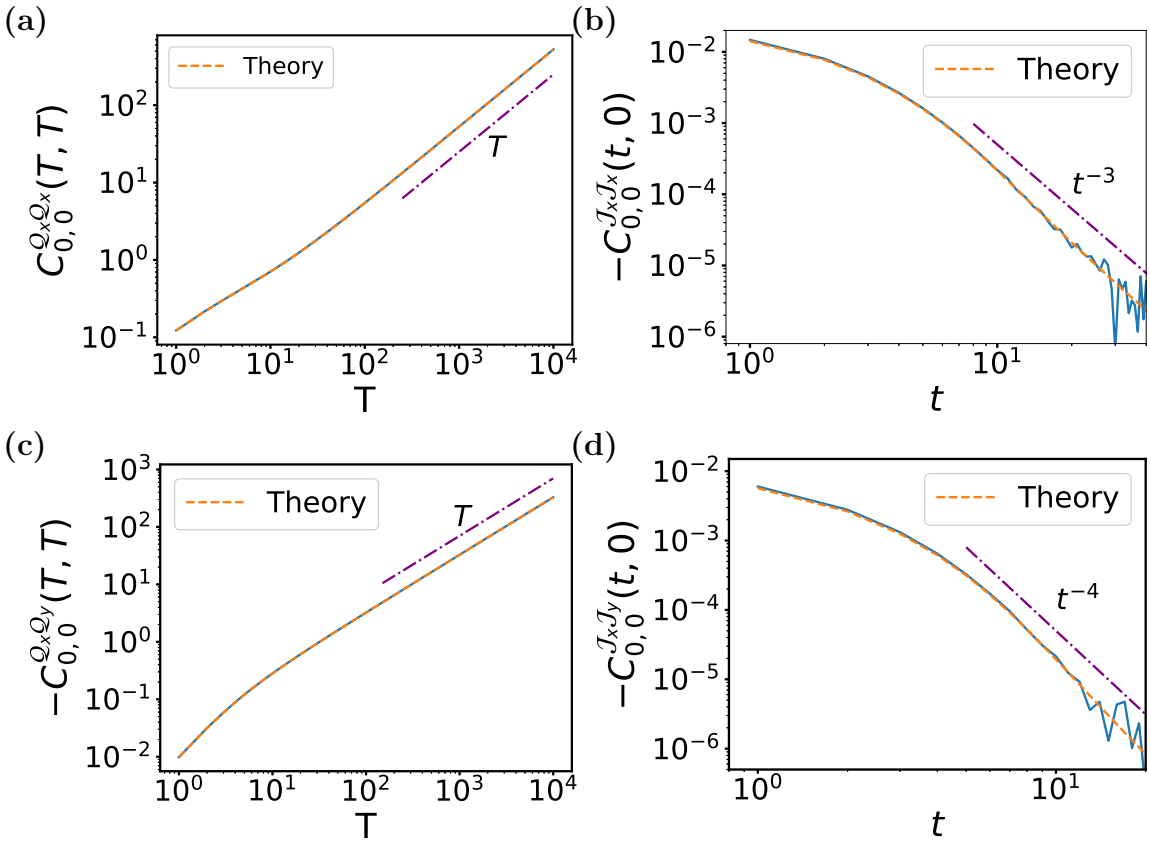

Figure 3.11: *MCM-COM II in two dimensions.* Panel (a): The bond-current fluctuation $C^{\mathcal{Q}_x\mathcal{Q}_x}_{0,0}(T,T)$ is plotted as a function of time T. Panel (b): Negative of instantaneous current correlation $C^{\mathcal{J}_x\mathcal{J}_x}_{0,0}(t,0)$ is plotted as a function of time t. Panel (c): The negative of time-integrated cross-current correlation $C^{\mathcal{Q}_x\mathcal{Q}_y}_{0,0}$ is plotted as a function of time T. Panel (d) Negative of instantaneous cross-current correlation $C^{\mathcal{J}_x\mathcal{J}_y}_{0,0}(t,0)$ is plotted as a function of time t. The orange dashed lines in panels (a), (b), (c) and (d) represent the theory lines and the asymptotic (purple dashed-dotted lines) are obtained from Eqs. (3.71), (3.73), (3.77), and (3.78), respectively. We take a periodic system of area 100×100 and the global density $\rho = 1.0$.

where $\omega(\mathbf{q}) = \sum_\alpha \lambda(q_\alpha)$. To obtain the general solution of the above two equations, namely Eqs. (3.79) and (3.80), we also require the equal-time current-current and mass-current correlation functions. First, we write the time evolution of equal-time current-current correlation function as

$$\frac{d}{dt}\tilde{C}_{\mathbf{q}}^{\mathcal{Q}_\alpha \mathcal{Q}_\beta}(t,t) = D(1-e^{iq_\alpha})\tilde{C}_{\mathbf{q}}^{m\mathcal{Q}_\beta}(t,t) + D(1-e^{iq_\beta})\tilde{C}_{\mathbf{q}}^{m\mathcal{Q}_\alpha}(t,t) + \tilde{\Gamma}_{\mathbf{q}}^{\alpha\beta}(\rho), \quad (3.81)$$

where $\tilde{\Gamma}_{\mathbf{q}}^{\alpha\beta}(\rho)$ is a model-dependent quantity. The equal-time mass-current correlation can be expressed as

$$\frac{d}{dt}\tilde{C}_{\mathbf{q}}^{m\mathcal{Q}_\beta}(t,t) = -D\omega(\mathbf{q})\tilde{C}_{\mathbf{q}}^{m\mathcal{Q}_\beta}(t,t) + \tilde{f}_{\mathbf{q}}^{\beta}(\rho), \quad (3.82)$$

where

$$\tilde{f}_{\mathbf{q}}^{\beta}(\rho) = (1-e^{-iq_\beta})G_\beta^{I/II}(\mathbf{q},\rho). \quad (3.83)$$

Here $G_\beta^I(\mathbf{q},\rho) = [D\tilde{C}_{\mathbf{q}}^{mm}(\rho) - g^I(\rho)\sum_\alpha \lambda(q_\alpha)]$ and $G_\beta^{II}(\mathbf{q},\rho) = [D\tilde{C}_{\mathbf{q}}^{mm}(\rho) - g^{II}(\rho)\sum_\alpha \lambda(q_\alpha)\delta_{\alpha,\beta}]$, and $g^I(\rho) = \mu_2\langle m^2\rangle/8$ and $g^{II}(\rho) = \mu_2\langle m^2\rangle/16$ are two model-dependent constants; also, in the above equation, case I corresponds to simultaneous mass transfer along all d axes and case II corresponds to mass transfer along a β-axis (chosen randomly during a mass transfer event), whereas CoM is conserved in both cases. By integrating Eq. (3.82), we obtain

$$\tilde{C}_{\mathbf{q}}^{m\mathcal{Q}_\beta}(t',t') = \int_0^{t'} dt'' e^{-D\omega_{\mathbf{q}}(t'-t'')}\tilde{f}_{\mathbf{q}}^{\beta}(\rho). \quad (3.84)$$

Then by integrating Eq. (3.81) and using Eq. (3.84), finally we obtain the equal-time current correlation function in the Fourier space,

$$\tilde{C}_{\mathbf{q}}^{\mathcal{Q}_\alpha \mathcal{Q}_\beta}(t,t) = \int_0^t dt \tilde{\Gamma}_{\mathbf{q}}^{\alpha\beta}(\rho) + D\Lambda(q_\alpha,q_\beta)G_\beta^{I/II}(\mathbf{q},\rho)\int_0^t dt' \int_0^{t'} dt'' e^{-D\omega_{\mathbf{q}}(t'-t'')}. \quad (3.85)$$

Now integrating Eq. (3.79) and using Eqs. (3.85), (3.80), and (3.84), finally, we obtain the unequal-time current correlation in the Fourier space as

$$\tilde{C}_{\mathbf{q}}^{\mathcal{Q}_\alpha \mathcal{Q}_\beta}(t,t') \quad (3.86)$$
$$= \tilde{\Gamma}_{\mathbf{q}}^{\alpha\beta}t' + D\Lambda(q_\alpha,q_\beta)G_{\mathbf{q}}^{I/II}(\rho)\left[\int_0^{t'} dt'' \int_0^{t''} dt''' e^{-D\omega_{\mathbf{q}}(t''-t''')} + \frac{1}{2}\int_{t'}^{t} dt'' \int_0^{t''} dt''' e^{-D\omega_{\mathbf{q}}(t''-t''')}\right],$$

where $\Lambda(q_\alpha,q_\beta) = [\lambda(q_\alpha) + \lambda(q_\beta) - \lambda(q_\alpha - q_\beta)]$. After performing the integration of Eq. (3.86) and putting $t = t' = T$, we have equal time bond current fluctuation as

$$\tilde{C}_{\mathbf{q}}^{\mathcal{Q}_\alpha \mathcal{Q}_\beta}(T,T) = \tilde{\Gamma}_{\mathbf{q}}^{\alpha\beta}T + D\Lambda(q_\alpha,q_\beta)G_\beta^{I/II}(\mathbf{q},\bar{\rho})\left[\frac{T}{D\omega_q} - \frac{1-e^{-D\omega_q T}}{(D\omega(\mathbf{q}))^2}\right]. \quad (3.87)$$

Above current correlation in real space can be obtained by taking the inverse Fourier transform on both sides as

$$C_{\mathbf{r}}^{\mathcal{Q}_\alpha \mathcal{Q}_\beta}(T,T) = \frac{T}{L^d}\sum_{\mathbf{q}} \tilde{\Gamma}_{\mathbf{q}}^{\alpha\beta} e^{-i\mathbf{q}\cdot\mathbf{r}} + \frac{T}{L^d}\sum_{\mathbf{q}\neq 0} \frac{\Lambda(q_\alpha,q_\beta) G_\beta^{I/II}(\mathbf{q},\bar{\rho})}{\omega(\mathbf{q})} e^{-i\mathbf{q}\cdot\mathbf{r}} \\ -\frac{1}{L^d}\sum_{\mathbf{q}\neq 0} \frac{\Lambda(q_\alpha,q_\beta) G_\beta^{I/II}(\mathbf{q},\bar{\rho})(1-e^{-D\omega_q T})}{D\omega^2(\mathbf{q})} e^{-i\mathbf{q}\cdot\mathbf{r}} \tag{3.88}$$

For $t > 0$, the unequal-time (instantaneous) bond current correlation function can be written from the above equation as

$$C_{\mathbf{r}}^{\mathcal{J}_\alpha \mathcal{J}_\beta}(t,0) = \frac{D}{2}\int_{BZ} d^d\mathbf{q} \Lambda(q_\alpha,q_\beta) G_\beta^{I/II}(\mathbf{q},\bar{\rho}) e^{-D\omega_{\mathbf{q}} t} e^{-\mathbf{i}\mathbf{q}\cdot\mathbf{r}}. \tag{3.89}$$

Now, we have, in the small wave-number limit,

$$\Lambda(q_\alpha,q_\beta) \simeq \begin{cases} \frac{q_\alpha^2 q_\beta^2}{2} & \text{for } \alpha \neq \beta, \\ 2q_\alpha^2 & \text{for } \alpha = \beta \end{cases} \tag{3.90}$$

and $G_{\mathbf{q}}^{I/II} \sim \mathcal{O}(q_\alpha^2, q_\beta^2)$; these can be used in (3.89) to derive the asymptotic expression for the bond current correlation function as given in Eqs. (3.91) and (3.93).

3.7 Generalization to arbitrary dimensions

In the previous sections, we have explicitly calculated the steady-state dynamic correlation functions for instantaneous and time-integrated bond current in MCMs with CoM conservation (MCM-CoMCs) in $d = 1$ and 2 dimensions; moreover, the corresponding exponents governing the decay (or, growth) of these dynamic correlations have been exactly determined. In this section, we discuss how the long-time asymptotics can be generalized to d dimensions through simple dimensional scaling analysis. For example, the (two-point) unequal-time bond-current correlation function $C_0^{\mathcal{J}_\alpha \mathcal{J}_\alpha}(t,0)$ has the following asymptotic power-law decay in d dimensions as a function of time t,

$$C_0^{\mathcal{J}_\alpha \mathcal{J}_\alpha}(t,0) \sim -\int_0^\infty q^4 e^{-Dq^2 t} q^{d-1} dq \sim -t^{-(2+d/2)}, \tag{3.91}$$

where $\alpha \in [x,y]$ denote x or y direction, and we have approximated $\omega(\mathbf{q}) \approx q^2$, with q being the magnitude of the wave-number vector $\mathbf{q}$ in d-dimensions. The above asymptotic form has been derived by simple power counting of q_α's in the integrands of Eqs. (3.54) and (3.73) for the MCM-CoMC models I and II, respectively. Alternatively, the expression can also be derived directly from the general expression of current correlations given in Eq. (3.89) by replacing β by α and using the scale transformation $q_\alpha = q'_\alpha/\sqrt{t}$; for details, see 3.6. The power spectrum for the correlation function for the bond currents along a particular direction α in the small-frequency regime has an asymptotic form,

$$S_J(f) = \int_{-\infty}^{\infty} dt C_0^{\mathcal{J}_\alpha \mathcal{J}_\alpha}(t,0) e^{i2\pi f t} \simeq A_1 + \text{Const.} f^{(1+d/2)}, \tag{3.92}$$

where $A_1 \equiv S_J(0)$, the zero-frequency mode, can be expressed in the thermodynamic limit as $A_1 = \lim_{T\to\infty}\langle \mathcal{Q}_\alpha^2(T)\rangle/T$. In one dimension, as demonstrated in Secs. 3.2 and 3.3, the coefficient A_1 vanishes, signifying that the dynamic current fluctuations exhibit "class-I" hyperuniformity [4], albeit in the time domain, as previously observed for a different quantity - activity fluctuations - in a sandpile model [50]. However, in higher dimensions ($d > 1$), A_1 can be nonzero, depending on the microscopic details (e.g., for MCM CoMC II, $A_1 > 0$, as shown in (3.68)). Consequently, dynamic hyperuniformity may be lost even though static fluctuations remain hyperuniform, with $S(q \to 0) \to 0$.

One can also calculate the "cross"-correlation functions for currents in two orthogonal directions; that is, if a current is initially ($t = 0$) generated in a bond in the x-direction, one may ask how it is correlated to the current across a bond in (orthogonal) y-direction at a later time t. The asymptotic form of the cross correlation functions in d-dimension can be written as

$$C_0^{\mathcal{J}_\alpha \mathcal{J}_\beta}(t,0) \sim -\int_0^\infty q^6 e^{-Dq^2 t} q^{d-1} dq \sim -t^{-(3+d/2)}. \tag{3.93}$$

The above asymptotic form has been derived by power counting of q_α's in the integrands of Eqs. (3.65) and (3.78) in the MCM-CoMC models I and II, respectively. Alternatively, it can be derived from Eq. (3.89) by replacing β by α and using the transformation $q_\alpha = q'_\alpha/\sqrt{t}$; for details, see 3.6. The asymptotic forms in Eqs. (3.91), (3.92) and (3.93) are expected to be generic for diffusive systems with CoM conservation, regardless of microscopic details; however, the existence of phase transition in the system (e.g., in the presence of a threshold condition in dynamics) can change the scenario. As there are no cross-correlations in one dimension, Eq. (3.93) is applicable only for $d > 1$.

Equivalently, one can also obtain the variance (second cumulant) $\langle \mathcal{Q}_\alpha^2(T)\rangle_c$ of time-integrated bond-current in a fixed time interval T, having the following asymptotic form in the thermodynamic limit,

$$\langle \mathcal{Q}_\alpha^2(T)\rangle_c \equiv C_{0,0}^{\mathcal{Q}_\alpha \mathcal{Q}_\alpha}(T,T) \simeq A_1 T + A_2 + A_3 T^{-d/2}, \tag{3.94}$$

where A_i's are density- and parameter-dependent constants. The above asymptotic form has been obtained by power counting of q_α's in the integrands of Eqs. (3.50) and (3.71) in the MCM-CoMC models I and II, respectively. It can also be obtained by taking the inverse Fourier transform of Eq. (3.86), replacing β by α and then using the scale transformation $q_\alpha = q'_\alpha/\sqrt{t}$. Quite strikingly, depending on dimensions and the microscopic details of the models, the variance of time-integrated bond current saturates at long times, i.e, $A_1 = 0$ vanishes [see Eqs. (3.32) and (3.49)]. Though this feature is presumably generic in one dimension, however in higher dimensions $d > 1$, the coefficient A_1 need not always vanish [see Eq. (3.68) for MCM-CoMC II in $d = 2$]. We can also calculate the cross-correlation function $C_{0,0}^{\mathcal{Q}_\alpha \mathcal{Q}_\beta}(T,T)$, which has an asymptotic form,

$$C_{0,0}^{\mathcal{Q}_\alpha \mathcal{Q}_\beta}(T,T) \simeq B_1 T + B_2 + B_3 T^{-(1+d/2)}, \tag{3.95}$$

where B_i's are constant (density- and parameter-dependent) coefficients. The asymptotic form has been obtained by power counting of q_α's in the integrands of Eqs.

(3.61) and (3.77) in the MCM-CoMC models I and II, respectively. It can also be derived by taking the inverse Fourier transform of Eq. (3.86), using $\alpha \neq \beta$ and then the scale transformation $q_\alpha = q'_\alpha/\sqrt{t}$. As in the case of the correlation function for time-integrated bond currents (in the same direction), the cross-correlation function for currents in the two orthogonal (e.g., x and y) directions can also saturate at long times, and B_1 in that case is zero (i.e., no long-time linear growth of correlation function), depending on the microscopic details, as demonstrated in the two-dimensional case of MCM-CoMC I [see Eq. (3.60)].

3.8 Summary and concluding remarks

In this chapter, we have theoretically investigated steady-state dynamic correlations for currents in a broad class of mass transport processes, known as mass chipping models (MCMs), which have both mass and *center of mass* (CoM) being conserved. We study these models - MCMs with CoM conservation, called here MCM-CoMCs - specifically in $d = 1$ and 2 dimensional periodic domain of size L; the results can be suitably generalized to arbitrary dimensions. Notably, the MCM-CoMCs belong to the generalized Kipnis-Marchioro-Pressutti (KMP) models [15, 34, 57, 58, 60, 116, 117], where masses fragment (i.e, get chipped off from parent masses), diffuse and then coalesce with neighboring masses with constant rate. They have broken time-reversal symmetry, thus no detailed balance, in the bulk and, in most cases, their steady states cannot be described by the equilibrium Boltzmann-Gibbs distribution. Recently, the role of detailed-balance violation and the CoM conservation have received significant attention in the context of an exotic state of matter, that of "hyperuniform" systems, which are examples of many-body correlated systems with their density fluctuations anomalously suppressed. Indeed, unlike in typical diffusive systems having a single conserved quantity (e.g., mass), the fluctuation properties of the MCM having both mass and CoM conservation are fundamentally different. We show that both dynamic and static fluctuations in the MCM-CoMCs are greatly suppressed in spatial and temporal domains, leading to the emergence of an extreme form of ("class I") hyperuniform state of matter.

In these models, we show that, in the limit of small wave numbers $q \to 0$, the static structure factor $S(q)$ vanishes as q^2. Indeed, this particular dependence of the static structure factor at small wave numbers is a signature of an extreme form of ("class-I" [4]) hyperuniformity in the spatial domain, implying an extreme suppression of density fluctuations in the systems. Furthermore, we analytically calculate various time-dependent quantities, including the time-varying density profiles that relax from a given initial condition and the dynamic correlation functions for currents. We show that the two-point dynamic correlation $C_0^{\mathcal{J}_\alpha \mathcal{J}_\alpha}(t, 0)$ for bond current in a particular direction, with $\alpha \in x, y$, varies as $\sim -t^{-(2+d/2)}$ as a function of time t in d-dimensions. For example, in $d = 1$ dimension, the temporal decay is described by a power law $t^{-5/2}$; this should be contrasted with that in the one-dimensional symmetric simple exclusion processes (SSEPs) [78] or the MCMs [103], having only a single (mass) conservation law, where the dynamic correlation function for current decays slower, $\sim t^{-3/2}$, as a function of time. Likewise, in the thermodynamic limit, the power-spectrum $S_J(f)$ for bond current in the models studied here has an asymptotic form as $S_J(f) \simeq A_1 + \text{Const.} f^{1+d/2}$ for small frequencies

$f \to 0$. That is, in one dimension where we have $A_1 = 0$, the small-frequency power spectrum for MCM-CoMCs is much suppressed as compared to that in, e.g. the one-dimensional SSEP, where the corresponding behavior is described by the $f^{1/2}$ power law [78]. However, the long-time behavior of the second cumulant, or the variance, $\langle \mathcal{Q}_\alpha^2(T) \rangle_c$ of the time-integrated bond current $\mathcal{Q}_\alpha(T)$ in a time interval T has a long-time asymptotic form $\langle \mathcal{Q}_\alpha^2(T) \rangle_c \equiv C_{0,0}^{\mathcal{Q}_\alpha \mathcal{Q}_\alpha}(T,T) \simeq A_1 T + A_2 + A_3 T^{-d/2}$, which is quite nuanced and has an intricate behavior, depending on the dimension and microscopic details of the models. While, in one dimension, the variance $\langle \mathcal{Q}_\alpha^2(T) \rangle_c$, quite strikingly, saturates at long times, the variance in higher dimensions (say, $d = 2$) could either saturate or grow linearly with time. Another quantity of interest in higher dimensions is the cross-correlation function $C_0^{\mathcal{J}_\alpha \mathcal{J}_\beta}(t,0) \sim -t^{-(3+d/2)}$ for currents in two orthogonal (e.g., x and y) directions α and β (with $\alpha \neq \beta$); the correlation function decays as a power law, which is however faster than that when $\alpha = \beta$. The cross-correlation function $C_{0,0}^{\mathcal{Q}_\alpha \mathcal{Q}_\beta}(T,T)$ for currents $\mathcal{Q}_\alpha$ and $\mathcal{Q}_\beta$ in the two orthogonal directions α and β (e.g., x and y) has a long-time asymptotic form $C_{0,0}^{\mathcal{Q}_\alpha \mathcal{Q}_\beta}(T,T) \simeq B_1 T + B_2 + B_3 T^{-(1+d/2)}$, which, depending on the microscopic details, can also saturate at long times, and B_1 in that case simply vanishes. The subtle effects due to the formation of current loops (vortices [132]), generated at later times due to the bond current at an initial time ($t = 0$), could physically explain the reduction of current fluctuations, as well as the vanishing of the coefficients A_1 and B_1 in some cases, in the presence of CoM conservation. Usually, in higher dimensions without CoM conservation, these current loops would typically feed in (positive feedback) the current at later times (as well as the cumulative current overall), thus typically enhancing the current fluctuations. However, the CoM conservation generates opposing current loops (clockwise and anticlockwise), which decrease current fluctuations in the systems. Furthermore, depending on the microscopic details, a greater number of opposing current loops can be formed, such as in the case of the first variant MCM-COMC-I, where mass is transported simultaneously along all axes and directions. The precise quantitative characterization of the spatio-temporal structure of these current loops (or, vortices) is however beyond the scope of the present study, and will be considered elsewhere [133].

Though MCMs have been extensively investigated throughout the past several decades, the role of an additional conservation law, such as the CoM conservation, on relaxation and fluctuation properties of such systems however remains unexplored and lacks good theoretical understanding. Indeed, recently, there has been growing interest in characterizing large-scale properties of systems having multiple conserved quantities, especially in the context of quantum many-body systems, like fractonic fluids and spin-systems with dipole-like (or, multipole-like) conservation laws [127, 128]. In the latter cases, the density relaxation are found to be subdiffusive [126, 134]; however, it must be noted that these models of course have time-reversal symmetry, lack of which, as we have demonstrated here, can indeed have a drastic impact on the relaxation processes. To systematically investigate the issue, here we ask what happens when the time-reversal symmetry, or detailed balance, is actually broken in the bulk, which is the case for the broad class of models studied in this work. Indeed, in the context of the MCM-CoMCs considered here, we find that, despite highly constrained microscopic dynamics with CoM conservation, the density relaxation in the absence of time-reversal symmetry need not be subdiffusive [44,

135, 136], and we show that the density relaxation in MCM-CoMCs is diffusive. Nevertheless, the fluctuation properties of MCM-CoMCs differ significantly from those of typical diffusive systems with a single conserved quantity, such as symmetric exclusion processes [78, 137] and MCMs without CoM conservation [103].

We conclude the paper with a few remarks. Despite having a nonequilibrium steady state, which is not described by the Boltzmann-Gibbs distribution and has a nontrivial steady-state structure having finite spatial correlations in the bulk, MCM-CoMCs are amenable to analytical calculations. The analytical tractability arises from the fact that not only the MCM-CoMCs have a "gradient property" [137], but also the bulk-diffusion coefficient is *independent* of density; in other words, the local diffusive current is a *linear* function of local masses as seen in Eq. (3.11). In fact, the latter aspect - the *linearity property* of Eq. (3.11) - is quite crucial for performing explicit analytical calculations as done in the present work. We show that the above linearity property leads to the time-evolution equations for the two-point (in general, n-point) correlation functions to *not* involve higher-order correlations and thus to close onto themselves. Of course, many other dynamical variations of these models are possible. For example, adding a threshold condition on the mass transfer rules (in other words, mass-dependent chipping rates) would certainly make the model more interesting because of the possibility of a nonequilibrium phase transition in the system, similar to the absorbing phase transition observed in the BRO model [93] or the continuous-mass version of the celebrated Manna sandpile [12, 105]. However, it would immediately make the correlation functions have an infinite BBGKY-like hierarchy, rendering the model analytically almost intractable in even one dimension. Indeed, it remains a challenge to derive rigorous results for time-dependent properties of the latter class of systems, and the exact results derived in this work could provide some useful insights in that direction.

4

Generic power laws in higher-dimensional lattice models

4.1 Introduction

Lattice models have played a crucial role in developing a statistical mechanics framework for systems driven out of equilibrium, particularly those having a conserved quantity (e.g., mass) [19, 36, 38, 138, 139]; for reviews, see [9, 54]. However, most analytical studies rely on approximation techniques [139] and phenomenological field theories [36, 38], and exact results are relatively rare [33, 140–142]. Despite decades of intense numerical and theoretical investigations, the precise nature of spatial structures in nonequilibrium systems lacks a good theoretical understanding [7, 95, 143, 144].

It is well known that out-of-equilibrium systems exhibit power-law correlations when translational symmetry is broken − such as in boundary-driven [11, 54, 138, 145, 146] or disordered systems [147] − or when rotational symmetry is absent [148, 149]. However, whether such systems can have scale-invariant spatial structures when all underlying (lattice) symmetries are preserved remains an open issue [150]. If scale invariance indeed emerges under these symmetries, an important question arises: What classes of nonequilibrium systems are capable of generating such spatial structures? A good theoretical understanding of this issue is still lacking. Perhaps not surprisingly, the fact that, in higher dimensions, a wide class of conserved-mass transport processes, e.g., those studied in Refs. [13, 19, 43, 105], possess "generic scale invariance" in the presence of all symmetries of the lattice and even far from a phase transition (critical) point is hitherto unknown (presumably due in part to

This chapter is based on the paper, **Generic power laws in higher-dimensional lattice models with multidirectional hopping**, Animesh Hazra, Tanmoy Chakraborty, Anirban Mukherjee and Punyabrata Pradhan (accepted in Phys. Rev. E; arXiv.2503.18365)

the weak strength of the power-law correlations). Indeed, the latter scenario − the appearance of power laws far from the "critical point" − does not quite conform to the conventional understanding of critical phenomena, where criticality is achieved at a particular point in the parameter space. This issue is also intriguingly connected to the idea of self-organized criticality (SOC) proposed by Bak, Tang, and Wiesenfeld (BTW) [11] as an explanation for the scale-invariant structures abundant in nature.

More specifically, consider, e.g., the Ising model, a paradigm for equilibrium systems with short-ranged interactions, where correlations decay algebraically only at the critical point and short-ranged elsewhere. Usually, in isotropic systems far from criticality, the correlation function $C(\mathbf{r})$ for densities at two spatially points separated by position vector $\mathbf{r} \equiv \{r_\alpha\}$ on a $d-$dimensional space, with $\alpha = 1, 2, \ldots, d$, is short-ranged. Consequently, in the thermodynamic limit, the static structure factor $S(\mathbf{q})$ − Fourier transform of $C(\mathbf{r})$ − as a function of wave-vector $\mathbf{q} \equiv \{q_\alpha\}$ is analytic and, in the leading order of small $q = |\mathbf{q}| \to 0$, $S(\mathbf{q}) \simeq S_0(\bar{\rho}) - S_1(\bar{\rho})|\mathbf{q}|^2$; here, the two coefficients $S_0(\bar{\rho})$ and $S_1(\bar{\rho})$ depend on global density $\bar{\rho} = M/L^d$ with M being total mass (conserved) in the system. Taking a cue from equilibrium, the prevalent view even in nonequilibrium is that " ... *as for the Ising model, SOC typically exists at a critical point in the relevant parameter space.*" (see page 1 in Ref. [38]). That is, closed and isotropic systems such as conserved sandpiles [36, 38], are scale-invariant only at the (absorbing) phase transition point, and likely have a finite correlation length otherwise. We, however, argue that, unlike in equilibrium, this particular scenario is atypical, and scale invariance is rather generic in nonequilibrium, even in the presence of the lattice rotation and translation symmetries. We characterize a class of lattice models by identifying an interesting feature common to such rotation-symmetric systems − namely, a specific kind of dynamics referred to as *multidirectional hopping* − which plays a central role in generating the scale-invariant behavior.

In this paper, we show that higher-dimensional lattice models with mass-conserving and multidirectional hopping have power-law correlations, quite contrary to the expectations, for *generic* parameter values and even far from (above) "critical" (absorbing-phase transition) point, if any. We substantiate our assertion in (i) conserved mass chipping models (MCMs) − generalized versions of random average processes − involving fragmentation, diffusion, and aggregation of masses [13, 14, 19, 20, 86] and (ii) conserved sandpiles [36, 38, 43, 45, 105, 113, 119, 140, 151] − the paradigm for systems undergoing absorbing-phase transition from active to absorbing phase below a critical density. These models typically have multidirectional hopping, where *multiple* fragments of mass (*multiple* particles) at a lattice site hop out simultaneously in *several* directions with certain rate and thus violate detailed balance. They have been extensively studied in the past, but, to our knowledge, have never been reported to have scale invariance far from a phase transition point.

In this chapter, using both hydrodynamic and microscopic theories, we show that, on a periodic hypercubic lattice in dimensions $d > 1$, steady-state static density-density and "activity"-density correlation functions in these systems decay, in the thermodynamic limit and at large distance $r = |\mathbf{r}|$, as a power law $\sim 1/r^\eta$ with exponent $\eta = d + 2$; in threshold-activated systems like sandpiles, local "activity" at a site indicates whether there can be toppling of "grains" or particles ("active")

or not ("inactive") [11]. The strength of the power law is calculated exactly for several models and expressed in terms of the bulk-diffusion coefficient and the Onsager matrix (or, the mobility tensor). Strikingly, in models having axial bidirectional hopping of masses, the *scaled* "activity"-density and density-density (two-point) static correlation functions (connected), $C^{\mathcal{A}m}_{\mathbf{r}} = \langle \mathcal{A}(\mathbf{0})m(\mathbf{r})\rangle_c$ and $C^{mm}_{\mathbf{r}} = \langle m(\mathbf{0})m(\mathbf{r})\rangle_c$, respectively, have a generic asymptotic form [see Eq. (4.2)]; in two dimensions, we have, for $\mathbf{r} = (x, 0)$ with x large,

$$\frac{2}{(\gamma_1 - \gamma_2)} C^{\mathcal{A}m}_{x,0} = \frac{2D}{(\gamma_1 - \gamma_2)} C^{mm}_{x,0} \simeq \frac{6}{\pi x^4}, \tag{4.1}$$

where D is the bulk-diffusion coefficient and the coefficients γ's are related to the Onsager matrix [see Eqs. (4.7) and (4.8), and Fig. (4.6)].

To demonstrate our arguments, the systems we investigate here are arguably the simplest in the class: They are described by continuous-time Markov processes with nearest-neighbor hopping, and are closed (mass-conserving), *diffusive* (reflection-symmetric hopping), spatially homogeneous (translation-invariant) and "isotropic" (lattice-rotation-symmetric); of course, they have *no* net mass current in the steady state. Most crucially, though, they possess multidirectional hopping, which, we demonstrate, leads to *nonanalyticity* in the static structure factor. In other words, under certain symmetry conditions as observed for lattice models on a periodic domain, the emergence of power laws in higher dimensions depends on the violation of detailed balance and the presence of multidirectional hopping. Indeed, for such systems, we find that the static structure factor for small wave vector $\mathbf{q} = \{q_\alpha\}$ on a d-dimensional hypercubic lattice has a generic form,

$$S(\mathbf{q}) \simeq S_0(\bar{\rho}) - S_1(\bar{\rho})|\mathbf{q}|^2 + S_2(\bar{\rho}) \frac{\sum_{\alpha=1}^{d} q_\alpha^4}{|\mathbf{q}|^2}, \tag{4.2}$$

where $S_2(\bar{\rho})$ is another density-dependent coefficient. The structure factor and the correlation functions are "isotropic" in the sense that they still have the rotational symmetry of the lattice. However, the higher-order derivatives of the third term in the rhs of Eq. (4.2) (corresponding to the prefactor S_2) are nonanalytic, and results in power-law density correlations $C(\mathbf{r}) \sim \int d^d\mathbf{q} S(\mathbf{q}) e^{-i\mathbf{q}.\mathbf{r}} \sim 1/r^{d+2}$ for large r.

The rest of the chapter is organized as follows. In Sec. 4.2, we present a hydrodynamic theory applicable to isotropic diffusive systems in general. In Sec. 4.3, we define several nearest-neighbor mass transport models considered in this study. In Sec. 4.4, to substantiate the hydrodynamic theory, we provide microscopic calculations for variants of MCMs and threshold-activated systems like sandpiles and density correlation for these models in 4.4.3. Finally, in Sec. 4.5, we summarize with some concluding remarks.

4.2 Hydrodynamic theory

To physically understand the dynamical origin of the nonanalyticity of the static structure factor, let us simply begin by formulating a linearized hydrodynamic theory of a *closed diffusive* system on a periodic domain, albeit out of equilibrium due to violation of detailed balance in (microscopic) configuration space. To proceed

further, let us define a coarse-grained (fluctuating) density $m(\mathbf{r},t)$ at position $\mathbf{r}$ and time t. The density fluctuation $\delta m(\mathbf{r},t) = m(\mathbf{r},t) - \bar{\rho}$ around a homogeneous state with global density $\bar{\rho} = \langle m(\mathbf{r}, t \to \infty)\rangle = M/L^d$, satisfy a (discrete) continuity equation due to mass conservation,

$$\partial_t \delta m(\mathbf{r},t) = -\nabla.\left[\mathbf{j}^{(d)}(\mathbf{r},t) + \mathbf{j}^{(fl)}(\mathbf{r},t)\right], \tag{4.3}$$

where ∇ denotes (discrete) gradient and the local instantaneous current $\mathbf{j} = \mathbf{j}^{(d)} + \mathbf{j}^{(fl)}$ in the rhs is decomposed into two parts, with $\mathbf{j}^{(d)}$ and $\mathbf{j}^{(fl)}$ being called diffusive and fluctuating ("noise") currents, respectively. The diffusive current has the following form,

$$\mathbf{j}^{(d)}(\mathbf{r},t) = -\nabla \mathcal{A}[m(\mathbf{r},t)], \tag{4.4}$$

where $\mathcal{A}[m(.)]$ is a coarse-grained fluctuating observable, a generalized "activity", which is typically a fast (nonconserved) variable and, in the hydrodynamic framework, can be considered "slave" to the local (conserved and slowly varying) density field $m(\mathbf{r},t)$ [41]; for explicit form of the model-specific quantity $\mathcal{A}$, see microscopic calculations presented in Secs. 4.4.2. Now, considering small fluctuations $\delta m \ll \bar{\rho}$ and performing a small-gradient expansion, the diffusive current $\mathbf{j}^{(d)}(\mathbf{r},t)$ in Eq. (4.4) is written as the gradient (discrete on a lattice) of the density field $m(\mathbf{r},t)$,

$$\mathbf{j}^{(d)}(\mathbf{r},t) \simeq -D(\bar{\rho})\nabla m(\mathbf{r},t), \tag{4.5}$$

where we define the bulk-diffusion coefficient $D(\bar{\rho}) = d\langle\mathcal{A}\rangle/d\bar{\rho}$. In the hydrodynamic framework, the bulk-diffusion coefficient, in principle, depends on local density. But, here it is simply treated as a constant $D(\bar{\rho})$ with $\bar{\rho}$ being the global density around which the small fluctuations are considered, thus justifying the linearized hydrodynamics discussed below. The fluctuating current has the properties $\langle j_\alpha^{(fl)}(\mathbf{r},t)\rangle = 0$, and its strength can be written as

$$\langle j_\alpha^{(fl)}(\mathbf{r},t) j_\beta^{(fl)}(\mathbf{r}',t')\rangle = \Gamma^{\alpha\beta}(\mathbf{r}'-\mathbf{r},\bar{\rho})\delta(t-t'). \tag{4.6}$$

Here, the Onsager transport-coefficient matrix $\mathbf{\Gamma} \equiv \{\Gamma^{\alpha\beta}(\mathbf{r}'-\mathbf{r},\bar{\rho})\}$ represents the strength of the fluctuating current along any two directions α and β; the elements of the Onsager matrix are nonzero in general and depend on density and other model-specific parameters. From microscopic calculations for models considered here, we can analytically calculate the Onsager transport coefficients and thus obtain the strength of the fluctuating ("noise") current correlation along the same direction α,

$$\Gamma_{\mathbf{q}}^{\alpha\alpha}(\bar{\rho}) = \gamma_0(\bar{\rho}) + \gamma_1(\bar{\rho})\lambda(q_\alpha), \tag{4.7}$$

and that along two orthogonal directions $\alpha \neq \beta$,

$$\Gamma_{\mathbf{q}}^{\alpha\beta}(\bar{\rho}) = \gamma_2(\bar{\rho})(1-e^{\mathbf{i}q_\alpha})(1-e^{-\mathbf{i}q_\beta}), \tag{4.8}$$

where $\lambda(q_\alpha) = 2(1-\cos q_\alpha)$. Here we have introduced a set of density-dependent coefficients γ_0, γ_1 and γ_2. As we show later, for unidirectional mass transfer (or, 1-particle transfer along a randomly chosen direction), the fluctuating currents along two orthogonal directions are uncorrelated, and we have the following form of $\Gamma^{\alpha\beta} = \gamma_0(\bar{\rho})\delta_{\alpha,\beta}\delta(\mathbf{r}-\mathbf{r}')$. However, this particular (delta-correlated) form of $\Gamma^{\alpha\beta}(\mathbf{r}-\mathbf{r}')$

is not valid for multidirectional hopping, where cross-correlations between currents along two orthogonal directions also generally appear and moreover $\Gamma^{\alpha\beta}$ has now finite spatial correlations.

We note that, in principle, the hydrodynamic equation (4.3) involves nonlinear terms, which arise from the density-dependence of the bulk diffusion coefficient D and Onsager matrix $\Gamma^{\alpha\beta}$ – related to the noise strength – thus making the noise multiplicative. Indeed, for the specific models studied here, the density-dependence of the relevant transport coefficients appearing in the hydrodynamics are later calculated using a microscopic dynamical approach. Nevertheless, it is still quite instructive to follow the linearized hydrodynamic theory, which, though approximate, captures the structure factor, and thus the correlation function, remarkably well.

By taking Fourier transform of both sides of Eq. (4.3) and using Eq. (4.5), we obtain

$$\delta m(\mathbf{q},t) = \sum_{\alpha} \int_0^t dt' e^{-D\omega(\mathbf{q})(t-t')}(e^{\mathrm{i}q_\alpha}-1) j_\alpha^{(fl)}(\mathbf{q},t'), \tag{4.9}$$

where $\delta m(\mathbf{q},t) = \sum_{\mathbf{r}} \delta m(\mathbf{r},t) e^{\mathrm{i}\mathbf{q}\cdot\mathbf{r}}$ and $\omega(\mathbf{q}) = \sum_\alpha \lambda(q_\alpha)$ are the Fourier transforms of excess density $\delta m(\mathbf{r},t)$ and eigenvalue of the (discrete) Laplacian operator, respectively. Equation (4.9) leads to the dynamic structure factor $S(\mathbf{q},t) = L^{-d}\langle|\delta m(\mathbf{q},t)|^2\rangle$,

$$S(\mathbf{q},t) = \sum_{\alpha,\beta}\left(1-e^{-2D\omega(\mathbf{q})t}\right)\frac{(1-e^{-\mathrm{i}q_\alpha})(1-e^{\mathrm{i}q_\beta})\Gamma^{\alpha\beta}_{\mathbf{q}}}{2D\omega(\mathbf{q})}, \tag{4.10}$$

and the static structure factor (by taking $t\to\infty$),

$$S(\mathbf{q}) = \frac{1}{2D\omega(\mathbf{q})}\sum_{\alpha,\beta}(1-e^{-\mathrm{i}q_\alpha})(1-e^{\mathrm{i}q_\beta})\Gamma^{\alpha\beta}_{\mathbf{q}} \equiv \frac{\mathcal{B}(\mathbf{q})}{2D\omega(\mathbf{q})}, \tag{4.11}$$

where we construct a scalar quantity out of the Onsager matrix,

$$\mathcal{B}(\mathbf{q}) = \sum_{\alpha,\beta}(1-e^{-\mathrm{i}q_\alpha})(1-e^{\mathrm{i}q_\beta})\Gamma^{\alpha\beta}_{\mathbf{q}}. \tag{4.12}$$

Now, using Eqs. (4.7) and (4.8), we explicitly obtain

$$\mathcal{B}(\mathbf{q}) = \omega(\mathbf{q})\left[\gamma_0 + \gamma_2\sum_\alpha \lambda(q_\alpha) + (\gamma_1-\gamma_2)\frac{\sum_\alpha \lambda^2(q_\alpha)}{\sum_\alpha \lambda(q_\alpha)}\right] \tag{4.13}$$

as a function of $\mathbf{q}$. Indeed, later we resort to a microscopic approach and derive the above expressions for $\mathcal{B}(\mathbf{q})$ and $S(\mathbf{q},t)$ for all models (MCMs and sandpiles) considered in this chapter. Now, by comparing Eq. (4.2) to Eq. (4.13), one can see that the structure factor can be written in the leading order of small $\mathbf{q}$ as given in Eq. (4.2), and thus we immediately obtain,

$$S_0(\bar{\rho}) = \frac{\gamma_0}{2D}, \tag{4.14}$$

$$S_1(\bar{\rho}) = -\frac{\gamma_2}{2D}, \tag{4.15}$$

$$S_2(\bar{\rho}) = \frac{(\gamma_1-\gamma_2)}{2D}, \tag{4.16}$$

in terms of the transport coefficients D and γ's (density-dependent in general). The above equations (4.11)-(4.16) constitute the main results of this chapter. In fact, the coefficients D and γ's can be calculated exactly for MCMs and in terms of the activity for sandpiles (see Table 4.1).

Importantly, we can now see that the third term (i.e., its higher-order derivatives) in Eq. (4.2), corresponding to the coefficient S_2, is nonanalytic. Also, from Eq. (4.13), we find that the case with $\gamma_1 \neq \gamma_2$ corresponds to nonzero coefficient $S_2 \neq 0$ in Eq. (4.2) and thus to correlations that exhibit a power-law behavior; otherwise, $S_2 = 0$ and the correlations are short-ranged. Furthermore, Eq. (4.11) could be thought of as a modified fluctuation-dissipation relation, connecting the structure factor, density relaxation and current fluctuation in these out-of-equilibrium systems.

4.3 Models

To derive hydrodynamics discussed in the previous section, we consider a broad class of microscopic models, with and *without* detailed balance, on a periodic $d-$dimensional hypercubic lattice of volume L^d. Notably, the systems have mass-conserving dynamics with *symmetric* hopping, which results in diffusive relaxations at large spatio-temporal scales. We consider both unidirectional and multidirectional hopping; also, some of the models we consider have an additional center-of-mass conservation (CoMC), i.e., where both mass and center of mass (CoM) are conserved. The models evolve through a continuous-time stochastic Markov dynamics as described below.

For simplicity, we define the models (and later present the simulation results) in two dimensions; generalization to higher dimensions is straightforward.

4.3.1 Unidirectional (one-particle) hopping

In this class of models, a *single* particle hops from a site (i, j) with rate $u(i, j)$, which depends on the amount of mass at that site. The particle is then attempted to get transferred to one of its nearest neighbors with equal probability ($1/2d$ on a d-dimensional square lattice); the move is accepted depending on the presence of hardcore constraint. For example, in symmetric simple exclusion process (SSEP) having hardcore exclusion [142], the hop rate is given by $u(i, j) = m(i, j)$, with the occupation variable $m(i, j) \in \{0, 1\}$ taking value 1 (occupied) or 0 (vacant), provided the destination site is vacant; otherwise, $u(i, j) = 0$. On the other hand, in the zero-range processes (ZRPs) having unbounded occupation (no hardcore constraint) [61], one can have the hop rate, $u(i, j) = 1 + b/m(i, j)$, where mass $m(i, j) \in \{0, 1, 2, \ldots\}$ can take any nonnegative integer value, and $b \geq 0$ is a model parameter.

4.3.2 Multidirectional (multi-particle) hopping

Mass chipping models (MCMs)

Another class of conserved-mass transport processes [13, 34] we consider here involve fragmentation, diffusion, and coalescence of masses, with total mass in the system

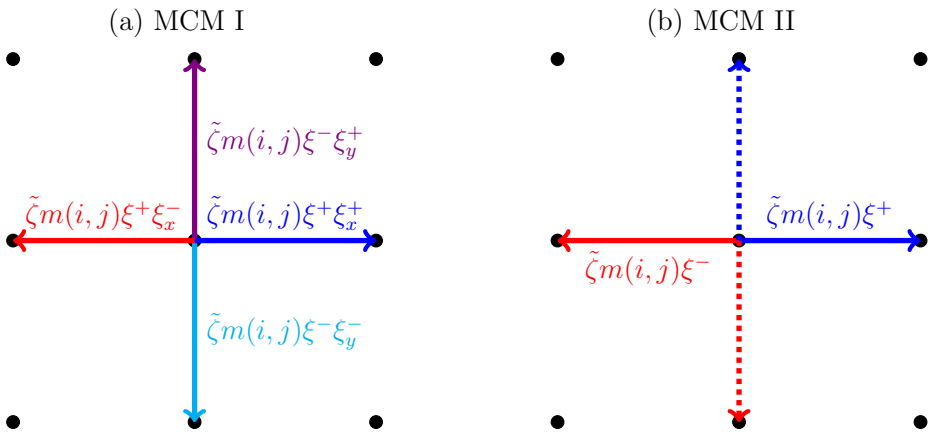

Figure 4.1: Schematic representation of dynamical update rules in mass transport processes in two-dimensional space for two variants: (a) MCM I and (b) MCM II. The arrows indicate the direction of mass transfer from the central site (i, j) to its neighbors, with color-coded expressions representing the corresponding fractions of masses transferred during the particular update. Panel (a): In MCM I, mass is distributed simultaneously to all four nearest neighbors along both $x-$ and $y-$ axes. Panel (b): On the other hand, in MCM II, mass is transferred to only two neighboring sites along either horizontal (solid line) or vertical (dotted line) axis, with equal probability. For other variants (not shown here), when center of mass (CoM) is conserved, the two chunks of masses transferred from site (i, j), in +ve and −ve directions along a particular axis, are the same; the respective variants are referred to as MCM-CoMC I and MCM-CoMC II.

being conserved. These models are variants of random average processes [16, 19, 20], which belong to the generalized Kipnis-Marchioro-Presutti (KMP) class of models [15, 22, 57, 117, 118], and have been intensively studied in the literature over the past decades. In these systems, a site (i, j) is updated with unit rate as following. The site retains a constant fraction ζ of its mass $m(i, j) \geq 0$, while the remaining mass is randomly fragmented and redistributed among its neighbors. To proceed further, let us first define a parameter $\tilde{\zeta} = 1 - \zeta$ (a constant, model parameter) and the random variables $\xi^+ \in (0, 1)$ and $\xi^- = (1 - \xi^+)$, where ξ^+ is drawn from a uniform distribution (for simplicity), with mean μ_1 and second moment μ_2; similarly, we also define random variables ξ_x^+ and $\xi_x^- = (1 - \xi_x^+)$, and ξ_y^+ and $\xi_y^- = (1 - \xi_y^+)$, where ξ_x^+ and ξ_y^+ are i.i.d and uniformly distributed in unit interval.

In the first variant of MCM, which we refer to as *MCM I*, the remaining mass is fragmented into four random parts, $\tilde{\zeta}m(i, j)\xi^+\xi_x^+$, $\tilde{\zeta}m(i, j)\xi^+\xi_x^-$, $\tilde{\zeta}m(i, j)\xi^-\xi_y^+$ and $\tilde{\zeta}m(i, j)\xi^-\xi_y^-$ and coalesces to four nearest neighbors $(i + 1, j)$, $(i - 1, j)$, $(i, j + 1)$ and $(i, j - 1)$, respectively (see Fig. 4.1(a)). In second variant of MCM, refered to as *MCM II*, the chipped-off mass is randomly fragmented into two parts, $\tilde{\zeta}m(i, j)\xi^+$ and $\tilde{\zeta}m(i, j)\xi^-$, and then coalesces with either the nearest neighbors in the $x-$direction, $(i + 1, j)$ and $(i - 1, j)$, or with the nearest neighbors in the $y-$direction, $(i, j + 1)$ and $(i, j - 1)$, respectively with equal probability. The mass-transfer rules are schematically presented in Fig. 4.1. Later, we show that both MCM I and II have power-law correlations.

Further, to explore the role of conservation laws, one can think of a variant of MCM I, which, in addition to mass conservation, can now have a center-of-mass conservation (CoMC). In that case, a random fraction of the mass is retained $\xi m(i,j)$, and the remaining fraction is split into four *equal* parts (thus imposing CoM conservation on the microscopic dynamics), each of which is then redistributed to each of the four nearest-neighbor sites; we call this CoM-conserving variant as *MCM-CoMC I*. In another variant of MCM II with CoMC, simply called *MCM-CoMC II*, the chipped-off mass is divided into two equal parts, which are transferred in the opposite directions along either $x-$direction or $y-$direction, chosen with equal probability. Interestingly, while MCM-CoMC I has short-ranged correlations, MCM-CoMC II has power-law correlations.

Sandpile models

Here, we consider two variants of conserved ("fixed-energy") stochastic sandpiles − the Oslo [18] and Manna [12] models, which have been extensively studied in the literature. For simplicity, in the present chapter, we study two particular variants of the conserved sandpiles with center-of-mass conservation (CoMC) − the Oslo [43] and Manna [40] models with CoMC; generalization to other particle transfer rules (say, that without CoMC [12, 140] or having continuous mass variables [119]) is not difficult. In the Oslo model [43], an active site with mass $m(i,j) \geq m^\star(i,j)$ greater than or equal to a threshold value topples with unit rate: Two particles *simultaneously* hop out, with one particle transferred to one its nearest neighbors along a randomly chosen axis, either $(i \pm 1, j)$ or $(i, j \pm 1)$, i.e., axial transfer in opposite directions. Here, the threshold $m^\star(i,j)$ is a random variable that takes value 2 or 3; after each toppling, $m^\star(i,j)$ is reset randomly. The difference between the Oslo model and the Manna model with CoMC [40] is that, in the latter model, $m^\star(i,j) = 2$ is fixed, but, in the Oslo model, $m^\star(i,j) \in [2,3]$ is chosen randomly during a toppling event. As discussed later, both the Oslo and Manna models with CoMC have power-law correlations.

Notably, unlike the models studied in Refs. [147, 149, 152, 153], hopping rates in the models considered in this work satisfy all symmetries of the lattice. However, unlike the equilibrium models such as the SSEP and ZRPs, the MCMs and sandpile models do not possess time-reversal symmetry, meaning they lack detailed balance in the configuration space. Nevertheless, because the hopping rates in the models are "isotropic", there is no biasing in any direction and, therefore, the systems have no mass current in the real space. The violation of detailed balance arises because, in MCMs and sandpiles, when multiple particles or chunks of mass simultaneously hop out from a lattice site to several neighboring sites (a forward transition), there is, by definition, no corresponding reverse transition. Therefore, the multidirectional hopping implies that the Kolmogorov criterion − a necessary and sufficient condition for detailed balance to hold − is not satisfied in these processes [80, 154]. Consequently, unlike in equilibrium systems, which have detailed balance, there can now be a steady-state probability current in the configuration space, thus driving the systems out of equilibrium. However, large-scale relaxation dynamics (above the absorbing-phase transition point in sandpiles) still remain diffusive. In fact, one can derive and verify an exact diffusion equation (nonlinear in general) that governs the

time evolution of the density field in such models [41, 56, 103].

4.4 Characterization of fluctuations: A Microscopic Approach

4.4.1 Current fluctuations and derivation of hydrodynamics

In this section, we substantiate the hydrodynamic theory as presented in Sec. 4.2 by deriving the hydrodynamics from microscopic dynamical calculations. To this end, we define time-integrated (cumulative) bond current $\mathcal{Q}_\alpha(\mathbf{r}, T)$, along direction α, as the net mass flux along the bond between lattice sites $\mathbf{r}$ and $\mathbf{r}+\hat{e}_\alpha$ over a time interval T, where $\hat{e}_\alpha$ is unit vector along $+\alpha$ direction. More specifically, consider two mass-transfer events during time interval T where amount of masses δm^+ and δm^- are transferred from site $\mathbf{r}$ to $\mathbf{r}+\hat{e}_\alpha$ and from site $\mathbf{r}+\hat{e}_\alpha$ to $\mathbf{r}$, respectively. Then the cumulative bond current increases by $\mathcal{Q}_\alpha(\mathbf{r}, T) \to \mathcal{Q}_\alpha(\mathbf{r}, T) + \delta m^+ - \delta m^-$. Accordingly, instantaneous bond current, $j_\alpha(\mathbf{r}, t)$, represents the net mass flow per unit time at position $\mathbf{r}$ and time t. That is, the time-integrated bond current up to time t along a given direction α can be written as

$$\mathcal{Q}_\alpha(\mathbf{r}, t) = \int_0^t dt' j_\alpha(\mathbf{r}, t'), \tag{4.17}$$

where $j_\alpha(\mathbf{r}, t)$ is the instantaneous current. Now the local bond current $j_\alpha(\mathbf{r}, t)$ can be decomposed into two parts − diffusive (slow or hydrodynamic) and fluctuating (fast or "noise") components,

$$j_\alpha(\mathbf{r}, t) = j_\alpha^{(d)}(\mathbf{r}, t) + j_\alpha^{(fl)}(\mathbf{r}, t), \tag{4.18}$$

such that $\langle j_\alpha(\mathbf{r}, t)\rangle = \langle j_\alpha^{(d)}(\mathbf{r}, t)\rangle$ and therefore $\langle j_\alpha^{(fl)}\rangle = 0$. The first term corresponds to the diffusive current $j_\alpha^{(d)}(\mathbf{r}, t)$, while the second term represents the fluctuating current $j_\alpha^{(fl)}(\mathbf{r}, t)$ along direction α.

For diffusive systems (as considered in this work), the first and second moments of the (time-integrated) bond current are related to the two transport coefficients (density-dependent in general), called the bulk-diffusion coefficient D and the mobility tensor or the Onsager matrix $\Gamma^{\alpha\beta}$ [54, 67]. These transport coefficients can, in general, be a tensor quantity, but, for the models considered here, only the latter one is a tensor, while the former one (D) is a scalar due to isotropy (lattice-rotation symmetry). More specifically, as shown later using microscopic calculations, the average bond current can be written as a gradient of local mass,

$$\frac{d\langle \mathcal{Q}_\alpha(\mathbf{r}, t)\rangle}{dt} = \langle j_\alpha^{(d)}(\mathbf{r}, t)\rangle = -\frac{\partial\langle \mathcal{A}\rangle}{\partial x_\alpha} \equiv -D(\rho)\frac{\partial \rho}{\partial x_\alpha}, \tag{4.19}$$

where we define a density field $\rho(\mathbf{r}, t) = \langle m(\mathbf{r}, t)\rangle$, $\mathcal{A}(\mathbf{r})$ is a local observable [called "genaralized activity" identified later in Eq. (4.55)] and $D(\rho) = d\langle \mathcal{A}\rangle(\rho)/d\rho$ is the density-dependent bulk-diffusion coefficient. In the last step, we have used a local-equilibrium property where the observable $\mathcal{A}$ is slave to the density field. To characterize the second moment, or more generally, the two-point correlations

of bond current, we calculate unequal-time ($t > t'$) correlation function for bond current in different directions α and β through the following time-evolution equation,

$$\frac{d}{dt}C_{\mathbf{r}}^{\mathcal{Q}_\alpha \mathcal{Q}_\beta}(t,t') = C_{\mathbf{r}}^{j_\alpha^{(d)} \mathcal{Q}_\beta}(t,t'), \tag{4.20}$$

where we have defined dynamic correlation as $C_{\mathbf{r}}^{\mathcal{Q}_\alpha \mathcal{Q}_\beta}(t,t') = \langle \mathcal{Q}_\alpha(\mathbf{0},t)\mathcal{Q}_\beta(\mathbf{r},t')\rangle_c$ of two observable $\mathcal{Q}_\alpha$ and $\mathcal{Q}_\beta$. To solve the above equation, we need to obtain equal-time current-current correlation, which satisfies the following equation,

$$\frac{d}{dt}C_{\mathbf{r}}^{\mathcal{Q}_\alpha \mathcal{Q}_\beta}(t,t) = C_{\mathbf{r}}^{j_\alpha^{(d)} \mathcal{Q}_\beta}(t,t) + C_{\mathbf{r}}^{\mathcal{Q}_\alpha j_\beta^{(d)}}(t,t) + \Gamma_{\mathbf{r}}^{\alpha\beta}. \tag{4.21}$$

The first two terms in the rhs of the above equation correspond to an infinitesimal change of bond current either in α or in β direction, whereas the third term $\Gamma_{\mathbf{r}}^{\alpha\beta}$ arise from the simultaneous update of current in both (orthogonal) directions α and β [see Eqs. (4.7) and (4.8)]. Now, using some algebraic manipulations, it can be shown that the source term in the above equation is directly related to the strength of the fluctuating current through the Onsager matrix $\Gamma^{\alpha\beta}$ as given below:

$$C_{\mathbf{r}}^{j_\alpha^{(fl)} j_\beta^{(fl)}}(t,t') = \Gamma^{\alpha\beta}(\mathbf{r})\delta(t-t'); \tag{4.22}$$

see appendix for details. In mass transport processes with nearest-neighbor mass transfer (see Table 4.1), one can find from the infinitesimal-time update rules for currents that the strength of fluctuating current along the same direction (say, α), denoted as $\Gamma^{\alpha\alpha}(\mathbf{r})$, is "positive" at the origin $\delta(\mathbf{r})$ and "negative" at the nearest neighbors $\mathbf{r} \pm \hat{e}_\alpha$. This leads to the following form in d dimensions,

$$\Gamma^{\alpha\alpha}(\mathbf{r}) = (\gamma_0 + 2\gamma_1)\delta(\mathbf{r}) - \gamma_1[\delta(\mathbf{r}+\hat{e}_\alpha) + \delta(\mathbf{r}-\hat{e}_\alpha)], \tag{4.23}$$

which has the lattice-reflection symmetry ($\mathbf{r} \to -\mathbf{r}$). Note that, for unidirectional mass transfer (e.g., in the SSEP and ZRPs), we have $\gamma_1 = 0$; on the other hand, in models with center-of-mass conservation, we have $\gamma_0 = 0$. Furthermore, the strength $\Gamma^{\alpha\beta}(\mathbf{r})$ of the fluctuating current along two orthogonal directions α and β is interestingly *nonzero* if the systems allow multidirectional hopping along orthogonal directions (e.g., MCM I). Indeed, we can explicitly write down the analytic expressions for the strength of the cross-correlation functions for fluctuating currents, along two orthogonal directions $\alpha \neq \beta$ in d dimensions as given below:

$$\Gamma^{\alpha\beta}(\mathbf{r}) = \Gamma^{\beta\alpha}(-\mathbf{r}) = \gamma_2[\delta(\mathbf{r}) - \delta(\mathbf{r}-\hat{e}_\alpha) - \delta(\mathbf{r}+\hat{e}_\beta) + \delta(\mathbf{r}-\hat{e}_\alpha+\hat{e}_\beta)]. \tag{4.24}$$

Now, after taking Fourier transform of Eqs. (4.23) and (4.24), we immediately obtain Eqs. (4.7) and (4.8), respectively. In Fig. 4.2, we have schematically represented the spatial range of the fluctuating-current strength along the same direction, $\Gamma^{\alpha\alpha}(\mathbf{r})$ [in panel (a)], as well as along the two perpendicular directions, $\Gamma^{\alpha\beta}(\mathbf{r})$ and $\Gamma^{\alpha\beta}(\mathbf{r})$ [in panels (b) and (c)].

Furthermore, we define a "scalar" (density-dependent) mobility χ – constructed out of the Onsager matrix $\Gamma^{\alpha\beta}$ – as the variance of the space-time-integrated fluctuating current, integrated over time interval T and over the entire system of volume $V = L^d$. That is, for nearest-neighbor hopping, if δm_α amount of mass is transferred in $+\alpha$ or $-\alpha$ direction, one adds or subtracts $+\delta m_\alpha$ or $-\delta m_\alpha$, respectively,

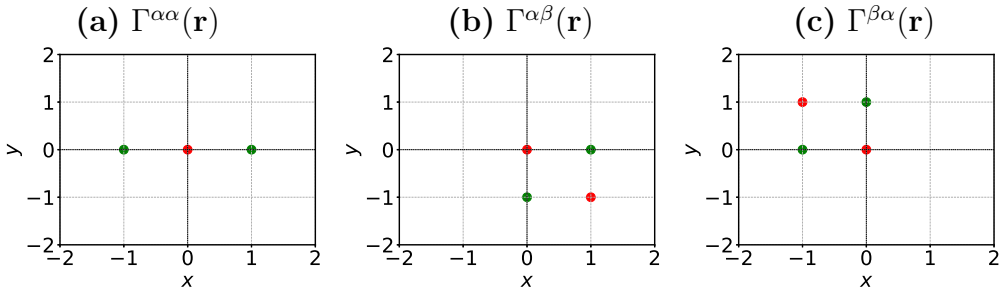

Figure 4.2: *MCM I:* The spatial range of fluctuating current strength is illustrated both along the same direction ($\alpha = x$) (panel (a)) and the perpendicular direction ($\alpha = x$ and $\beta = y$) (panels (b) and (c)) for different nearest-neighbor mass transport processes of the model in $d = 2$ considered here. In both panels (a) and (b), the same color represents the same magnitude and sign: red for positive and green for negative values.

and then considers the variance of the weighted sum of total mass transferred in a time interval T. The scaled variance of the weighted sum is related to the mobility χ through the space-time-integrated currents as

$$2\chi \equiv \lim_{T\to\infty,V\to\infty} \frac{1}{VTd}\left\langle \left[\sum_{\alpha,\mathbf{r}} \mathcal{Q}_\alpha(\mathbf{r},T)\right]^2\right\rangle = \lim_{T\to\infty,V\to\infty} \frac{1}{VTd}\left\langle \left[\sum_{\alpha,\mathbf{r}} \mathcal{Q}^{(fl)}_\alpha(\mathbf{r},T)\right]^2\right\rangle \tag{4.25}$$

$$= \lim_{T\to\infty,V\to\infty} \frac{1}{VTd}\left\langle \sum_{\alpha,\beta,\mathbf{r},\mathbf{r}'} \mathcal{Q}^{(fl)}_\alpha(\mathbf{r},T)\mathcal{Q}^{(fl)}_\beta(\mathbf{r}',T)\right\rangle = \frac{1}{d}\sum_{\alpha,\beta}\sum_{\mathbf{r}}\int_{-\infty}^{\infty} C_{\mathbf{r}}^{j^{(fl)}_\alpha j^{(fl)}_\beta}(t,0)dt,$$

where in the first step we used $\mathcal{Q}_\alpha = \mathcal{Q}^{(d)}_\alpha + \mathcal{Q}^{(fl)}_\alpha$ and that the sum over diffusive (gradient) current $\sum_{\mathbf{r}} \mathcal{Q}^{(d)}_\alpha(\mathbf{r},T) \equiv \int dt \sum_{\mathbf{r}} j^{(d)}_\alpha(\mathbf{r},t) = \int dt(-\sum_{\mathbf{r}} \partial_\alpha \mathcal{A}) = 0$ over a periodic domain vanishes. Note that the order of limits (of T and V) does not matter if one considers integrated current over the entire system. Using Eq. (4.22) in the above equation, we can relate the scalar mobility to the spatial correlations involving mass and activity,

$$2\chi = \frac{1}{d}\sum_{\alpha,\beta}\sum_{\mathbf{r}} \delta_{\alpha\beta}\Gamma^{\alpha\beta}_{\mathbf{r}} = 2D\sum_{\mathbf{r}} C^{mm}_{\mathbf{r}} = 2\sum_{\mathbf{r}} C^{\mathcal{A}m}_{\mathbf{r}}, \tag{4.26}$$

where, in the first step, we have used an identity, for $\alpha \neq \beta$,

$$\sum_{\mathbf{r}} \Gamma^{\alpha\beta}_{\mathbf{r}} = 0, \tag{4.27}$$

leading to the scalar mobility expressed in terms of the trace of the Onsager matrix,

$$2\chi = \frac{1}{d}\sum_{\alpha}\sum_{\mathbf{r}} \Gamma^{\alpha\alpha}_{\mathbf{r}} = \gamma_0. \tag{4.28}$$

In Fig. 4.3, we verify the above relation Eq. (4.28) by comparing the scaled variance of space-time-integrated current $\langle[\sum_{\alpha,\mathbf{r}} \mathcal{Q}_\alpha(\mathbf{r},T)]^2\rangle/(VTd) \equiv 2\chi$ obtained from simulations (points) and the quantity $\gamma_0(\bar{\rho})$ obtained from theory (dashed lines;

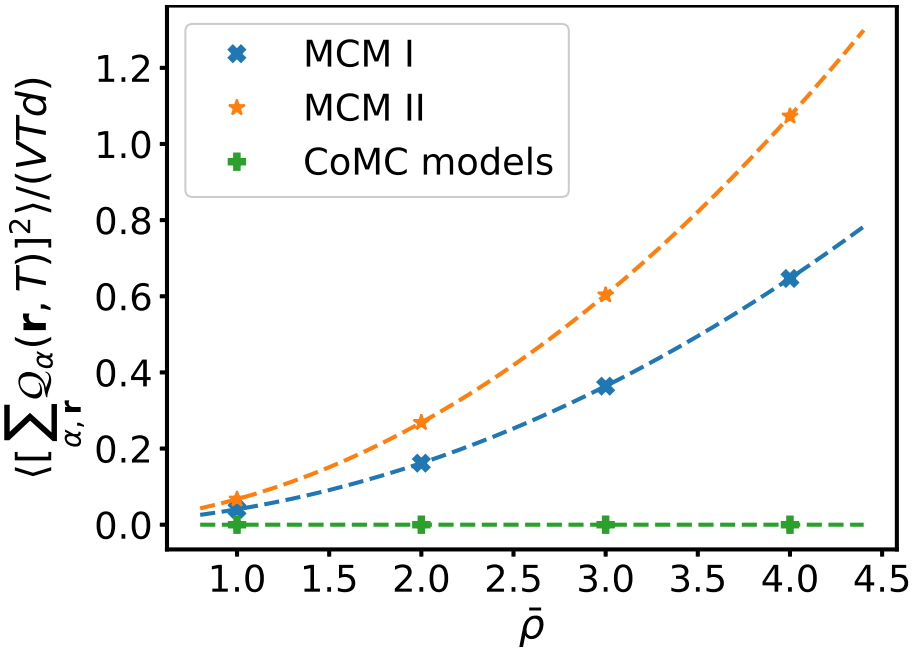

Figure 4.3: The scaled variance of space-time-integrated currents, $\langle[\sum_{\alpha,\mathbf{r}} \mathcal{Q}_\alpha(\mathbf{r},T)]^2\rangle/(VTd)$ is plotted as a function of global density $\bar{\rho}$ for MCM I (blue cross), MCM II (orange star), and centre-of-mass conserving models - Manna CoMC and Oslo CoMC (green plus). Points are obtained from simulations, and dotted lines represent $\gamma_0(\bar{\rho})$ [as in Eq. (4.28); the analytic expressions of $\gamma_0(\bar{\rho})$ are given in Table 4.1 for respective models].

see Table 4.1) as a function of global density $\bar{\rho}$ for three different models. Both simulations and theory agree with each other quite well.

Fluctuation-dissipation relation.– Interestingly, despite the violation of detailed balance at the microscopic scale, there exists a nonequilibrium fluctuation-dissipation (Green-Kubo) relation, analogous to the equilibrium Einstein relation, connecting mass and current fluctuations to density relaxation characterized by the bulk-diffusion coefficient. To derive the relation, we construct a scalar density-dependent transport coefficient, or simply the "mobility", out of the Onsager matrix $\Gamma^{\alpha\beta}$,

$$\begin{aligned}\chi(\bar{\rho}) &\equiv \frac{1}{2d}\sum_{\alpha,\beta}\delta_{\alpha\beta}\Gamma^{\alpha\beta}_{\mathbf{q}\to 0} = \frac{1}{2d}\sum_{\alpha,\beta}\sum_{\mathbf{r}}\Gamma^{\alpha\beta}_{\mathbf{r}} \\ &= D(\bar{\rho})\sum_{\mathbf{r}} C^{mm}_{\mathbf{r}}(\bar{\rho}) = DS(\mathbf{q}\to 0),\end{aligned} \tag{4.29}$$

where, in the second step, we have used the identity $\Gamma^{\alpha\beta}_{\mathbf{q}\to 0} = 0$ for $\alpha \neq \beta$ from Eq. (4.8). In other words, by using Eq. (4.2), we have an exact relationship $\chi(\bar{\rho}) = DS_0(\bar{\rho})$, between the mobility, bulk-diffusion coefficient and scaled mass fluctuation – an Einstein relation for nonequilibrium models studied here.

4.4.2 Calculation of the Onsager matrix

In this section, we calculate the Onsager matrix $\Gamma^{\alpha\beta}$ and express the matrix elements in terms of the coefficients γ's as defined in Eq. (4.13). For simplicity, we consider

below only the models in dimensions $d = 2$; generalizing the calculations to higher dimensions can be suitably done.

MCM I in $d = 2$ dimensions

First we exactly calculate the Onsager matrix for a particular variant of MCMs, called MCM I, in $d = 2$ dimensions. For other variants of MCMs and in higher dimensions, one can proceed along the lines of the calculation scheme provided below.

In MCM I, a random fraction of the chipped-off mass from a site hops to one of its nearest neighbors (for details of the model in dimensions $d = 2$, see Sec. 4.3). We now verify below that the time-evolution equation for the density field indeed has a gradient form [54]. To this end, we first write down the time-evolution equation for local mass $m(\mathbf{r}, t)$ using the following microscopic infinitesimal-time update rules,

$$m(\mathbf{r}, t + dt) = \begin{cases} \textbf{events} & \textbf{prob.} \\ m(\mathbf{r}, t) - \tilde{\zeta} m(\mathbf{r}, t) & dt \\ m(\mathbf{r}, t) + \tilde{\zeta} m(\mathbf{r} + \hat{e}_\alpha, t)\xi^+\xi_x^- & dt \\ m(\mathbf{r}, t) + \tilde{\zeta} m(\mathbf{r} - \hat{e}_\alpha, t)\xi^+\xi_x^+ & dt \\ m(\mathbf{r}, t) + \tilde{\zeta} m(\mathbf{r} + \hat{e}_\beta, t)\xi^+\xi_y^- & dt \\ m(\mathbf{r}, t) + \tilde{\zeta} m(\mathbf{r} - \hat{e}_\beta, t)\xi^+\xi_y^+ & dt \\ m(\mathbf{r}, t) & 1 - 5dt. \end{cases} \tag{4.30}$$

From the above update rules, the time-evolution equation for the average local mass can be written as

$$\partial_t \rho(\mathbf{r}, t) = D(\tilde{\zeta}) \nabla^2 \rho(\mathbf{r}, t), \tag{4.31}$$

where we denote the density field $\rho(\mathbf{r}, t) = \langle m(\mathbf{r}, t) \rangle$, $D(\tilde{\zeta}) = \tilde{\zeta}/4$ is the bulk-diffusion coefficient and ∇^2 is the discrete Laplacian operator in d dimensions. Notably, in this model (and MCMs in general), the bulk-diffusion coefficient D is independent of density, but the mobility (or, equivalently, the coefficients γ's) is proportional to the square of the density (see the analytic expressions given in Table 4.1).

Time evolution of average bond current.– The infinitesimal-time stochastic update rules for bond current $\mathcal{Q}_\alpha(\mathbf{r}, t)$ along direction $\alpha \in \{x, y\}$ can be written as

$$\mathcal{Q}_\alpha(\mathbf{r}, t + dt) = \begin{cases} \textbf{events} & \textbf{prob.} \\ \mathcal{Q}_\alpha(\mathbf{r}, t) + \tilde{\zeta} m(\mathbf{r}, t)\xi^+\xi_x^+ & dt \\ \mathcal{Q}_\alpha(\mathbf{r}, t) - \tilde{\zeta} m(\mathbf{r} + \hat{e}_\alpha, t)\xi^+\xi_x^- & dt \\ \mathcal{Q}_\alpha(\mathbf{r}, t) & 1 - 2dt. \end{cases} \tag{4.32}$$

Using the above update rule, we get

$$\partial_t \langle \mathcal{Q}_\alpha(\mathbf{r}, t) \rangle = D_\alpha(\tilde{\zeta}) \langle m(\mathbf{r}, t) - m(\mathbf{r} + \hat{e}_\alpha, t) \rangle \equiv \langle j_\alpha^{(d)} \rangle, \tag{4.33}$$

from which one can identify the local diffusive current

$$j_\alpha^{(d)}(\mathbf{r}, t) = D_\alpha(\tilde{\zeta})[m(\mathbf{r}, t) - m(\mathbf{r} + \hat{e}_\alpha, t)], \tag{4.34}$$

where $D_\alpha(\tilde{\zeta}) = D(\tilde{\zeta}) = \tilde{\zeta}/4$ is the bulk-diffusion coefficient, which is the same (i.e., isotropic) along any direction $\alpha \in \{x, y\}$. Note that, for MCM I (and MCMs in general), we can identify the explicit form of the observable $\mathcal{A}(\mathbf{r}, t) = D(\tilde{\zeta})m(\mathbf{r}, t)$, which enters into the hydrodynamic theory through Eq. (4.4). Next we characterize the fluctuating current by calculating its strength $\Gamma^{\alpha\beta}$ as in Eq. (4.21) or, equivalently, in Eq. (4.22).

Time evolution of equal-time bond-current correlations.– Now we proceed to calculate dynamic bond-current correlations. The infinitesimal-time stochastic update rules for equal-time bond current can be written as

$\mathcal{Q}_\alpha(\mathbf{r}, t+dt)\mathcal{Q}_\alpha(\mathbf{0}, t+dt) =$

$$\begin{cases} \textbf{events} & \textbf{prob.} \\ [\mathcal{Q}_\alpha(\mathbf{r},t) + \tilde{\zeta}m(\mathbf{r},t)\xi^+\xi_x^+]\mathcal{Q}_\alpha(\mathbf{0},t) & dt \\ [\mathcal{Q}_\alpha(\mathbf{r},t) - \tilde{\zeta}m(\mathbf{r}+\hat{e}_\alpha,t)\xi^+\xi_x^-]\mathcal{Q}_\alpha(\mathbf{0},t) & dt \\ \mathcal{Q}_\alpha(\mathbf{r},t)[\mathcal{Q}_\alpha(\mathbf{0},t) + \tilde{\zeta}m(\mathbf{0},t)\xi^-\xi_y^+] & dt \\ \mathcal{Q}_\alpha(\mathbf{r},t)[\mathcal{Q}_\alpha(\mathbf{0},t) - \tilde{\zeta}m(\hat{e}_\alpha,t)\xi^-\xi_y^-] & dt \\ \mathcal{Q}_\alpha(\mathbf{r},t)\mathcal{Q}_\alpha(\mathbf{0},t) + \tilde{\zeta}^2\{\xi^+\xi_x^+ m(\mathbf{r},t)\}^2 & \delta(\mathbf{r})dt \\ \mathcal{Q}_\alpha(\mathbf{r},t)\mathcal{Q}_\alpha(\mathbf{0},t) + \tilde{\zeta}^2\{\xi^+\xi_x^- m(\hat{e}_\alpha,t)\}^2 & \delta(\mathbf{r})dt \\ \mathcal{Q}_\alpha(\mathbf{r},t)\mathcal{Q}_\alpha(\mathbf{0},t) - (\tilde{\zeta}\xi^+)^2\xi_x^+\xi_x^- m^2(\mathbf{r},t) & \delta(\mathbf{r}-\hat{e}_\alpha)dt \\ \mathcal{Q}_\alpha(\mathbf{r},t)\mathcal{Q}_\alpha(\mathbf{0},t) - (\tilde{\zeta}\xi^+)^2\xi_x^+\xi_x^- m^2(\mathbf{0},t) & \delta(\mathbf{r}+\hat{e}_\alpha)dt \\ \mathcal{Q}_\alpha(\mathbf{r},t)\mathcal{Q}_\alpha(\mathbf{0},t) & 1-\Xi dt, \end{cases} \tag{4.35}$$

where $\Xi = 4 + 2\delta(\mathbf{r}) + \delta(\mathbf{r}+\hat{e}_\alpha) + \delta(\mathbf{r}-\hat{e}_\alpha)$ is the total exit rate. Using the above update rules, we obtain the following time-evolution equation for the equal-time bond current correlation function,

$$\partial_t C_{\mathbf{r}}^{\mathcal{Q}_\alpha\mathcal{Q}_\alpha}(t,t) = 2D(\tilde{\zeta})C_{\mathbf{r}}^{m\mathcal{Q}_\alpha}(t,t) + \Gamma^{\alpha\alpha}(\mathbf{r}), \tag{4.36}$$

where $C_{\mathbf{r}}^{m\mathcal{Q}_\alpha}(t,t) = \langle m(\mathbf{0},t)\mathcal{Q}_\alpha(\mathbf{r},t)\rangle_c$ is the equal-time dynamic mass-current correlation function. Here the associated source term is given by

$$\Gamma^{\alpha\alpha}(\mathbf{r}) = \frac{\tilde{\zeta}^2\langle m^2\rangle}{18}[4\delta(\mathbf{r}) - \delta(\mathbf{r}-\hat{e}_\alpha) - \delta(\mathbf{r}+\hat{e}_\alpha)], \tag{4.37}$$

which can be shown to be equal to the strength of fluctuating current-current correlation [see Eq. (4.22) and the proof given in the Appendix]. Here, the quantity $\langle m^2\rangle$ is the second moment of the onsite mass, which can be calculated by explicitly solving the density correlation function [derived later in Eq. (4.65)].

Now, we write the infinitesimal-time stochastic update rule for bond-current correlations along two orthogonal directions α and β as

$\mathcal{Q}_\alpha(\mathbf{r},t+dt)\mathcal{Q}_\beta(\mathbf{0},t+dt) =$

$$\begin{cases} \textbf{events} & \textbf{prob.} \\ [\mathcal{Q}_\alpha(\mathbf{0},t)+\tilde{\zeta}m(\mathbf{0},t)\xi^+\xi_x^+]\mathcal{Q}_\beta(\mathbf{r},t) & dt \\ [\mathcal{Q}_\alpha(\mathbf{0},t)-\tilde{\zeta}m(\hat{e}_\alpha,t)\xi^+\xi_x^-]\mathcal{Q}_\beta(\mathbf{r},t) & dt \\ \mathcal{Q}_\alpha(\mathbf{0},t)[\mathcal{Q}_\beta(\mathbf{r},t)+\tilde{\zeta}m(\mathbf{r},t)\xi^-\xi_y^+] & dt \\ \mathcal{Q}_\alpha(\mathbf{0},t)[\mathcal{Q}_\beta(\mathbf{r},t)-\tilde{\zeta}m(\mathbf{r}+\hat{e}_\beta,t)\xi^-\xi_y^-] & dt \\ \mathcal{Q}_\alpha(\mathbf{0},t)\mathcal{Q}_\beta(\mathbf{r},t)+\tilde{\zeta}^2\xi^+\xi^-\xi_x^+\xi_y^+m^2(\mathbf{0},t) & \delta(\mathbf{r})dt \\ \mathcal{Q}_\alpha(\mathbf{0},t)\mathcal{Q}_\beta(\mathbf{r},t)-\tilde{\zeta}^2\xi^+\xi^-\xi_x^-\xi_y^+m^2(\hat{e}_\alpha,t) & \delta(\mathbf{r}-\hat{e}_\alpha)dt \\ \mathcal{Q}_\alpha(\mathbf{0},t)\mathcal{Q}_\beta(\mathbf{r},t)-\tilde{\zeta}^2\xi^+\xi^-\xi_x^+\xi_y^-m^2(\mathbf{0},t) & \delta(\mathbf{r}+\hat{e}_\beta)dt \\ \mathcal{Q}_\alpha(\mathbf{0},t)\mathcal{Q}_\beta(\mathbf{r},t)+\tilde{\zeta}^2\xi^+\xi^-\xi_x^-\xi_y^-m^2(\hat{e}_\alpha,t) & \delta(\mathbf{r}-\hat{e}_\alpha+\hat{e}_\beta)dt \\ \mathcal{Q}_\alpha(\mathbf{0},t)\mathcal{Q}_\beta(\mathbf{r},t) & 1-\Xi dt, \end{cases} \tag{4.38}$$

where total exit rate $\Xi = 4+\delta(\mathbf{r})+\delta(\mathbf{r}-\hat{e}_\alpha)+\delta(\mathbf{r}+\hat{e}_\beta)+\delta(\mathbf{r}-\hat{e}_\alpha+\hat{e}_\beta)$. Using the above update rules, we immediately obtain the time-evolution equation for time-integrated bond current correlations,

$$\partial_t C_{\mathbf{r}}^{\mathcal{Q}_\alpha\mathcal{Q}_\beta}(t,t) = D[C_{\mathbf{r}}^{m\mathcal{Q}_\beta}(t,t)+C_{\mathbf{r}}^{\mathcal{Q}_\alpha m}(t,t)]+\Gamma^{\alpha\beta}(\mathbf{r}), \tag{4.39}$$

where, for $\alpha \neq \beta$, we have

$$\Gamma^{\alpha\beta}(\mathbf{r}) = \frac{\tilde{\zeta}^2\langle m^2\rangle}{24}[\delta(\mathbf{r})-\delta(\mathbf{r}-\hat{e}_\alpha)-\delta(\mathbf{r}+\hat{e}_\beta)+\delta(\mathbf{r}-\hat{e}_\alpha+\hat{e}_\beta)], \tag{4.40}$$

for MCM I in dimensions $d = 2$. Now, by comparing Eqs. (4.37) and (4.40) with Eqs. (4.23) and (4.24), we finally obtain the set of coefficients γ's as given below:

$$\gamma_0 = 2\gamma_1 = \langle m^2\rangle\frac{\tilde{\zeta}^2}{9}, \tag{4.41}$$

and

$$\gamma_2 = \langle m^2\rangle\frac{\tilde{\zeta}^2}{24}. \tag{4.42}$$

As shown later through explicit calculations of the density correlation function, we indeed have a power-law correlation in MCM I since $\gamma_1 \neq \gamma_2$ (see Table 4.1 and Fig. 4.6).

Oslo Model in $d = 2$ dimensions

In this section, we calculate the Onsager matrix for the two−dimensional version of the Oslo model [43]. The microscopic infinitesimal-time stochastic update rules for local mass can be written as

$$m(\mathbf{r},t+dt) = \begin{cases} \textbf{events} & \textbf{prob.} \\ m(\mathbf{r},t)-2 & a(\mathbf{r},t)dt \\ m(\mathbf{r},t)+1 & \sum_\alpha a(\mathbf{r}+\hat{e}_\alpha,t)dt/2 \\ m(\mathbf{r},t)+1 & \sum_\alpha a(\mathbf{r}-\hat{e}_\alpha,t)dt/2 \\ m(\mathbf{r},t) & 1-\Xi dt, \end{cases} \tag{4.43}$$

where $\Xi = a(\mathbf{r},t) + \sum_\alpha \sum_{s\in\{1,-1\}} a(\mathbf{r}+s\hat{e}_\alpha,t)/2$ and $a(\mathbf{r},t)$ is an indicator function if the site $\mathbf{r}$ is active at time t, i.e., $a=1$ if the site is active, otherwise $a=0$. Using the above update rules, we straightforwardly obtain the time-evolution equation for the first moment of local mass,

$$\partial_t \langle m(\mathbf{r},t)\rangle = \frac{1}{2}\nabla^2 \langle a(\mathbf{r},t)\rangle. \tag{4.44}$$

Here, the rhs of the time-evolution equation is written in terms of the discrete Laplacian of the local average activity. Now, assuming a local-equilibrium (or, local steady state) property where, on a large spatio-temporal scale, the local activity is slave to local density $\langle a(\mathbf{r},t)\rangle = \mathsf{a}(\rho(\mathbf{r},t))$ [41, 54], we obtain the density evolution equation,

$$\partial_t \rho(\mathbf{r},t) = \frac{1}{2}\nabla^2 \mathsf{a}(\rho(\mathbf{r},t)), \tag{4.45}$$

where we define density field $\rho(\mathbf{r},t) = \langle m(\mathbf{r},t)\rangle$ and steady-state activity (density of active sites) $\langle \hat{a}(\mathbf{r})\rangle^{st}_{\bar{\rho}=\rho} = \mathsf{a}(\rho)$, and $\langle . \rangle^{st}_{\bar{\rho}}$ denotes steady-state average provided that the global density is $\bar{\rho}$. The local diffusive current $\langle \mathbf{j}^{(d)}(\mathbf{r},t)\rangle = -(1/2)\nabla \mathsf{a}(\rho(\mathbf{r},t)) = -D(\rho)\nabla\rho(\mathbf{r},t)$ can be immediately identified by casting the above density evolution equation as a continuity equation, where the bulk-diffusion coefficient is given by $D(\rho) = (1/2)d\mathsf{a}/d\rho$, thus justifying diffusive relaxation in Eq. (4.5) used in the hydrodynamic theory formulated in the previous section.

Next, we proceed to write the infinitesimal-time stochastic update rules for equal-time spatial (two-point) correlation function involving time-integrated bond current,

$\mathcal{Q}_\alpha(\mathbf{r},t+dt)\mathcal{Q}_\alpha(\mathbf{0},t+dt) =$

$$\begin{cases} \textbf{events} & \textbf{prob.} \\ [\mathcal{Q}_\alpha(\mathbf{r},t)+1]\mathcal{Q}_\alpha(\mathbf{0},t) & a(\mathbf{r},t)\frac{dt}{2} \\ [\mathcal{Q}_\alpha(\mathbf{r},t)-1]\mathcal{Q}_\alpha(\mathbf{0},t) & a(\mathbf{r}+\hat{e}_\alpha,t)\frac{dt}{2} \\ \mathcal{Q}_\alpha(\mathbf{r},t)[\mathcal{Q}_\alpha(\mathbf{0},t)+1] & a(\mathbf{0},t)\frac{dt}{2} \\ \mathcal{Q}_\alpha(\mathbf{r},t)[\mathcal{Q}_\alpha(\mathbf{0},t)-1] & a(\hat{e}_\alpha,t)\frac{dt}{2} \\ \mathcal{Q}_\alpha(\mathbf{r},t)\mathcal{Q}_\alpha(\mathbf{0},t)+1 & a(\mathbf{r},t)\delta(\mathbf{r})\frac{dt}{2} \\ \mathcal{Q}_\alpha(\mathbf{r},t)\mathcal{Q}_\alpha(\mathbf{0},t)-1 & a(\mathbf{r},t)\delta(\mathbf{r}-\hat{e}_\alpha)\frac{dt}{2} \\ \mathcal{Q}_\alpha(\mathbf{r},t)\mathcal{Q}_\alpha(\mathbf{0},t)+1 & a(\hat{e}_\alpha,t)\delta(\mathbf{r})\frac{dt}{2} \\ \mathcal{Q}_\alpha(\mathbf{r},t)\mathcal{Q}_\alpha(\mathbf{0},t)-1 & a(\hat{e}_\alpha,t)\delta(\mathbf{r}+\hat{e}_\alpha)\frac{dt}{2} \\ \mathcal{Q}_\alpha(\mathbf{r},t)\mathcal{Q}_\alpha(\mathbf{0},t) & 1-\Xi dt, \end{cases} \tag{4.46}$$

with Ξ is the total exit rate. Using the above update rules, we obtain the following time-evolution equation for the dynamic current correlation function,

$$\partial_t C^{\mathcal{Q}_\alpha\mathcal{Q}_\alpha}_{\mathbf{r}}(t,t) = 2C^{\mathcal{A}\mathcal{Q}_\alpha}_{\mathbf{r}}(t,t) + \Gamma^{\alpha\alpha}(\mathbf{r}), \tag{4.47}$$

where we denote local activity as $\mathcal{A} \equiv a(\mathbf{r},t)/2$ on the right-hand side and write the strength of the fluctuating current simply as

$$\Gamma^{\alpha\alpha}(\mathbf{r}) = \frac{\mathsf{a}(\bar{\rho})}{2}[2\delta(\mathbf{r}) - \delta(\mathbf{r}+\hat{e}_\alpha) - \delta(\mathbf{r}-\hat{e}_\alpha)]. \tag{4.48}$$

From the above equation, we find that

$$\gamma_0 = \gamma_2 = 0, \tag{4.49}$$

and

$$\gamma_1 = \frac{\mathsf{a}(\bar{\rho})}{2}. \tag{4.50}$$

Notably, the fact that the coefficient $\gamma_0 = 0$ results in hyperuniform density fluctuation is a consequence of the additional center-of-mass conservation in the Oslo model. Indeed, the dynamical structure of the Manna model with center-of-mass conservation (CoMC) is quite similar to that of the Oslo model and can be characterized similarly (calculations not presented here); see Table 4.1 for comparison between the two models. Now, another coefficient γ_2 can be calculated from the infinitesimal-time-update rules for bond-current correlations along the orthogonal directions α and β as given below:

$$\mathcal{Q}_\alpha(\mathbf{0}, t+dt)\mathcal{Q}_\beta(\mathbf{r}, t+dt) = \begin{cases} \textbf{events} & \textbf{prob.} \\ [\mathcal{Q}_\alpha(\mathbf{0},t)+1]\mathcal{Q}_\beta(\mathbf{r},t) & a(\mathbf{0},t)\frac{dt}{2} \\ [\mathcal{Q}_\alpha(\mathbf{0},t)-1]\mathcal{Q}_\beta(\mathbf{r},t) & a(\hat{e}_\alpha,t)\frac{dt}{2} \\ \mathcal{Q}_\alpha(\mathbf{0},t)[\mathcal{Q}_\beta(\mathbf{r},t)+1] & a(\mathbf{r},t)\frac{dt}{2} \\ \mathcal{Q}_\alpha(\mathbf{0},t)[\mathcal{Q}_\beta(\mathbf{r},t)-1] & a(\mathbf{r}+\hat{e}_\beta,t)\frac{dt}{2} \\ \mathcal{Q}_\alpha(\mathbf{0},t)\mathcal{Q}_\beta(\mathbf{r},t) & 1-\Xi dt, \end{cases} \tag{4.51}$$

with $\Xi = [a(\mathbf{0},t) + a(\hat{e}_\alpha,t) + a(\mathbf{r},t) + a(\mathbf{r}+\hat{e}_\beta,t)]/2$. From the above update rules, we obtain time evolution of the equal-time current correlation function,

$$\partial_t C_{\mathbf{r}}^{\mathcal{Q}_\alpha \mathcal{Q}_\beta}(t,t) = D[C_{\mathbf{r}}^{m\mathcal{Q}_\beta}(t,t) + C_{\mathbf{r}}^{\mathcal{Q}_\alpha m}(t,t)] + \Gamma^{\alpha\beta}(\mathbf{r}), \tag{4.52}$$

where, for $\alpha \neq \beta$, we have

$$\Gamma^{\alpha\beta}(\mathbf{r}) = 0, \tag{4.53}$$

implying $\gamma_2 = 0$ for the Oslo model. Notably, $\gamma_1 \neq 0$ is still nonzero and, as a result, the system exhibits power-law correlations. However, quite interestingly, the long-wavelength density fluctuations still vanish in the thermodynamic limit: $S_0 = \gamma_0/2D = 0$ as $\gamma_0 = 0$. That is, unlike systems at an equilibrium critical point, the Oslo model in higher dimensions and even above the (absorbing-phase transition) critical density exhibits hyperuniformity − suppressed density fluctuations − and long-ranged correlations at the same time.

Comparison of coefficients $\{\gamma_0, \gamma_1, \gamma_2\}$ in various models

As demonstrated in the previous sections, we can also calculate the Onsager matrix $\Gamma_{\mathbf{q}}^{\alpha\beta}$ and the quantity $\mathcal{B}(\mathbf{q})$ as given in Eq. (4.13) for various other mass-transport processes directly from the microscopic dynamics. Indeed, as discussed below, for sandpiles, these coefficients can be expressed in terms of the density-dependent activity $\mathsf{a}(\bar{\rho})$ − the "order parameter" in the system. In table 4.1, we provide the expressions of the sets of three coefficients γ's $\gamma = \{\gamma_0, \gamma_1, \gamma_2\}$, which essentially encode the information determining whether the mass-mass correlations $C_{\mathbf{r}}^{mm}$, or equivalently activity-mass correlations $C_{\mathbf{r}}^{\mathcal{A}m}$, are power law (PL) or short ranged (SR).

Table 4.1: *Transport coefficients in $d = 2$ dimensions.*– We provide in this Table the schematic hop directions and the coefficients $\gamma = \{\gamma_0, \gamma_1, \gamma_2\}$, which parametrize the Onsager transport coefficients $\Gamma^{\alpha\beta}$ (the mobility tensor) for a wide class of conserved-mass transport processes, both with and *without* detailed balance, in two dimensions. We have $\langle \mathcal{A} \rangle \equiv \mathsf{a}(\bar{\rho})/2$ and $\langle \mathcal{A} \rangle \equiv u(\bar{\rho})/2$ – the activity for conserved sandpiles and the average (mass-dependent) hopping rate in the zero-range process (ZRP), respectively; both quantities depend on the global density $\bar{\rho}$ and other parameters of the models. Also, we denote "PL" and "SR" as power-law and short-ranged behavior, respectively, of the respective correlation functions (far from the absorbing-phase transition point, if any).

Models	Hop direction	γ_0	γ_1	γ_2
I. SSEP / ZRP (Case 1: SR)	$[\rightarrow, \leftarrow, \uparrow, \downarrow]$	$\frac{\bar{\rho}(1-\bar{\rho})}{2} \Big/ \frac{u(\bar{\rho})}{2}$	0	0
II. MCM I (Case 3: PL)	$[\updownarrow]$	$\frac{\tilde{\zeta}^2 \pi \bar{\rho}^2}{(9\pi - \tilde{\zeta}(5\pi+2))}$	$\frac{\gamma_0}{2}$	$\frac{3\gamma_0}{8}$
III. MCM II (Case 3: PL)	$[\leftrightarrow, \updownarrow]$	$\frac{\tilde{\zeta}^2 \bar{\rho}^2 \pi}{2(3\pi - \tilde{\zeta}(\pi+4))}$	$\frac{\gamma_0}{2}$	0
IV. MCM CoMC II[56] (Case 4: PL)	$[\leftrightarrow, \updownarrow]$	0	$\frac{\mu_1 \mu_2 \pi \bar{\rho}^2}{8(\pi\mu_1 - 2\mu_2)}$	0
V. Manna model CoMC[40] (Case 4: PL)	$[\leftrightarrow, \updownarrow]$	0	$\frac{\mathsf{a}(\rho)}{2}$	0
VI. Oslo model[43] (Case 4: PL)	$[\leftrightarrow, \updownarrow]$	0	$\frac{\mathsf{a}(\rho)}{2}$	0

4.4.3 Mass fluctuations: Calculations of two-point spatial correlations

In this section, we finally calculate the desired two-point correlation functions involving mass (density) and activity and then directly connect the strength of the correlation functions to the Onsager transport coefficients $\Gamma^{\ alpha\beta}$ (or, equivalently, γ's). To this end, we begin our discussion in a somewhat general setting, where we consider a broad class of microscopic models with multidirectional hopping of masses. For simplicity, here we shall confine ourselves to models with nearest-neighbor hopping of masses (or particles).

During an infinitesimal time interval $(t, t+dt)$, mass at a site $\mathbf{r}$ loses some fraction of the original mass, $\delta m_0(\mathbf{r}, t)$, with rate $a(\mathbf{r}, t)$ and gains some amount of mass $\delta m_\alpha(\mathbf{r} \pm \hat{e}_\alpha)$ with rate $a(\mathbf{r} \pm \hat{e}_\alpha, t)$ from a nearest-neighbor site $\mathbf{r} \pm \hat{e}_\alpha$ [e.g., $\alpha \in (x, y)$ for a $d = 2$ dimensional square lattice] with $\hat{e}_\alpha$ is the unit vector along direction α.

Then, the time-evolution equation for density can be written as

$$\partial_t \langle m(\mathbf{r},t)\rangle = -\langle \delta m_0(\mathbf{r},t) a(\mathbf{r},t)\rangle\, r + \sum_{\alpha=1}^{d} \sum_{s\in\{1,-1\}} \langle \delta m_\alpha(\mathbf{r}+s\hat{e}_\alpha,t) a(\mathbf{r}+s\hat{e}_\alpha,t)\rangle\,, \tag{4.54}$$

where the *indicator function* $a(\mathbf{r},t) = \theta_{\mathbf{r}}(m(\mathbf{r},t) - m^\star)$ denotes whether the site $\mathbf{r}$ is active. For MCMs, $m^* = 0$ and $a(\mathbf{r},t) = 1$ at all times. For conserved sandpiles, m^* is called threshold height and takes nonzero integer value(s), depending on the details of the models. That is, if $m(\mathbf{r}) \geq m^*$, $a(\mathbf{r},t) = 1$, otherwise it is zero. Provided that a site is updated with unit rate, $a(\mathbf{r},t)$ can essentially be thought of as the (instantaneous) rate with which mass transfer occurs at site $\mathbf{r}$ and time t. The steady-state average of $a(\mathbf{r},t)$, or $\mathsf{a}(\bar{\rho})$, depends on global density $\bar{\rho}$, but is independent of $\mathbf{r}$ for translation-invariant systems considered here. Also, e.g., for MCM II, the following two quantities – mass loss $\delta m_0(\mathbf{r},t)$ from site $\mathbf{r}$ and mass gain $\delta m_\alpha(\mathbf{r}\pm\hat{e}_\alpha,t)$ from site $\mathbf{r}\pm\hat{e}_\alpha$ – are given by $\tilde{\zeta}m(\mathbf{r},t)$ and $\xi^{\mp}(\mathbf{r}\pm\hat{e}_\alpha,t)\tilde{\zeta}m(\mathbf{r}\pm\hat{e}_\alpha,t)$, respectively; in conserved sandpiles with 2-particle hopping, the corresponding particle (mass) loss and gain are given by 2 and 1 for the Manna and Oslo models, respectively.

Now we define a stochastic variable, called generalized "activity", as given below:

$$\mathcal{A}(\mathbf{r},t) \equiv \frac{1}{2d}\delta m_0(\mathbf{r},t) a(\mathbf{r},t), \tag{4.55}$$

which is activity $a(\mathbf{r},t)$ weighted by chipped-off mass $\delta m_0(\mathbf{r},t)$. Therefore, we obtain the time-evolution equation for density field $\rho(\mathbf{r},t) = \langle m(\mathbf{r},t)\rangle$,

$$\partial_t \rho(\mathbf{r},t) = \nabla^2 \langle \mathcal{A}(\mathbf{r},t)\rangle = -\nabla\langle \mathbf{j}^{(d)}(\mathbf{r},t)\rangle, \tag{4.56}$$

where the local diffusion current can be written in the form of a (discrete) gradient,

$$\mathbf{j}^d(\mathbf{r},t) = -\nabla \mathcal{A}(\mathbf{r},t), \tag{4.57}$$

a "gradient"-property [54, 138] satisfied by the models considered in this chapter. In Eq. (4.56), we have defined a discrete Laplacian operator as

$$\nabla^2 \mathcal{A}(\mathbf{r},t) \equiv \sum_{\alpha=1}^{d} \sum_{s\in\{1,-1\}} \mathcal{A}(\mathbf{r}+s\hat{e}_\alpha,t) - 2d\mathcal{A}(\mathbf{r},t). \tag{4.58}$$

Also, as mentioned in Eq. (4.4), Eq. (4.57) is Fick's law for mass current in the systems. Note that, on large spatio-temporal scale, we can then define local average diffusive current $\langle \mathbf{j}^{(d)}(\mathbf{r},t)\rangle = -\nabla\langle\mathcal{A}\rangle(\rho(\mathbf{r},t))$ by invoking a local-equilibrium (local steady state) property where the average $\langle\mathcal{A}\rangle$ is slave to the density field $\rho(\mathbf{r},t)$ on large spatio-temporal scale [41, 54].

Now, using the infinitesimal-time update rules similar to those given explicitly in Eqs. (4.30) and (4.43), the time-evolution equation for equal-time density correlation function $C^{mm}(\mathbf{r}_1,\mathbf{r}_2,t) = \langle \delta m(\mathbf{r}_1,t)\delta m(\mathbf{r}_2,t)\rangle$, with $\delta m(\mathbf{r},t) = m(\mathbf{r},t) - \bar{\rho}$, can be exactly written as

$$\partial_t C^{mm}(\mathbf{r}_1,\mathbf{r}_2,t) = \nabla^2_{\mathbf{r}_1}\langle \mathcal{A}(\mathbf{r}_1,t) m(\mathbf{r}_2,t)\rangle_c + \nabla^2_{\mathbf{r}_2}\langle m(\mathbf{r}_1,t)\mathcal{A}(\mathbf{r}_2,t)\rangle_c + B(\mathbf{r}_1,\mathbf{r}_2). \tag{4.59}$$

Since the correlation functions are dependent on relative position vector $\mathbf{r} = \mathbf{r}_2 - \mathbf{r}_1$, we have

$$\partial_t C^{mm}(\mathbf{r}, t) = 2\nabla^2 C^{\mathcal{A}m}(\mathbf{r}, t) + B(\mathbf{r}), \tag{4.60}$$

where the quantity $B(\mathbf{r})$ is a model-specific source term and is strictly short-ranged for models having nearest-neighbor hopping of masses; see Fig. 4.4 for a schematic representation of $B(\mathbf{r})$ on a two-dimensional square lattice.

Calculation of $B(\mathbf{r})$ for MCMs in $d = 2$ dimensions

In this section, we derive the results specifically for MCM I in dimensions $d = 2$. Using the infinitesimal-time update rules for local mass in MCM I as given in Eq. (4.30), we obtain the time-evolution equation for the two-point mass-mass spatial correlation function, which satisfies the following equation,

$$\partial_t C^{mm}(\mathbf{r}, t) = 2D(\tilde{\zeta})\nabla^2 C^{mm}(\mathbf{r}, t) + B(\mathbf{r}), \tag{4.61}$$

where the bulk-diffusion coefficient $D(\tilde{\zeta}) = \tilde{\zeta}/2$ and the source term $B(\mathbf{r})$ can be explicitly written as

$$B(\mathbf{r}) = \frac{\tilde{\zeta}^2\langle m^2\rangle}{36}\Bigg[52\delta(\mathbf{r}) + \sum_{\substack{\alpha\in\{x,y\}\\ s\in\{-1,1\}}}\{2\delta(\mathbf{r}+2s\hat{e}_\alpha) - 18\delta(\mathbf{r}+s\hat{e}_\alpha)\} + \frac{3}{2}\sum_{\substack{\alpha\neq\beta\\ s\in\{-1,1\}}}\{\delta(\mathbf{r}+s\hat{e}_\alpha+s\hat{e}_\beta) + \delta(\mathbf{r}+s\hat{e}_\alpha-s\hat{e}_\beta)\}\Bigg] \tag{4.62}$$

with the second moment of mass being denoted as $\langle m^2\rangle \equiv \int m^2 \text{Prob.}[m(\mathbf{r}) = m]dm$. Note that the range of $B(\mathbf{r})$ for MCM I is shown in panel (d) of Fig. 4.4. In steady-state, by putting $\partial_t C^{mm}(\mathbf{r}, t) = 0$ and then taking the Fourier transform of Eq. (4.61), we have steady-state structure factor as

$$S(\mathbf{q}) = \frac{\tilde{\zeta}\langle m^2\rangle}{36\omega(\mathbf{q})}\left[8\omega(\mathbf{q}) + 3\omega^2(\mathbf{q}) + \sum_\alpha \lambda^2(q_\alpha)\right], \tag{4.63}$$

where $S(\mathbf{q})$ is the Fourier transform of steady-state density correction function $C^{mm}(\mathbf{r}) \equiv C^{mm}(\mathbf{r}, t \to \infty)$. Integrating the steady-state structure factor, as mentioned in Eq. (4.63), over the first Brillouin zone, we obtain:

$$C^{mm}(0) \equiv (2\pi)^{-2}\int_{BZ} S(\mathbf{q})d\mathbf{q} = (C^{mm}(0) + \bar{\rho}^2) \times (2\pi)^{-2}\frac{\tilde{\zeta}}{36}\int_{BZ} d\mathbf{q}\left[8 + 3\omega(q) + \frac{\sum_{\alpha\in\{x,y\}}\lambda^2(q_\alpha)}{\omega(\mathbf{q})}\right] \tag{4.64}$$

where we have used $\langle m^2\rangle = (C^{mm}(0) + \bar{\rho}^2)$. After performing some algebraic manipulations, we do the above integral and obtain the variance of onsite mass as

$$\langle m^2\rangle = \frac{9\pi\bar{\rho}^2}{9\pi - \tilde{\zeta}(5\pi+2)}. \tag{4.65}$$

Using above equation in (4.63), we have

$$\mathcal{B}(\mathbf{q}) = \frac{\tilde{\zeta}^2 \pi \bar{\rho}^2}{8(9\pi - \tilde{\zeta}(5\pi+2))} \left[8\omega(\mathbf{q}) + 3\omega^2(\mathbf{q}) + \sum_{\alpha} \lambda^2(q_\alpha) \right]. \tag{4.66}$$

The above expression is a special case of Eq. (4.13), where the model-dependent coefficients γ's are nonzero. It is worth noting that $\mathcal{B}(\mathbf{q})$ can also be obtained from the fluctuating relation

$$\mathcal{B}(\mathbf{q}) = \sum_{\alpha,\beta} (1 - e^{-\mathbf{i}q_\alpha})(1 - e^{\mathbf{i}q_\beta}) \Gamma^{\alpha\beta}_{\mathbf{q}}, \tag{4.67}$$

by knowing the fluctuating current strength $\Gamma^{\alpha\beta}_{\mathbf{q}}$ as mentioned in Eq. (4.11). In other words, in the real space, the quantities $B(\mathbf{r})$ and $\Gamma^{\alpha\beta}(\mathbf{r})$ are related through derivatives (discrete on a lattice)

$$B(\mathbf{r}) = -\sum_{\alpha,\beta} \partial_\alpha \partial_\beta \Gamma^{\alpha\beta}(\mathbf{r}), \tag{4.68}$$

can be thought of as a fluctuation relation connecting static and dynamic fluctuations, i.e., mass and current correlations, in the system. Indeed, from the microscopic infinitesimal-time update rules, we can explicitly show that the above relation holds for other models considered here and is quite generic for diffusive systems with nearest-neighbor mass transfer; see Table 4.1. Equivalently, using Eqs. (4.23) and (4.24), one can write down the following general expression for $B(\mathbf{r})$ in $d = 2$ dimensions,

$$\begin{aligned} B(\mathbf{r}) = (4\gamma_0 + 12\gamma_1 + 8\gamma_2)\delta(\mathbf{r}) + \sum_{\substack{\alpha\in\{x,y\} \\ s\in\{-1,1\}}} \{-(\gamma_0 + 4\gamma_1 + 4\gamma_2)\delta(\mathbf{r} + s\hat{e}_\alpha) + \gamma_1 \delta(\mathbf{r} + 2s\hat{e}_\alpha)\} \\ + \gamma_2 \sum_{\substack{\alpha\neq\beta \\ s\in\{-1,1\}}} \{\delta(\mathbf{r} + s\hat{e}_\alpha + s\hat{e}_\beta) + \delta(\mathbf{r} + s\hat{e}_\alpha - s\hat{e}_\beta)\}, \end{aligned} \tag{4.69}$$

explicitly in terms of the coefficients γ's, which depend on global density and other parameters of the models. The Fourier transform of the above equation is nothing but the expression of $B(\mathbf{r})$ as given in Eq. (4.2). In Fig. 4.4, we plot the spatial range of $B(\mathbf{r})$ for different values of γ's corresponding to various models in $d = 2$ dimensions (see Table 4.1).

Calculation of $B(\mathbf{r})$ in sandpiles in $d = 2$ dimensions

Let us first consider the conserved Oslo model in $d = 2$ dimensions. Using the infinitesimal-time stochastic update rules for local mass as given in Eq. (4.43), the time-evolution equation for the two-point mass-mass correlation function can be written as

$$\partial_t C^{mm}(\mathbf{r}, t) = 2C^{\mathcal{A}m}(\mathbf{r}, t) + B(\mathbf{r}), \tag{4.70}$$

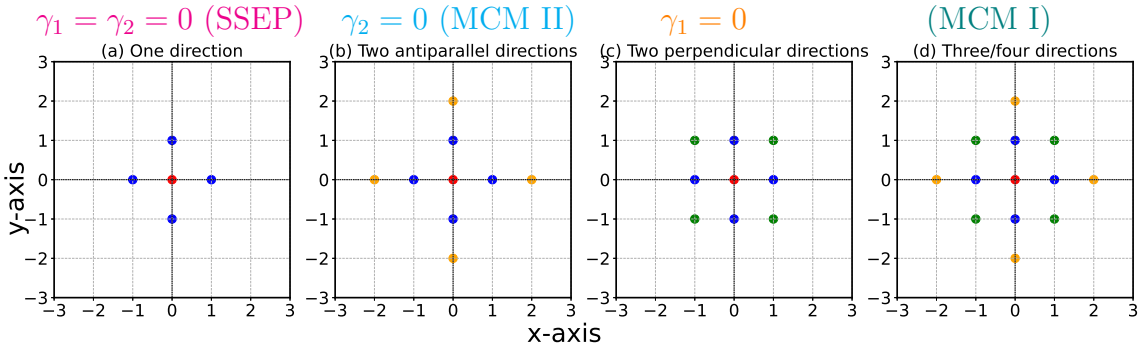

Figure 4.4: The range of $B(\mathbf{r})$ for various nearest-neighbor mass-transfer rules considered in $d = 2$ dimensions in this chapter (see Eq. (4.69)) is analyzed. The quantity $B(\mathbf{r})$ is strictly localized in the sense that it is nonzero on a finite plaque but zero otherwise. Panels (a) (e.g., SSEP, ZRP), (b) (e.g., MCM II, Manna CoMC, Oslo; see Eq. (4.71)), and (d) (e.g., MCM I; see Eq. (4.62)) illustrate the range of $B(\mathbf{r})$ for different models. In panel (c), mass is transported along two randomly chosen perpendicular directions. The same color in each panel represents the same magnitude and sign, as the lattice reflection symmetry $B(\mathbf{r}) = B(-\mathbf{r})$ holds for the models discussed here.

where the source term is given by

$$B(\mathbf{r}) = \frac{\mathsf{a}(\bar{\rho})}{2}\Big[12\delta(\mathbf{r}) + \sum_{\substack{\alpha\in\{x,y\}\\ s\in\{-1,1\}}} \{\delta(\mathbf{r}+2s\hat{e}_\alpha) - 4\delta(\mathbf{r}+s\hat{e}_\alpha)\}\Big]. \tag{4.71}$$

Here, the quantity $\mathsf{a}(\bar{\rho})$ is the steady-state activity, which is a function of global density $\bar{\rho}$. Notably, for the Manna model with center-of-mass conservation [40], the equation for $B(\mathbf{r})$ has exactly the same structure, with $\mathsf{a}(\bar{\rho})$ being the density-dependent activity in the respective system. Also, it is not difficult to show that the relationship between $B(\mathbf{r})$ and $\Gamma^{\alpha\beta}(\mathbf{r})$ remains the same as given in Eq. (4.68).

Correlation functions in d dimensions

In this section, we derive the correlation functions in arbitrary spatial dimensions $d > 1$, find the large-distance asymptotics, and then verify the results by simulations in dimensions $d = 2$.

Irrespective of the specific details of the models considered in this work, we can write down the equations for static spatial correlation function involving density (mass) and local activity. By using Eqs. (4.4) and (4.5) and then taking inverse Fourier transform of Eq. (4.11), we find that the static two-point density-density and activity-density correlation functions, $C^{mm}(\mathbf{r}) = \langle \delta m(\mathbf{0})\delta m(\mathbf{r})\rangle$ and $C^{\mathcal{A}m}(\mathbf{r}) = \langle \delta\mathcal{A}(\mathbf{0})\delta m(\mathbf{r})\rangle$, respectively, in the real space satisfy a Poisson equation,

$$2\nabla^2 C^{\mathcal{A}m}(\mathbf{r}) + B(\mathbf{r}) = 0, \tag{4.72}$$

$$2D\nabla^2 C^{mm}(\mathbf{r}) + B(\mathbf{r}) = 0, \tag{4.73}$$

where $B(\mathbf{r})$, the inverse Fourier transform of $\mathcal{B}(\mathbf{q})$, can be thought of as a charge distribution in an electrostatic problem. Also, from mass conservation and rotation symmetry, we have $\int B(\mathbf{r})d\mathbf{r} = 0$ and $\int \mathbf{r}B(\mathbf{r})d\mathbf{r} = 0$ (analogous to quadrupole

charge distribution). Note that the Eq. (4.72) involving activity-density correlation is exact for both MCMs and sandpiles (in *active* phase). The second equation (4.73) is exact for MCMs. For sandpiles, to arrive at Eq. (4.73), we have used an approximation $\nabla C^{\mathcal{A}m}(\mathbf{r}) = \langle \nabla \delta\mathcal{A}(\mathbf{r})\delta m(\mathbf{0})\rangle \simeq D(\bar{\rho})\langle \nabla \delta m(\mathbf{r})\delta m(\mathbf{0})\rangle = D(\bar{\rho})\nabla C^{mm}(\mathbf{r})$. Here, we have essentially assumed that, on large spatio-temporal (hydrodynamic) scales, activity $\mathcal{A}(\mathbf{r}) = \mathcal{A}[m(\mathbf{r})]$ is slave to the local density field $m(\mathbf{r})$ [41].

We remark here that, for MCMs, both equations are exact and essentially encode the same information. Also, in all models considered here, the fluctuating-current correlation function $\Gamma^{\alpha\beta}(\mathbf{r})$ has been calculated exactly from the infinitesimal-time microscopic dynamics of currents and masses at two different space points with spatial separation $r = |\mathbf{r}|$. As shown through the explicit microscopic calculations in the previous sections, the source term $B(\mathbf{r})$ appearing in Eqs. (4.72) and (4.73) is indeed directly related to the Onsager transport coefficients $\Gamma^{\alpha\beta}(\mathbf{r})$ through a fluctuation-response relation given in Eq. (4.68). It is worth mentioning that, although the quadrupole moments (diagonal part) of $B(\mathbf{r})$ are nonzero in these models, they are all equal due to the isotropic nature of the systems. Consequently, the large-distance $1/r^{(d+2)}$ power-law behavior we observe are generated by the higher-order (octupole) moments of $B(\mathbf{r})$, not the quadrupole ones, which are known to govern the $1/r^d$ algebraic decay of the two-point density correlation function in anisotropic models [149].

Now, taking Fourier transform of Eqs. (4.72) and (4.73), we explicitly obtain the density-density and activity-density correlation function, in terms of density and all other parameters,

$$C^{\mathcal{A}m}(\mathbf{r}) = \frac{1}{(2\pi)^d}\int_{BZ} d^d\mathbf{q} e^{-\mathbf{i}\mathbf{q}\cdot\mathbf{r}}\frac{\mathcal{B}(\mathbf{q})}{2\omega(\mathbf{q})}, \tag{4.74a}$$

$$C^{mm}(\mathbf{r}) = \frac{1}{(2\pi)^d}\int_{BZ} d^d\mathbf{q} e^{-\mathbf{i}\mathbf{q}\cdot\mathbf{r}}\frac{\mathcal{B}(\mathbf{q})}{2D\omega(\mathbf{q})}, \tag{4.74b}$$

where we have essentially performed the inverse Fourier transform of the structure factor $S(\mathbf{q})$, by taking the thermodynamic limit ($L \to \infty$) and performing the $\mathbf{q}$-integration over the first Brillouin zone (BZ). Using the general expression of $\mathcal{B}(\mathbf{q})$ from Eq.(4.13) in Eq.(4.74), we obtain the correlation function in real space,

$$C^{\mathcal{A}m}(\mathbf{r}) = DC^{mm}(\mathbf{r}) = \frac{\gamma_0 + 2d\gamma_2}{2}\delta(\mathbf{r}) - \gamma_2\sum_{\alpha=1}^{d}\sum_{s\in[-1,1]}\delta(\mathbf{r}+s\hat{e}_\alpha) + \frac{\gamma_1-\gamma_2}{2}C^{LR}(\mathbf{r}). \tag{4.75}$$

Here, the first two terms in the rhs of the above equation refer to the short-ranged spatial correlations; the last term contains the power-law decay, which can be expressed as,

$$C^{LR}(\mathbf{r}) = \frac{1}{(2\pi)^d}\int_{BZ} d\mathbf{q}\frac{\sum_\alpha \lambda^2(q_\alpha)}{\sum_\alpha \lambda(q_\alpha)}e^{-\mathbf{i}\mathbf{q}\cdot\mathbf{r}} \tag{4.76}$$

where $\lambda(q_\alpha) = 2(1-\cos q_\alpha)$ is the eigenvalue of the Laplacian operator in the lattice along α direction, and the Brillouin zone is $[-\pi,\pi]^d$. We now express the numerator

$\sum_\alpha \lambda^2(q_\alpha)$ as the Fourier transform of a real-space kernel:

$$\sum_\alpha \lambda^2(q_\alpha) = \sum_{\mathbf{r}'} K(\mathbf{r}')e^{\mathbf{i}\mathbf{q}\cdot\mathbf{r}'}, \tag{4.77}$$

where $K(\mathbf{r}')$ can be explicitly written as

$$\begin{aligned} K(\mathbf{r}') = 6d\delta(\mathbf{r}') - 4\sum_{\alpha=1}^{d}[\delta(\mathbf{r}'+\hat{e}_\alpha) + \delta(\mathbf{r}'-\hat{e}_\alpha)] \\ + \sum_{\alpha=1}^{d}[\delta(\mathbf{r}'+2\hat{e}_\alpha) + \delta(\mathbf{r}'-2\hat{e}_\alpha)]. \end{aligned} \tag{4.78}$$

Using (4.77) in (4.76), we have

$$C^{LR}(\mathbf{r}) = \sum_{\mathbf{r}'} K(\mathbf{r}')\mathcal{G}(\mathbf{r}-\mathbf{r}') \simeq \sum_{\alpha=1}^{d} \frac{\partial^4}{\partial x_\alpha^4}\mathcal{G}(\mathbf{r}), \tag{4.79}$$

where $\mathcal{G}(\mathbf{r})$ is the lattice Green's function,

$$\mathcal{G}(\mathbf{r}) = \int_{BZ} \frac{d^d\mathbf{q}}{(2\pi)^d} \frac{1}{\sum_\alpha \lambda(q_\alpha)} e^{-\mathbf{i}\mathbf{q}\cdot\mathbf{r}}. \tag{4.80}$$

After some algebraic manipulation, the above equation can be expressed in the following form,

$$\mathcal{G}(\mathbf{r}) = \int_0^\infty dt e^{-2td}\Pi_\alpha \mathcal{I}_{x_\alpha}(2t), \tag{4.81}$$

where we have used the identity $1/A = \int_0^\infty e^{-At}dt$ with $A = \sum_\alpha \lambda(q_\alpha)$ and have defined

$$\mathcal{I}_{x_\alpha}(2t) = \frac{1}{2\pi}\int_{-\pi}^{\pi} dq_\alpha e^{2t\cos q_\alpha} e^{\mathbf{i}q_\alpha x_\alpha}, \tag{4.82}$$

the modified Bessel function of the first kind [155].

Large-Distance Behavior.– For distance large, the asymptotic behavior of the above integral in Eq.(4.82) is governed by the small $\mathbf{q}$ behavior of the integrand and the corresponding asymptotics can be evaluated as follows. By using the approximation $\cos q_\alpha \simeq (1 - q_\alpha^2/2)$ for small q_α, Eq. (4.82) has following asymptotic form for large $x_\alpha \gg 1$,

$$\mathcal{I}_{x_\alpha}(2t) \simeq \frac{e^{2t}}{2\pi}\int_{-\infty}^{\infty} dq_\alpha e^{-tq_\alpha^2} e^{-\mathbf{i}q_\alpha x_\alpha} = \frac{e^{2t}}{\sqrt{4\pi t}} e^{-x_\alpha^2/4t}, \tag{4.83}$$

which can then be substituted in Eq. (4.81) to obtain the following equation,

$$\mathcal{G}(\mathbf{r}) \simeq \frac{1}{(4\pi)^{d/2}}\int_0^\infty dt e^{-r^2/4t} t^{-d/2}. \tag{4.84}$$

By substituting the above equation in Eq.(4.79), we find that, in higher dimensions $d \geq 2$, the long-range part of the correlation function can be expressed as:

$$\begin{aligned} C^{LR}(\mathbf{r}) &\simeq \sum_{\alpha} \frac{\partial^4}{\partial x_\alpha^4} \mathcal{G}(\mathbf{r}) \\ &\simeq \frac{1}{(4\pi)^{d/2}} \int_0^\infty dt e^{-r^2/4t} \frac{(\sum_\alpha x_\alpha^2 + 12dt^2 - 12r^2 t)}{16 t^{4+d/2}} \qquad (4.85) \\ &= \frac{1}{\Omega_d} \frac{d(d+2)(d+4)\sum_\alpha x_\alpha^4 - 3d(d+4)r^4}{r^{d+6}}, \qquad (4.86) \end{aligned}$$

where $\Omega_d = 2\pi^{d/2}/\Gamma(d/2)$ is the solid angle in d dimensions. For $r \gg 1$ being large, we have $C^{LR}(\mathbf{r}) \sim 1/r^{d+2}$; the algebraic decay is valid for $d > 1$, as seen in the above equation. Putting $d = 2$ and performing some algebraic manipulations, the above equation leads to the following expression of the long-ranged correlation in two dimensions,

$$C^{LR}(x, y) = \frac{6\,(x^4 - 6x^2y^2 + y^4)}{\pi\,(x^2 + y^2)^4}. \qquad (4.87)$$

Thus, in the case of a two-dimensional system, the scaled correlation functions are given by

$$\frac{2}{(\gamma_1 - \gamma_2)} C_{x,0}^{\mathcal{A}m} = \frac{2D}{(\gamma_1 - \gamma_2)} C_{x,0}^{mm} \simeq \frac{6}{\pi x^4}, \qquad (4.88)$$

in the limit of distance $(1 \ll |\mathbf{r}| \ll L)$ being large. However, in a finite system, the power law is essentially cut-off at very large $|\mathbf{r}|$ with $|\mathbf{r}|/L$ being finite, and there are finite-size corrections of $\mathcal{O}(1/L^d)$ to the correlation functions.

Classification of models.– Indeed, based on the calculations of various transport coefficients γ's in the previous sections and their relationship to the coefficients S_0, S_1 and S_2 appearing in the structure factor in the small$-\mathbf{q}$ limit, one can categorize various possible scenarios as given below. To this end, we consider a broad class of models intensively studied in the past several decades:

(i) Symmetric simple exclusion processes (SSEPs) [142] – a *single* particle hops to a randomly chosen nearest-neighbor site if the site is vacant;

(ii) zero range processes (ZRPs) [61] – a *single* particle hops to a randomly chosen nearest-neighbor site;

(iii) mass chipping models (MCMs) [13, 14, 19, 20] – random fractions of (continuous) mass at a site hop to randomly chosen nearest-neighbor sites;

(iv) conserved sandpiles [12, 43] – two (or more) particles from an *active* site hop to randomly chosen nearest-neighbor sites.

Categories (ii), (iii) and (iv) have *no* hardcore constraint. Also, only the categories (iii) and (iv) have *multidirectional* hopping of masses, i.e., at each elementary (infinitesimal) time step, mass from the departure site gets redistributed to *at least*

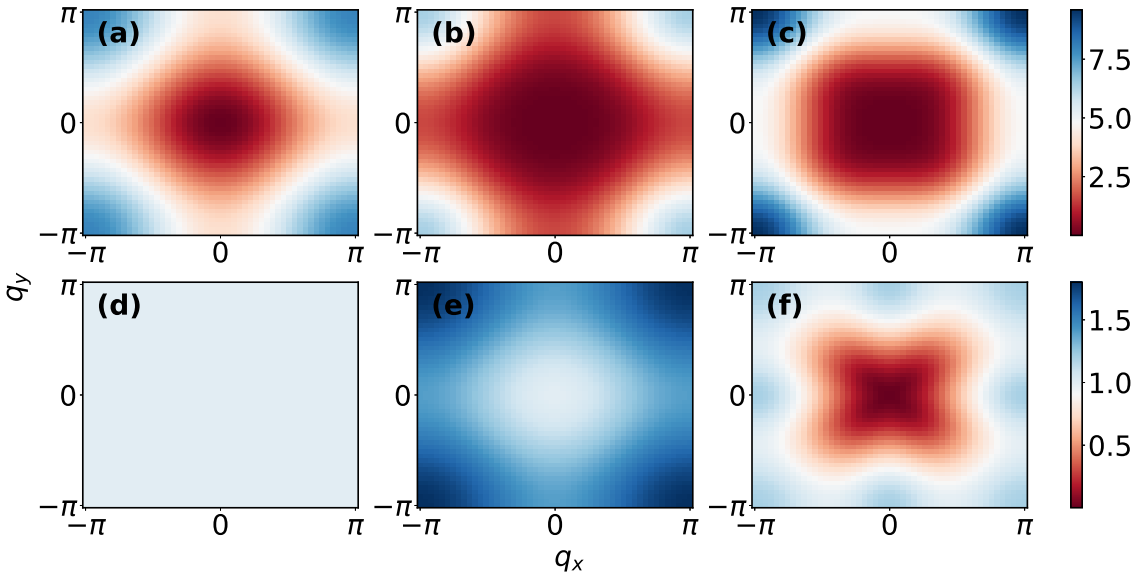

Figure 4.5: In Panels (a)-(c) and (d)-(f), the quantity $\mathcal{B}(\mathbf{q})$ and scaled structure factor $2DS(\mathbf{q})$, respectively, as defined in Eq. (4.11), are plotted for three representative sets of the Onsager transport coefficients (equivalently, the mobility tensor) γ's as defined in Eqs. (4.7) and (4.8). Panels (a) and (d) are for SSEP- or ZRP-like systems (delta-correlated) where $\gamma_0 \neq 0$ and $\gamma_1 = \gamma_2 = 0$. Panels (b) and (e) represent the cases where $\gamma_0 = 0$ and $\gamma_1 = \gamma_2 \neq 0$; these systems exhibit short-ranged $C(r)$. Panels (c) and (f) illustrate the cases where $\gamma_0 = 0$ and $\gamma_1 > \gamma_2 = 0$; these systems exhibit power-law $C(r) \sim 1/r^{d+2}$.

two different destination sites simultaneously. We consider several variants of MCMs and sandpiles (see Fig. 4.6), some of which may have an additional *center-of-mass conservation* (CoMC) and consequently exhibit hyperuniformity [4]. In all cases, we analytically calculate the structure factors, which are expressed in terms of the transport coefficients γ's (for details, see Table 4.1). Now, according to Eq. (4.13), we have the following representative scenarios.

Case 1: Unidirectional hopping, $\gamma_0 \neq 0$ and $\gamma_1 = \gamma_2 = 0$; this case could correspond to with or without detailed balance and correlations $C(r)$ are short-ranged, e.g., SSEP, ZRP, and some variants of MCMs (results not presented).

Case 2: Multidirectional hopping, $\gamma_0 \neq 0$ and $\gamma_1 = \gamma_2 \neq 0$; in this case, detailed balance is violated, and correlations $C(r)$ are short-ranged, e.g., some variants of MCMs (results not presented).

Case 3: Multidirectional hopping, $\gamma_0 \neq 0$ and $\gamma_2 \neq \gamma_1$; detailed balance is violated, power-law correlations $C(r) \sim r^{-(d+2)}$ are observed, e.g., MCM I.

Case 4: Multidirectional hopping, $\gamma_0 = 0$; the systems are hyperuniform [3], e.g., CoM-conserving models, and correlations are short-ranged $C(r)$ for $\gamma_2 = \gamma_1$ (e.g., MCM CoMC I) and power law otherwise (e.g., MCM-CoMC II, Manna model with CoMC and Oslo model as in Fig. 4.6).

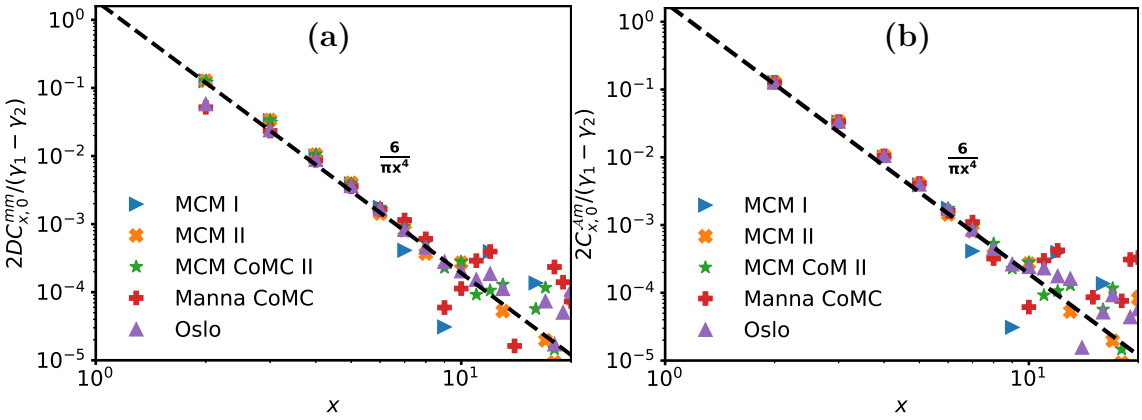

Figure 4.6: *Panel (a):* Steady-state scaled density-density correlation function, $2DC^{mm}_{x,0}/(\gamma_1-\gamma_2)$, is plotted as a function of axial distance x. *Panel (b):* Scaled activity-density correlation function, $2C^{\mathcal{A}m}_{x,0}/(\gamma_1-\gamma_2)$, as a function of spatial distance x is plotted for the Oslo model [43] and Manna model with CoMC [40]; here $D = \mathsf{a}'(\bar{\rho})/2$, $\gamma_1(\bar{\rho})$ and $\gamma_2(\bar{\rho})$ all depend on global density $\bar{\rho}$, where $\mathsf{a}(\bar{\rho})$ is the density-dependent activity – the "order parameter" for conserved sandpiles [38]. In mass chipping models (MCMs) [13], D is independent of density. Theory (black dotted line) predicts a generic power law $(6/\pi)x^{-4}$ [Eq. (4.1)]. In simulations, we take a periodic 250×250 square lattice and global density $\bar{\rho} = 4.0$ (far from criticality for the Manna and Oslo models).

To verify the above theoretical predictions, we have performed Monte-Carlo simulations of various microscopic models in two dimensions. In panels (a) – (c) and (d) – (f) of Fig. 4.5, we present heat maps of the quantity $2D\mathcal{B}(\mathbf{q})$ and the scaled structure factor $2DS(\mathbf{q})$, respectively, in the two-dimensional $\mathbf{q}$-plane for different sets of $\gamma \equiv \{\gamma_0, \gamma_1, \gamma_2\}$ values. The non-analyticity emerges when the condition $\gamma_1 \neq \gamma_2$ is satisfied. We also construct model-independent scaled density-density and activity-density correlation functions $2DC^{mm}_{\mathbf{r}}/(\gamma_1-\gamma_2)$ and $2C^{\mathcal{A}m}_{\mathbf{r}}/(\gamma_1-\gamma_2)$, respectively, which are plotted as a function of spatial distance $\mathbf{r} = (x, 0)$ in panels (a) and (b) of Fig. 4.6. We take global density $\bar{\rho} = 4.0$ [far from (above) the absorbing-phase transition points for the Manna model with CoMC and Oslo model], and a periodic square lattice of area $L \times L = 250 \times 250$. The black-dotted line in both panels demonstrates that the scaled correlations indeed exhibit a generic power-law decay $(6/\pi)x^{-4}$ along $x-$axis [as obtained in Eq. (4.88)].

4.5 Conclusions

In this chapter, we have provided a theoretical characterization of spatial structures in a broad class of conserved-mass transport processes defined on a periodic $d-$dimensional ($d > 1$) hypercubic lattice. The models are governed by continuous-time Markov jump processes and, importantly, involve *multidirectional* hopping, which respects all symmetries of the lattice. We focus on the often-studied two-point spatial correlation functions involving density and activity. We show that these models exhibit power-law correlations in higher dimensions for generic parameter values, even when the systems are far from a phase transition point (if any).

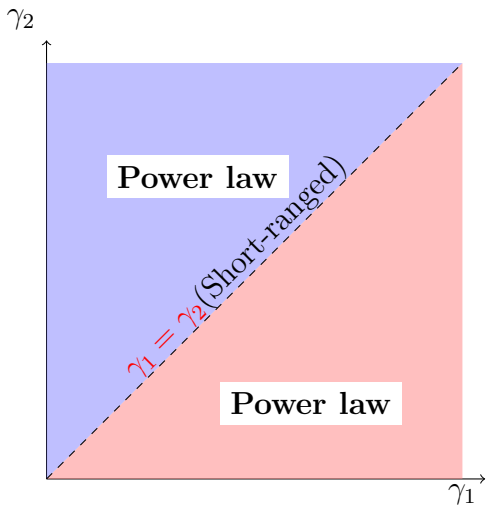

Figure 4.7: Schematic "phase diagram" of conserved-mass transport processes on a $d-$dimensional lattice in the plane of parameters γ_1 and γ_2 as defined in Eqs. (4.7) and (4.8). The black-dotted line depicts the "phase boundary", where the correlation function is short-ranged and elsewhere it is a power-law.

The crucial mechanism behind the algebraic decay is the multidirectional hopping dynamics, where multiple chunks of mass or particles can simultaneously hop out of a lattice site in various directions, thereby breaking detailed balance and generically leading to long-ranged correlations. Indeed, using a hydrodynamic and microscopic approach, the strength of the correlation functions have been determined in terms of the bulk-diffusion coefficient and the Onsager matrix (or, the mobility tensor). More specifically, for the class of models considered here, we parametrize the transport properties, and consequently the correlations, in terms of three coefficients (density-dependent in general), γ_0, γ_1 and γ_2 [see Eq. (4.13)]. Indeed, the presence (or, absence) of the power-law correlations can be understood as follows. For $\gamma_1 \neq \gamma_2$, irrespective of the values of γ_0, the correlation functions decay as a power law. However, in some special cases, where $\gamma_1 = \gamma_2$, and therefore $S_2 = 0$ [see Eq. (4.2)], the correlation functions can be short-ranged too; for a schematic "phase diagram", see Fig. 4.7.

In particular, our theory explains why center-of-mass-conserving dynamics with axial bidirectional (opposite) hopping of masses generically leads to long-ranged correlations, which manifest into a remarkable state of nonequilibrium disordered matter, called *hyperuniformity* [3, 40]. In that case, we have $\gamma_0 = \gamma_2 = 0$, but the coefficient of the *nonanalytic* term in static structure factor is nonzero [$S_2 \neq 0$ in Eq. (4.2)]. Therefore, the systems have anomalously suppressed long-wave-length density fluctuations $S(\mathbf{q} \to 0) = 0$, resulting in hyperuniformity [$S(q) \sim q^\alpha$ with hyperuniformity exponent $\alpha = 2$] and long-ranged correlations at the same time.

Importantly, the systems studied in this work are isotropic (i.e., symmetric under lattice rotations) and homogeneous, yet they violate detailed balance. Moreover, the symmetric nature of mass hopping ensures that there is no net current in real space (though probability current in the configuration space is nonzero), and the systems exhibit diffusive relaxation at large spatio-temporal scales. While such systems

were widely studied over past several decades [13, 19, 43, 105], so far it has not been realized that they possess generic scale invariance in higher dimensions, even far from phase transition point.

In contrast, in open current-carrying systems, e.g., in the presence of a temperature or density gradient (therefore, anisotropic) [156–159], long-ranged correlations are rather the rule and were studied before [138, 160–163] (in equilibrium, apart from the critical state, continuous-symmetry-broken ordered phase can also have long-ranged correlations [164]). Furthermore, it is known that also closed systems with localized drive ("disorder") can induce long-ranged correlations [147]. But, this raises an important question: What happens in closed, homogeneous and isotropic systems? Is the violation of detailed balance sufficient to generate power laws, even on a lattice, which has more restricted symmetry compared to that in a continuum? The answers to these questions are not obvious. Previously, it has been explained why correlations in closed *anisotropic* systems have $1/r^d$ decay [145, 148, 149, 152, 153, 165]. However, the behavior when all symmetries of the lattice are present in the system is not well understood. One prior attempt to address this issue used an approximate kinetic theory to illustrate that an isotropic lattice model too can exhibit algebraic decay, albeit a faster one $1/r^{d+2}$ on a hypercubic lattice [150]. Still, a detailed characterization of the class of microscopic dynamics for which such decays occur is lacking. In this scenario, here we elucidate, in terms of the Onsager transport coefficients, its precise dynamical mechanism, that crucially requires *multidirectional* hopping to violate detailed balance and generate algebraic decay. From a general perspective, our findings could shed light on why power laws are so ubiquitous in nature [11] − the question posed by Bak, Tang, and Wiesenfeld in their seminal chapter more than three decades ago.

5

Summary and Discussions

The thesis presents a detailed analytical study of steady-state fluctuations—both static and dynamic—in nonequilibrium mass transport processes on $d-$dimensional periodic hypercubic lattice. Two broad classes of models are considered: mass chipping models (MCMs) [13–15, 19–22], which describe fragmentation, diffusion, and aggregation of continuous mass variables, and conserved-mass sandpile models, such as the Oslo model [18] and the centre-of-mass (CoM) conserving Manna model [40]. Using a microscopic dynamical approach, we characterise fluctuation properties in exactly solvable minimal models, including cases with nontrivial spatio-temporal correlations and violation of detailed balance. We then extend the analysis to more complex scenarios of many-body systems with additional conservation laws.

The central focus of our study is to characterize the role of CoM conservation (analogous to dipole-moment conservation in systems with charged particles), which has recently attracted significant attention in diverse contexts, including quantum fluids [126, 127, 166] and equilibrium lattice models [134]. Indeed, our results demonstrate how the CoM conservation fundamentally alters fluctuation behavior, suppressing current and density fluctuations and giving rise to emergent hyperuniform structures. Before summarizing the results, let us provide a brief description of the models considered in this thesis.

5.1 Summary of the models studied

I. Models with only mass conservation: The models studied in this thesis are defined on periodic hypercubic lattices of volume L^d, considered in both one and two dimensions. At each lattice site, the mass is a non-negative continuous variable, and the dynamics are such that the global density is conserved, given by $\bar{\rho} = M/L^d$, where M denotes the total mass of the system. The dynamics proceed via local chipping of mass from a site, followed by random redistribution of the

chipped mass to neighboring sites. We investigate three different one-dimensional variants, referred to as MCM I, MCM II, and MCM III (see schematic diagram in Sec. 2.2).

In MCM I, a site retains a fraction of its mass, while the chipped-off fraction is split between the left and right nearest neighbors, with a random proportion directed to each. In MCM II, the chipped-off fraction is transferred entirely to either the left or the right neighbor with equal probability, while the remaining fraction is deposited back at the same site. In MCM III, mass chipped off from two neighboring sites is first recombined and then randomly fragmented before being redistributed back to the same two sites. Notably, MCM III is a generalized version of the Kipnis-Marchioro-Presutti (KMP) model [15].

II. Models with both mass and centre-of-mass conservation – Two types of models have been considered with both mass and centre-of-mass (CoM) conservation.

(a) *Mass chipping models with CoMC:* In these models, with unit rate, a site with continuous mass retains a random fraction of its mass, and the remaining portion is *equally* fragmented and deposited to all $2d$ nearest neighbors (MCM CoMC I). In another variant, the chipped-off mass is equally divided into *two* parts and deposited at neighboring sites along one of the lattice axes, chosen with equal probability (MCM CoMC II).

(b) *Threshold-activated CoM-conserving models:* In addition to the MCMs, we have also studied the CoM-conserving threshold-activated models; the Oslo model [18] and a CoM-conserving version of the Manna model [167]. In these systems, with unit rate, an active site (where mass is greater than or equal to the threshold mass) deterministically transfers two particles – one each to its right and left neighboring sites so that the center of mass is conserved.

5.2 Summary of the main results

The main results are summarized below.

1. Dynamic fluctuation of diffusive models with mass conservation: In Chapter 2, exact microscopic calculations are employed to analyze the second cumulant of time-integrated bond currents, $\langle \mathcal{Q}_i^2(T) \rangle_c$. Three distinct temporal regimes emerge for the bond current variance:

- Short-time regime ($T \sim \mathcal{O}(1)$): Linear growth as $\sim T$.
- Intermediate-time regime ($1 \ll T \ll L^2$): Subdiffusive growth as $\sim T^{1/2}$.
- Long-time regime ($T \gg L^2$): Diffusive growth as $\sim T$.

Interestingly, these two different scaling regimes are unified through a *single*, universal scaling function $\mathcal{W}(y)$, with the scaling variable being $y = DT/L^2$, where D is the bulk diffusion coefficient. Furthermore, we show that, even in the presence

of spatial finite spatial correlations, the instantaneous current correlation is shown to have the following form $\langle \mathcal{J}_i(t)\mathcal{J}_i(0)\rangle \sim -t^{-(1+d/2)}$; the corresponding power spectrum is given by $S_J(f) \sim S_J(0) + \text{Const.}\, f^{d/2}$, for bond currents in systems with a *single* (mass) conservation law.

2. Dynamic fluctuation in models with centre of mass conservation – With the additional constraint of center-of-mass (CoM) conservation, the mass chipping models, although violating detailed balance, remain *diffusive*. We have calculated the steady-state bond current fluctuations exactly for these models and found a generic asymptotic behavior of the form $\langle \mathcal{Q}(T)^2\rangle = A_1 T + A_2 + A_3 T^{-d/2}$, where the coefficient A_1 may vanish depending on the details of the model. When $A_1 = 0$, the long-time current fluctuations saturate, implying *dynamical hyperuniformity*. Furthermore, we have computed the instantaneous current correlation, which decays as $\sim -t^{-(2+d/2)}$ – significantly faster than in models with only mass conservation, where the decay is $t^{-(1+d/2)}$. This behavior is consistent with the corresponding power spectrum of the current, $S_J(f) \sim A_1 + \text{Const.}\, f^{1+d/2}$, highlighting how the power-law decay exponent changes depending on the conservation laws present in the systems. Moreover, all CoM-conserving models studied in the thesis exhibit a steady-state structure factor that vanishes as $S(q) \sim q^2$, characteristic of class-I hyperuniformity, the most extreme form of suppression of the density fluctuations [168].

3. Generic power laws in higher-dimensional mass transport models: In a broad class of nonequilibrium lattice models, we have computed the structure factor by combining microscopic analysis with hydrodynamic theory. Interestingly, in models with multidirectional hopping, where multiple chunks of mass or particles can simultaneously leave a lattice site and be deposited at two or more neighboring destinations. We find that, within a specific parameter regime, the structure factor exhibits a non-analytic q^2 dependence. This non-analyticity gives rise to a robust power-law decay of correlations, $\sim 1/r^{d+2}$ (for $d > 1$), in real space, even though the systems still preserve isotropy and homogeneity.

Overall, the thesis provides a unified framework, based on exact microscopic theory, explaining both dynamic and spatial fluctuation behavior in nonequilibrium mass transport systems. Much of the work focuses on simple, exactly solvable models that nevertheless exhibit non-trivial spatial correlations. Remarkably, several nonequilibrium phenomena can be observed in such minimal lattice models, such as mass chipping processes. These findings open new avenues for advancing a rigorous understanding of the emergence of power-law correlations and hyperuniformity in out-of-equilibrium systems and provide promising directions for future research into designing hyperuniform materials and achieving efficient transport in driven systems in general.

A

Appendix

A.1 Fluctuating current correlations

The time-integrated bond current up to time t along a given direction α can be written as

$$\mathcal{Q}_\alpha(\mathbf{r},t) = \int_0^t dt' j_\alpha(\mathbf{r},t'), \tag{A.1}$$

where $j_\alpha(\mathbf{r},t)$ is instantaneous current, which can be written as a sum of diffusive and fluctuating current components,

$$j_\alpha(\mathbf{r},t) = j_\alpha^{(d)}(\mathbf{r},t) + j_\alpha^{(fl)}(\mathbf{r},t). \tag{A.2}$$

Then, to characterize the second moment, or more generally, the two-point correlations of bond current, we calculate unequal-time ($t > t'$) correlation function for bond current in different directions α and β through the following time-evolution equations,

$$C_{\mathbf{r}}^{j_\alpha \mathcal{Q}_\beta}(t,t') \equiv \frac{d}{dt} C_{\mathbf{r}}^{\mathcal{Q}_\alpha \mathcal{Q}_\beta}(t,t') = C_{\mathbf{r}}^{j_\alpha^{(d)} \mathcal{Q}_\beta}(t,t'), \tag{A.3}$$

where we have defined dynamic correlation as $C_{\mathbf{r}}^{\mathcal{Q}_\alpha \mathcal{Q}_\beta}(t,t') = \langle \mathcal{Q}_\alpha(\mathbf{0},t)\mathcal{Q}_\beta(\mathbf{r},t')\rangle_c$ of two observable $\mathcal{Q}_\alpha$ and $\mathcal{Q}_\beta$. The above equation implies that, for $t > t'$,

$$\langle (j_\alpha(\mathbf{r},t) - j_\alpha^{(d)}(\mathbf{r},t))\mathcal{Q}_\beta(\mathbf{0},t')\rangle = C_{\mathbf{r}}^{j_\alpha^{(fl)} \mathcal{Q}_\beta}(t,t') = 0. \tag{A.4}$$

Also, we have, by definition,

$$\frac{d}{dt'} C_{\mathbf{r}}^{\mathcal{Q}_\alpha \mathcal{Q}_\beta}(t,t') = C_{\mathbf{r}}^{\mathcal{Q}_\alpha j_\beta}(t,t') \tag{A.5}$$

Note that, in the above two equations (A.3) and (A.5), we have considered that the correlation between the fluctuating current $j_\alpha^{(fl)}(\mathbf{r},t)$ at a later time t and any dynamical observable, say $\mathcal{A}(\mathbf{r}',t')$, at an earlier time t' (i.e.,$t>t'$) is uncorrelated,

$$\langle j_\alpha^{(fl)}(\mathbf{r},t)\mathcal{A}(\mathbf{r}',t')\rangle_c = \langle j_\alpha^{(fl)}(\mathbf{r},t)\mathcal{A}(\mathbf{r}',t')\rangle = 0, \tag{A.6}$$

for any $\mathbf{r}$ and $\mathbf{r}'$. However, the time ordering is important and $\langle \mathcal{A}(\mathbf{r},t)j_\alpha^{(fl)}(\mathbf{r}',t')\rangle \neq 0$ is not necessarily zero for $t>t'$. To solve eq. (A.3), we require to obtain an equal-time current-current correlation, which satisfies the following equation,

$$\frac{d}{dt}C_{\mathbf{r}}^{\mathcal{Q}_\alpha\mathcal{Q}_\beta}(t,t) = C_{\mathbf{r}}^{j_\alpha^{(d)}\mathcal{Q}_\beta}(t,t) + C_{\mathbf{r}}^{\mathcal{Q}_\alpha j_\beta^{(d)}}(t,t) + \Gamma_{\mathbf{r}}^{\alpha\beta}. \tag{A.7}$$

The first two terms in the rhs of the above equation correspond to an infinitesimal change of bond current either in α or in β directions, whereas the third term $\Gamma_{\mathbf{r}}^{\alpha\beta}$ represents the simultaneous update of current in both directions (α and β) [see Eqs. (4.7) and (4.8)]. Using Eqs. (A.3) and (A.7), we obtain the solution of unequal-time ($t>t'$) current correlations as given below:

$$C_{\mathbf{r}}^{\mathcal{Q}_\alpha\mathcal{Q}_\beta}(t,t') = \Gamma_{\mathbf{r}}^{\alpha\beta}t' + \int_0^{t'} dt''\big[C_{\mathbf{r}}^{j_\alpha^{(d)}\mathcal{Q}_\beta}(t'',t'') + C_{\mathbf{r}}^{\mathcal{Q}_\alpha j_\beta^{(d)}}(t'',t'')\big] + \int_{t'}^{t} dt'' C_{\mathbf{r}}^{j_\alpha^{(d)}\mathcal{Q}_\beta}(t'',t'). \tag{A.8}$$

Considering the time-ordering, we now write in a general form the time-integrated bond-current correlation fluctuation for an arbitrary time t and t' as

$$C_{\mathbf{r}}^{\mathcal{Q}_\alpha\mathcal{Q}_\beta}(t,t') = \Theta(t-t')C_{\mathbf{r}}^{\mathcal{Q}_\alpha\mathcal{Q}_\beta}(t,t') + \Theta(t'-t)C_{\mathbf{r}}^{\mathcal{Q}_\alpha\mathcal{Q}_\beta}(t',t), \tag{A.9}$$

where the Heaviside step function $\Theta(t)$ equals $1, 1/2$ and 0 for $t>0$, $t=0$ and $t<0$, respectively. First differentiating Eq. (A.9) w.r.t. t', then w.r.t. t and finally considering (for simplicity) $t'=0$ and $t\geq t'$, we have

$$C_{\mathbf{r}}^{j_\alpha j_\beta}(t,t'=0) = \left[\frac{d}{dt}\frac{d}{dt'}C_{\mathbf{r}}^{\mathcal{Q}_\alpha\mathcal{Q}_\beta}(t,t')\right]_{t'=0,(t-t')\geq 0} \tag{A.10}$$

$$= \frac{d}{dt}\Big[-\delta(t-t')\{C_{\mathbf{r}}^{\mathcal{Q}_\alpha\mathcal{Q}_\beta}(t,t') - C_{\mathbf{r}}^{\mathcal{Q}_\alpha\mathcal{Q}_\beta}(t',t)\} + \Theta(t-t')\frac{d}{dt'}C_{\mathbf{r}}^{\mathcal{Q}_\alpha\mathcal{Q}_\beta}(t,t') + \Theta(t'-t)\frac{d}{dt'}C_{\mathbf{r}}^{\mathcal{Q}_\alpha\mathcal{Q}_\beta}(t',t)\Big]_{t'=0,(t-t')\geq 0} \tag{A.11}$$

$$= \Gamma_{\mathbf{r}}^{\alpha\beta}\delta(t) + \Theta(t)C_{\mathbf{r}}^{j_\alpha^{(d)}j_\beta}(t,0) + \Theta(-t)C_{\mathbf{r}}^{j_\alpha^{(d)}j_\beta}(0,t). \tag{A.12}$$

The above equation implies that, for $t=t'=0$, we have $C_{\mathbf{r}}^{j_\alpha j_\beta}(0,0) = \Gamma_{\mathbf{r}}^{\alpha\beta}\delta(0)$ as, in leading order, only the first term containing $\delta(0)$ dominates and the other two terms in rhs are negligibly small compared the first term. On the other hand, for $t>t'=0$, we have $C_{\mathbf{r}}^{j_\alpha j_\beta}(t,0) = C_{\mathbf{r}}^{j_\alpha^{(d)}j_\beta}(t,0)$ as, in that case, the first term is vanishingly small and, due to Heaviside theta function, only one of the remaining terms survives. Furthermore, for arbitrary times t and t', the fluctuating current-current correlation

function can be written as

$$C_{\mathbf{r}}^{j_\alpha^{(fl)} j_\beta^{(fl)}}(t,t') = \langle (j_\alpha(0,t) - j_\alpha^{(d)}(0,t))(j_\beta(\mathbf{r},t') - j_\beta^{(d)}(\mathbf{r},t'))\rangle_c \tag{A.13}$$

$$= C_{\mathbf{r}}^{j_\alpha j_\beta}(t,t') - C_{\mathbf{r}}^{j_\alpha j_\beta^{(d)}}(t,t') - C_{\mathbf{r}}^{j_\alpha^{(d)} j_\beta}(t,t') + C_{\mathbf{r}}^{j_\alpha^{(d)} j_\beta^{(d)}}(t,t')$$

$$= C_{\mathbf{r}}^{j_\alpha j_\beta}(t,t') - C_{\mathbf{r}}^{j_\alpha^{(d)} j_\beta}(t,t'), \tag{A.14}$$

which becomes zero for $t > t'$, where we have used $\langle j_\alpha^{(fl)} j_\beta^{(d)}(t,t')\rangle_c = 0$ and $C_{\mathbf{r}}^{j_\alpha j_\beta^{(d)}}(t,t') = C_{\mathbf{r}}^{j_\alpha^{(d)} j_\beta^{(d)}}(t,t')$ for $t > t'$ [also see Eq. (A.6)] – the first equality implies that the diffusive current at the initial time t' is uncorrelated with the fluctuating current at the latter time t and then the second equality immediately follows. For $t = t'$, from Eq. (A.12), one can see that $C_{\mathbf{r}}^{j_\alpha^{(d)} j_\beta}(t,t')$ is of order $\mathcal{O}(1)$. In other words, we obtain the strength of the fluctuating current through the Onsager transport coefficients or the mobility tensor $\Gamma^{\alpha\beta}$ as given below:

$$C_{\mathbf{r}}^{j_\alpha^{(fl)} j_\beta^{(fl)}}(t,t') = \Gamma^{\alpha\beta}(\mathbf{r})\delta(t-t'). \tag{A.15}$$

Bibliography

[1]S. Ramaswamy, "The Mechanics and Statistics of Active Matter", Annu. Rev. Condens. Matter Phys., 323–345 (2010).

[2]A. Gabrielli, M. Joyce, and F. Sylos Labini, "Glass-like universe: Real-space correlation properties of standard cosmological models", Phys. Rev. D **65**, 083523 (2002).

[3]S. Torquato and F. H. Stillinger, "Local density fluctuations, hyperuniformity, and order metrics", Phys. Rev. E **68**, 041113 (2003).

[4]S. Torquato, "Hyperuniform states of matter", Phys. Rep. **745**, 1–95 (2018).

[5]Y. Liu, D. Chen, J. Tian, W. Xu, and Y. Jiao, "Universal Hyperuniform Organization in Looped Leaf Vein Networks", Phys. Rev. Lett. **133**, 028401 (2024).

[6]Y. Jiao, T. Lau, H. Hatzikirou, M. Meyer-Hermann, J. C. Corbo, and S. Torquato, "Avian photoreceptor patterns represent a disordered hyperuniform solution to a multiscale packing problem", Phys. Rev. E **89**, 022721 (2014).

[7]A. Donev, F. H. Stillinger, and S. Torquato, "Unexpected Density Fluctuations in Jammed Disordered Sphere Packings", Phys. Rev. Lett. **95**, 090604 (2005).

[8]F. Spitzer, "Interaction of Markov processes", Adv. Math. **5**, 246–290 (1970).

[9]T. M. Liggett, *Interacting Particle Systems* (Springer, New York, NY, USA, 1985).

[10]R. J. Harris, A. Rákos, and G. M. Schütz, "Current fluctuations in the zero-range process with open boundaries", J. Stat. Mech.: Theory Exp. **2005**, P08003 (2005).

[11]P. Bak, C. Tang, and K. Wiesenfeld, "Self-organized criticality: An explanation of the 1/f noise", Phys. Rev. Lett. **59**, 381–384 (1987).

[12]S. S. Manna, "Two-state model of self-organized criticality", J. Phys. A: Math. Gen. **24**, L363 (1991).

[13]S. Bondyopadhyay and P. K. Mohanty, "Conserved mass models with stickiness and chipping", J. Stat. Mech.: Theory Exp. **2012**, P07019 (2012).

[14]R. Rajesh and S. N. Majumdar, "Conserved Mass Models and Particle Systems in One Dimension", J. Stat. Phys. **99**, 943–965 (2000).

[15]C. Kipnis, C. Marchioro, and E. Presutti, "Heat flow in an exactly solvable model", J. Stat. Phys. **27**, 65–74 (1982).

[16]P. A. Ferrari and L. Fontes, "Fluctuations of a Surface Submitted to a Random Average Process", Electron. J. Probab. **3**, 1–34 (1998).

[17]M. R. Evans and T. Hanney, "Nonequilibrium statistical mechanics of the zero-range process and related models", J. Phys. A: Math. Gen. **38**, R195 (2005).

[18]K. Christensen, Á. Corral, V. Frette, J. Feder, and T. Jøssang, "Tracer Dispersion in a Self-Organized Critical System", Phys. Rev. Lett. **77**, 107–110 (1996).

[19]D. Aldous and P. Diaconis, "Hammersley's interacting particle process and longest increasing subsequences", Probab. Theory Related Fields **103**, 199–213 (1995).

[20]J. Krug and J. García, "Asymmetric Particle Systems on $\mathbb{R}$", J. Stat. Phys. **99**, 31–55 (2000).

[21]A. Chakraborti and B. K. Chakrabarti, "Statistical mechanics of money: how saving propensity affects its distribution", Eur. Phys. J. B **17**, 167–170 (2000).

[22]F. Redig and F. Sau, "Generalized immediate exchange models and their symmetries", Stochastic Processes Appl. **127**, 3251–3267 (2017).

[23]S. K. Friedlander and W. H. Marlow, "Smoke, Dust and Haze: Fundamentals of Aerosol Behavior", Phys. Today **30**, 58–59 (1977).

[24]S. N. Coppersmith, C.-h. Liu, S. Majumdar, O. Narayan, and T. A. Witten, "Model for force fluctuations in bead packs", Phys. Rev. E **53**, 4673–4685 (1996).

[25]A. E. Scheidegger, "A stochastic model for drainage patterns into an intramontane treinch", International Association of Scientific Hydrology. Bulletin **12**, 15–20 (1967).

[26]A. Dutta and D. Kumar Sinha, "Turnover of the actomyosin complex in zebrafish embryos directs geometric remodelling and the recruitment of lipid droplets", Sci. Rep. **5**, 1–14 (2015).

[27]D. Chowdhury, L. Santen, and A. Schadschneider, "Statistical physics of vehicular traffic and some related systems", Phys. Rep. **329**, 199–329 (2000).

[28]J. R. Norris, *Markov Chains* (Cambridge University Press, Cambridge, England, UK, Feb. 1997).

[29]N. G. Van Kampen, *Stochastic Processes in Physics and Chemistry* (North Holland, 2007).

[30]M. R. Evans, "Phase transitions in one-dimensional nonequilibrium systems", Braz. J. Phys. **30**, 42–57 (2000).

[31]C. Godrèche, "Dynamics of condensation in zero-range processes", J. Phys. A: Math. Gen. **36**, 6313 (2003).

[32]T. Chakraborty, P. Pradhan, and K. Jain, "Current fluctuations in the symmetric zero-range process below and at critical density", Phys. Rev. E **110**, L052103 (2024).

[33]B. Derrida and J. L. Lebowitz, "Exact Large Deviation Function in the Asymmetric Exclusion Process", Phys. Rev. Lett. **80**, 209–213 (1998).

[34]A. Das, S. Chatterjee, and P. Pradhan, "Spatial correlations, additivity, and fluctuations in conserved-mass transport processes", Phys. Rev. E **93**, 062135 (2016).

[35]P. K. Mohanty, "Generic features of the wealth distribution in ideal-gas-like markets", Phys. Rev. E **74**, 011117 (2006).

[36]A. Vespignani, R. Dickman, M. A. Muñoz, and S. Zapperi, "Driving, Conservation, and Absorbing States in Sandpiles", Phys. Rev. Lett. **81**, 5676–5679 (1998).

[37]A. Hazra, T. Chakraborty, A. Mukherjee, and P. Pradhan, "Generic power laws in higher-dimensional lattice models with multidirectional hopping", arXiv, 10.48550/arXiv.2503.18365 (2025).

[38]R. Dickman, A. Vespignani, and S. Zapperi, "Self-organized criticality as an absorbing-state phase transition", Phys. Rev. E **57**, 5095–5105 (1998).

[39]S. Lübeck, "Universal scaling behavior of non-equilibrium phase transitions", Int. J. Mod. Phys B **18**, 3977–4118 (2004).

[40]D. Hexner and D. Levine, "Noise, Diffusion, and Hyperuniformity", Phys. Rev. Lett. **118**, 020601 (2017).

[41]D. Tapader, P. Pradhan, and D. Dhar, "Density relaxation in conserved Manna sandpiles", Phys. Rev. E **103**, 032122 (2021).

[42]A. Mukherjee and P. Pradhan, "Dynamic correlations in the conserved Manna sandpile", Phys. Rev. E **107**, 024109 (2023).

[43]P. Grassberger, D. Dhar, and P. K. Mohanty, "Oslo model, hyperuniformity, and the quenched Edwards-Wilkinson model", Phys. Rev. E **94**, 042314 (2016).

[44]A. Mukherjee, D. Tapader, A. Hazra, and P. Pradhan, "Anomalous relaxation and hyperuniform fluctuations in center-of-mass conserving systems with broken time-reversal symmetry", Phys. Rev. E **110**, 024119 (2024).

[45]D. Hexner and D. Levine, "Hyperuniformity of Critical Absorbing States", Phys. Rev. Lett. **114**, 110602 (2015).

[46]Z.-Q. Li, Q.-L. Lei, and Y.-Q. Ma, "Fluidization and anomalous density fluctuations in 2D Voronoi cell tissues with pulsating activity", Proc. Natl. Acad. Sci. U.S.A. **122**, e2421518122 (2025).

[47]Y.-E. Keta and S. Henkes, "Long-range order in two-dimensional systems with fluctuating active stresses", Soft Matter **21**, 5710–5719 (2025).

[48]Y. Tang, X. Li, and D. Bi, "Tunable Hyperuniformity in Cellular Structures", arXiv, 10.48550/arXiv.2408.08976 (2024).

[49]J. Toner and Y. Tu, "Long-Range Order in a Two-Dimensional Dynamical XY Model: How Birds Fly Together", Phys. Rev. Lett. **75**, 4326–4329 (1995).

[50]R. Garcia-Millan, G. Pruessner, L. Pickering, and K. Christensen, "Correlations and hyperuniformity in the avalanche size of the Oslo model", Europhys. Lett. **122**, 50003 (2018).

[51]H. Spohn, *Large Scale Dynamics of Interacting Particles* (Springer, Berlin, Germany, Dec. 2012).

[52]B. Derrida, "Non-equilibrium steady states: fluctuations and large deviations of the density and of the", J. Stat. Mech.: Theory Exp. **2007**, P07023 (2007).

[53]B. Derrida, J. L. Lebowitz, and E. R. Speer, "Exact Free Energy Functional for a Driven Diffusive Open Stationary Nonequilibrium System", Phys. Rev. Lett. **89**, 030601 (2002).

[54]L. Bertini, A. De Sole, D. Gabrielli, G. Jona-Lasinio, and C. Landim, "Macroscopic fluctuation theory", Rev. Mod. Phys. **87**, 593–636 (2015).

[55]T. Bodineau and B. Derrida, "Current Fluctuations in Nonequilibrium Diffusive Systems: An Additivity Principle", Phys. Rev. Lett. **92**, 180601 (2004).

[56]A. Hazra, A. Mukherjee, and P. Pradhan, "Hyperuniformity in mass transport processes with center-of-mass conservation: some exact results", J. Stat. Mech.: Theory Exp. **2025**, 023201 (2025).

[57]C.-H. Liu, S. R. Nagel, D. A. Schecter, S. N. Coppersmith, S. Majumdar, O. Narayan, and T. A. Witten, "Force Fluctuations in Bead Packs", Science **269**, 513–515 (1995).

[58]V. M. Yakovenko and J. B. Rosser, "Colloquium: Statistical mechanics of money, wealth, and income", Rev. Mod. Phys. **81**, 1703–1725 (2009).

[59]M. Patriarca, E. Heinsalu, and A. Chakraborti, "Basic kinetic wealth-exchange models: common features and open problems", Eur. Phys. J. B **73**, 145–153 (2010).

[60]F. Zielen and A. Schadschneider, "Exact Mean-Field Solutions of the Asymmetric Random Average Process", J. Stat. Phys. **106**, 173–185 (2002).

[61]M. R. Evans, S. N. Majumdar, and R. K. P. Zia, "Factorized steady states in mass transport models", J. Phys. A: Math. Gen. **37**, L275 (2004).

[62]L. Onsager and S. Machlup, "Fluctuations and Irreversible Processes", Phys. Rev. **91**, 1505–1512 (1953).

[63]L. D. Landau and E. M. Lifshitz, *Statistical Physics: Volume 5, Volume 5* (Elsevier Science, Oxford, England, UK, 2013).

[64]L. Bertini, A. De Sole, D. Gabrielli, G. Jona-Lasinio, and C. Landim, "Fluctuations in Stationary Nonequilibrium States of Irreversible Processes", Phys. Rev. Lett. **87**, 040601 (2001).

[65]P. I. Hurtado and P. L. Garrido, "Test of the Additivity Principle for Current Fluctuations in a Model of Heat Conduction", Phys. Rev. Lett. **102**, 250601 (2009).

[66]P. Rizkallah, A. Grabsch, P. Illien, and O. Bénichou, "Duality relations in single-file diffusion", J. Stat. Mech.: Theory Exp. **2023**, 013202 (2023).

[67]B. Derrida, B. Douçot, and P.-E. Roche, "Current Fluctuations in the One-Dimensional Symmetric Exclusion Process with Open Boundaries", J. Stat. Phys. **115**, 717–748 (2004).

[68]B. Derrida and A. Gerschenfeld, "Current Fluctuations of the One Dimensional Symmetric Simple Exclusion Process with Step Initial Condition", J. Stat. Phys. **136**, 1–15 (2009).

[69]D. Gabrielli and P. L. Krapivsky, "Gradient structure and transport coefficients for strong particles", J. Stat. Mech.: Theory Exp. **2018**, 043212 (2018).

[70]C. E. Fiore, P. E. Harunari, C. E. F. Noa, and G. T. Landi, "Current fluctuations in nonequilibrium discontinuous phase transitions", Phys. Rev. E **104**, 064123 (2021).

[71]A. Grabsch, P. Rizkallah, A. Poncet, P. Illien, and O. Bénichou, "Exact spatial correlations in single-file diffusion", Phys. Rev. E **107**, 044131 (2023).

[72]A. Grabsch, A. Poncet, P. Rizkallah, P. Illien, and O. Bénichou, "Exact closure and solution for spatial correlations in single-file diffusion", Sci. Adv. **8**, 10.1126/sciadv.abm5043 (2022).

[73]L. Bertini, A. D. Sole, D. Gabrielli, G. Jona-Lasinio, and C. Landim, "Non Equilibrium Current Fluctuations in Stochastic Lattice Gases", J. Stat. Phys. **123**, 237–276 (2006).

[74]R. A. Blythe and M. R. Evans, "Nonequilibrium steady states of matrix-product form: a solver's guide", J. Phys. A: Math. Theor. **40**, R333 (2007).

[75]J. Cividini, A. Kundu, S. N. Majumdar, and D. Mukamel, "Exact gap statistics for the random average process on a ring with a tracer", J. Phys. A: Math. Theor. **49**, 085002 (2016).

[76]A. Prados, A. Lasanta, and P. I. Hurtado, "Nonlinear driven diffusive systems with dissipation: Fluctuating hydrodynamics", Phys. Rev. E **86**, 031134 (2012).

[77]G. Basile, C. Bernardin, and S. Olla, "Momentum Conserving Model with Anomalous Thermal Conductivity in Low Dimensional Systems", Phys. Rev. Lett. **96**, 204303 (2006).

[78]T. Sadhu and B. Derrida, "Correlations of the density and of the current in nonequilibrium diffusive systems", J. Stat. Mech.: Theory Exp. **2016**, 113202 (2016).

[79]R. Dandekar and A. Kundu, "Mass fluctuations in random average transfer process in open set-up", J. Stat. Mech.: Theory Exp. **2023**, 013205 (2023).

[80]A. Das, A. Kundu, and P. Pradhan, "Einstein relation and hydrodynamics of nonequilibrium mass transport processes", Phys. Rev. E **95**, 062128 (2017).

[81]R. Rajesh and S. N. Majumdar, "Exact calculation of the spatiotemporal correlations in the Takayasu model and in the q model of force fluctuations in bead packs", Phys. Rev. E **62**, 3186–3196 (2000).

[82]R. Rajesh and S. N. Majumdar, "Exact tagged particle correlations in the random average process", Phys. Rev. E **64**, 036103 (2001).

[83]G. M. Schütz, "Exact Tracer Diffusion Coefficient in the Asymmetric Random Average Process", J. Stat. Phys. **99**, 1045–1049 (2000).

[84]A. Kundu and J. Cividini, "Exact correlations in a single-file system with a driven tracer", Europhys. Lett. **115**, 54003 (2016).

[85]F. Zielen and A. Schadschneider, "Matrix product approach for the asymmetric random average process", J. Phys. A: Math. Gen. **36**, 3709 (2003).

[86]S. Chatterjee, P. Pradhan, and P. K. Mohanty, "Gammalike Mass Distributions and Mass Fluctuations in Conserved-Mass Transport Processes", Phys. Rev. Lett. **112**, 030601 (2014).

[87]D. K. C. MacDonald, *Noise and Fluctuations: An Introduction* (Dover Publications, Incorporated, Dec. 2013).

[88]D. Gabrielli and D. R. M. Renger, "Dynamical Phase Transitions for Flows on Finite Graphs", J. Stat. Phys. **181**, 2353–2371 (2020).

[89]F. Bonetto, G. Gallavotti, A. Giuliani, and F. Zamponi, "Chaotic Hypothesis, Fluctuation Theorem and Singularities", J. Stat. Phys. **123**, 39–54 (2006).

[90]R. J. Harris, A. Rákos, and G. M. Schütz, "Breakdown of Gallavotti-Cohen symmetry for stochastic dynamics", Europhys. Lett. **75**, 227 (2006).

[91]M. Baus, "On the compressibility of a one-component plasma", J. Phys. A: Math. Gen. **11**, 2451 (1978).

[92]M. N. Tamashiro, Y. Levin, and M. C. Barbosa, "The one-component plasma: a conceptual approach", Physica A **268**, 24–49 (1999).

[93]L. Corté, P. M. Chaikin, J. P. Gollub, and D. J. Pine, "Random organization in periodically driven systems", Nat. Phys. **4**, 420–424 (2008).

[94]L. Berthier, P. Chaudhuri, C. Coulais, O. Dauchot, and P. Sollich, "Suppressed Compressibility at Large Scale in Jammed Packings of Size-Disperse Spheres", Phys. Rev. Lett. **106**, 120601 (2011).

[95]C. E. Zachary, Y. Jiao, and S. Torquato, "Hyperuniform Long-Range Correlations are a Signature of Disordered Jammed Hard-Particle Packings", Phys. Rev. Lett. **106**, 178001 (2011).

[96]S. Wilken, R. E. Guerra, D. J. Pine, and P. M. Chaikin, "Hyperuniform Structures Formed by Shearing Colloidal Suspensions", Phys. Rev. Lett. **125**, 148001 (2020).

[97]S. Wilken, A. Chaderjian, and O. A. Saleh, "Spatial Organization of Phase-Separated DNA Droplets", Phys. Rev. X **13**, 031014 (2023).

[98]M. Salvalaglio, M. Bouabdellaoui, M. Bollani, A. Benali, L. Favre, J.-B. Claude, J. Wenger, P. de Anna, F. Intonti, A. Voigt, and M. Abbarchi, "Hyperuniform Monocrystalline Structures by Spinodal Solid-State Dewetting", Phys. Rev. Lett. **125**, 126101 (2020).

[99]R. Maire and A. Plati, "Enhancing (quasi-)long-range order in a two-dimensional driven crystal", J. Chem. Phys. **161**, 054902 (2024).

[100]Q.-L. Lei and R. Ni, "Hydrodynamics of random-organizing hyperuniform fluids", Proc. Natl. Acad. Sci. U.S.A. **116**, 22983–22989 (2019).

[101]Q.-L. Lei, M. P. Ciamarra, and R. Ni, "Nonequilibrium strongly hyperuniform fluids of circle active particles with large local density fluctuations", Sci. Adv. **5**, 10.1126/sciadv.aau7423 (2019).

[102]A. De Masi and P. A. Ferrari, "Flux Fluctuations in the One Dimensional Nearest Neighbors Symmetric Simple Exclusion Process", J. Stat. Phys. **107**, 677–683 (2002).

[103]A. Hazra, A. Mukherjee, and P. Pradhan, "Dynamic fluctuations of current and mass in nonequilibrium mass transport processes", J. Stat. Mech.: Theory Exp. **2024**, 083205 (2024).

[104]E. Barkai and R. Silbey, "Theory of Single File Diffusion in a Force Field", Phys. Rev. Lett. **102**, 050602 (2009).

[105]R. Dickman, M. Alava, M. A. Muñoz, J. Peltola, A. Vespignani, and S. Zapperi, "Critical behavior of a one-dimensional fixed-energy stochastic sandpile", Phys. Rev. E **64**, 056104 (2001).

[106]S. Wilken, R. E. Guerra, D. Levine, and P. M. Chaikin, "Random Close Packing as a Dynamical Phase Transition", Phys. Rev. Lett. **127**, 038002 (2021).

[107]Z. Ma and S. Torquato, "Hyperuniformity of generalized random organization models", Phys. Rev. E **99**, 022115 (2019).

[108]L. Corté, S. J. Gerbode, W. Man, and D. J. Pine, "Self-Organized Criticality in Sheared Suspensions", Phys. Rev. Lett. **103**, 248301 (2009).

[109]G. I. Menon and S. Ramaswamy, "Universality class of the reversible-irreversible transition in sheared suspensions", Phys. Rev. E **79**, 061108 (2009).

[110]S. Torquato, T. M. Truskett, and P. G. Debenedetti, "Is Random Close Packing of Spheres Well Defined?", Phys. Rev. Lett. **84**, 2064–2067 (2000).

[111]E. Tjhung and L. Berthier, "Hyperuniform Density Fluctuations and Diverging Dynamic Correlations in Periodically Driven Colloidal Suspensions", Phys. Rev. Lett. **114**, 148301 (2015).

[112]C. E. Maher, Y. Jiao, and S. Torquato, "Hyperuniformity of maximally random jammed packings of hyperspheres across spatial dimensions", Phys. Rev. E **108**, 064602 (2023).

[113]K. J. Wiese, "Hyperuniformity in the Manna Model, Conserved Directed Percolation and Depinning", Phys. Rev. Lett. **133**, 067103 (2024).

[114]R. Dandekar, "Exact hyperuniformity exponents and entropy cusps in models of active-absorbing transition", Europhys. Lett. **132**, 10008 (2020).

[115]H. Spohn, "Generalized Gibbs Ensembles of the Classical Toda Chain", J. Stat. Phys. **180**, 4–22 (2020).

[116]M. Patriarca, A. Chakraborti, K. Kaski, and G. Germano, "Kinetic Theory Models for the Distribution of Wealth: Power Law from Overlap of Exponentials", in *Econophysics of Wealth Distributions* (Springer, Milano, Italy, 2005), pp. 93–110.

[117]G. Carinci, C. Giardinà, C. Giberti, and F. Redig, "Duality for Stochastic Models of Transport", J. Stat. Phys. **152**, 657–697 (2013).

[118]B. van Ginkel, F. Redig, and F. Sau, "Duality and Stationary Distributions of the "Immediate Exchange Model" and Its Generalizations", J. Stat. Phys. **163**, 92–112 (2016).

[119]M. Basu, U. Basu, S. Bondyopadhyay, P. K. Mohanty, and H. Hinrichsen, "Fixed-Energy Sandpiles Belong Generically to Directed Percolation", Phys. Rev. Lett. **109**, 015702 (2012).

[120]A. Chatterjee, B. K. Chakrabarti, and S. S. Manna, "Pareto law in a kinetic model of market with random saving propensity", Physica A **335**, 155–163 (2004).

[121]H. Spohn, "Hydrodynamic equations for the Ablowitz–Ladik discretization of the nonlinear Schrödinger equation", J. Math. Phys. **63**, 10.1063/5.0075670 (2022).

[122]C. Boldrighini, R. L. Dobrushin, and Y. M. Sukhov, "One-dimensional hard rod caricature of hydrodynamics", J. Stat. Phys. **31**, 577–616 (1983).

[123]O. A. Castro-Alvaredo, B. Doyon, and T. Yoshimura, "Emergent Hydrodynamics in Integrable Quantum Systems Out of Equilibrium", Phys. Rev. X **6**, 041065 (2016).

[124]O. Ogunnaike, J. Feldmeier, and J. Y. Lee, "Unifying Emergent Hydrodynamics and Lindbladian Low-Energy Spectra across Symmetries, Constraints, and Long-Range Interactions", Phys. Rev. Lett. **131**, 220403 (2023).

[125]J. Feldmeier, P. Sala, G. De Tomasi, F. Pollmann, and M. Knap, "Anomalous Diffusion in Dipole- and Higher-Moment-Conserving Systems", Phys. Rev. Lett. **125**, 245303 (2020).

[126]A. Morningstar, V. Khemani, and D. A. Huse, "Kinetically constrained freezing transition in a dipole-conserving system", Phys. Rev. B **101**, 214205 (2020).

[127]V. B. Shenoy and R. Moessner, "(k, n)-fractonic Maxwell theory", Phys. Rev. B **101**, 085106 (2020).

[128]A. Gromov, A. Lucas, and R. M. Nandkishore, "Fracton hydrodynamics", Phys. Rev. Res. **2**, 033124 (2020).

[129]A. Das, S. Chatterjee, P. Pradhan, and P. K. Mohanty, "Additivity property and emergence of power laws in nonequilibrium steady states", Phys. Rev. E **92**, 052107 (2015).

[130]H. Sachdeva and M. Barma, "Analytical Study of Giant Fluctuations and Temporal Intermittency", J. Stat. Phys. **154**, 950–987 (2014).

[131]D. Karevski and G. M. Schütz, "Conformal Invariance in Driven Diffusive Systems at High Currents", Phys. Rev. Lett. **118**, 030601 (2017).

[132]T. Bodineau, B. Derrida, and J. L. Lebowitz, "Vortices in the Two-Dimensional Simple Exclusion Process", J. Stat. Phys. **131**, 821–841 (2008).

[133]A. Hazra, T. Chakraborty, A. Mukherjee, and P. Pradhan, "Spatial structure of current fluctuation in mass transport processes in d dimensions", (Unpublished).

[134]J. H. Han, E. Lake, and S. Ro, "Scaling and Localization in Multipole-Conserving Diffusion", Phys. Rev. Lett. **132**, 137102 (2024).

[135]T. Bertrand, D. Chatenay, and R. Voituriez, "Nonlinear diffusion and hyperuniformity from Poisson representation in systems with interaction mediated dynamics", New J. Phys. **21**, 123048 (2019).

[136]J. Guo, P. Glorioso, and A. Lucas, "Fracton Hydrodynamics without Time-Reversal Symmetry", Phys. Rev. Lett. **129**, 150603 (2022).

[137]C. Arita, P. L. Krapivsky, and K. Mallick, "Generalized exclusion processes: Transport coefficients", Phys. Rev. E **90**, 052108 (2014).

[138]H. Spohn, "Long range correlations for stochastic lattice gases in a non-equilibrium steady state", J. Phys. A: Math. Gen. **16**, 4275 (1983).

[139]S. N. Majumdar, S. Krishnamurthy, and M. Barma, "Nonequilibrium Phase Transitions in Models of Aggregation, Adsorption, and Dissociation", Phys. Rev. Lett. **81**, 3691–3694 (1998).

[140]D. Dhar, "Self-organized critical state of sandpile automaton models", Phys. Rev. Lett. **64**, 1613–1616 (1990).

[141]B. Derrida, M. R. Evans, V. Hakim, and V. Pasquier, "Exact solution of a 1D asymmetric exclusion model using a matrix formulation", J. Phys. A: Math. Gen. **26**, 1493 (1993).

[142]B. Derrida, J. L. Lebowitz, and E. R. Speer, "Free Energy Functional for Nonequilibrium Systems: An Exactly Solvable Case", Phys. Rev. Lett. **87**, 150601 (2001).

[143]P. Rissone, E. I. Corwin, and G. Parisi, "Long-Range Anomalous Decay of the Correlation in Jammed Packings", Phys. Rev. Lett. **127**, 038001 (2021).

[144]R. Kürsten, S. Stroteich, M. Z. Hernández, and T. Ihle, "Multiple Particle Correlation Analysis of Many-Particle Systems: Formalism and Application to Active Matter", Phys. Rev. Lett. **124**, 088002 (2020).

[145]J. R. Dorfman, T. R. Kirkpatrick, and J. V. Sengers, "Generic Long-Range Correlations in Molecular", Annu. Rev. Phys. Chem., 213–239 (1994).

[146]D. Dhar and P. Pradhan, "Probability distribution of residence times of grains in sand-pile models", J. Stat. Mech.: Theory Exp. **2004**, P05002 (2004).

[147]T. Sadhu, S. N. Majumdar, and D. Mukamel, "Long-range correlations in a locally driven exclusion process", Phys. Rev. E **90**, 012109 (2014).

[148]G. Grinstein, D.-H. Lee, and S. Sachdev, "Conservation laws, anisotropy, and ''self-organized criticality" in noisy nonequilibrium systems", Phys. Rev. Lett. **64**, 1927–1930 (1990).

[149]P. L. Garrido, J. L. Lebowitz, C. Maes, and H. Spohn, "Long-range correlations for conservative dynamics", Phys. Rev. A **42**, 1954–1968 (1990).

[150]H. J. Bussemaker and M. H. Ernst, "Microscopic theory for long-range spatial correlations in lattice gas automata", Phys. Rev. E **53**, 5837–5851 (1996).

[151]M. Rossi, R. Pastor-Satorras, and A. Vespignani, "Universality Class of Absorbing Phase Transitions with a Conserved Field", Phys. Rev. Lett. **85**, 1803–1806 (2000).

[152]C. Maes, "Kinetic limit of a conservative lattice gas dynamics showing long-range correlations", J. Stat. Phys. **61**, 667–681 (1990).

[153]C. Maes and F. Redig, "Long-range spatial correlations for anisotropic zero-range processes", J. Phys. A: Math. Gen. **24**, 4359 (1991).

[154]A. Kolmogoroff, "Zur Theorie der Markoffschen Ketten", Math. Ann. **112**, 155–160 (1936).

[155]M. Abramowitz and I. A. Stegun, *Handbook of mathematical functions* (Dover Publications, New York, 1972).

[156]I. Procaccia, D. Ronis, and I. Oppenheim, "Light Scattering from Nonequilibrium Stationary States: The Implication of Broken Time-Reversal Symmetry", Phys. Rev. Lett. **42**, 287–291 (1979).

[157]T. Kirkpatrick, E. G. D. Cohen, and J. R. Dorfman, "Kinetic Theory of Light Scattering from a Fluid Not in Equilibrium", Phys. Rev. Lett. **42**, 862–865 (1979).

[158]B. M. Law, R. W. Gammon, and J. V. Sengers, "Light-scattering observations of long-range correlations in a nonequilibrium liquid", Phys. Rev. Lett. **60**, 1554–1557 (1988).

[159]B. Derrida, C. Enaud, C. Landim, and S. Olla, "Fluctuations in the Weakly Asymmetric Exclusion Process with Open Boundary Conditions", J. Stat. Phys. **118**, 795–811 (2005).

[160]M. Q. Zhang, J.-S. Wang, J. L. Lebowitz, and J. L. Vallés, "Power law decay of correlations in stationary nonequilibrium lattice gases with conservative dynamics", J. Stat. Phys. **52**, 1461–1478 (1988).

[161]T. Hwa and M. Kardar, "Dissipative transport in open systems: An investigation of self-organized criticality", Phys. Rev. Lett. **62**, 1813–1816 (1989).

[162]B. Doyon, G. Perfetto, T. Sasamoto, and T. Yoshimura, "Emergence of Hydrodynamic Spatial Long-Range Correlations in Nonequilibrium Many-Body Systems", Phys. Rev. Lett. **131**, 027101 (2023).

[163]L. Bertini, A. De Sole, D. Gabrielli, G. Jona-Lasinio, and C. Landim, "Stochastic interacting particle systems out of equilibrium", J. Stat. Mech.: Theory Exp. **2007**, P07014 (2007).

[164]H. Wang, R. Samajdar, and S. Torquato, "Correlations in interacting electron liquids: Many-body statistics and hyperuniformity", Phys. Rev. B **110**, 104201 (2024).

[165]H. van Beijeren, "Long-range spatial correlations in a simple diffusion model", J. Stat. Phys. **60**, 845–849 (1990).

[166]S. Scherg, T. Kohlert, P. Sala, F. Pollmann, B. Hebbe Madhusudhana, I. Bloch, and M. Aidelsburger, "Observing non-ergodicity due to kinetic constraints in tilted Fermi-Hubbard chains", Nat. Commun. **12**, 1–8 (2021).

[167]D. Hexner, P. M. Chaikin, and D. Levine, "Enhanced hyperuniformity from random reorganization", Proc. Natl. Acad. Sci. U.S.A. **114**, 4294–4299 (2017).

[168]S. Torquato, "Hyperuniformity and its generalizations", Phys. Rev. E **94**, 022122 (2016).